Dissertation
submitted to the
Combined Faculties for the Natural Sciences and for Mathematics
of the Ruperto-Carola University of Heidelberg, Germany,
for the degree of
Doctor of Natural Sciences

presented by

Denis Scholz

born in Ludwigshafen am Rhein, Germany

Oral examination: 26.01.2005

U-series dating of

diagenetically altered fossil reef corals

and the application for sea level reconstructions

Referees: **Prof. Dr. Augusto Mangini**

Prof. Dr. Kurt Roth

Zusammenfassung

Mithilfe von fossilen Riffkorallen ist eine exakte Rekonstruktion der Meeresspiegelschwankungen der Vergangenheit möglich. Ein bekanntes Problem bei der Uranreihen-Datierung fossiler Riffkorallen sind initiale ($^{234}U/^{238}U$) Aktivitätsverhältnisse, die nicht durch den radioaktiven Zerfall in einem geschlossenen System erklärt werden können. Dieses Phänomen ist unter dem Begriff *diagenetische Veränderungen* bekannt.

In der vorliegenden Arbeit werden fossile Riffkorallen aus Aqaba, Jordanien, und Barbados, Westindische Inseln, untersucht. Die *Porites* Korallen aus Aqaba zeigen einen hohen Grad diagenetischer Veränderungen und sind daher ideal geeignet, um die diagenetischen Prozesse zu untersuchen. Mithilfe eines numerischen Modells wird gezeigt, dass die Aktivitätsverhältnisse dieser Korallen durch nachträgliche Uranaufnahme gefolgt von teilweisem Verlust des aufgenommenen Urans erklärt werden können. Auf dieser Basis wird ein Korrekturverfahren (das *Isochronenverfahren*) entwickelt, das es ermöglicht, glaubwürdige Uranreihen-Alter für Korallen zu berechnen, die nicht mit den herkömmlichen Methoden datiert werden können.

Die *Acropora palmata* und *Diploria strigosa* Korallen aus Barbados zeigen einen geringeren Grad diagenetischer Veränderungen. Es wird gezeigt, dass diese Korallen durch einen anderen Prozess beeinflusst wurden als die Korallen aus Aqaba. Daher können sie nicht mit der Isochronenmethode datiert werden. Dennoch ist es möglich, Höhe, Beginn und Dauer des Meeresspiegel Hochstands während des Marinen Isotopen Stadiums (MIS) 6.5 (~175000 Jahre vor heute) zu bestimmen. MIS 6.5 ist eine außergewöhnliche Klimaphase innerhalb der letzen 300000 Jahre. Die vorliegende Meeresspiegelkurve ist die erste, exakt datierte, direkte Meeresspiegelrekonstruktion für das Marine Isotopen Stadium 6.5.

Abstract

The age/height relationship of fossil reef coral terraces provides an accurate measurement of past sea level changes. An outstanding problem of U-series dating of fossil reef corals is that many corals show initial ($^{234}U/^{238}U$) activity ratios that cannot be explained by closed system decay. This phenomenon is denoted by the term *diagenetic* alterations.

In this work fossil reef corals from Aqaba, Jordan, and Barbados, West Indies, are investigated by U-series methods. The corals of the genus *Porites* from Aqaba show a very high degree of diagenetic alteration. Therefore, they are ideally suited to study the diagenetic processes. It is demonstrated by numerical modelling that the activity ratios of these corals can be explained by post depositional U uptake followed by partial loss of the additional U. On the basis of these results a correction technique (the *isochron dating method*) is developed which enables to calculate reliable U-series ages for corals which could not be dated by the conventional methods.

The corals of the genus *Acropora palmata* and *Diploria strigosa* from Barbados show less degree of diagenetic alteration. It is shown that these corals have been affected by a different process than the Aqaba corals. Therefore, they cannot be dated by the isochron dating method. Nevertheless, the results allow an accurate reconstruction of the magnitude, timing, and duration of the sea level peak during Marine Isotope Substage (MIS) 6.5 (~175,000 before present), a period of extraordinary climate signature within the last 300,000 years. The presented record is the first precisely dated direct measurement of sea level during this period.

Table of contents

1 Introduction

The climate of the Earth was subject to considerable variations in the past. One way to investigate the forcing and feedback mechanisms of Earth's climate is to use climate models, another way is the reconstruction of past climate variations by investigation of climate archives such as deep sea sediments, ice cores, tree rings, or speleothems. Such data can then be used as boundary conditions in climate models or to verify the model outputs. In recent years a better cooperation between paleoclimate researchers and climate modellers has emerged with regard to understand past and to predict future climate changes.

An outstanding climatic feature within the Quaternary are global sea level fluctuations of different magnitude and periodicity. These sea level changes are for example recorded in the $\delta^{18}O$ signals of deep sea sediments and ice cores. Beyond the ^{14}C-dating range of ~40,000 years, the chronologies of such climate archives are mainly based on the *Milankovitch theory of climate change* which suggests that the change between Glacials and Interglacials is primarily driven by variations in the total solar summer insolation received in northern latitudes where major ice sheets have formed in the past (*Milankovitch, 1941*). These insolation changes arise from variations in Earth's orbital parameters. However, during the last decade the results from several climate archives have indicated that orbital forcing is not the only trigger for major changes in global ice volume. Furthermore, there are several problems associated with the reconstruction of the magnitude of sea level changes from $\delta^{18}O$ signals (*Broecker, 1995*).

An alternative method of sea level reconstruction is the use of fossil reef corals. As some coral species live in the upper five meters below sea level only, they provide an accurate measure of past sea level change. In addition, the carbonate skeletons of fossil reef corals can be dated by U-series methods providing absolute ages independent from the Milankovitch theory. *Mesolella et al.* (*1969*) have firstly applied this method of sea level reconstruction successfully on the island of Barbados, West Indies. However, in the following years it turned out that many fossil reef corals display so-called *diagenetic* alterations and their U-series ages cannot be considered as strictly reliable. Although many researchers have investigated this phenomenon in the last ~15 years, the processes which produce these isotopic anomalies have remained unidentified. Consequently, coral diagenesis is a subject of ongoing research, and just recently, two new models that try to explain the diagenetic processes have been published (*Thompson et al., 2003; Villemant & Feuillet, 2003*).

In this work fossil and recent corals of the genus *Porites* from Aqaba, Jordan, as well as fossil corals of the genus *Acropora palmata* and *Diploria strigosa* from Barbados, West Indies, are studied. As the corals from Aqaba show a very high degree of diagenetic alteration, they are ideally qualified to investigate the involved processes. On the basis of the results the *isochron dating method*, a correction technique that allows to estimate reliable ages for corals that cannot be dated by conventional U-series methods, is developed (*Scholz et al., 2004*). The results obtained from the corals from Barbados allow a reconstruction of the magnitude, timing, and duration of the sea level highstand within *Marine Isotope Substage (MIS) 6.5* (~175,000 years before present), a relatively warm phase within the penultimate glacial period. The presented record is the first precisely dated direct measurement of sea level for MIS 6.5 which is a period of extraordinary climate signature and therefore of particular interest.

In the second chapter of this work the basics of the U-series dating method are explained. Subsequently, a description of coral growth, reef development, and the incorporation of U-series isotopes into coral skeletons is given. As the focus of this work lies on the investigation of the diagenetic processes, a detailed discussion of this topic is included comprising indications for open-system behaviour, the reliability criteria used by other authors, and the diagenetic scenarios and open-system-models proposed in previous studies.

In chapter three the basics of sea level reconstruction using fossil reef corals and the other available methods (i.e. stable isotopes and submerged speleothems) are described and discussed. Afterwards, the current state of the sea level record based on coral dating is shown, and a short summary of other possible utilizations of fossil corals as paleoclimate archives is given.

Chapter four represents the main part of this work. In the first section the investigation of the Aqaba corals is described in detail. Afterwards, the new isochron dating method that has been developed on the basis of these results is presented. After a brief discussion of the paleo sea level at Aqaba, a detailed discussion of the calculation of the isochron age uncertainties follows, and an algorithm which is based on a Monte Carlo simulation is proposed. This algorithm can be generally used to estimate the uncertainty of all kinds of isochrons used in geochronology. In the second part of chapter four the Barbados data and the sea level reconstruction for MIS 6.5 are presented and discussed.

In chapter five the major results of this work are summarized, and a short outlook on future studies is given.

This investigation was carried out within the framework of the “Deutsches Klimaforschungsprogramm” (DEKLIM) which is funded by the German Federal Ministry for Education and Research. Different working groups, including specialists for several kinds of paleoclimate archives as well as climate modellers, work in close collaboration in order to compare their results. The corals from Aqaba, Jordan, have been collected by Dr. Thomas Felis from the University of Bremen, who performed most of the pre-treatment of these coral samples (see chapter four) as well. The coral sampling on Barbados has been assisted by Prof. Dr. D. Meischner (University of Göttingen).

2 Basics

2.1 U-series dating methods

There are three naturally occurring radioactive decay chains; each starts with an actinide nuclide (^{238}U, ^{235}U, and ^{232}Th) having a long half live ($T_{1/2}$ > 0.7 Gyr) and ends with a stable isotope of lead (Fig. 2.1). Processes that fractionate nuclides within a decay chain produce parent-daughter disequilibrium. The return to equilibrium then allows quantification of time (*Bourdon et al., 2003*).

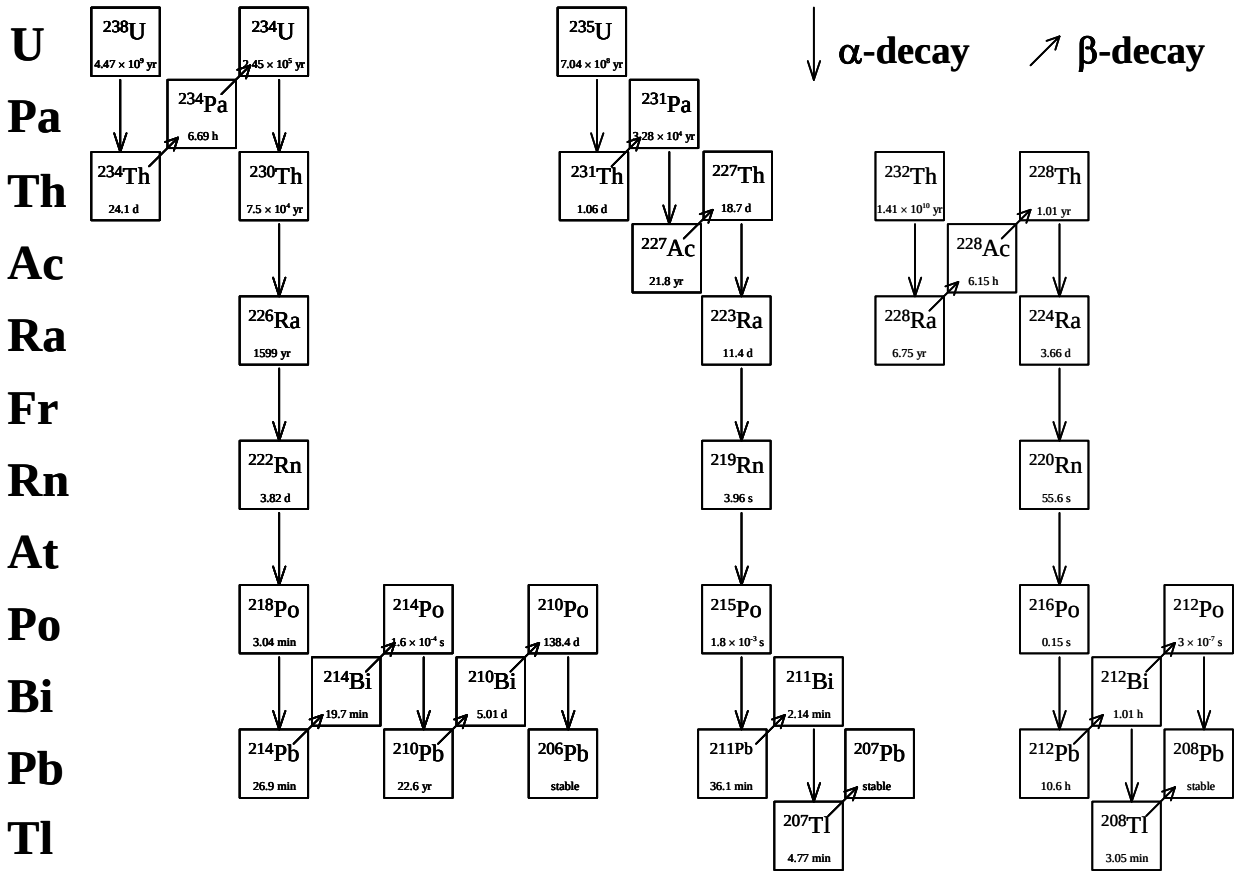

Fig. 2.1: Schematic drawing of the ^{238}U, ^{235}U and ^{232}Th decay chains (modified from *Bourdon et al.* (*2003*)).

2.1.1 U, Th, and Pa geochemistry

Typical U concentrations of the continental crust range from 0.1 (basalts) to 6 ppm (granites), but there have also been found much higher values (up to 100 ppm) for example in speleothems. The average Th/U ratio in crustal rocks is ~3.5, and the constancy of this value among many different igneous rock types indicates the general lack of fractionation of the two elements during magmatic processes (*Ivanovich & Harmon, 1992*).

The half-lives of the parent isotopes in the ^{238}U, ^{235}U, and ^{232}Th decay-series are much longer than those of their intermediate daughters (see Fig. 2.1). In naturally occurring materials with an age of several million years the parent and daughter isotopes will be in a state of secular equilibrium. The key to the utility of the U-series dating methods is that several natural processes are capable of disrupting this state of equilibrium. In general, two types of mechanisms need to be distinguished:

Firstly, U-series isotopes can become fractionated because of their different geochemical behaviour. U mainly exists in two oxidation states in nature (U^{4+} and U^{6+}), being dominantly in the soluble U^{6+} form at the surface of the earth, and is soluble as uranyl ion $(UO_2)^{2+}$ and in various uranyl carbonate forms (*Edwards et al., 2003*). However, in a reducing environment it will be in the U^{4+} state where it is insoluble and therefore generally far less mobile than U^{6+}. In contrast, Pa (in terrestrial material mainly in the 5+ oxidation state) and Th (mainly Th^{4+}) are insoluble in natural waters (*Ivanovich & Harmon, 1992; Bourdon et al., 2003*). Therefore, under natural conditions Pa and Th are mainly transported adsorbed to particles or in minerals. Consequently, Th and Pa will not be incorporated during the precipitation of secondary carbonates from aqueous solutions (e.g. corals, molluscs, speleothems or travertines) resulting in Th/U and Pa/U disequilibria respectively.

The second fractionation mechanism takes place as a result of radioactive decay and is generally described as α-recoil effect. During an α-decay (e.g. decay of ^{238}U) the resulting particles are emitted with finite kinetic energy. The effect of recoil is twofold: firstly, the atom is displaced from its original site and can either be more easily removed subsequently or be ejected directly into an adjacent phase, secondly the site is damaged by the α-particle (*Bourdon et al., 2003*). This results in the daughter nuclide to be more easily mobilized than its parent during weathering processes. Therefore U isotope compositions potentially can provide an important tool for tracing groundwaters from different aquifer conditions, although clear interpretations of ($^{234}U/^{238}U$) activity ratios, and quantification of the responsible processes, remain difficult (*Porcelli & Swarzenski, 2003*).

2.1.2 The calculation of Th/U- and Pa/U-ages

The activity A of a number of atoms of a nuclide is the number of decay events per a unit of time. In this work all activities and activity ratios are indicated by parenthesis (e.g. (^{238}U)) and are given in *decays per minute [dpm]*. The equation of decay for given a number of atoms, N, of a nuclide can be written as follows:

$$\frac{dN}{dt} = -\lambda N \tag{2.1}$$

By integration of eq. (2.1) we obtain:

$$N(t) = N_0 \cdot e^{-\lambda t} \tag{2.2}$$

with : N(t): Number of atoms at the time t
N_0: Number of atoms at the time t = 0
λ: decay constant [yr^{-1}]

λ is related to the half-live $T_{1/2}$ by: $$\lambda = \frac{\ln 2}{T_{1/2}} \tag{2.3}$$

The equation of decay for the daughter atoms can be written as:

$$\frac{dN_2}{dt} = -\lambda_2 N_2 + \lambda_1 N_1 \tag{2.4}$$

where the first term describes the decay of the daughter nuclide and the second term describes the production of the daughter nuclide by decay of the mother.

For Th/U- and Pa/U-dating the following assumptions need to be made:

1. (^{230}Th)$_{initial}$ and (^{231}Pa)$_{initial}$ are zero, because both isotopes are not incorporated during the precipitation of secondary carbonates due to their insolubility (see chapter 2.1).
2. The system remains closed after deposition, i.e. U, Th, and Pa are not remobilised.

With these assumptions the development of the (^{234}U/^{238}U), (^{230}Th/^{238}U), and (^{231}Pa/^{235}U) activity ratios with time can be expressed as follows (see *Ivanovich & Harmon* (*1992*) for derivation):

$$\left(\frac{^{234}U}{^{238}U}\right)(t) = \left(\left(\frac{^{234}U}{^{238}U}\right)_{init.} - 1\right) \quad e^{-\lambda_{234}\, t} + 1 \tag{2.5}$$

$$\left(\frac{^{230}Th}{^{238}U}\right)(t) = (1 - e^{-\lambda_{230}\, t}) + \left(\left(\frac{^{234}U}{^{238}U}\right)(t) - 1\right)\frac{\lambda_{230}}{\lambda_{230} - \lambda_{234}}(1 - e^{-(\lambda_{230} - \lambda_{234})\, t}) \tag{2.6}$$

$$\left(\frac{^{231}Pa}{^{235}U}\right)(t) = 1 - e^{-\lambda_{231}\, t} \tag{2.7}$$

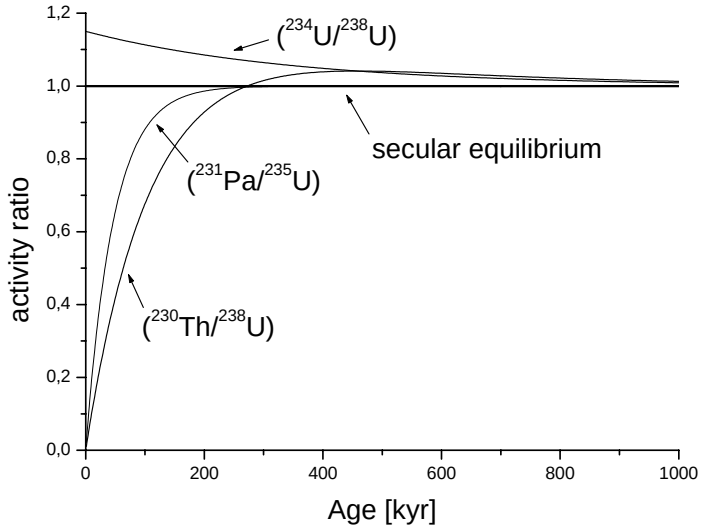

Fig. 2.2: Evolution of the (^{234}U/^{238}U), (^{230}Th/^{238}U), and (^{231}Pa/^{235}U) activity ratios under closed system conditions with no initial Th and Pa. The initial (^{234}U/^{238}U) activity ratio was assumed to be 1.15. Because of the shorter half-live (~ 32,500 yrs) of Pa, the (^{231}Pa/^{235}U) activity ratio reaches secular equilibrium about two times faster than (^{230}Th/^{238}U). The dating ranges of both methods are about 250,000 yrs for Pa/U- and 600,000 yrs for Th/U (*Edwards et al., 2003*).

The ($^{234}U/^{238}U$) activity ratio can also be given in the δ-notation in per mill:

$$\delta^{234}U = \frac{\left(\frac{^{234}U}{^{238}U}\right)_{meas} - \left(\frac{^{234}U}{^{238}U}\right)_{eq}}{\left(\frac{^{234}U}{^{238}U}\right)_{eq}} \cdot 1000 = \left(\left(\frac{^{234}U}{^{238}U}\right)_{meas} - 1\right) \cdot 1000 \qquad (2.8)$$

where $\left(\frac{^{234}U}{^{238}U}\right)_{eq}$ indicates the secular equilibrium.

While the Pa/U age equation (eq. (2.7)) can be solved analytically for t, this is not possible for the Th/U age equation. Therefore, the age calculation must be done either graphically or numerically (e.g. by the Newton-Raphson-method). The error of the Th/U age can be calculated by a Monte-Carlo-simulation (see chapter 4.1.9.2 for an extended description of this method). In the context of this work for the age- as well as the age-error-calculation Visual Basic scripts have been written which can be integrated into Microsoft Excel (see Appendix B1).

2.1.3 Correction for detrital contamination

As mentioned above one of the two basic assumptions of Th/U- and Pa/U-dating is that during carbonate growth no ^{230}Th and ^{231}Pa respectively are incorporated. Unfortunately, this basic requirement is not generally fulfilled for all kinds of samples, e.g. for deep-sea corals or lacustrine carbonates (*Edwards et al., 2003*). In such a case, a correction for initial (or non-radiogenic) ^{230}Th and ^{231}Pa will be necessary. As an indicator for the degree of detrital contamination the ^{232}Th content of the sample can be used, because ^{232}Th has the same chemical properties as ^{230}Th. If there is some knowledge of the initial ($^{230}Th/^{232}Th$) activity ratio of the detritus and the magnitude of the correction is small but significant, such a correction can be performed by the introduction of an additional term into equation (2.6) (see *Edwards et al.* (*2003*)):

$$\begin{aligned} &\left(\left(\frac{^{230}Th}{^{238}U}\right)(t) - \left(\frac{^{232}Th}{^{238}U}\right)\left(\frac{^{230}Th}{^{232}Th}\right)_{init.} e^{-\lambda_{230} t}\right) = \\ &= (1 - e^{-\lambda_{230} t}) + \left(\left(\frac{^{234}U}{^{238}U}\right)(t) - 1\right)\frac{\lambda_{230}}{\lambda_{230} - \lambda_{234}}(1 - e^{-(\lambda_{230} - \lambda_{234}) t}) \end{aligned} \qquad (2.9)$$

There have been several strategies developed to estimate initial ($^{230}Th/^{232}Th$) activity ratios. Many authors (e.g. *Stirling et al.* (*1998*)) use an initial $^{230}Th/^{232}Th$ atomic ratio of 4.4 □ 10^{-6} assuming a bulk earth $^{232}Th/^{238}U$ ratio of 3.8 ± 1.0 (*Wedepohl, 1995*) and presuming secular equilibrium. It is also possible to estimate initial ($^{230}Th/^{232}Th$) ratios by analysing modern analogues to the samples in question (*Cobb et al., 2003*).

In cases where the initial ^{230}Th concentration is that large that $^{230}Th/^{232}Th$ must be known precisely, isochron methods can be used. Such methods consider the sample to be composed of a mixture of two components, an authigenic fraction and a detrital one. On a so-called isochron-plot the activity ratios of different sub-samples of the same age with different proportions of the two components will plot on straight line. Depending on the choice of the axes, the activity ratios of the radiogenic endmember can be obtained either from the slope or the intercept of the isochron plot (for a discussion of the advantages and disadvantages of the respective plots see *Ludwig* (*2003*)). If the points do not plot on a line, an additional U or Th component must be present in the mixture (*Edwards et al., 2003*).

Another possibility is to separate the authigenic fraction physically from the detrital one, but often this is not possible because of cementation or small grain size. Chemical separation methods have been proven to be problematic, because of different adsorption of U and Th onto the solid residue or different leaching of U and Th from the residue. In such cases a total sample dissolution (TSD) scheme may be applied (*Bischoff & Fitzpatrick, 1991; Luo & Ku, 1991*). Further discussion and a comparison of various approaches can be found for example in *Kaufman* (*1993*), *Ludwig* (*2003*), or *Ludwig & Titterington* (*1994*).

Initial ($^{231}Pa/^{235}U$) activity ratios have not been studied in detail for most carbonates, but it can be shown that the initial ($^{231}Pa/^{235}U$) = 0 assumption holds for a number of corals that have low ^{232}Th concentrations. In contrast to Th, there is no long-lived isotope of Pa that can be used as an index isotope. Therefore, corrections for initial ^{231}Pa assume that ^{232}Th is an isotope of Pa and assume bulk earth $^{232}Th/^{238}U$ ratio and secular equilibrium between ^{231}Pa and ^{235}U (*Edwards et al., 2003*).

Altogether there are various approaches available to correct for detrital contamination, but the uncertainty of the estimated age will always be greater than for pure material.

2.2 U-series dating of fossil reef corals

2.2.1 The behaviour of U-series isotopes in seawater

The dominant supply of U to the oceans is from the continents by river runoff with a total flux of ~11 × 10^9 g/yr (± 35%) (*Ivanovich & Harmon, 1992*). Additional U sources are dissolution of wind-blown dust and groundwater discharge. Whereas the former is unlikely to be significant (< 3% of the riverine U flux), the latter is extremely difficult to estimate as both the total flux of groundwater and the average U concentration of such waters are poorly known (*Dunk et al., 2002*). U is removed from the oceans principally into reducing marine sediments where U concentrations are lowered, because U becomes reduced and consequently insoluble (see chapter 2.1.1). A compilation of the different oceanic U sources and sinks is given in *Henderson & Anderson* (*2003*). At the level of uncertainty, the oceanic U budget is in balance. Therefore, U has a reasonably constant seawater concentration of 3.3 ppb (*Chen et al., 1986*) in both space and time, varying only in line with salinity (*Ku et al., 1977*). This indicates an oceanic residence time for U of ~400 kyr.

Seawater ($^{234}U/^{238}U$) is higher than secular equilibrium due to α-recoil (see chapter 2.1.1) on the continents and in marine sediments. The average riverine U flux to the oceans has a ($^{234}U/^{238}U$) activity ratio lying somewhere close to 1.25 (*Chabaux et al., 2003*). Considering the long residence time of U, there is time for a portion of the excess ^{234}U to decay before it is removed again. A simple calculation suggests that, if rivers were the only source of excess ^{234}U, the oceans would have a ($^{234}U/^{238}U$) activity ratio of ~1.08 (*Henderson & Anderson, 2003*). As the observed values are much higher than this (1.146 ± 0.002) (*Chen et al., 1986; Delanghe et al., 2002*), there needs to be an additional ^{234}U source to the oceans, probably related to marine sediments. Although the size of the ^{234}U flux from sediments to bottom waters has not yet been independently assessed, the mismatch between riverine input and the observed ($^{234}U/^{238}U$) values suggests that it must be of approximately equal importance (*Henderson, 2002*). Changes in seawater ($^{234}U/^{238}U$) with time are most likely to be induced by changes in the riverine input. An extended discussion of the history of seawater ($^{234}U/^{238}U$) will be given in chapter 2.2.4.

Th generally exists as a neutral hydroxide species in the oceans and is highly insoluble. Because of its high particle reactivity, it has a distinct tendency to become incorporated in colloids or adsorbed to particle surfaces (*Ivanovich & Harmon, 1992*). Therefore, ^{230}Th produced by decay of ^{234}U in the water column is rapidly removed by sorption to particles, which settle from the water column. The average residence time of Th isotopes in seawater is ~20 yr (*Henderson & Anderson, 2003*). Decay produced ^{231}Pa is also removed from the water column by sorption to settling particles, but is slightly less insoluble than Th leading to a longer residence time of ~130 yr in seawater (*Henderson & Anderson, 2003*).

In summary, the different solubility of U and Th and Pa respectively results in seawater (^{230}Th/^{238}U) values 10^5 times lower than secular equilibrium (*Moore, 1981*), and (^{231}Pa/^{235}U) values 10^4 times lower than secular equilibrium (*Nozaki & Nakanishi, 1985*).

2.2.2 Stony or scleractinian corals and reef development

Reef building corals only live in marine environments and belong to the class of the Anthozoa. They are closely related to sea anemones (*Schuhmacher, 1988*) and may be visualized as colonial anemones that secrete limestone foundations providing structural support and protection (*Barnes & Hughes, 1988*). The largest order of the anthozoans are the stony (or scleractinian) corals which produce a calcium carbonate skeleton (*Ruppert & Barnes, 1994*).

The living organism of the coral consists of polyps and coenosarc which constitute a thin layer over the block of limestone they have secreted (*Barnes & Hughes, 1988*) (Fig. 2.3). Each polyp sits in a cup-like depression, the calyx. In times of danger or physical stress, the polyp contracts and retreats into the calyx, at other times it extends to varying degrees, depending on time of day and species. The polyps (Fig. 2.3) are connected to each other in one colony by a thin sheet of tissue, the coenosarc, covering the limestone between the calyces (*Barnes & Hughes, 1988*). Some corals, such as the Indo-Pacific reef-inhabitating *Fungia* and some deep-water species, are solitary and have large polyps (~25 cm in diameter), but the majority are colonial with hundreds to thousands of small polyps averaging 1 to 3 mm in diameter (*Ruppert & Barnes, 1994*).

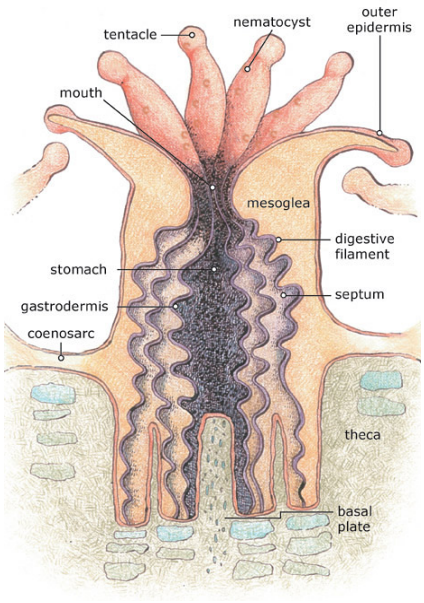

Fig. 2.3: Diagram of a single coral polyp. Much of the polyp's body is taken up by a stomach filled with digestive filaments. Open at one end only, the polyp takes in food and expels waste through its mouth. A ring of tentacles surrounding the mouth aids in capturing food, expelling waste and clearing away debris. (Picture source: http://www.nos.noaa.gov/education/corals/media/supp_coral01a.html).

The calcium carbonate skeletons of stony corals are circular and continually secreted by the lower portion of the polyp, the basal epidermis. In many corals the polyps periodically lift their bases and deposit a new floor to their calyx (*Ruppert & Barnes, 1994*). Although all corals secrete calcium carbonate, not all of them produce sufficient quantities to form reefs. Corals that calcify at high rates are known as hermatypic or reef-building corals (*Barnes & Hughes, 1988*) and can be divided into massive and branching forms, although there are intermediates between both types. While massive corals grow slowly (not much more than 1 cm per year), branching forms tend to grow rapidly, on the order of 10 cm per year (*Levinton, 2001*).

The driving force behind reef growth is the mutualism between hermatypic corals and photosynthetic zooxanthellae which are specialised single-celled algae. These algae live intracellularly within the endodermal tissues of scleractinian corals and are concentrated in the tentacles (*Levinton, 2001*). Zooxanthellae benefit from the corals by protection and perhaps by access to nutrients derived from coral excretion. The benefits of the algae to hermatypic corals include coral nutrition and lipid synthesis, but most importantly they enhance coral calcification (*Levinton, 2001*).

According to *Barnes & Hughes* (*1988*), the chemical equation describing the equilibrium between carbonate dissolution and precipitation in seawater can be summarized as:

$$Ca^{2+} + 2HCO_3^- \leftrightarrow Ca(HCO_3)_2 \leftrightarrow CaCO_3 + H_2CO_3 \qquad (2.10)$$

In the light, the zooxanthellae use CO_2 for photosynthesis and permanently remove carbon dioxide (as carbonic acid) from the system. This shifts the equilibrium in equation (2.10) to conditions favourable for calcium carbonate precipitation. Consequently, the calcium carbonate precipitation rate in corals living in symbiosis with zooxanthellae is about 10 times higher than in algae free corals (*Schuhmacher, 1988*).

Light availability is probably the most important limiting factor for coral reef growth. Because light intensity decreases exponentially with increasing depth, reef building ceases below depths of 25-50 m (*Levinton, 2001*). Another important factor is water temperature and salinity. Optimal values range from 23 to 29° C and 28 to 48 ‰ salinity (*Schellmann & Radtke, 2004*). Turbidity and sedimentation both have negative effects on hermatypic corals. Turbid waters intercept light and reduce photosynthesis, while sedimentation tends to smother corals and inhibit feeding (*Levinton, 2001*). Finally, corals are often located in areas of high wave energy, because the moving water is clear and brings nutrients and zooplankton to the corals.

These limiting factors result in shallow water coral reefs being confined to tropical and subtropical waters, generally between 30° north and 30° south latitude (Fig. 2.4).

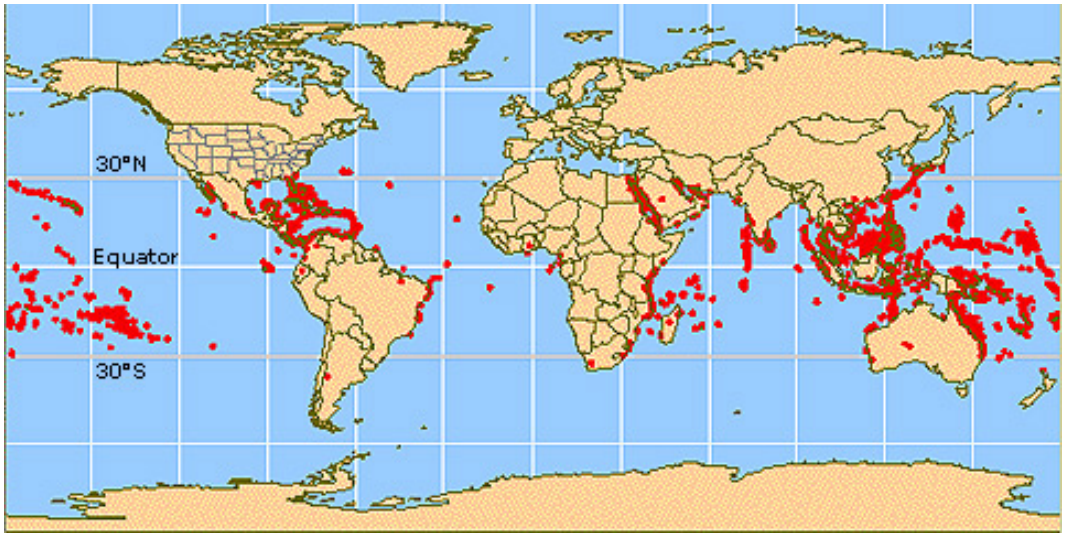

Fig. 2.4: Regions where reef building corals can be found. The red dots indicate the location of the major stony corals reefs of the world. (The picture has been taken from: http://www.nos.noaa.gov/education/corals/media/supp_coral05a.html).

Many scleractinian corals show significant growth bands, which may be compared to tree rings. Isotope (e.g. $\delta^{18}O$ or $\delta^{13}C$) or element studies (e.g. Sr/Ca) show that coral growth is seasonal and reflects changes in various parameters, like water temperature, wave stress, salinity and other factors (*Schellmann & Radtke, 2004*). This offers the possibility of (i) precise age estimation of young corals by growth band counting and (ii) reconstruction of several climate parameters (see chapter 3.2 for an extended discussion).

Coral reefs can be differentiated into several geomorphic units as types defined by their shape, size, and location in relationship to the coastline (e.g. fringing reefs, barrier reefs, platform reefs, atolls, and others). They can be further classified based on their position relative to sea-level, as for example drowned, shallow-water, or emerged reefs. In the Caribbean Sea, fringing reefs are the most common reef types (*Schellmann & Radtke, 2004*, see Fig. 2.5). However, reef development and the distribution of different coral species on the reef strongly depends on a complex interplay of local ecological factors.

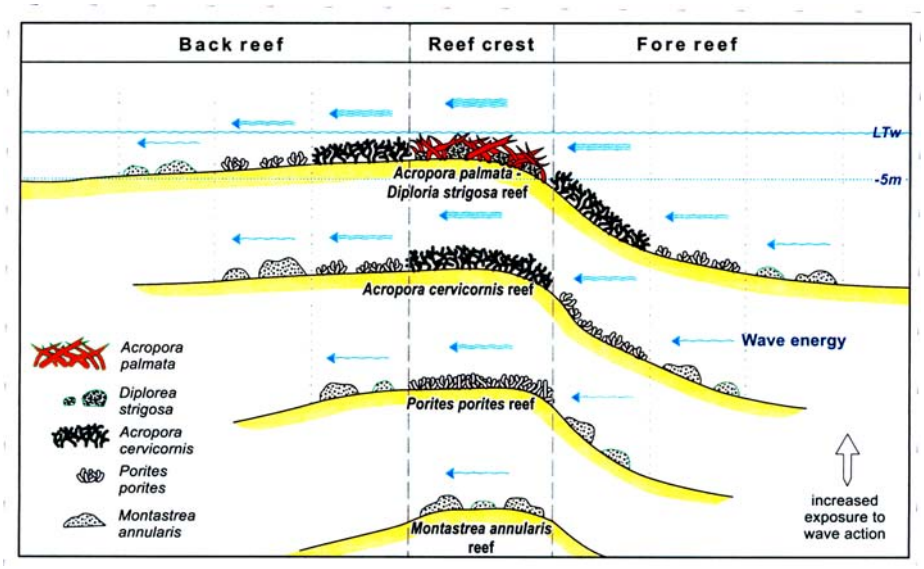

Fig. 2.5: The most common reef zones in the Caribbean are correlated with wave energy: (a) The *Acropora palmata* zone located in shallow water depths (up to 5 m) on the reef crest, (b) the *Acropora cervicornis* zone in deeper water (4-7 m in depth), and (c) the *Montastrea annularis* zone in depths up to 10 m. The picture has been taken from *Schellmann & Radtke* (*2004*).

In this work mainly three coral species have been investigated: *Porites sp.*, *Diploria strigosa*, and *Acropora palmata*, which is the most common shallow water coral species in the Caribbean. It is resistant to strong wave action and therefore grows on the upper reef crest (Fig. 2.5). It grows in water depths ranging from 5 m to low tide water levels (*Schellmann & Radtke, 2004*) and is therefore ideally suited for sea level reconstructions. The *Acropora palmata* grows rather fast and reaches growth rates of up to 15 cm/yr under optimal ecological conditions (*Bak, 1977*). Because of its characteristic form the *Acropora palmata* is also called the “elkhorn coral” (Fig. 2.6).

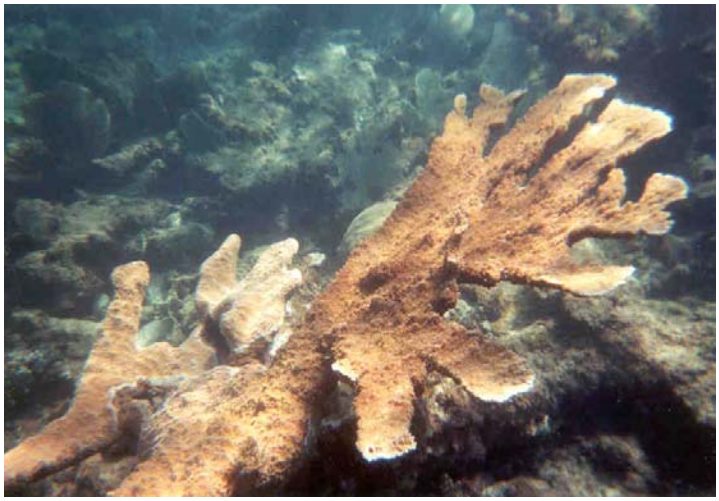

Fig. 2.6: Under water photography of an *Acropora palmata* coral. (Picture source: http://www.hsu.edu/faculty/engmanj/jamaica/acropalm.jpg)

The surface structure and body of *Diploria strigosa* look like a brain. Therefore, this coral is commonly called “brain coral”. It reaches more than 30 cm in thickness and up to 2 m in diameter. *Diploria strigosa* inhabits water depths ranging from 1 to 43 m below sea level, but due to its compact body, it withstands extreme wave action and is frequently found on reef crests in association with *Acropora palmata* (*Schellmann & Radtke, 2004*).

The *Porites sp.* (“finger coral”) can be easily identified by its morphology and short branches. The branches of *Porites sp.* can reach up to 2 cm in diameter. It is a reef forming coral that grows in dense colonies under calm surf conditions (Fig. 2.5), and it is relatively frequent in the Caribbean. It inhabits great water depths (up to 53 m) and cannot be used for sea level reconstructions in general (*Schellmann & Radtke, 2004*).

2.2.3 The incorporation of U-series isotopes into coral skeletons

There are three naturally occurring polymorphs of calcium carbonate ($CaCO_3$): calcite, aragonite, and vaterite which is very rare. While calcite has a trigonal symmetry, the symmetry of aragonite and vaterite is orthorhombic and hexagonal respectively. The most stable mineral of all three is calcite. Aragonite is metastable under normal surface temperatures and pressures, and it will convert to calcite with time. Nearly all hermatypic scleractinian corals secrete calcium carbonate as aragonite.

When coralline aragonite forms from surface seawater, there is potential to fractionate U, Th, and Pa isotopes. To date the U incorporation mechanism into coral skeletons is not completely understood. In seawater the dominant form of U is the large anion, uranyl carbonate ($UO_2(CO_3)_3^{4-}$), and with descending pH, the species $UO_2(CO_3)_3^{2-}$ and $UO_2(CO_3)_3^{0}$ prevail (*Shen & Dunbar, 1995*). There is a large difference between the U content of calcite, which ranges from 0.02 to 10 ppm in molluscs and can take even higher values in speleothems (*Holzkämper, 2004*), and aragonite (2–4 ppm). According to *Reeder et al.* (*2000*), U is less compatible in the rhombohedral conformation of calcite than in the orthorhombic form of aragonite. Most likely, this is because of the similar equatorial coordination of UO_2^{2+} in aragonite and $UO_2(CO_3)_3^{4-}$ (*Reeder et al., 2000*). This indicates that a change in UO_2^{2+} coordination is required for incorporation into calcite and that U is taken up by calcium carbonates as a large complex ion and not as a simple ion (U^{6+}, U^{4+}) (*Shen & Dunbar, 1995*). If this is the case, U/Ca ratios of corals would be influenced by the carbonate ion content of seawater. *Shen & Dunbar* (*1995*) compared several U substitution mechanisms and concluded - in agreement with *Swart & Hubbard* (*1982*) - the following reaction to be the likeliest in coral skeletogenesis:

$$CaCO_3 + UO_2(CO_3)_2^{2-} \leftrightarrow CaUO_2(CO_3)_2 + CO_3^{2-} \qquad (2.11)$$

Furthermore, a variety of studies have shown that U/Ca ratios of scleractinian corals are influenced by water temperature, as seasonal variations up to 20% have been identified (*Min et al., 1995; Shen & Dunbar, 1995*), absolute U concentration of seawater (and consequently seawater salinity, see chapter 2.2.1) (*Swart & Hubbard, 1982; Shen & Dunbar, 1995*), coral growth rate, and coral species (*Cross & Cross, 1983*). However, despite of these effects molar U/Ca ratios of surface corals are within about 30% of the seawater value of 1.3×10^{-6} (*Edwards et al., 2003*).

Fractionation between the different U isotopes (^{234}U and ^{238}U respectively) does not occur during coral growth. The distribution of δ^{234}U in the ocean is homogenous at an average of 149.6 ± 3 ‰ (1σ-error, n = 23 (*Delanghe et al., 2002*)). δ^{234}U values measured in modern corals average 146.6 ± 1.4 ‰ (1σ-error, n = 10 (*Delanghe et al., 2002*)) and are in good agreement with the seawater value within error.

Molar ^{232}Th/^{238}U values of young surface corals are typically a bit lower than seawater values, but within a factor of 3 of this value (*Chen et al., 1986; Edwards et al., 1986*). ^{231}Pa values for modern corals have not been measured directly because of their extremely low concentration, but there has been placed an upper limit of 5×10^{-10} on the initial molar ^{231}Pa/^{235}U ratio (*Edwards et al., 1997*). This value is in agreement with the limited number of surface seawater ^{231}Pa/^{235}U measurements (*Edwards et al., 2003*).

It turns out that U, Th, and Pa are not largely fractionated during aragonite formation (i.e. less than a factor of two), and are incorporated into the coral skeletons in approximately their proportions in seawater. Therefore the main fractionation leading to the close to zero initial (^{230}Th/^{238}U) and (^{231}Pa/^{235}U) activity ratios of scleractinian corals is that between solids and natural waters resulting from the different solubility of U and Th and Pa, respectively.

2.2.4 Testing the dating assumptions for fossil reef corals

The two basic assumptions of U-series dating are that (i) initial (^{230}Th/^{238}U) and (^{231}Pa/^{235}U) values are zero, and (ii) the system remains closed after deposition (see chapter 2.1.2). To evaluate the reliability of U-series ages of fossil reef corals, it is necessary to test if both assumptions are valid.

As discussed above, the first assumption is fulfilled for almost all reef building surface corals (chapter 2.2.3). This can be tested by U-series dating of corals with ages known a priori from counting of annual density bands (see chapter 3.2). Such age comparisons showed that initial ^{230}Th levels are negligible in corals containing less than 100 ppt ^{232}Th, which is the case for most reef building corals (*Edwards et al., 2003*), though there have been reported ^{232}Th concentrations between several hundred and 1000 ppt (*Cobb et al., 2003*) or even higher (*Stirling et al., 1998*). For corals older than several thousand years even values of this

magnitude are not likely to produce significant shifts in Th/U-ages, because the detrital ^{230}Th will be negligible compared to that produced by in situ decay of U. However, for very young corals (i.e. younger than several thousand years) high ^{232}Th content indicates the presence of significant levels of initial ^{230}Th and makes an appropriate correction necessary. To apply such a correction, knowledge of the initial (^{230}Th/^{232}Th) activity ratio is required. Investigation of samples with known age resulted in atomic ^{230}Th/^{232}Th ratios between 0 and 2×10^{-5} for marine and ~ 4×10^{-6} for terrestrial sources (*Cobb et al., 2003*). With these values upper and lower limits for the correction can be estimated. In the case of a very high ^{232}Th content, isochron methods can be used (see chapter 2.1.3).

To test the first assumption for ^{231}Pa is more difficult, because there is no long-lived isotope of Pa that can be used as an index isotope (*Edwards et al., 2003*). It has been shown that initial ^{231}Pa is negligible for surface corals with ^{232}Th content lower than 100 ppt (*Edwards et al., 1997*). Whether or not corals with elevated ^{232}Th require correction for initial ^{231}Pa is an open question (*Edwards et al., 2003*).

Testing the second (the closed-system) assumption is more complicated. During periods of low sea level (glacial and interstadial periods) most fossil reef corals have been exposed to meteoric waters for a substantial period of their depositional history. This bears the risk of the aragonitic coral skeletons to be recrystallised to the more stable polymorph of $CaCO_3$, calcite, by dissolution or reprecipitation processes (see *Matthews* (*1968*) and also chapter 2.2.3). As calcite is known to incorporate much less U than aragonite (*Reeder et al., 2000*), such processes are supposed to be associated with significant loss of U. The calcite content of fossil corals can be easily measured by X-ray diffraction.

In some corals also significant amounts of secondary aragonite or aragonite cements have been detected. *Bar-Matthews et al.* (*1993*) tried to correlate such petrologic changes which are an indication for open system behaviour with shifts in isotope ratios and U-series ages, but did not find any clear correlation. Other authors used minor element abundances like Sr and Mg to identify disturbed corals (*Amiel et al., 1973a; Cross & Cross, 1983*).

Another indication for open-system behaviour are elevated ^{232}Th concentrations. These need not necessarily result from initial incorporation during coral growth, but can also be produced by post-depositional isotopic change and contamination from detrital sources.

Information about possible open system behaviour can also be obtained by comparison of the total U content of fossil corals and their modern counterparts. A variety of studies on various coral species showed that primary surface coral U concentrations lie between 1.5 and 4 ppm (e.g. *Amiel et al., 1973b; Gvirtzman et al., 1973; Swart & Hubbard, 1982; Cross & Cross, 1983*). U/Ca ratios in scleractinian corals depend on many factors, such as temperature, U availability, and coral species (see chapter 2.2.3). Overall, even variations of several percent are possible in one and the same coral (*Min et al., 1995; Shen & Dunbar, 1995*). For

this reason, total U concentration can only serve as a broad indication for open system behaviour, but not as a strict criterion for dating reliability.

Stony corals incorporate ^{234}U and ^{238}U exactly in the ratio as they occur in modern seawater ($\delta^{234}U_{seawater}$ = 149.6 ± 3 ‰, see chapter 2.2.4). If the coral behaves as a closed system after growth, the timely development of the activity ratios can be calculated from equations (2.5) and (2.6). This can be clearly illustrated on a plot of $\delta^{234}U$ vs. ($^{230}Th/^{238}U$) (Fig. 2.7). Equivalently, the initial $\delta^{234}U$ value can be calculated by inserting the coral age into equation (2.5).

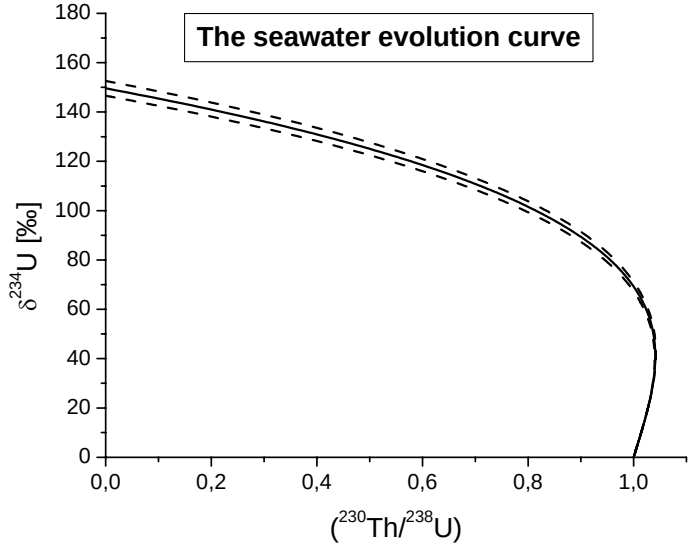

Fig. 2.7: The development of the activity ratios with time with an initial $\delta^{234}U$ value of 149.6‰ (modern seawater). The dashed lines indicate the uncertainty of this value (3 ‰). In the following this curve will be referred to as the *seawater evolution curve*.

In the earliest studies the activity ratios were measured by α-counting techniques (e.g. *Barnes et al., 1956; Broecker, 1963; Mesolella et al., 1969*). These studies demonstrated the general possibility to apply U-series dating methods to reef-building corals and to use the results for paleoclimate reconstructions. With increasing instrumental precision, it was recognized that $\delta^{234}U_{initial}$ varies significantly between different corals and that, in general, higher $\delta^{234}U_{initial}$ values correspond to higher ages (*Bender et al., 1979*). With the development of thermal ionisation mass spectrometry (TIMS, see Appendix A) the analytical precision again improved by several orders of magnitude (*Edwards et al., 1986*), revealing that most fossil reef corals display $\delta^{234}U_{initial}$ values in excess of modern seawater and recent corals (e.g. *Edwards et al., 1987; Ku et al., 1990; Bard et al., 1991; Henderson et al., 1993*). This phenomenon is shown in Fig. 2.8.

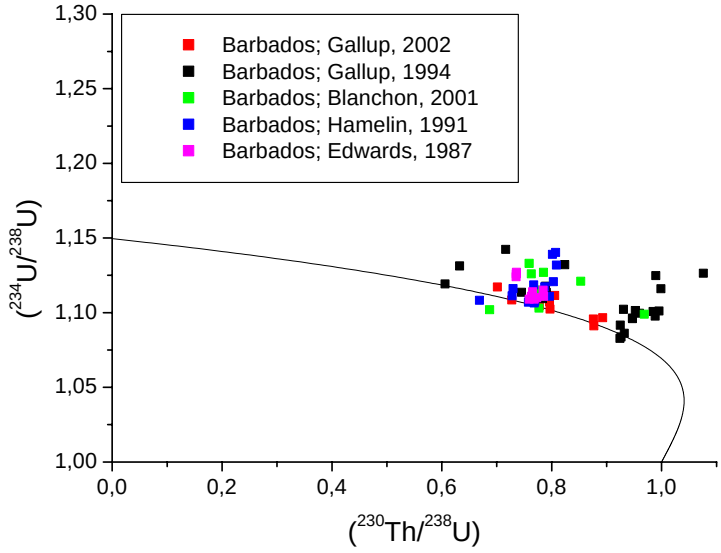

Fig. 2.8: A compilation of the activity ratios measured on fossil reef corals from Barbados, West Indies. The error bars are smaller than the plotted symbols. All corals are of the genus *Acropora palmata*. It is evident that most corals show significantly elevated initial ($^{234}U/^{238}U$) activity ratios.

The question is: Do these variations reflect changes in the marine U isotopic composition or do they represent open system behaviour of fossil corals?

Several workers have used models to place limits on how much the marine $\delta^{234}U$ value could have changed over Late Quaternary time scales (e.g. *Chen et al., 1986; Edwards, 1988; Hamelin et al., 1991; Richter & Turekian, 1993*). All studies agree that large and long-lasting variations in the activity ratios of the earth's major rivers would be necessary to produce changes of large magnitude and that $\delta^{234}U_{seawater}$ should not have changed more than 10-20 ‰ compared to its modern value during the last several hundred thousand years. This is further confirmed by U-series dating of U-rich slope sediments from the Bahamas suggesting that $\delta^{234}U_{seawater}$ has remained within 15‰ of the modern value for the last 360 kyr (*Henderson, 2002*). Unfortunately, the scatter of the older data of this study is rather large, but there is no indication of a trend in seawater $\delta^{234}U$ with age. Even if there were significant variations of past $\delta^{234}U_{seawater}$, corals which behaved as closed systems should reproduce these values. But even coeval corals from one and the same reef display large differences in $\delta^{234}U_{initial}$ and not one uniform value. The fact that even apparently pristine samples show elevated $\delta^{234}U_{initial}$ values suggests that the isotopic systems are more sensitive to isotopic change than is any petrographic or general geochemical parameter (*Chen et al., 1991; Zhu et al., 1993*). Therefore the established opinion is that the premise of closed systems behaviour is not generally warranted for fossil reef building corals, and the accuracy of U-series ages is more limited due to these isotopic anomalies than to analytical precision (*Bard et al., 1992; Stirling et al., 1995*). Today, these isotopic anomalies of fossil reef corals are denoted by the term *diagenetic alterations*. Originally, the term *diagenesis* stands for "physical, chemical, and

biological changes occurring in sediments during and after the period of initial deposition, including lithification, but excluding surficial alteration (weathering) and metamorphism" (*Geyh & Schleicher, 1990*). This traces back to the time when geochronologists thought that the isotopic anomalies would result from mineralogical or petrological effects. It must be emphasized that the processes which produce *diagenetical alterations* in fossil reef corals are not satisfyingly understood.

Therefore, various reliability criteria for U-series ages of fossil reef corals have been developed (e.g. *Stirling et al., 1998; Muhs et al., 2002*):

a) $\delta^{234}U_{initial}$ lying within the strict range of 149 ± 4 ‰
b) ^{238}U concentration lying within the range of modern analogues from the same region
c) ^{232}Th concentrations lower than 1 ppb
d) Less than 1% calcite
e) Primary aragonitic textures

Only U-series ages that fulfil all these requirements are believed to be strictly reliable and can be used for paleoclimate reconstructions.

Perhaps the most rigorous test for open system behaviour is combined ^{231}Pa and ^{230}Th dating (*Edwards et al., 2003*). By the application of both dating methods to the same coral sample it is possible to identify isotopically altered corals which would have passed all the above listed tests. Recent measurements on some corals from Barbados, West Indies (*Gallup et al., 2002; Cutler et al., 2003*), showed that of 14 corals all with $\delta^{234}U_{initial}$ values within 8‰ of the modern seawater value, 6 had discordant ^{231}Pa and ^{230}Th ages, demonstrating without ambiguity, processes that have affected Pa, Th, and/or U, but not $\delta^{234}U$ (*Edwards et al., 2003*). Apart from detecting disturbed samples, combined ^{231}Pa and ^{230}Th dating provides additional information about the processes that produce elevated $\delta^{234}U_{initial}$ values in fossil reef corals (see the extended discussion in the next chapter). Because mass spectrometric ^{231}Pa techniques are still rather new, to date there is still limited data of this sort (*Edwards et al., 1997; Gallup et al., 2002; Cutler et al., 2003*), but in coming years, ^{231}Pa measurements will play a major role in assessing the accuracy of ^{230}Th-based chronologies (*Edwards et al., 2003*).

2.2.5 Modelling diagenetic effects in fossil reef corals

To explain the isotopic anomalies in fossil reef corals several authors have proposed diagenetic scenarios, like U, Th, and Pa gain and loss as well as various combinations of those (e.g. *Chen et al., 1991; Hamelin et al., 1991; Bar-Matthews et al., 1993; Henderson et al., 1993; Fruijtier et al., 2000*). Fig. 2.9 illustrates the general effects of these processes on a (^{234}U/^{238}U)-(^{230}Th/^{238}U)-plot.

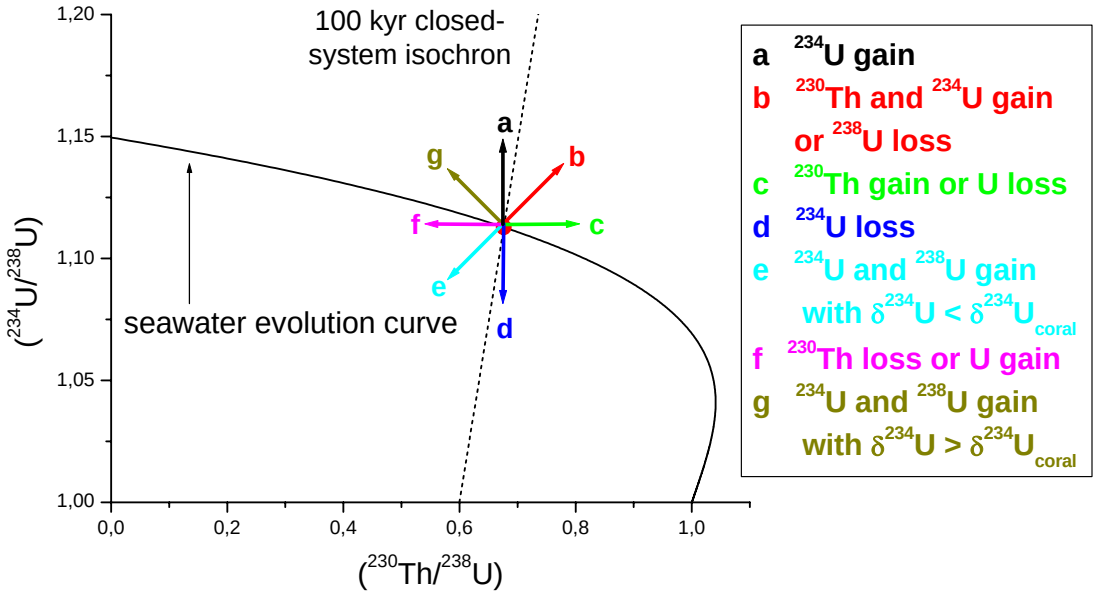

Fig. 2.9: The effect of different diagenetic processes on the coral isotopic composition. The intersection point of all arrows corresponds to a coral which has behaved as a closed system for 100 kyr. Different diagenetic processes are indicated by different arrow colours. The straight curve is the seawater evolution curve. The dotted line is the 100 kyr closed-system isochron which indicates all combinations of (^{230}Th/^{238}U) and (^{234}U/^{238}U) activity ratios yielding a Th/U-age of 100 kyr. Diagenetic processes which shift the activity ratios to the right of this straight line produce apparent "older" coral ages, the others produce apparent "younger" coral ages.

It must be emphasized that Fig. 2.9 is rather illustrative. The exact effect of all shown processes strongly depends on the timing (direct after coral growth or later), duration (episodic or continuous), frequency, magnitude, and – for all processes where two or more isotopes are involved – on the ratio of the added or lost isotopes (see also the discussion in the above mentioned references). It also must be considered that two or more processes happen simultaneously or one after another. Nevertheless, this schematic diagram allows to divide the processes into different groups. These groups are shown in Table 2.1:

Group	Effect on coral age	Effect on coral $\delta^{234}U$	Processes
1	older	higher	b, c
2	older	lower	d
3	younger	higher	a, g
4	younger	lower	e, f

Table 2.1: Classification of the diagenetic processes by their effect on coral age and $\delta^{234}U$.

In general, the most diagenetically altered fossil reef corals show elevated $\delta^{234}U_{initial}$ values, suggesting one of the processes of groups 1 and 3. Many authors detected some correlation between elevated measured $\delta^{234}U$ values and Th/U-age (*Stein et al., 1993; Zhu et al., 1993; Fruijtier et al., 2000*) as well as ($^{230}Th/^{238}U$) activity ratio (*Gallup et al., 1994; Stirling et al., 1998; Thompson et al., 2003; Villemant & Feuillet, 2003*). According to Fig. 2.9, this would be an indication for a process belonging to group 1, although it needs to be emphasized that in other studies no general correlations have been found (*Chen et al., 1991*). While process c produces only slightly elevated $\delta^{234}U$ values (see the discussion in *Hamelin et al.* (*1991*)), the development of the activity ratios in scenario b strongly depends on the ratio of the ^{234}U and ^{230}Th added.

Bender et al. (*1979*) were the first who presented a diagenetic open system model for fossil reef corals. They applied combined Th/U- and ^{4}He/U-dating to some *Acropora palmata* samples from Barbados, West Indies, and found that all corals older than 150 kyr had excess ^{230}Th and all samples older than 250 kyr had excess ^{234}U. Therefore they assumed that all their corals suffered continuous ^{234}U and ^{230}Th addition (according to scenario b in Fig. 2.9). *Ku et al.* (*1990*) proposed a model which takes into account gain or loss of both ^{234}U and ^{238}U through continuous exchange with U in ground or soil water.

Subsequently, *Gallup et al.* (*1994*) documented a rough correlation between initial $\delta^{234}U$ values and Th/U-ages by extensive dating of Barbados corals. On the basis of the observed trend on a ($^{234}U/^{238}U$)-($^{230}Th/^{238}U$)-plot, they modelled the diagenetic processes affecting these corals assuming continuous addition of ^{234}U and ^{230}Th. While they allowed different rates of addition to different coral samples, they assumed the $(^{230}Th/^{234}U)_{additional}$ ratio to be constant. In fact, this ratio was chosen so that the model reproduced the isotopic composition of an altered coral whose age was known by ^{4}He/U-dating from the previous study by *Bender et al.* (*1979*). They derived an age equation that describes the isotopic composition resulting from adding ^{234}U and ^{230}Th in a fixed ratio and to varying degrees to samples of a given true age. This results in so-called “addition lines” on a ($^{234}U/^{238}U$)-($^{230}Th/^{238}U$)-plot (Fig. 2.9) which followed the trends in their data, suggesting that the addition is broadly continuous and that ^{234}U and ^{230}Th are added in atomic proportions of 0.71. This ratio of addition corresponds to an increase of the ^{230}Th age of 1 kyr for every 4‰ rise in initial $\delta^{234}U$ and provided a semi-quantitative criterion for reliable Th/U-ages for corals that have similar trends in isotopic

composition. Because the data scattered about the addition lines, *Gallup et al.* (*1994*) did not attempt to use their model to correct the Th/U-ages of their samples. In the following, the *Gallup et al.* (*1994*) model (i.e. the reliability criterion based on it) has been used for corals from many areas, including the Western Atlantic (e.g. *Blanchon & Eisenhauer, 2001*), the Western Pacific (e.g. *Stirling et al., 1995; Stirling et al., 1998; Esat et al., 1999*), and the Eastern Pacific (e.g. *Szabo et al., 1994; Stirling et al., 2001*). However, there are two serious problems with this model:

a) When there are a limited number of coeval samples, it is difficult to show that the diagenetic trends are such as described by the model, or even worse, in some cases, such as in Papua New Guinea, corals do not seem to show the same diagenetic trends (*Edwards et al., 2003*).
b) As mentioned by the authors themselves, it is surprising that ^{234}U and ^{230}Th should be added at similar rates, because of their very different chemical behaviour (see chapters 2.1.1 and 2.2.1). In theory, the redistribution of the isotopes should rely on transport by ground- or porewaters, but the model results suggest that the different solubilities of U and Th do not play a significant role in how they are transported and deposited. For this reason, *Gallup et al.* (*1994*) proposed that the nuclides may be transported on particles in the water, such as organic colloids.

Many authors have proposed mechanisms to give an explanation for the second problem. *Chen et al.* (*1991*) suggested that some ^{238}U, ^{234}U, and ^{230}Th may be leached out of one part of the coral by chemical reactions and deposited onto another part. As a mechanism for ^{234}U addition they proposed that ^{234}Th, which is the recoil daughter nuclide of ^{238}U (see Fig. 2.1), is likely to be hydrolysed and adsorbed onto a solid surface before decaying to ^{234}U. *Bar-Matthews et al.* (*1993*) argued that such a model would require very large amounts of aragonite dissolution and considered it to be highly speculative. *Fruijtier et al.* (*2000*) also provided two speculative scenarios of adding both ^{234}U and ^{230}Th to fossil corals in near equimolar amounts and at the same time highlighted the difficulties in finding a plausible mechanism. The proposed processes again consider particle reactive ^{234}Th to be involved in producing elevated $\delta^{234}U$ values, but in contrast to *Chen et al.* (*1991*) they suggest direct ejection of daughter nuclides from the aragonitic structure by α-recoil (see chapter 2.1.1). An important aspect of these processes is that they would not leave any obvious chemical or petrographic signature, unlike U loss, that might be expected to be more evident from dissolution features (*Fruijtier et al., 2000*).

Recently, two models dealing with open system behaviour of fossil reef corals have been published (*Thompson et al., 2003; Villemant & Feuillet, 2003*). These models pick up one of the mechanisms suggested by *Fruijtier et al.* (*2000*) and are an extension of a similar idea proposed by *Henderson & Slowey* (*2001*) in the context of U-series dating of carbonate bank sediments. *Villemant & Feuillet's* (*2003*) model takes into account possible initial ^{230}Th excess (see chapters 2.1.3 and 2.2.4 for an extended discussion of this assumption) and continuous selective redistribution (gain or loss) of ^{234}U, ^{234}Th, and ^{230}Th that is controlled by α-recoil processes. The model of *Thompson et al.* (*2003*) explains the positive correlation between measured (^{234}U/^{238}U) and (^{230}Th/^{238}U) activity ratios by coupled addition of particle-reactive ^{234}Th and ^{230}Th, which is produced by decay of dissolved U and α-recoil mobilisation of U daughters. In contrast to *Gallup et al.* (*1994*), the authors of both models suggest that their models can be used to correct ages of samples with non-marine δ^{234}U, and term these ages "open-system ages". As both models assume the same redistribution mechanisms except for very slight differences, the slopes of the resulting "addition-lines" as well as the calculated "open-system ages" are rather similar. However, the trends observed at different localities worldwide are not the same, an in general, the data points from a given terrace are not all co-linear within analytical error, as required for an exact age correction using either the *Gallup et al.* (*1994*) or one of these models (*Edwards et al., 2003*). Thus, an age correction with these models should only be performed (i) in localities where trends can be demonstrated to be particularly robust and (ii) for scientific problems that allow significant error in age (*Edwards et al., 2003*). A further problem with the α-recoil based models is that impossibly large volumes of carbonate are needed to maintain the dissolved U concentrations required to produce the isotopic anomalies observed in most fossil reef corals (*Thompson et al., 2003*).

All the diagenetic processes discussed above (Fig. 2.9 and Table 2.1) can also be modelled for the U-Th-Pa system (*Edwards et al., 1997; Cheng et al., 1998; Edwards et al., 2003*). The effects of these scenarios can be clearly demonstrated on so-called concordia diagrams (Fig. 2.10, see next page).

Cheng et al. (*1998*) presented a general solution of a model for continuous ^{234}U, ^{230}Th, and ^{231}Pa input together with continuous loss or gain of U and illustrated the effects of these scenarios on concordia diagrams. In the same study it has been shown that, if a suite of coeval samples which experienced different degrees of the same diagenetic process, the data will plot along a straight line or a curve which is very close to that in a concordia diagram. The intersection point of this straight line with the closed system curve then represents the 'true' age of the sample (*Cheng et al., 1998*).

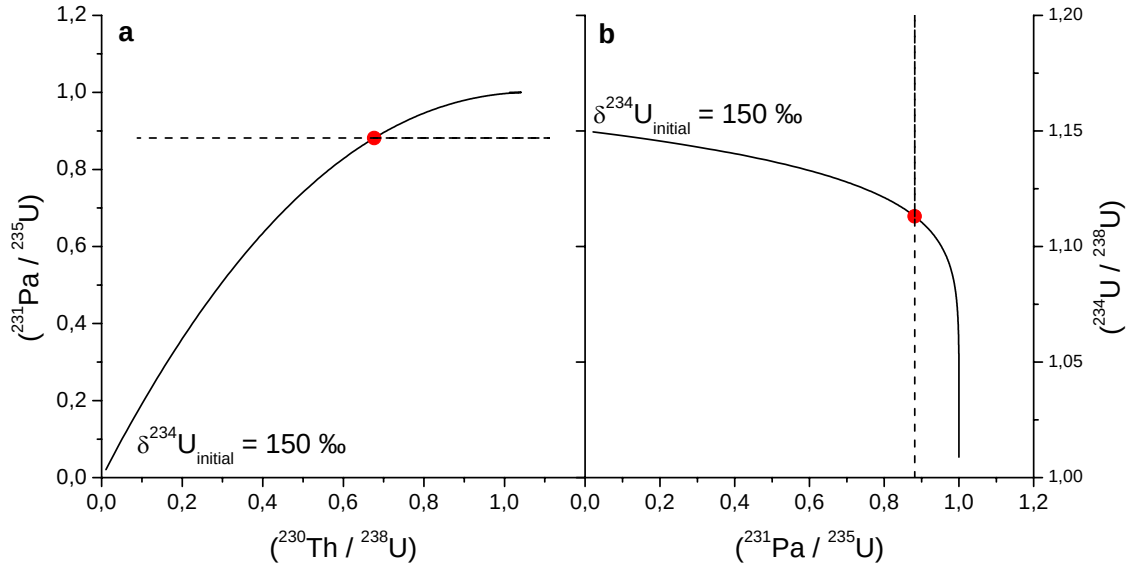

Fig. 2.10: Concordia diagrams for the U-Th-Pa system. The straight lines show the timely development of the (^{230}Th/^{238}U), (^{234}U/^{238}U), and (^{231}Pa/^{235}U) activity ratios with an initial (^{234}U/^{238}U) activity ratio of 1.1496 (modern seawater). The red circle indicates a coral which has behaved as a closed system for 100 kyr. The dashed lines indicate the 100-kyr-closed-system isochrons. The different diagenetic processes have the following effects on such plots:
Plot a: Samples that lost U relativ to both ^{230}Th and ^{231}Pa (and equivalently samples that gained both ^{230}Th and ^{231}Pa relative to U) plot above concordia, samples that gained U relativ to both ^{230}Th and ^{231}Pa (and equivalently samples that lost both ^{230}Th and ^{231}Pa relative to U) plot below concordia.
Plot b: Points that lie to the right of the concordia indicate U loss or gain of both ^{230}Th and ^{231}Pa. Points that lie to the left indicate U gain or loss of both ^{230}Th and ^{231}Pa.

The α-recoil models proposed by *Thompson et al.* (*2003*) and *Villemant & Feuillet* (*2003*) would affect the Pa/U-system in a similar way as Th/U, because there is also a particle-reactive short-lived daughter nuclide for ^{235}U, ^{231}Th (see Fig. 2.1). Consequently, ^{231}Pa should be redistributed in almost the same manner as ^{230}Th and ^{234}U. This would produce activity ratios which plot above concordia in the respective diagrams (Fig. 2.10). Older samples from the Huon Peninsula, Papua New Guinea, plot on concordia, above concordia, and below concordia (*Cutler et al., 2003*). Thus, diagenetic processes affecting the Huon Peninsula samples appear to be more complex than for other locations (e.g. Barbados) and cannot have been produced by these models.

After all, despite of more than 30 years of intensive examination of the U-series systematics in fossil reef corals, a number of aspects that produce increased $\delta^{234}U_{initial}$ values have not been satisfactorily explained so far. Thus, it has not been possible to develop a general correction technique for diagenetically altered fossil reef corals, although a variety of approaches have been proposed.

3 The application of fossil reef corals as paleoclimate archives

3.1 Reconstruction of past sea level fluctuations

The Quaternary is characterized by periodic changes between global stages of cold and warm climate, respectively. While the cold periods are denoted as Glacials, the phases of warm climate are named Interglacials. These phases correspond to stages of globally low and high sea level, respectively, due to storage of large ice volumes in high latitudes. There have been several methods of sea level reconstruction established, with each of them being associated with its assets and drawbacks.

3.1.1 The utilization of stable isotopes measured in deep sea sediments

Oxygen isotopes are a common tool to identify climate variations in paleoclimate archives. Stable isotope ratios are usually expressed in the δ-notation, i.e. the deviation of the isotopic ratio of the analysed sample relative to that of a standard:

$$\delta^{18}O = \left[\frac{\left({}^{18}O/{}^{16}O\right)_{sample}}{\left({}^{18}O/{}^{16}O\right)_{standard}} - 1 \right] \cdot 1000 \qquad [‰] \qquad (3.1)$$

The $^{18}O/^{16}O$ isotope ratio measured on snow accumulated on ice caps is depleted in heavy oxygen relative to ocean water by ~40 ‰. This depletion is created because the water which condenses to form precipitation in a cooling air mass is enriched in the heavier isotope, ^{18}O, while the residual vapour will correspondingly be enriched in the light isotope, ^{16}O. This yields the air masses that reach the cold regions of the ice caps being progressively depleted in the heavy isotopes. If large ice volumes are stored on the continents (with very low $\delta^{18}O$ values), the $\delta^{18}O$ value of sea water will accordingly be slightly higher than at times with less global ice volume. Roughly estimated, a sea level rise of about 120 m will produce a $\delta^{18}O$-enrichment of 1.26 ‰ in the ocean (*Broecker, 1995*). These changes in ocean $\delta^{18}O$ are

recorded in the carbonate shells of foraminifera found in deep sea sediments. Consequently, the oxygen isotope ratio of these shells provides potential information about global ice volume and sea level change, respectively. The observed stable isotope variations provide the basis for the division of the climate record into so-called *Marine Isotope Stages (MIS)*. In this terminology, uneven numbers denote relatively warm phases (e.g. MIS 5 stands for the Last Interglacial), while the cold phases (Glacials) are labelled by even numbers (Fig. 3.1). The Glacials as well as the Interglacials are again subdivided into periods of cooler and warmer climate, respectively. These sea level oscillations of smaller magnitude are denoted as Stadials and Interstadials, respectively, and are labelled by additional letters (Fig. 3.1). Sometimes they are also referred to as Substages.

However, the utilization of the $\delta^{18}O$ signal from deep sea cores for sea level reconstructions is difficult, because $\delta^{18}O$ is not uniformly distributed in the oceans. Additionally, the isotope signal recorded in foraminifera is also largely influenced by the temperature of carbonate precipitation, as a cooling of 1 degree Celcius will produce an increase of 0.23 ‰ in $\delta^{18}O$. Thus, the temperature effect also makes a significant contribution to the heavier isotopic signal during glacial times. Both problems can be avoided to some extent by relying on the record kept by the shells of benthic foraminifera, which live on the sea floor, because (i) the $\delta^{18}O$ content of deep sea waters is far more homogenous than that of surface water, and (ii) the deep sea at polar regions could not have been much colder during glacial time than today minimizing the effect of deep water cooling. Nevertheless, it has been shown that disturbances by the temperature effect cannot be completely avoided (*Broecker, 1995*). Consequently, additional information is needed to untangle the temperature from the ice volume component to reconstruct sea level with the $\delta^{18}O$ signal from deep sea cores.

Further difficulties arise from the dating of deep-sea sediment cores. Beyond the ^{14}C-dating range of ~40,000 yr most $\delta^{18}O$-records are so-called “astronomically” or “orbitally tuned”. This method relies on the *Milankovitch theory of climate change*, which says that the change between Glacials and Interglacials is primarily driven by variations in the total summer insolation received in northern latitudes where major ice sheets have formed in the past, near 65° north (*Milankovitch, 1941*). These variations are caused by changes in orbital parameters, namely in the precession of the equinoxes, in the eccentricity of the earth’s orbit, and in the earth’s tilt, which occur on periods of 19 and 23 kyr/cycle, 413 and 100 kyr/cycle, and 41 kyr/cycle, respectively. As these periodicities can also be identified in the $\delta^{18}O$ records of deep-sea sediments, the extracted signals can be used to “tune” the sedimentary to the astronomical record. Based on this dating method the SPECMAP chronology (*Imbrie et al., 1984*) has been set up (Fig. 3.1).

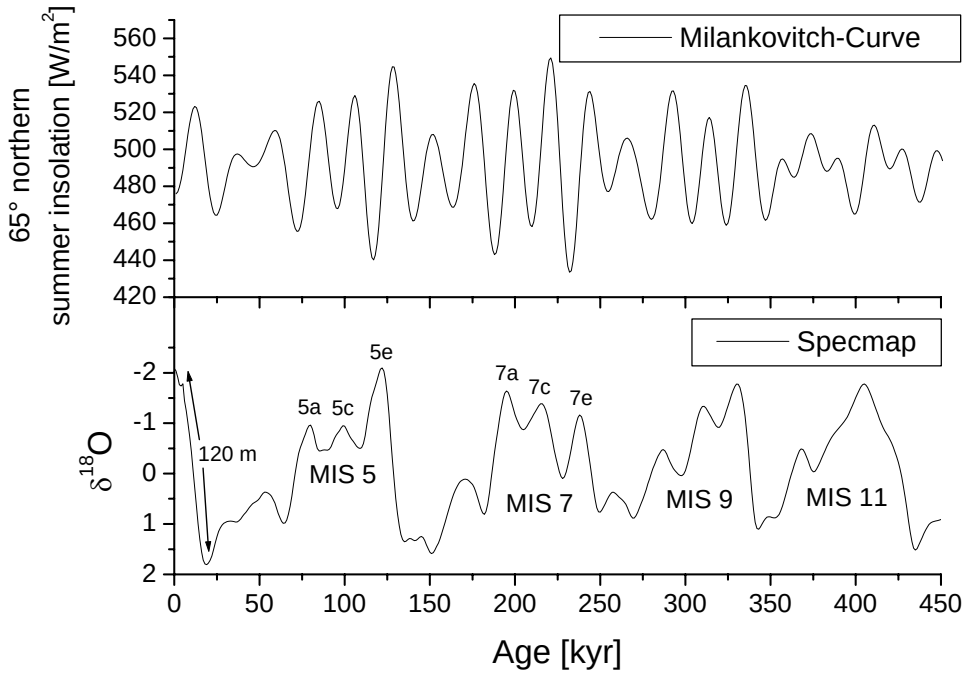

Fig. 3.1: (Upper part) Variations in 65° northern summer insolation as calculated by *Berger & Loutre* (*1991*). The signal is composed of the timely variations in eccentricity, obliquity, and precession. (Lower part) The SPECMAP curve, which has been dated by locking the phase of the observed cycles to an orbital template (*Imbrie et al., 1984*). Periods of high sea level are indicated by low $\delta^{18}O$ values (the scale of the y-axis has been inverted) and conversely. The magnitude of sea level change between Glacials and Interglacials is about 120 m. The last four Interglacials (Marine Isotope Stages (MIS) 5, 7, 9, and 11) can be easily identified in the $\delta^{18}O$-signal. The labels above the peaks denote Interstadials or Substages, respectively.

To date, the most deep-sea records are dated by matching their $\delta^{18}O$-signal with the SPECMAP curve. As the theory of orbital tuning presupposes that the variations of $\delta^{18}O$ are the result of insolation changes, it is obvious that the reliability of the assigned ages strongly depends on the validity of this assumption. Though the Milankovitch theory is adequate to explain the long term sea level fluctuations, absolute dates have shown that it is not sufficient to explain all features of past climate. For example, there have been several studies which suggest that the beginning of the Last Interglacial (MIS 5) was between 132 and 135 kyr (e.g. *Winograd et al., 1992; Henderson & Slowey, 2000; Gallup et al., 2002*), while the SPECMAP chronology suggests that MIS 5 did not start before 128 kyr, raising the question what initiated the termination of the penultimate Glacial.

3.1.2 The utilization of the height/age relationship of fossil reef corals

It has been described in chapter 2.2.2 that there are some coral genera that are generally found on the reef crest (i.e. the highest position relative to sea level (Figs. 2.5 and 3.2)) and that inhabit water depths not greater than 5 m (e.g. *Acropora palmata*). As such corals grow considerably fast, they have the possibility to follow even rapid sea level rises. Therefore, these species are ideally suited to document past sea level changes.

To describe the development of a coral reef under conditions of successively varying sea level, generally two different situations must be considered: (i) tectonically stable conditions and (ii) locations that are subject to significant tectonic movement.

Locations that are far from the margins of tectonic plates can be considered as tectonically stable, at least in the time interval of interest (i.e. two or three Glacial cycles). Such locations are for example western and eastern Australia, Hawaii, the Bahamas, or Bermuda. At such locations the reef structure will develop as illustrated in Fig. 3.2:

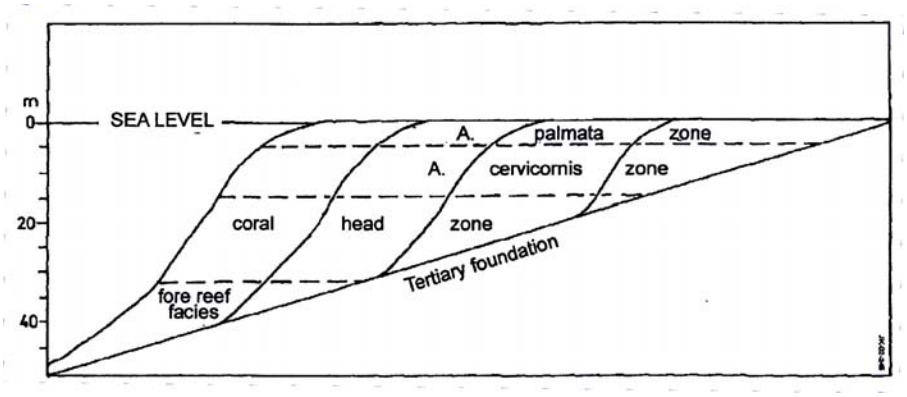

Fig. 3.2: Reef development under conditions of relative tectonic stability. It is assumed that all successive past sea level highstands had the same magnitude. This results in a seaward migration of the reef, forming one single terrace with a reef-crest community "pavement" (in this case consisting of corals of the genus *Acropora palmata*). The drawing has been taken from *Schellmann & Radtke* (*2004*).

If the age of an *in situ* (i.e. still in its natural growth position) reef-crest community coral can be determined at a tectonically stable site, the only uncertainty in the estimation of sea level at the time of coral growth arises from the uncertainty in the living depth, which is also referred to as the *paleodepth* sometimes (e.g. *Cabioch & Ayliffe, 2001*). As mentioned above, it can be shown that the paleodepth varies between 0 and 5 m only for specific coral genera. Unfortunately, there are two major drawbacks associated with sea level reconstructions at tectonically stable locations. Firstly, all corals that grew in periods with lower sea level than today are located below present sea level. As we are living in a period of warm climate and accordingly high sea level (MIS 1/*Holocene*, see Fig. 3.1), this is the case for almost all corals

except for those that grew during previous Interglacials. Therefore, it is very difficult to sample such corals. Even worse, it is evident from Fig. 3.2 that the reefs corresponding to the older sea level maxima will be overlain by the younger ones, which makes sampling of the older reefs almost impossible.

For this reason, it could be established from several stable sites that sea level during MIS 5 was about 3 to 6 m higher than today (*Broecker, 1995*), but the investigation of past sea level fluctuations was not possible. The only way to obtain corals from submerged reefs is by off shore borings. For the first time, this method has been successfully applied off the coast of Barbados, West Indies, where *Acropora palmata* sequences that documented the sea level rise from the Last Glacial Maximum till today could be obtained (*Fairbanks, 1989*). By U-series dating of these corals (*Bard et al., 1990b*) it could be established that the sea level difference between peak Glacial and today was about 120 m (Fig. 3.1). Subsequently, several authors have undertaken such drillings which confirmed the magnitude as well as the timing of the post-glacial sea level rise (e.g. *Chappell & Polach, 1991; Edwards et al., 1993; Bard et al., 1996; Cutler et al., 2003*).

At localities that are subject to significant tectonic movement during the time interval of interest (e.g. Barbados, Papua New Guinea, or Haiti) the development of the reef structure will be as shown in Fig. 3.3:

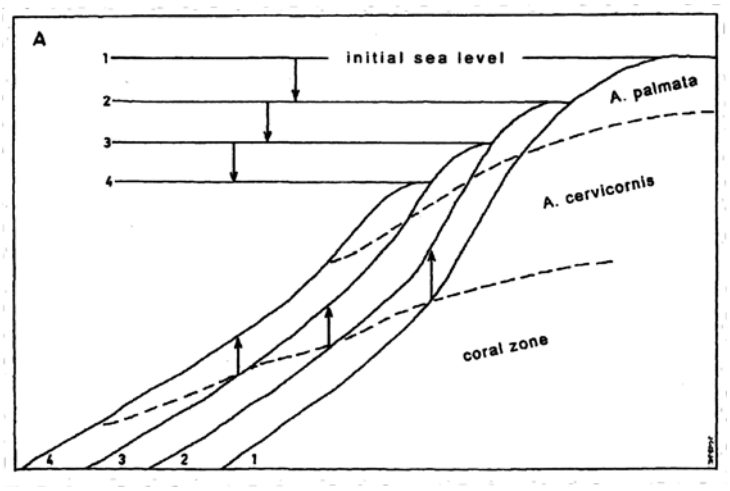

Fig. 3.3: Reef development under conditions of constant tectonic uplift. It is assumed that all successive past sea level highstands had the same magnitude. This results in a characteristic terrace structure which can be found at various locations worldwide, with each terrace corresponding to a past sea level highstand. The oldest terraces will have the highest elevation. In the case of a higher uplift rate the *Acropora palmata* zone will be interrupted by a fore reef species like *Acropora cervicornis* instead of being continuous. The drawing has been taken from *Schellmann & Radtke* (*2004*).

In the case of a rather large uplift rate, terraces corresponding to past sea level maxima will not only be located above present sea level, but also will not be overlain by the subsequent terraces. Consequently, each terrace represents an individual past sea level highstand corresponding to an Interglacial or Interstadial. At locations with very high uplift rate, like the Huon Peninsula, Papua New Guinea, even sea level oscillations of small magnitude can be identified (*Chappell, 2002*). If *in situ* corals from reef-crest communities can be collected, the magnitude of past sea level can be calculated using the following formula:

$$S = H - (U \times T), \tag{3.2}$$

where S is the paleo sea level relative to present [m], H is the actual height of the coral reef terrace relative to present sea level [m], R is the rate of tectonic uplift [m/kyr], and T is the age of the coral [kyr].

Some authors also include the paleodepth P [m] in their estimation (e.g. *Cabioch & Ayliffe, 2001*):

$$S = (H + P) - (U \times T) \tag{3.3}$$

It is evident from equations (3.2) and (3.3) that the advantage of the separation of individual sea level oscillations which is produced by tectonic uplift is at least partly compensated by the additional uncertainty which arises from the estimation of the uplift rate.

Usually, the uplift rate is assumed to be continuous and is estimated by the use of so-called reference horizons for which the paleo sea level is known. Often, the MIS 5e sea level highstand is used as a reference horizon, because its paleo sea level has been accurately established at stable sites. If the age and actual height of the reference horizon at the tectonically unstable sight can be determined, a mean uplift rate can be calculated with equation (3.2) or (3.3). One of the main criticisms of paleo sea level reconstructions using elevated coral reef terraces is that the uplift rate is generally assumed to be continuous. In fact, it has been shown by several authors that this assumption is not necessarily true on timescales of thousands of years, possibly due to the combination of coseismic uplifts followed by periods of interseismic subsidence. Nevertheless, the variations over short periods can be considered to be continuous over long periods, because the long term uplift rate should be an average of the short term variations (*Cabioch & Ayliffe, 2001*). However, to avoid mistakes in the estimation of the uplift rate generally at least two reference horizons with accurately known paleo sea levels should be used.

This method of sea level reconstruction has firstly been applied in the late 1960's on the Caribbean island of Barbados, West Indies, and the results strongly supported the theory that sea level followed the Milankovitch cycles (*Broecker et al., 1968; Mesolella et al., 1969*). Since then, numerous authors have investigated the degree to which this relationship holds and the details of this relationship by U-series dating of uplifted fossil reef coral terraces.

At tectonically stable as well as unstable sites relative sea level change reflects variations in global ice volume as well as the response of the Earth to changes in surface loading in the form of surface deformation and geoid changes, or glacio-hydro-isostasy. As past sea levels are measured relative to present-day sea levels, they are a function of the isostatic state of the Earth at that time relative to the present day isostatic state. These effects can produce apparent discrepancies in the estimates of relative sea level for a given event at different locations. This has been demonstrated very nicely for the Marine Isotope Substage 5a by *Potter & Lambeck* (*2003*).

3.1.3 The utilization of submerged speleothems

While fossil reef corals mainly provide information about periods of sea level rise or maximum, speleothems found below present sea level can be used as a complimentary evidence about the timing and elevation of *low* past sea levels (*Richards & Dorale, 2003*). This is because speleothems can of course only have formed when the caves were air-filled and not submerged. Thus, the growth phases of submerged speleothems do not provide direct information of the magnitude of past sea level, but rather such as "sea level was not higher than". Conversely, hiatuses (i.e. periods during those no speleothem growth occurred) are evidence for periods of higher sea level. To date, there have been several studies on submerged speleothems which provided constraints for the timing of the Interglacials (MIS 7, 5, and 1) as well as the maximum elevation of sea level fluctuations during glacial times (e.g. *Richards et al., 1994; Smart et al., 1998; Bard et al., 2002a*).

Speleothems can be dated very precisely by U-series dating methods. An extended discussion about U-series dating of speleothems as well as their application for paleoclimate reconstruction can be found in *Richards & Dorale* (*2003*).

3.1.4 Comparison of the different reconstruction methods

Each of the three sea level reconstruction methods described in this chapter has its assets and drawbacks. These are summarized and compared with each other in Table 3.1. To take advantage of the benefits of all methods several authors have tried to combine the results obtained from different methods. For example, absolutely dated fossil coral data have been used to develop a timescale for an isotope curve which is independent from orbital tuning (*Shackleton et al., 2002*). Other authors used relative sea level estimates based on fossil corals to correct their $\delta^{18}O$ records for the temperature component (*Waelbroeck et al., 2002*).

Method	**Reconstruction of the *magnitude* of past sea level change**		**Reconstruction of the *timing* of past sea level change**	
	+	**-**	**+**	**-**
$\delta^{18}O$ in deep sea cores	- records go far back in time - continuous records	- $\delta^{18}O$ signal is also influenced by deep sea temperature - provides only relative information about sea level change		- beyond ^{14}C dating range orbitally tuned - no absolute age control
Fossil reef corals	- direct measurement of the magnitude	- uncertainty in the estimation of the uplift rate - sea level lowstands cannot be determined - relative sea level change is also affected by isostatic effects of the Earth - only selected species have a narrow depth habitat	- precise absolute dating by U-series methods	- coral diagenesis
Submerged speleothems		- provide only information such as “higher/not higher than” - possibly also influenced by effects of uplift or isostasy	- precise absolute dating by U-series methods	- absence of growth does not necessarily result from submergence - possibly also affected by diagenesis

Table 3.1: Summary and comparison of the three methods described in this chapter, subdivided into the reconstruction of the *magnitude* and the *timing* of past sea level fluctuations.

3.1.5 The Late Quaternary sea level curve from coral dating

Since the first studies in the late 1960's (*Broecker et al., 1968; Mesolella et al., 1969*) various authors have applied U-series dating of fossil reef corals for sea level reconstruction. Fig. 3.4 gives a summary of the current state of the coral based sea level record since the Last Interglacial period (MIS 5).

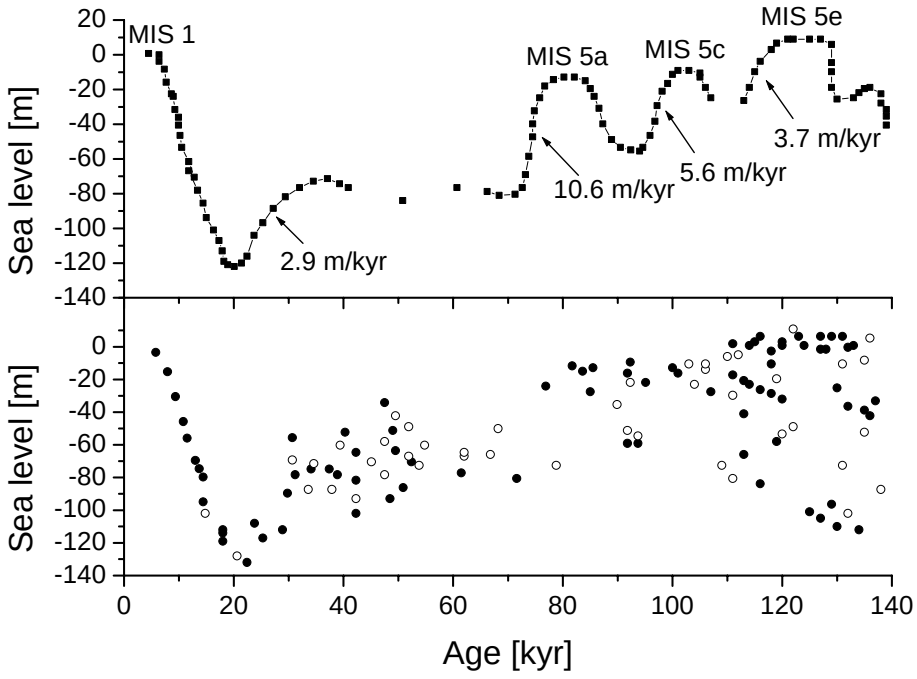

Fig. 3.4: **(Upper part)** The coral sea level record based upon samples showing no evidence of diagenesis (modified from *Cutler et al.* (*2003*)). The numbers give the estimated average rates of sea level fall for each drop.
(Lower part) All coral sea level data presently available (*Cutler et al.* (*2003*) and data from references therein). The picture has been modified from *Cutler et al.* (*2003*). Solid symbols represent samples having $\delta^{234}U_{initial}$ values within ± 8‰ of the modern marine value, open symbols represent samples that do not.

To compose the curve the following data sets have been used: The part prior to MIS 5e is based on the results of *Gallup et al.* (*2002*). The age limits of the MIS 5e peak have been fixed using the dataset of *Chen et al.* (*1991*). It must be noted that the dataset of *Stirling et al.* (*1995; 1998*) suggests a longer duration of MIS 5e, resulting in a more rapid rate of sea level fall for the 5e-5d transition. The MIS 5c sea level is based on two points only (*Bard et al., 1990a; Edwards et al., 1997*), because there are no data available with both marine initial $\delta^{234}U$ and concordant Th/U- and Pa/U-ages. The MIS 5b sea level minimum is constrained by one coral age from the Huon Peninsula (*Cutler et al., 2003*). The timing and magnitude of the

MIS 5a peak follow the results of the studies by *Ludwig et al.* (*1996*) and *Toscano & Lundberg* (*1999*). The curve is discontinuous during MIS 3 due to insufficient resolution where other climate proxies (ice- and deep sea-cores) suggest major fluctuations. The existing data for this period range from values between -74 and –85 m relative to present sea level (r.p.s.l.) (*Cutler et al., 2003*) to –45 m (*Chappell et al., 1996; Cabioch & Ayliffe, 2001; Chappell, 2002*). Thus, it is possible that MIS 3 sea level varied about 40 m during MIS 3. Finally, the sea level rise from the Last Glacial maximum till today is composed of the data of *Edwards et al.* (*1993*), *Bard et al.* (*1990b; 1996*), and *Cutler et al.* (*2003*).

The lower part of Fig. 3.4 shows a compilation of all coral sea level data presently available. It is evident that the resulting sea level curve (from the complete dataset as well as the $\delta^{234}U$ screened data, see Figure caption) has serious inconsistencies, particularly in the older portion. This shows that Pa/U concordancy or other tests are important to obtain reliable results and that – if strict criteria are applied - the remaining dataset is small.

3.2 Corals as high resolution paleoclimate archives

Apart from their application for past sea level reconstruction, fossil reef corals provide a paleoclimatic archive with seasonal resolution. As this work focuses on U-series dating of fossil corals and the calculated ages have been used in a paleoclimate study (*Felis et al., 2004*), a short review of this subject is given here.

During growth, alternating bands of high and low density are produced in the skeletons of massive scleractinian corals. These density variations result from changes in the coral's rate of calcification and/or growth, with each pair of bands representing on year. Based on counting the annual density band pairs, a precise continuous age model with seasonal resolution can be developed for living corals (e.g. *Linsley et al., 1994; Quinn et al., 1998*). Fossil corals can be dated by ^{14}C- and U-series methods providing a floating chronology for which top and bottom ages are known only approximately. The most commonly used corals in paleoclimatology are those of the genus *Porites* (see chapter 2.2.2) which are ideally suited for sub-annual sampling owing to their dense skeletons and rapid growth rates (about 1 cm per year, *Felis & Pätzold, 2003*).

As climate tracers in corals, mainly stable isotopes and trace elements are used. The $\delta^{18}O$ signal in corals is primarily influenced both by temperature and the $\delta^{18}O$ value of sea water during precipitation. If it can be shown for a certain locality that one of these environmental factors dominates the other, coral $\delta^{18}O$ records can provide information either on variations in sea surface temperature (SST) or in water $\delta^{18}O$ which is related to the hydrologic balance (evaporation, precipitation, runoff, or water mass transport). The interpretation of $\delta^{13}C$ values

in coral skeletons is complicated, because of disturbances by physiological processes. Therefore, this signal is difficult to use in paleoclimate research.

Similar to $\delta^{18}O$, the concentrations of various trace elements incorporated in coral skeletons are dependent on the precipitation temperature. Sr/Ca ratios provide a promising proxy for water temperature variability, even though there are still differences in the temperature calibrations between different studies (*Felis & Pätzold, 2003*). Due to the long residence time of Sr and Ca in the ocean, the Sr/Ca ratios of seawater are supposed to be constant on glacial-interglacial timescales. Therefore, the Sr/Ca signal can be used to remove the temperature component of the $\delta^{18}O$ signal. Other temperature sensitive trace elements in coral skeletons are U (see chapter 2.2.3) and Mg.

In summary, coral records have been successfully used during the last ten years for seasonal resolution paleoclimate reconstructions and have contributed substantially to the understanding of the dominant modes of the global climate system, like the El Nino-Southern Oscillation (ENSO) or the North Atlantic Oscillation (NAO). An extended overview of climate records derived from fossil corals can be found in *Felis & Pätzold* (*2003*).

4 Results and discussion

The fossil coral samples which have been analysed in the context of this work have been collected at two different regions. At Aqaba, Jordan, corals of the genus *Porites* have been sampled which have also been used in a high resolution paleoclimate study (*Felis et al., 2004*). The other corals are of the genus *Acropora palmata* and *Diploria strigosa* and have been collected on Barbados, West Indies.

4.1 The study of fossil reef corals from Aqaba, Jordan

4.1.1 Description of the study region and coral sampling

The studied fossil coral reef terraces are located south of the city of Aqaba on the Jordanian coast of the Gulf of Aqaba (29°27.12'N, 34°58.28'E) which is the narrow (180 km long, with 14 km average width) north-eastern extension of the northern Red Sea (Fig. 4.1). This site is one of the northernmost locations where annually banded corals grow on the Northern Hemisphere. The Gulf is a 1830-m-deep, desert-surrounded evaporative basin with negligible precipitation and runoff. The connection to the Red Sea in the south is via the Straits of Tiran, a shallow sill at a water depth of about 250 m. The Gulf is surrounded by a relatively narrow coastal plain bordered by 700-1000 m high mountain ranges, mostly of Precambrian basement build of metamorphic rocks with volcanic intrusions (*Reiss & Hottinger, 1984*). Mean sea surface temperature is 23.5°C and mean sea surface salinity is about 40.5‰. Mean precipitation is about 30 mm/year with the rainfall being restricted to the winter season, when the area is influenced by the Mediterranean climate regime.

Raised reef terraces of Late Quaternary age are a common landform on the Red Sea coast. A prominent site in the northern Red Sea are the fossil reef terraces at the southern tip of the Sinai Peninsula which were extensively studied by applying U-series dating (*Gvirtzman et al., 1992; Strasser et al., 1992; Gvirtzman, 1994; El-Asmar, 1997*). The raised reef terraces at Aqaba which are located 180 km to the north have been mentioned in the literature (*Taviani, 1998; Walter et al., 2000*), but until now U-series ages of fossil corals from these terraces have not been reported and their ages remain a matter of speculation (*Al-Rifaiy & Cherif, 1988*).

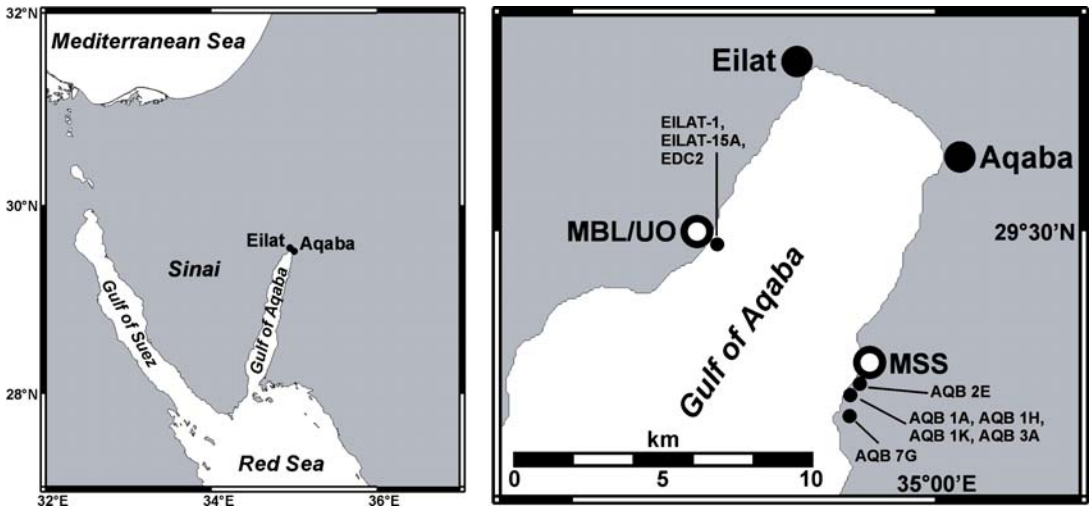

Fig. 4.1: Maps of the northern Red Sea and the northern end of the Gulf of Aqaba. The locations of coral collection are indicated. MBL/UO = The H. Steinitz Marine Biology Laboratory/Underwater Observatory Eilat (Israel); MSS = Marine Science Station Aqaba, Jordan.

At the study site, seven geomorphological terraces have been described on a length of about 1.5 km parallel to the coast. The terraces are highly dissected and reach a height of 30 m in a distance of a several 100 m to the coastline (*Al-Rifaiy & Cherif, 1988*). The area of the raised reef terraces is in the vicinity of a huge alluvial fan of a wadi. Exceptionally high rainfalls can generate floods along such wadis which are therefore areas of groundwater flow and discharge into the Gulf.

The corals analysed in this study are from the two lowermost clearly recognizable geomorphological terraces which have an elevation of 4-5 m (Figs. 4.2 and 4.3) and 7-10 m above present sea level (asl) (Fig. 4.4), respectively. The elevation of the two terraces is in the range reported for Last Interglacial reef terraces along the Red Sea coast of the Sinai Peninsula and Africa (*Walter et al., 2000*).

Fig. 4.2: Photography of the lower coral reef terrace at Aqaba which has an elevation of 4-5 m asl and is located in a distance of 50-100 m to the sea. The picture has been provided by T. Felis.

Fig. 4.3: More detailed picture of the lower terrace. On top of the terrace which has a width of about 50 m is the Aqaba coast road. The picture has been provided by T. Felis.

Fig. 4.4: Photography of the upper coral reef terrace at Aqaba which has an elevation of 7-10 m asl. Also shown is the Aqaba coast road which is located on top of the lower terrace and takes course along the upper one. The picture has been provided by T. Felis.

Originally, the main intention was to obtain material for high-resolution paleoclimate reconstructions (*Felis et al., 2004*). Therefore, corals of the genus *Porites* have been collected (see chapter 3.2). In contrast to many other studies, complete coral colonies were recovered in order to determine the parts of each colony that are best suited for high resolution paleoclimatic studies and U-series dating (i.e. that are relatively unaffected by diagenesis). The size of the coral colonies which were separated from the reef using hammers and chisels ranges from 13-60 cm for the height and 10-25 cm for the diameter (Fig. 4.5).

Fig. 4.5: Photography of coral colony AQB 3A, which has been collected on top of the lower terrace. This coral was located not in situ near the bottom of the upper terrace. Therefore, it cannot be definitely assigned to one of the terraces. The coral is of the genus *Porites*. It is about 60 cm high and 25 cm in diameter. The photo has been provided by T. Felis.

Coral colonies AQB 1A, AQB 1H, and AQB 1K were collected *in situ* from the lower terrace whereas colonies AQB 2E and AQB 7G were collected *in situ* from the higher terrace. Coral colony AQB 3A cannot be definitely assigned to one of the terraces (see Fig. 4.5 captions). While AQB 1A, AQB 1H, AQB 1K, and AQB 3A were collected close together (<100 m relative distance), AQB 2E was collected about 350 m to the north and AQB 7G was collected about 500 m to the south, the latter location being close to a nearby alluvial fan of a wadi (Fig. 4.1).

Furthermore, a fossil late Holocene coral was recovered from a canal cut through the modern reef platform at a distance of about 8 km to the south of the raised reef terraces. The age of this *Porites* colony which is 60 cm high with a diameter of 28 cm is 2963 cal yrs before 2003 AD (2σ error range: 3055-2860), based on ^{14}C- Accelerator Mass Spectrometry (AMS) dating (*Felis et al., 2004*). This age has been corrected for the global and local reservoir effect of the ocean.

As a modern reference, material from three living coral colonies of the genus *Porites* from a location near Eilat (Israel), in a distance of about 6 km on the opposite shore of the Gulf, was used (Fig. 4.1). These corals (EILAT-1, EILAT-15A, and EDC-2) have also been used in stable isotope based paleoceanographic studies (*Felis et al., 1998; Felis et al., 2003*).

4.1.2 Pre-treatment of the coral samples

Each coral colony was sliced into 4-6 mm thick slabs parallel to the axis of growth. As revealed by X-radiograph positive prints of these slabs, the annual density pattern was well preserved in all analysed coral colonies (Fig. 4.6). Diagenetic alterations which are visible as areas of relatively high density due to secondary precipitation of aragonite/calcite pore fillings can be identified only near the outer margin and in restricted parts of the interior of some colonies. Using the X-radiograph positive prints as a guide, samples for X-ray diffraction analysis were taken from parts of the slabs which were apparently unaffected by diagenesis. The X-ray diffraction analysis which was performed at the Department of Mineralogy of the Faculty of Geosciences at Bremen University revealed that with respect to these parts the aragonite content of all fossil corals is between 97-99%, except for colony AQB 2E where it is only 85% (Table 4.4, page 67).

Fig. 4.6: X-radiograph positive print of coral colony AQB 3A (see also **Fig. ???**). Alternating bands of high (dark colour) and low (light colour) density are clearly visible. One year is represented by one band pair. The white line indicates where the sampling for high resolution paleoclimate studies was done (*Felis et al., 2004*). The black bar represents 10 cm. The picture has been provided by T. Felis.

As corals AQB 3A and the late Holocene coral AQB 10B were also part of a high resolution paleoclimate study (*Felis et al., 2004*), they were investigated in more detail using petrographic thin sections. Those reveal that skeletal elements are occasionally coated with a thin layer (<20 µm thick) of secondary aragonite in both corals with respect to the analysed parts of the colonies. In addition, traces of calcite spar and patches of gypsum can be identified in coral AQB 3A. Due to its concentration in specific regions the gypsum was also identifiable in the X-radiographs. Apart from this minor cementation, the skeletal material itself shows no signs of alteration.

The time series of coral $\delta^{18}O$ and $\delta^{13}C$ show a clear seasonal cycle over the period of coral growth in both colonies, implying no occurrence of diagenetic alterations. However, the time series of coral Sr/Ca ratios shows a seasonal cycle only in restricted parts of colony AQB 3A. That coral Sr/Ca ratios can be affected by subtle diagenetic processes whereas coral $\delta^{18}O$ and $\delta^{13}C$ remain unaffected, was also reported from last interglacial corals from the Western Pacific (*Hughen et al., 1999; Tudhope et al., 2001*). An extended discussion of the diagenetic state of corals AQB 3A and AQB 10B is given in *Felis et al.* (*2004*).

4.1.3 Results of the U-series measurements

All U-series data presented in the context of this work have been measured by thermal ionisation mass spectrometry (TIMS). A detailed description of this method as well as the preceding sample preparation is given in Appendix A. During this work was done, a new calibration of the U- as well as the Th-spike-solution concentration has been performed (see Appendix A). This produces slight but significant differences in the calculated activity ratios and U-series ages of the analysed samples. The activity ratios of the Aqaba corals presented in this chapter refer to the old values of the spike-solution concentrations. They can be converted into the corrected ones by multiplying the ($^{230}Th/^{238}U$) activity ratio by a factor of 1.0115 (see Appendix A). It must be emphasized that this correction does not affect any of the conclusions drawn from the Aqaba data neither in the context of this work nor in the already published paper by *Scholz et al.* (*2004*).

For the U-series measurements four to six sub-samples have been cut out of each coral colony from Aqaba (Fig. 4.7).

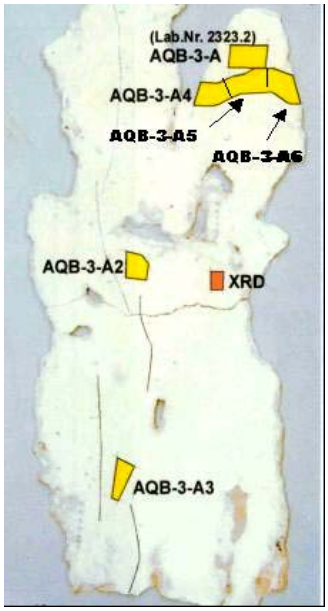

Fig. 4.7: Photo of ~5 mm thick slab sliced from coral colony AQB 3A. The locations from where samples for U-series dating (yellow) and X-ray diffraction analysis (orange) were taken are indicated. The samples were taken from that parts of each coral which showed the least evidence for diagenetic alteration on the X-radiograph positive prints (Fig. 4.6). Photo provided by T. Felis.

The U-series data and ages of the sub-samples of each coral from the raised reef terraces are listed in Tables C3 and C4 in Appendix C. The U-series ages range from 113.7 ± 1.2 to 151.6 ± 1.3 kyr, suggesting a Last Interglacial origin. ^{238}U concentrations are between 2.87 to 4.42 ppm, with an average of 3.67 ppm, and are generally higher than those reported in other studies (see chapter 2 and the references therein). The ^{232}Th concentrations of the Aqaba samples lie between 0.7 and 35 ppb, with an average of 8.13 ppb, and are higher than values measured normally in surface corals (see chapter 2), although values of this magnitude have already been reported for *Porites* corals (*Stirling et al., 1998*).

U-series data and ages of the sub-samples of the Holocene coral are given in Table C2 in Appendix C. The ^{238}U content ranges from 2.99 to 3.31 ppm, with an average of 3.11 ppm, and the ^{232}Th concentrations lie between 0.1 to 0.7 ppb, with an average of 0.44 ppb, both being within the usual range. The U-series ages of the sub-samples range from 3,070 to 3,171 years.

The results obtained from the recent corals collected at Eilat, Israel, are listed in Table C1 in Appendix C. While the ^{238}U concentrations range from 2.65 to 3.34 ppm (average: 2.96 ppm) and are within the usual range, the ^{232}Th contents lie between 0.07 to 3.85 ppb (average:1.53 ppb) and are slightly elevated. Due to very low counting rates, the ^{230}Th measurements of the recent corals have been significantly affected by the background current. Therefore, ($^{230}Th/^{238}U$) activity ratios and ages have not been calculated for these corals (Table C1, Appendix C).

The U-series results of all analysed Aqaba corals are presented on a $\delta^{234}U$-($^{230}Th/^{238}U$)-plot in Figure 4.8.

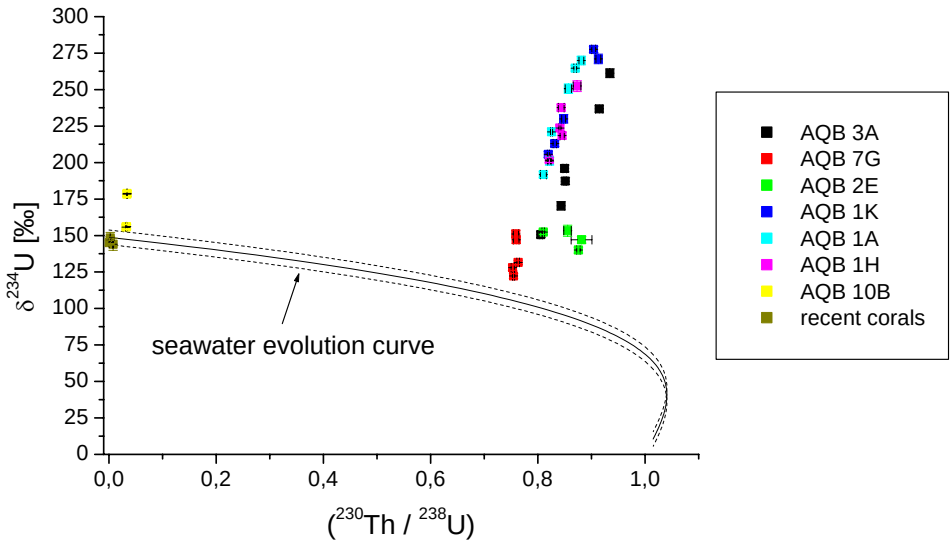

Fig. 4.8: The compilation of the U-series data measured on the Aqaba corals. Different sub-samples of the same coral are indicated by different colours. The dashed lines represent the uncertainty in the seawater evolution curve ($\delta^{234}U = 149.6 \pm 5$ ‰).

It is evident from Fig. 4.8 that the sub-samples of the Holocene as well as all Last Interglacial corals did not behave as closed systems, because all data points plot significantly above the seawater evolution curve. This is also manifested in the extremely elevated initial $\delta^{234}U$ values, which range from 171 ± 2 to 396 ± 3 ‰ for the Last Interglacial and from 156 ± 2 to 179 ± 2 ‰ for the Holocene corals. In contrast, the $\delta^{234}U$ values measured on the recent corals are between 144 ± 4 and 148 ± 4 ‰ reproducing the values measured on modern-day seawater and modern corals within error (see *Delanghe et al.* (*2002*) and also chapter 2 and the references therein). Applying the established criteria for age reliability (page 25, chapter 2.2.4), none of the calculated ages can be considered to be strictly reliable. This is also clear from the age differences up to 11 kyr observed in different sub-samples of one and the same coral that are also an evidence for a disturbed U-Th-system. However, as the $\delta^{234}U$ values of the Holocene as well as the Last Interglacial corals are much more elevated than those examined by other workers (compare for example the data presented in Fig. 2.8, chapter 2), the Aqaba corals should qualify very well to study the processes which produce elevated $\delta^{234}U$ values in fossil reef corals.

4.1.4 Discussion of ^{232}Th content

As mentioned above, the ^{232}Th contents of the Last Interglacial corals from Aqaba are higher than those of the Holocene and recent corals and those reported for fossil corals in most other studies. This indicates the presence of small fractions of non-radiogenic ^{230}Th (i.e. ^{230}Th not produced by in situ U decay), $^{230}Th_{nr}$, which needs to be corrected for. Such a correction can be performed using equation (2.9) if the initial ($^{230}Th/^{232}Th$) activity ratio of the non-radiogenic component is known (see also chapter 2.1.3). *Cobb et al.* (*2003*) give initial $^{230}Th_{nr}/^{232}Th_{nr}$ weight ratios (in the following activity ratios are given in parenthesis, but *weight ratios* are not) of 4×10^{-6} for continental sources and values between 5×10^{-6} and 1×10^{-5} for surface seawater. In general, two cases must be differentiated: (i) incorporation of non-radiogenic components during coral growth and (ii) post-depositional addition during subsequent periods. The former is the case if seawater is the source of the $^{232}Th_{nr}$ in the Aqaba corals. Sea level was between 0 and +6 m r.p.s.l. during the Last Interglacial and continuously lower throughout the following periods (see Fig. 3.4, page 39). Today, both fossil terraces at Aqaba are above sea level. Consequently, the non-radiogenic component must have been added during growth or shortly after death if seawater was its source. Therefore, the $^{230}Th_{nr}/^{232}Th_{nr}$ value must be corrected for radioactive decay since the time of addition. This is accounted for by the exponential term in equation (2.9). Using a maximum value of 3×10^{-5} for $^{230}Th_{nr}/^{232}Th_{nr}$ results in significant corrections for three Aqaba corals only (AQB 3A, AQB 3A 5, and AQB 1K 3). In contrast, if the ^{232}Th stems from a terrestrial source, it is not possible to estimate the time of addition. Consequently, a correction of $^{230}Th_{nr}/^{232}Th_{nr}$ for

radioactive decay is not recommended. However, the application of a correction using a (terrestrial) $^{230}Th_{nr}/^{232}Th_{nr}$ value of 4×10^{-6} is not significant for all Aqaba corals.

Although it is unlikely, it cannot be excluded that the non-radiogenic ($^{230}Th/^{232}Th$), ($^{234}U/^{232}Th$), and ($^{238}U/^{232}Th$) activity ratios of the Aqaba corals are much higher than the average crustal values. This has been investigated using $\delta^{234}U$-^{232}Th- and ($^{230}Th/^{238}U$)-^{232}Th-plots, respectively (see captions of Fig. 4.9 for details).

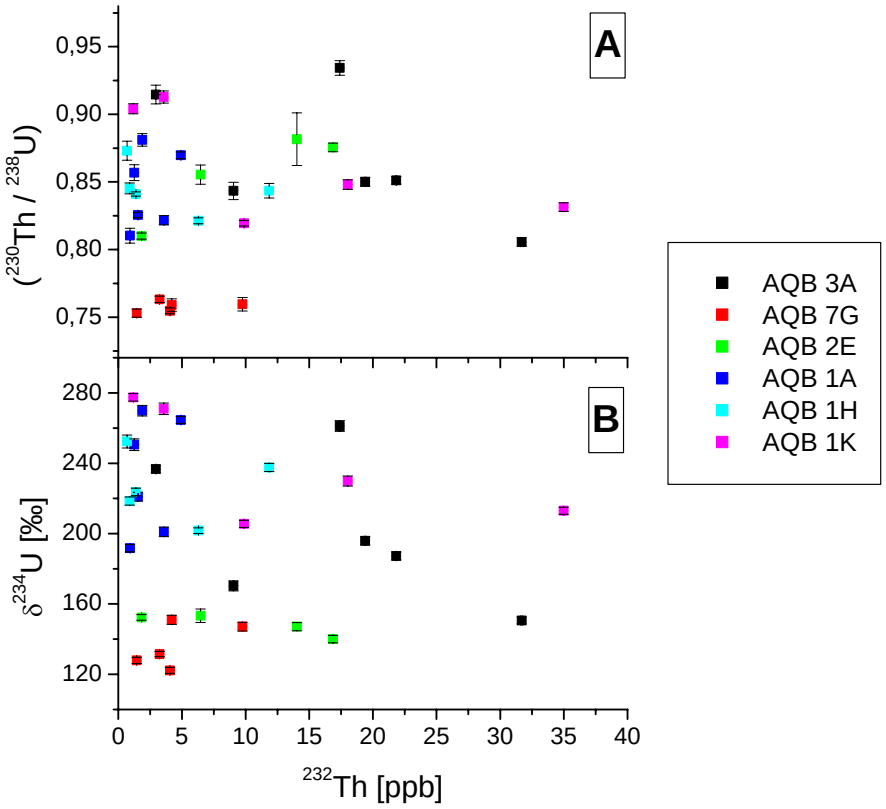

Fig. 4.9: ($^{230}Th/^{238}U$)-^{232}Th- (A) and $\delta^{234}U$-^{232}Th-plots (B) for the Last Interglacial corals from Aqaba. While there is no general correlation detectable, sub-samples of individual corals (as indicated by different colours) show moderate to high correlations, suggesting post-depositional uptake of ^{230}Th and ^{234}U along with ^{232}Th. However, while in some corals a positive correlation between ($^{230}Th/^{238}U$) and $\delta^{234}U$ with ^{232}Th is observable (AQB 1A and AQB 7G), in others they are negatively (AQB 3A and AQB 1K) or not correlated at all (AQB 1H). This suggests that ^{230}Th and ^{234}U have not been added in specific and unusually high ($^{230}Th/^{232}Th$) and ($^{234}U/^{232}Th$) ratios to the Aqaba corals. Interestingly, the strongest correlations are observed for coral AQB 2E which has the lowest aragonite content (85%), but again with opposite signs (R(($^{230}Th/^{238}U$)-^{232}Th)=0.98) and R($\delta^{234}U$-^{232}Th) = -0.88). This strengthens the previous conclusion.

Consequently, all activity ratios and ages listed in Tables C2, C3, and C4 (Appendix C) have been routinely corrected for detrital contamination assuming a silicate source with a $^{232}Th/^{238}U$ weight ratio of 3.8 (*Wedepohl, 1995*) and with ^{230}Th, ^{234}U, and ^{238}U in secular equilibrium. This has also been done in other studies of fossil reef corals before (e.g. *Stirling et al., 1998*). As mentioned above, the resulting differences between uncorrected and corrected ages are generally within the $\pm 2\sigma$ error range of the ages - despite of the higher ^{232}Th content of the Aqaba samples.

4.1.5 Discussion of ^{238}U content, $\delta^{234}U$, and ($^{230}Th/^{238}U$) activity ratio

As mentioned in chapter 4.1.3, the ^{238}U contents of the Last Interglacial *Porites* corals from Aqaba are higher than those of their Holocene and recent counterparts. They are also higher than those reported in other studies for *Porites* corals which range from 2 to 3.3 ppm (e.g. (*Henderson et al., 1993; Szabo et al., 1994; Stirling et al., 1998; Esat et al., 1999; McCulloch & Esat, 2000; Muhs et al., 2002*)).

U concentration in corals depends on the absolute U concentration of seawater (see chapter 2.2.3) which is correlated with salinity (chapter 2.2.1). As the Gulf of Aqaba is a partially enclosed body of slightly hypersaline water (41.5-43%) (*Friedman, 1968; Shemesh et al., 1994*), the elevated ^{238}U content of the Last Interglacial corals might result from a greater U availability. There are two arguments disproving this hypothesis: (i) A stable isotope based salinity reconstruction from the northern Red Sea suggests lower values for the Last Interglacial (37%) than today (*Geiselhart, 1998*), and (ii) the U contents of the recent corals which consequently grew under conditions of higher salinity than the Last Interglacial ones are within the normal range. From this follows that the Last Interglacial corals have gained significant U *after deposition.*

This conclusion is further supported by a significant correlation between $\delta^{234}U$ values and total U content suggesting post-depositional uptake of U with a higher $\delta^{234}U$ value (Fig. 4.10). In the context of Fig. 2.9 (page 26) this corresponds to scenario ‘g’ which would produce elevated $\delta^{234}U$ values and younger U-series ages at the same time.

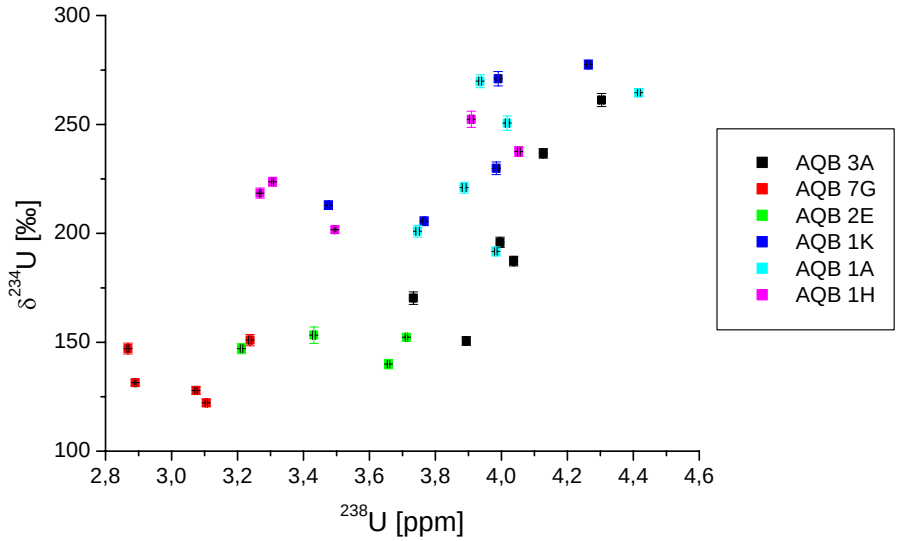

Fig. 4.10: Plot of $\delta^{234}U$ vs. ^{238}U content for the Last Interglacial corals from Aqaba. The positive correlation suggests that all samples gained significant amounts of a high $\delta^{234}U$ component after deposition.

Possible sources for such an additional high $\delta^{234}U$ component are ground- or porewaters (*Edwards et al., 1997*). As pointed out by *Edwards et al.* (*1997*), the additional U could either be added by (i) precipitation of secondary aragonite or (ii) addition of U to a minor component such as organic material. Organic matter in corals incorporates 40-70 ppm U by chelation, but overall the organic fraction is very low (0.1%) (*Amiel et al., 1973b*). The maximum U content of the Aqaba corals is 4.42 ppm, while the usual values for skeletal aragonite are about 3 ppm. If the whole additional U was added to an organic component and it is assumed, that this component contains the maximum value of 70 ppm U, it is required that the organic fraction of the coral would be 2.1%. Therefore, U addition to such a minor component seems to be rather unlikely. A similar estimation can be made for the first possibility: In some parts of corals AQB 3A and AQB 10B a thin layer of secondary aragonite was detected (see chapter 4.1.2). This layer is less than 20µm thick and does not exceed 5% of the total coral mass. If the whole additional U was added to secondary aragonite, it is required that it contained about 30 ppm U. U measurements on secondary aragonite in *Porites* corals from our study region resulted in a value of 4.12 ± 0.14 ppm (*Lazar et al., 2002*) showing that the additional U was most likely not added as secondary aragonite. Overall, there is no doubt that significant amounts of a high $\delta^{234}U$ component have been added to the Last Interglacial corals from Aqaba, but the mechanism of addition as well as the gaining component have yet to be identified.

To evaluate the isotopic composition of the additional component in the Aqaba corals in more detail, a simple two-component-mixing-model is used. This model assumes that the U and Th initially incorporated into the coral skeleton has been mixed with additional U and Th. The activity ratios of a sample that has gained significant amounts of U as well as Th are given by the following equations:

$$\left(\frac{^{230}Th}{^{238}U}\right)_{measured} = \frac{\left(\frac{^{230}Th}{^{238}U}\right)_{coral} \cdot {}^{238}U_{coral} + \left(\frac{^{230}Th}{^{238}U}\right)_{add} \cdot {}^{238}U_{add}}{{}^{238}U_{coral} + {}^{238}U_{add}} \tag{4.1}$$

$$\left(\frac{^{234}U}{^{238}U}\right)_{measured} = \frac{\left(\frac{^{234}U}{^{238}U}\right)_{coral} \cdot {}^{238}U_{coral} + \left(\frac{^{234}U}{^{238}U}\right)_{add} \cdot {}^{238}U_{add}}{{}^{238}U_{coral} + {}^{238}U_{add}} \tag{4.2}$$

The $^{238}U_i$'s are expressed in terms of activities. The measured uranium content of the sample is given by equation (4.3):

$$^{238}U_{measured} = {}^{238}U_{coral} + {}^{238}U_{add} \tag{4.3}$$

Solving equations (4.1) and (4.2) for $(^{230}Th/^{238}U)_{add}$ and $(^{234}U/^{238}U)_{add}$ gives the following equations:

$$\left(\frac{^{230}Th}{^{238}U}\right)_{add} = \frac{\left(\frac{^{230}Th}{^{238}U}\right)_{coral} \cdot {}^{238}U_{coral} - \left(\frac{^{230}Th}{^{238}U}\right)_{measured} \cdot {}^{238}U_{measured}}{{}^{238}U_{coral} - {}^{238}U_{measured}} \tag{4.4}$$

$$\left(\frac{^{234}U}{^{238}U}\right)_{add} = \frac{\left(\frac{^{234}U}{^{238}U}\right)_{coral} \cdot {}^{238}U_{coral} - \left(\frac{^{234}U}{^{238}U}\right)_{measured} \cdot {}^{238}U_{measured}}{{}^{238}U_{coral} - {}^{238}U_{measured}} \tag{4.5}$$

If the age of the coral is known, the activity ratios of the coral component ($(^{230}Th/^{238}U)$ and $(^{234}U/^{238}U)$ respectively) can be calculated using the closed-system equations ((2.5) and (2.6)) and the usual initial conditions for surface corals (i.e. no initial Th and $(^{234}U/^{238}U)_{initial} = 1.15$ (modern seawater)). For the calculations shown in this chapter the *isochron age* has been used as the 'true' coral age. The calculation of coral *isochron ages* will be explained in chapter 4.1.7. Another possibility would have been to use a Last Interglacial age, for example 125 kyr. As the recent corals have an average ^{238}U content of 2.96 ppm, a

value of 3 ppm has been used for the initial coral U concentration, $^{238}U_{coral}$. Three samples have a ^{238}U content lower than 3 ppm: AQB 10B-3, AQB 7G-3, and AQB 7G-5 (see Tables C2 and C3, Appendix C). Therefore, a ^{238}U value of 2.95 ppm has been used for coral AQB 10B, and 2.75 ppm for coral AQB 7G. As the single values of the recent corals range from 2.65 to 3.34 ppm, these values lie within the range of natural variations for *Porites* corals in the Gulf of Aqaba.

The activity ratios of the additional components at present time, $(^{230}Th/^{238}U)_{add}$ and $(^{234}U/^{238}U)_{add}$, respectively, can be calculated with equations (4.4) and (4.5). As the time of U and/or Th addition cannot be estimated, these values give only an upper (for $(^{230}Th/^{238}U)_{add}$) and a lower limit (for $(^{234}U/^{238}U)_{add}$) for each activity ratio. If the addition occurred directly after coral growth, a correction for radioactive decay is necessary. This can be done using the *isochron age* (see chapter 4.1.7) to calculate the initial additional activity ratios. Such a calculation can be done by solving for $(^{234}U/^{238}U)_{init}$ and $(^{230}Th/^{238}U)_{init}$ in equations (2.5) and (2.9), respectively. In Fig. 4.11 the resulting $(^{234}U/^{238}U)_{add}$ activity ratios are shown.

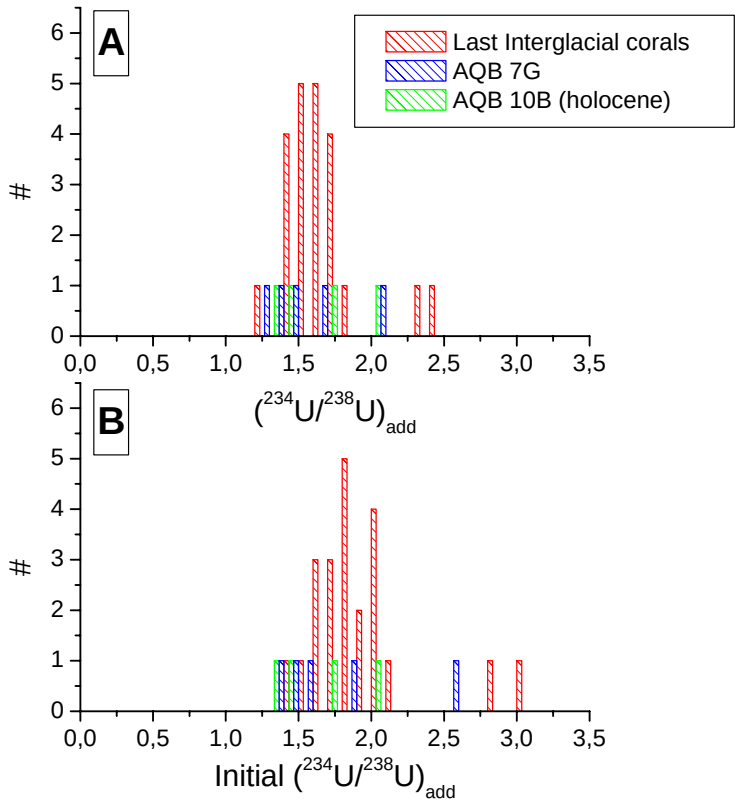

Fig. 4.11: Histograms of the calculated $(^{234}U/^{238}U)_{add}$ (A) and initial $(^{234}U/^{238}U)_{add}$ (B). The sub-samples of the Last Interglacial corals are shown in red, AQB 7G sub-samples in blue, and AQB 10B sub-samples (Holocene) in green.

The values for $(^{234}U/^{238}U)_{add}$ range from 1.25 to 2.46, with an average of 1.65. Most values are between 1.4 and 1.75. Between the Holocene (mean value: 1.63) and the Last Interglacial corals (mean value: 1.65) no general differences are observed (Fig. 4.11 A). The calculated initial $(^{234}U/^{238}U)_{add}$ values range from 1.34 to 3.03 for the Last Interglacial corals, with an average of 1.9, and from 1.33 to 2.03 for the Holocene coral, with an average of 1.64 (Fig. 4.11 B). This suggests that the $(^{234}U/^{238}U)$ activity ratio of the additional component was slightly higher during the Last Interglacial.

Fig. 4.12 shows the calculated $(^{230}Th/^{238}U)_{add}$ activity ratios.

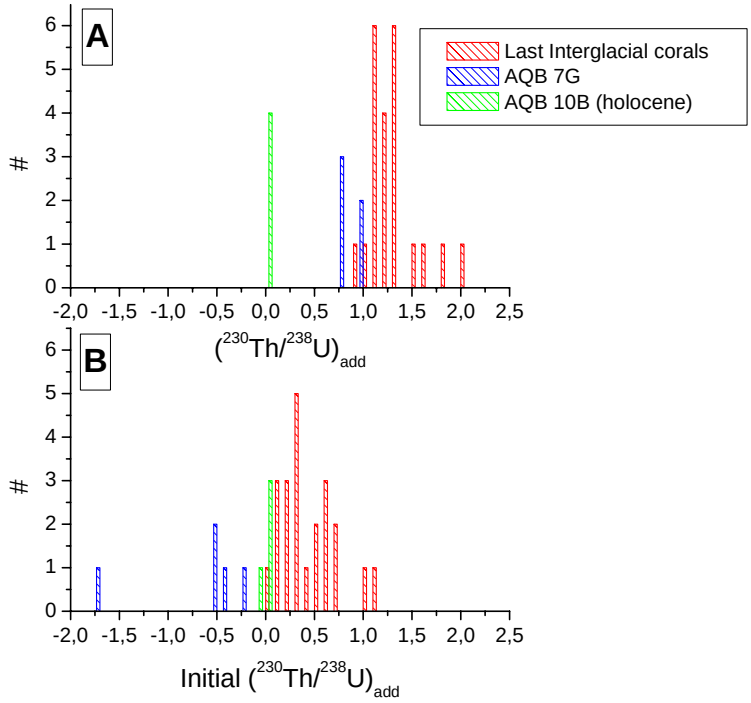

Fig. 4.12: Histograms of the calculated $(^{230}Th/^{238}U)_{add}$ (A) and initial $(^{230}Th/^{238}U)_{add}$ (B). The sub-samples of the Last Interglacial corals are shown in red, AQB 7G sub-samples in blue, and AQB 10B sub-samples (Holocene) in green.

While the calculation of the $(^{234}U/^{238}U)_{add}$ activity ratios gives similar values for the Holocene and the Last Interglacial corals, the calculation of the $(^{230}Th/^{238}U)_{add}$ ratios results in extreme differences (Fig. 4.12 A). For the four sub-samples of the Holocene coral very low $(^{230}Th/^{238}U)_{add}$ values between 0.03 and 0.08 are calculated. Given that this coral already gained substantial additional U, as it is manifested in its significantly elevated $\delta^{234}U$ as well as its slightly elevated U content compared to the recent corals (Tables C1 and C2, Appendix C), it can be concluded that U was added preferentially to Th. If any Th was added to the Holocene coral, then only at very small amounts. This is also confirmed by the very low initial $(^{230}Th/^{238}U)_{add}$ activity ratios calculated for the Holocene coral which range from –0.01 to 0.03 (Fig. 4.12 B) showing that initially no Th was added to this coral. In contrast, the

$(^{230}Th/^{238}U)_{add}$ activity ratios calculated for the Last Interglacial corals range from 0.76 to 2.03 with an average of 1.23 (Fig. 4.12 A). Most values are between 1.1 and 1.3. The different results obtained for the Holocene and the Last Interglacial corals suggest that either significant amounts of Th have been added to the Last Interglacial corals or that $(^{230}Th/^{238}U)_{add}$ increased with time by decay of the additional U. As Th is insoluble and consequently immobile in ground- and surface waters (see chapters 2.1.1 and 2.2.1), the former explanation is very unlikely. However, as the most values are in excess of secular equilibrium, the $(^{230}Th/^{238}U)_{add}$ activity ratios of the Last Interglacial corals can hardly be explained by closed system decay. This is also evident from the initial $(^{230}Th/^{238}U)_{add}$ values calculated for the Last Interglacial corals which range from –1.78 to 1.12 (Fig. 4.12 B), because activity ratios cannot take negative values. As addition of greater amounts of Th can be excluded due to the Holocene data, the only explanation for $(^{230}Th/^{238}U)_{add}$ values of this magnitude is U loss.

The calculation of the activity ratios of the additional component results in quite a range of $(^{230}Th/^{238}U)_{add}$ and $(^{234}U/^{238}U)_{add}$ values for different sub-samples of one and the same coral. This can be explained by the rather large uncertainties of the assumed initial U concentration, $^{238}U_{coral}$ (10%), and the *isochron age* (see chapter 4.1.7 and Table 4.4, page 67). Thus, the $(^{230}Th/^{238}U)_{add}$ and $(^{234}U/^{238}U)_{add}$ activity ratios have also been estimated with another method. It is a common approach to analyse two component mixing systems by plotting the measured $(^{230}Th/^{238}U)$ and $\delta^{234}U$ activity ratio, respectively, against the reciprocal of the ^{238}U activity (*Ivanovich & Harmon, 1992*). The $(^{230}Th/^{238}U)_{add}$ and $\delta^{234}U_{add}$, respectively, can then be obtained from the y-axis intercept. Fig. 4.13 shows the respective diagrams for coral AQB 1A:

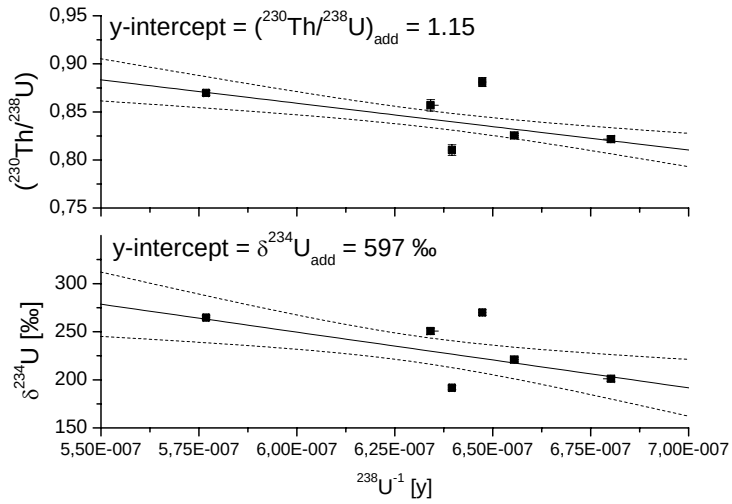

Fig. 4.13: Plots of $(^{230}Th/^{238}U)$ and $\delta^{234}U$ against the reciprocal ^{238}U activity for coral AQB 1A. The y-intercept gives the $(^{230}Th/^{238}U)_{add}$ and $\delta^{234}U_{add}$. The dashed curves are confidence bands at 68% confidence level. The 1σ-uncertainties of $(^{230}Th/^{238}U)_{add}$ and $\delta^{234}U_{add}$, respectively, are consequently given by the intersection points of the confidence bands and the y-axis.

The advantage of such plots compared to the approach using the two-component-mixing-model is that they are less sensitive to variations in the initial ^{238}U concentration of the coral. The determined $(^{234}U/^{238}U)_{add}$ activity ratios range from 1.11 ± 0.16 for coral AQB 7G to 2.02 ± 0.28 for coral AQB 3A. The $(^{230}Th/^{238}U)_{add}$ activity ratios are between 0.68 ± 0.05 for coral AQB 7G and 1.8 ± 0.37 for coral AQB 3A. Table 4.1 gives an overview of the $(^{230}Th/^{238}U)_{add}$ and $(^{234}U/^{238}U)_{add}$ activity ratios calculated with the two different methods.

Coral	$(^{234}U/^{238}U)_{add}$ Method I	$(^{230}Th/^{238}U)_{add}$ Method I	$^{230}Th/^{234}U$ Method I	$(^{234}U/^{238}U)_{add}$ Method II	$(^{230}Th/^{238}U)_{add}$ Method II	$^{230}Th/^{234}U$ Method II
AQB 3A	1.47 ± 0.12	1.19 ± 0.14	0.25 ± 0.04	2.02 ± 0.28	1.8 ± 0.37	0.28 ± 0.07
AQB 7G	1.53 ± 0.34	0.85 ± 0.1	0.17 ± 0.04	1.11 ± 0.16	0.68 ± 0.05	0.19 ± 0.03
AQB 1K	1.69 ± 0.12	1.43 ± 0.16	0.26 ± 0.03	1.57 ± 0.16	1.25 ± 0.28	0.25 ± 0.06
AQB 1H	1.98 ± 0.39	1.53 ± 0.38	0.24 ± 0.08	1.33 ± 0.12	0.82 ± 0.16	0.19 ± 0.04
AQB 1A	1.61 ± 0.11	1.19 ± 0.1	0.23 ± 0.02	1.6 ± 0.24	1.15 ± 0.15	0.22 ± 0.04

Table 4.1: Compilation of the activity ratios of the additional component calculated by the two methods described above. Method I refers to the approach using the two-component-mixing-model, Method II corresponds to the graphical approach. The values listed for Method I are the mean values of the respective sub-samples, the errors are given by the standard deviation. Method II errors have been calculated using confidence bands at 68% confidence level (Fig. 4.13). The respective initial activity ratios can be calculated as described above. Except for corals AQB 3A and AQB 1H all values agree within their errors. Also given are the atomic $^{230}Th/^{234}U$ proportions of the additional component.

Both methods calculate the lowest $(^{230}Th/^{238}U)_{add}$ activity ratios for coral AQB 7G (Table 4.1). The estimation of the initial $(^{230}Th/^{238}U)_{add}$ values with both methods even results in negative activity ratios for this coral. This clearly shows that the diagenetic history of this coral must have been substantially different than that of the other corals. Indeed, whereas the other four corals were collected close together (< 100 m relative distance), coral AQB 7G was collected at a distance of 500 m closer to a nearby alluvial fan of a wadi.

The estimation of the activity ratios of the additional component indicates that the Aqaba corals *apparently* have gained substantial U and Th. Several authors have suggested that α-recoil and other decay-related processes (*Fruijtier et al., 2000; Henderson et al., 2001; Thompson et al., 2003; Villemant & Feuillet, 2003*) or transport on particles in the water, such

as organic colloids (*Gallup et al., 1994*), could mobilise Th in spite of its low solubility (see also the extended discussion of the different diagenetic models in chapter 2.2.5). An important aspect of all these processes is that they would add ^{230}Th and ^{234}U in atomic proportions around 1. The atomic ^{230}Th/^{234}U proportions of the additional component of the Aqaba corals are given in Table 4.1. They are between 0.17 ± 0.04 and 0.28 ± 0.28 for the Last Interglacial corals and 0.01 ± 0.003 for the Holocene coral (not given in Table 4.1). As these values have not been corrected for radioactive decay (this correction can be done using the initial additional activity ratios), and such a correction would produce even smaller values, it can be concluded that the Aqaba corals have not been affected by one of the above mentioned processes. Instead, the remarkable difference between the Holocene and the Last Interglacial data suggests that they suffered addition of a high δ^{234}U component followed by partial loss of the additional component.

Nevertheless, the recently published open-system-dating methods of *Thompson et al.* (*2003*) and *Villemant & Feuillet* (*2003*) have been applied to coral AQB 3A. The results are shown in Table 4.2.

Sub-sample	**Conventional U-series age [kyr]**	**Age according to *Thompson et al.* (*2003*) [kyr]**	**Age according to *Villemant & Feuillet* (*2003*) [kyr]**	**Mean model age according to *Villemant & Feuillet* (*2003*) [kyr]**
AQB 3A	126.4 ± 1	98.9 ± 2.4	97	78 ± 13.5
AQB 3A 2	137.1 ± 1.6	54.5 ± 5.6	61	
AQB 3A 3	137.3 ± 2	64.9 ± 5	67	
AQB 3A 4	132.7 ± 2	93.5 ± 3.6	89	
AQB 3A 5	130.9 ± 0.9	84 ± 3.5	80	
AQB 3A 6	128.7 ± 1.1	78.1 ± 3.6	75	

Table 4.2: Coral ages calculated with the models of *Thompson et al.* (*2003*) and *Villemant & Feuillet* (*2003*), respectively. The model ages have been calculated using Excel spreadsheets provided by W. Thompson and B. Villemant. All age uncertainties are quoted at 2σ-level. Further details of the models can be found in the respective publications.

The ages calculated by the *Thompson et al.* (*2003*) model are between 54.5 ± 5.6 and 98.9 ± 2.4 kyr, while the model of *Villemant & Feuillet* (*2003*) results in ages between 61 and 97 kyr, with a mean model age of 77.96 ± 13.46 kyr. These large age discrepancies between several pieces of one and the same coral clearly show that the Aqaba data cannot be explained by these models. Furthermore, the calculated ages do not suggest a Last Interglacial origin of the corals, but rather a much younger age. As the raised reef terraces at Aqaba most likely grew during the Last Interglacial period (see chapter 4.1.1 and the following chapters), this also shows that the ages calculated by both models are too young. If the Aqaba corals have

been affected by coupled addition of ^{234}Th and ^{230}Th as proposed by these models, then only in combination with significant uptake of a high δ^{234}U component.

4.1.6 Numerical simulation of the Aqaba coral data

While in the compilation of the Aqaba data on a δ^{234}U-(^{230}Th/^{238}U)-plot only a rough trend between δ^{234}U and (^{230}Th/^{238}U) can be observed (Fig. 4.8, page 44), the (^{234}U/^{238}U) and (^{230}Th/^{238}U) activity ratios of different sub-samples of one and the same coral (e.g. AQB 3A to AQB 3A 6) are strongly linearly correlated (see also Table 4.4, page 67). In the following these straight lines will be called *isochrons*. The strong linear correlation is detectable in the Holocene coral AQB 10 B (Fig. 4.14) and in all Last Interglacial corals (Fig. 4.15 a-e) except for coral AQB 2E that has a significantly lower aragonite content of 85% (Fig. 4.15 f). The significant correlation between the activity ratios suggests that the processes that produced the elevated (^{234}U/^{238}U) activity ratios in the Aqaba corals follow specific rules. This may offer the possibility to model the diagenetic processes and to develop an adequate correction method. Figs. 4.14 and 4.15 show the respective plots for the Holocene and the Last Interglacial corals:

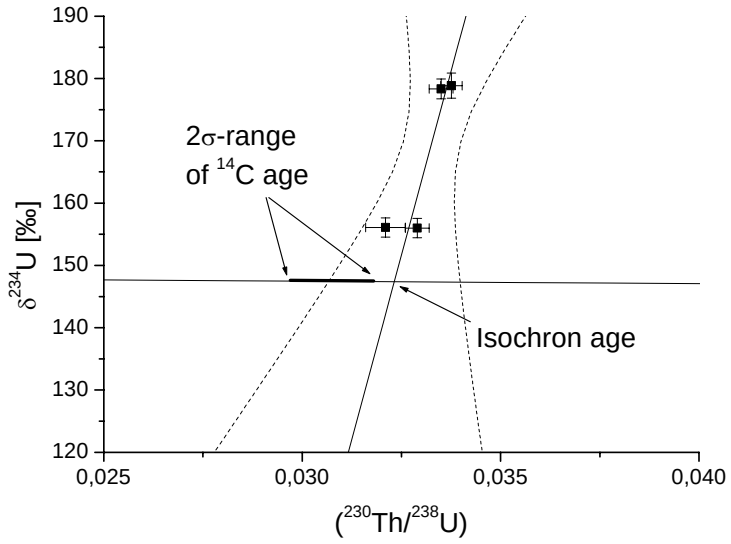

Fig. 4.14: δ^{234}U-(^{230}Th/^{238}U)-plot for the Holocene coral AQB 10B. The horizontal straight line is the seawater evolution curve. The bold section of the seawater evolution curve marks the 2σ-range of the ^{14}C age of the coral (2,860-3,055 cal yr BP). The linearly fitted straight line through the data points is the so-called *isochron*. By intersection of the isochron with the seawater evolution curve the *isochron age* which represents the 'true' age of the coral can be calculated (see chapter 4.1.7 for an extended discussion). The dotted lines around the isochron are confidence bands at 2σ-confidence-level (95%). The isochron age error can be calculated by intersecting these confidence bands with the seawater evolution curve. Isochron and ^{14}C age agree within age uncertainty.

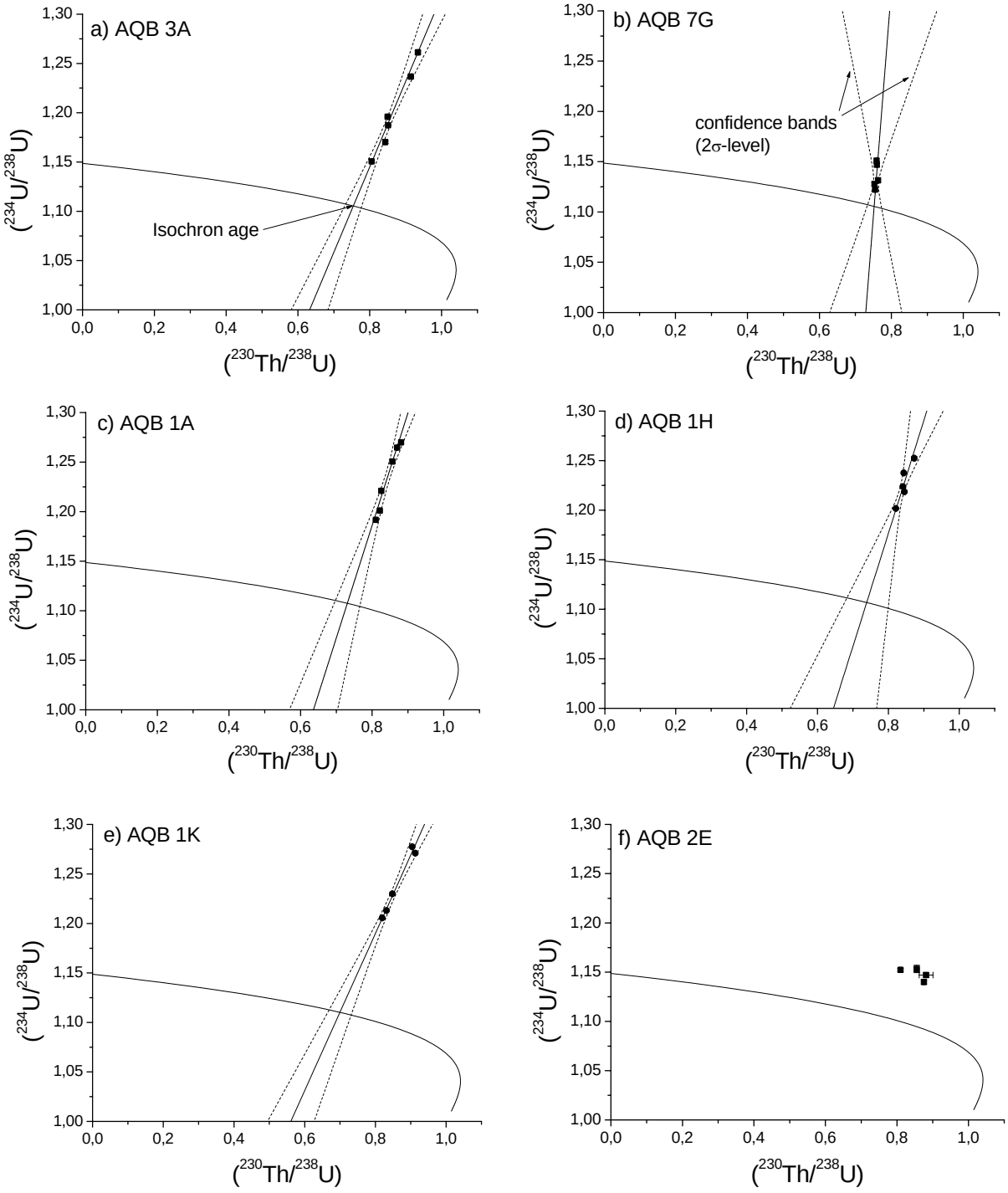

Fig. 4.15: Isochron plots for the six Last Interglacial corals from Aqaba. Dotted lines are confidence bands at 2σ-level. The intersection points of the confidence bands with the seawater evolution curve represent maximum and minimum isochron ages. While five corals show a strong linear correlation, the data of coral AQB 2E do not plot on a straight line. This may be due to the lower aragonite content (85%) of this coral.

Such a characteristic correlation between the ($^{234}U/^{238}U$) and ($^{230}Th/^{238}U$) activity ratio is generated if different parts of a coral gained different amounts of U with a fixed $\delta^{234}U$ value at the same time. As it has been shown in the previous chapter, the Aqaba corals clearly suffered addition of a high $\delta^{234}U$ component. The slope of the produced isochron strongly depends on the timing of addition, and the two extreme cases are defined by early and late U uptake. If the addition occurs soon after coral growth, the isochron corresponds to the respective closed-system isochron (denoted as 'uptake early' in Fig. 4.16). If the U is added ecently, an isochron with a negative slope is produced (denoted as 'uptake late' in Fig. 4.16). Fig. 4.16 shows the two extreme cases considering coral AQB 3A as an example:

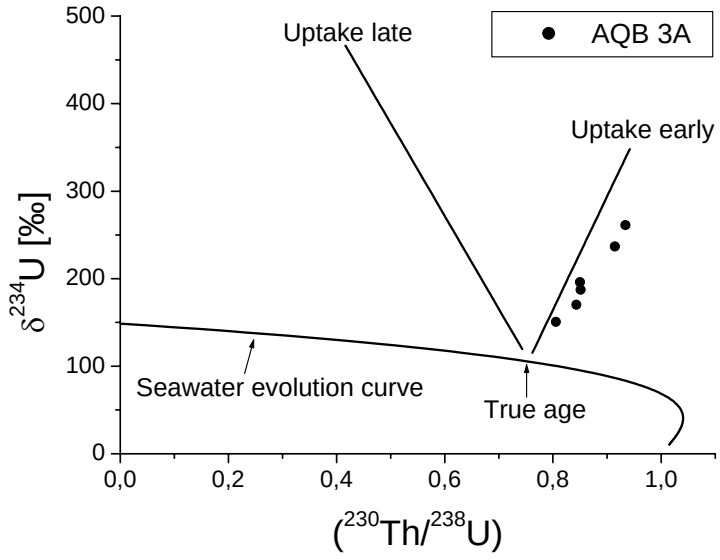

Fig. 4.16: Comparison of the results of the U uptake scenario with the data of coral AQB 3A. The straight lines denoted as 'uptake late' and 'uptake early' represent the maximum range that can be produced by U uptake. As the data of coral AQB 3A plot to the right of this range, the sample either must have gained ^{230}Th or lost ^{238}U.

It is evident from Fig. 4.16 that the data of coral AQB 3A cannot be explained by the high $\delta^{234}U$-uptake-scenario. Only the data of coral AQB 7G lie within the allowed range between the two extreme isochrons, whereas all other samples plot to the right of the early uptake isochron. To describe the isochron slopes of the Aqaba data correctly, either addition of ^{230}Th or loss of ^{238}U must be included in the modelling. As post-depositional ^{230}Th addition can be excluded because of the discussion in the previous chapter, in the following, the isochron slopes will be explained by U loss. When U is transported away, decay-produced ^{230}Th tends to sorb onto the solid due to its particle reactivity and consequently remains where it is (*Chen et al., 1991; Bar-Matthews et al., 1993; Edwards et al., 1997*). Therefore, the result of a combined U addition and loss scenario would be apparent ^{230}Th addition. To produce an isochron on a ($^{234}U/^{238}U$)-($^{230}Th/^{238}U$)-diagram it is required that U loss is proportional to the

U added before and that the timing of both addition and loss is the same for all sub-samples. Possible mechanisms for U loss in fossil reef coral skeletons are recrystallization or dissolution of aragonite. As the analysed parts of the Aqaba corals show no evidence for dissolution nor for recrystallization (except for coral AQB 2E which shows no isochron), it can be assumed that the U which was initially incorporated into the coral skeleton during growth has not been lost, but behaved as a closed system. Instead, the model proposed in the context of this work assumes that the additional U is at least partly remobilised. Though it must be admitted that there is no knowledge of as well the addition as the remobilisation mechanisms, the fact that six out of seven examined corals show an extremely high correlation suggests that U loss was proportional to addition. A potential explanation for this may be that some parts of the coral skeleton are more susceptible to that kind of processes. Periods of U addition and loss respectively may result from variations in the hydrologic regime of the coral reef, so that the timing as well as the rates of U addition and loss would be controlled by changes in the local ground- or porewater chemistry.

Based on the previous discussion, the U content, the ($^{234}U/^{238}U$) and the ($^{230}Th/^{238}U$) activity ratios of all well preserved Aqaba corals (aragonite content >97%) can be explained applying the above listed assumptions:

1. The U initially incorporated into the coral skeleton during growth behaves as a closed system.
2. All coral parts gain additional U with high $\delta^{234}U$ after deposition.
3. The $\delta^{234}U$ is the same for different sub-samples of one coral.
4. Different coral parts gain variable amounts of U.
5. The timing of addition is the same for all coral parts.
6. Some fraction of the additional U may be lost subsequently. If so, U loss is proportional to U gain and occurs at the same time in all coral parts.
7. ^{230}Th which is produced by decay of additional U sorbs onto the solid and is consequently not lost along with U.
8. Th is not mobilised (i.e. added or lost) during the whole time.

According to points 1 to 7, the Aqaba data can be modelled using a numerical model with two U components. One accounts for the U incorporated initially during growth, the other one for U which has been post-depositionally added during diagenetic processes. In the model the amount of the lost U is specified by a constant c [yr^{-1}] (*U loss coefficient*) which describes the fraction of additional U which is lost per year. Consequently, c can take values between 0 and 1, with 1 representing the case where the complete additional U is lost subsequently, and 0 standing for the case where no additional U is lost. Unfortunately, there is no method to estimate the timing of U addition and loss. Additionally, there needs not to be only one single period of U addition followed by one period of U loss. Just as well several periods of each

scenario can have taken place in random intervals. Therefore, a fixed number of so-called *events* when diagenetic processes take place have been defined. Each event is assumed to have a specific duration (e.g. 10 kyr), with U being added during the first half and lost during the second half of the event (i.e. 5 kyr of U addition and 5 kyr of U loss). In this work, five equidistant events with each of them lasting 10 kyr have been used for the modelling of the data of the Last Interglacial corals. According to the lower age of the Holocene coral, only one event with a duration of 3,000 yr has been used for modelling. It must be emphasized that the number as well as the duration of these events are arbitrary chosen values due to the fact that they cannot be evaluated from the data. The other values that are necessary for modelling, such as $^{238}U_{add}$ [µg per gram of coral mass and kyr], $\delta^{234}U_{add}$ [‰], the U loss coefficient c [yr^{-1}], and the initial ^{238}U concentration of the coral are adjusted such that the best agreement between measured data and model results is achieved. All model calculations have been performed using Visual Basic Scripts that can be integrated in Microsoft Excel. The Visual Basic code of the model can be found in Appendix B2.

Fig. 4.17 shows a comparison between the model results and the data of coral AQB 1K:

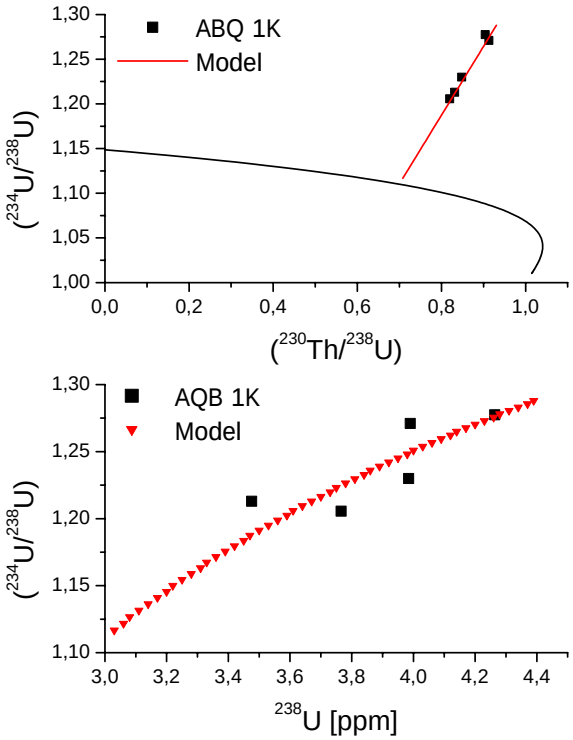

Fig. 4.17: Comparison of modelled and measured data for coral AQB 1K. Between 0 and 0.4 µg per g coral mass and kyr of a high $\delta^{234}U$ com-ponent have been added during five events lasting 10 kyr each. The best agreement between model and data is achieved using values of $c = 2.6 \times 10^{-4}$ yr^{-1} and $^{238}U_{init} = 3.25$ ppm.

The scatter of the data about the modelled trend arises from the natural $^{238}U_{init}$ variations of the corals (2.65 to 3.34 ppm for the recent corals). Table 4.3 gives an overview of the values which have been used to model the data of the Aqaba corals:

Sample	Init. ^{238}U conc. [ppm]	$^{238}U_{add}$ [ppm/kyr]	$\delta^{234}U_{add}$ [‰]	c [y^{-1}]	Number of events	Duration of event [kyr]
AQB 1K	3.25	0 – 0.4	1000	2.6×10^{-4}	5	10
AQB 1A	3.3	0 – 0.4	1000	1.75×10^{-4}	5	10
AQB 1H	3.1	0 – 0.4	1000	1.9×10^{-4}	5	10
AQB 3A	3.5	0 – 0.4	1000	2.5×10^{-4}	5	10
AQB 7G	2.8	0 – 0.05	600	6×10^{-5}	5	10
AQB 10B	3	0 – 0.4	600	6×10^{-4}	1	3

Table 4.3: Compilation of the values used for modelling the data of the Aqaba corals. The number and duration of the events are arbitrarily chosen values, because they cannot be estimated from the data. All other values have been adjusted such that the best agreement between model and data is achieved. The used $\delta^{234}U_{add}$ values are common in groundwaters all over the world (see summary in *Ivanovich & Harmon* (*1992*)).

For corals AQB 1K (Fig. 4.17), AQB 1A, AQB 1H, and AQB 3A rather similar values can be used for modelling. If the proposed number of events (5) with each of them corresponding to five kyr of U addition and five kyr of U loss are used, it is required to add between 0 and 0.4 µg per g coral mass and kyr of a U component with $\delta^{234}U = 1000‰$ (Table 4.3). Consequently, for the U loss coefficient, c, values between 1.75×10^{-4} and 2.6×10^{-4} yr^{-1} must be used to describe the coral data correctly (Table 4.3). Because the diagenetic history of coral AQB 7G seems to have been different than that of the other Last Interglacial corals, different values must be used to model the data of this coral. As described above, the assumption of post-depositional U loss is not necessary for modelling. With the proposed timing of U addition and loss, this coral would gain as well as subsequently lose significantly less U than all other Last Interglacial corals from Aqaba. Overall, the values used for $^{238}U_{add}$ and c are about one order of magnitude lower (Table 4.3). Again, as this coral was collected at 500 m distance from the other corals, this seems to be reasonable.

The data of the Holocene coral AQB 10B can be reproduced using similar values as for the four Last Interglacial corals (Table 4.3), although it has to be assumed that the diagenetic event lasted for 3 kyr only (i.e. 1,500 yr of U addition followed by 1,500 yr of U loss). The used initial ^{238}U contents lie within the range of the recent corals except for coral AQB 3A where an initial ^{238}U content of ~3.5 ppm must be assumed (Table 4.3). For $\delta^{234}U_{add}$, values between 600 and 1000‰ have been used for modelling (Table 4.3), being in good agreement with the values which have been estimated in the previous chapter. Unfortunately, no U-series measurements on groundwater are available for our study region, but values of this magnitude are common all over the world (see summary in *Ivanovich & Harmon* (*1992*)). The high $\delta^{234}U$ values at Aqaba may be the result of leaching of U from surrounding granitic rocks (*Lazar et al., 2002*). High initial $\delta^{234}U$ values measured on other corals from the region (*Gvirtzman et*

al., 1992; Strasser et al., 1992; Lazar et al., 2002) support the assumption that those are related to special hydrologic conditions which seem to be typical for this region. The values used for the added amount of U, $^{238}U_{add}$, and the U loss coefficient, c, cannot be compared to values measured in other materials, because they are estimated from the model and depend strongly on the number, duration, and the timing of the U addition and loss events. A similar scenario of post-depositional U uptake followed by partial loss has been developed for fossil teeth, but in this study no U loss coefficients have been calculated (*Hoffmann & Mangini, 2003*).

4.1.7 The calculation of isochron ages

As it has been shown in the previous chapter, the strong linear correlation between the ($^{234}U/^{238}U$) and ($^{230}Th/^{238}U$) activity ratios detected in the Aqaba corals can be explained by a two-component-model which assumes addition of a high $\delta^{234}U$ component followed by partial loss of the additional U, U_{add}. It has been demonstrated that the slope of the isochrons depends on a variety of factors. As the model assumes that different coral parts gain varying amounts of U_{add} (according to model assumption (MA) 4 (see chapter 4.1.6)) with the same $\delta^{234}U$ (MA 3) at the same time (MA 5), the $(^{234}U/^{238}U)_{add}$ activity ratio will be the same for all coral parts and independent from the amount of U_{add}. Subsequently, some fraction of the U_{add} may be remobilised. In the model U loss is assumed to be proportional to U_{add} (MA 6) which means that the amount of U loss will be larger in coral parts that gained more U_{add}, but the *fraction* of the lost U will be the same for all parts. As it is assumed that U loss happens simultaneously in all parts (MA 6), the activity ratios of the additional component, $(^{230}Th/^{238}U)_{add}$ and $(^{234}U/^{238}U)_{add}$ respectively, will develop in the same way in all coral parts. Consequently, the resulting total activity ratios of a fossil coral, $(^{230}Th/^{238}U)_{meas.}$ and $(^{234}U/^{238}U)_{meas.}$, respectively, can be interpreted as two-component-mixtures and can be described with equations (4.1) and (4.2). Solving equation (4.1) for $^{238}U_{add}$ and inserting into equation (4.2) results in the following equation which describes the isochron-function on a $(^{234}U/^{238}U)$-$(^{230}Th/^{238}U)$-plot:

$$\left(\frac{^{234}U}{^{238}U}\right)_{measured} = \frac{\left(\frac{^{234}U}{^{238}U}\right)_{coral}\cdot\left(\frac{^{230}Th}{^{238}U}\right)_{add} - \left(\frac{^{234}U}{^{238}U}\right)_{add}\cdot\left(\frac{^{230}Th}{^{238}U}\right)_{coral}}{\left(\frac{^{230}Th}{^{238}U}\right)_{add} - \left(\frac{^{230}Th}{^{238}U}\right)_{coral}} + \frac{\left(\frac{^{234}U}{^{238}U}\right)_{add} - \left(\frac{^{234}U}{^{238}U}\right)_{coral}}{\left(\frac{^{230}Th}{^{238}U}\right)_{add} - \left(\frac{^{230}Th}{^{238}U}\right)_{coral}} \times \left(\frac{^{230}Th}{^{238}U}\right)_{measured} \quad (4.6)$$

The addition of a high $\delta^{234}U$ component produces elevated $(^{234}U/^{238}U)_{meas.}$ and lower $(^{230}Th/^{238}U)_{meas.}$ activity ratios. As subsequent U loss is assumed to take place without isotope fractionation, this will not influence $(^{234}U/^{238}U)_{meas.}$, but will result in elevated $(^{230}Th/^{238}U)_{meas.}$ activity ratios. U loss is proportional to U addition. Therefore, the sub-samples which gained the most U_{add} will finally have the highest $(^{234}U/^{238}U)_{meas.}$ and $(^{230}Th/^{238}U)_{meas.}$ activity ratios. Conversely, a sub-sample which did neither gain nor lose any U will plot on the seawater evolution curve. This is equivalent to setting $(^{234}U/^{238}U)_{add}$ and $(^{230}Th/^{238}U)_{add}$ to zero in equation (4.6), because in this case $(^{234}U/^{238}U)_{meas.}$ and $(^{230}Th/^{238}U)_{meas.}$ will correspond to $(^{234}U/^{238}U)_{coral}$ and $(^{230}Th/^{238}U)_{coral}$, respectively. Therefore, in this model the intersection point of the isochron with the seawater evolution curve represents a coral which was not affected by diagenetic processes, and the corresponding activity ratios can be used to calculate the true age of the coral. In the following this is referred to as *isochron dating*.

The results of the application of isochron dating to the Aqaba corals are presented in Figs. 4.14 (page 60) and 4.15 (page 61) and Table 4.4.

Coral	Location	Isochron age [kyrs]	Correlation coefficient R	Isochron slope [‰]	Aragonite content [%]
AQB 3A	Probably upper terrace	121.9 (+7.0 -6.3)	0.987	866	98
AQB 7G	Upper terrace	121.0 (+6.7 -5.3)	0.48	4517	97
AQB 2E	Upper terrace	-	-	-	85
AQB 1K	Lower terrace	106.4 (+8.9 -8.1)	0.993	794	99
AQB 1A	Lower terrace	114.8 (+10.4 -9.2)	0.975	1134	99
AQB 1H	Lower terrace	117.1 (+19.7 -15.3)	0.949	1139	99

Table 4.4: Compilation of the results of isochron dating of the Aqaba corals. All isochron ages have been calculated graphically (see Figs. 4.14 and 4.15) using an initial $\delta^{234}U$ value of 150‰ (modern seawater). The age uncertainties have been estimated using confidence bands at 2σ-confidence-level. As sample AQB 3A was collected not in situ (see chapter 4.1.1), it can be assigned to upper as well as the lower terrace, but it is assumed that it stems from upper one. Because the data of coral AQB 2E do not show a linear correlation, isochron dating cannot be applied to this coral. Most likely this is due to its lower aragonite content.

The isochrons are obtained by performing an error-weighted linear fit. In general, the uncertainty of $(^{230}Th/^{238}U)$ is larger than that of the $(^{234}U/^{238}U)$. Therefore, an error-weighted x-on-y least squares regression has been performed. The age uncertainties have been estimated using confidence bands at 2σ-confidence-level (95%). By intersection of the upper and the lower confidence band with the seawater evolution curve maximum and minimum isochron ages have been calculated (see Figs. 4.14 (page 60) and 4.15 (page 61)). The dominating factors for the age uncertainty are the correlation coefficient *R* and the distance of

the data points from the seawater evolution curve. The larger the correlation coefficient and the closer the points lie to the curve, the smaller is the age uncertainty. To test the sensitivity of the method to the assumed initial $\delta^{234}U$ value, all ages have been recalculated using an initial $\delta^{234}U$ value of 144‰. The differences are always less than 0.6 kyr and generally within the uncertainties of the isochron ages.

Fig. 4.14 shows the isochron plot for the Holocene coral AQB 10B. The calculated isochron age is 3,116 (+167 –156) yr. The 2σ-range of the ^{14}C age of this coral (2,963 (+92 –103) yr) is shown as the bold section of the seawater evolution curve. Both ages agree within their error ranges.

The isochron age of coral AQB 7G which was collected from the higher terrace is 121 (+6.7 –5.3) kyr. For coral AQB 3A which was collected not in situ but was lying on top of the lower terrace an isochron age of 121.9 (+7 –6.3) kyr is calculated. The accordance of both ages suggests that coral AQB 3A stems from the upper terrace as well. Isochron ages of corals AQB 1K, AQB 1A, and AQB 1H that have all been collected from the lower terrace results in ages between 106.4 (+8.9 –8.1) and 117.1 (+19.7 –15.3) kyr (Table 4.4). All isochron ages that have been calculated for the Last Interglacial corals from Aqaba are shown in Fig. 4.18.

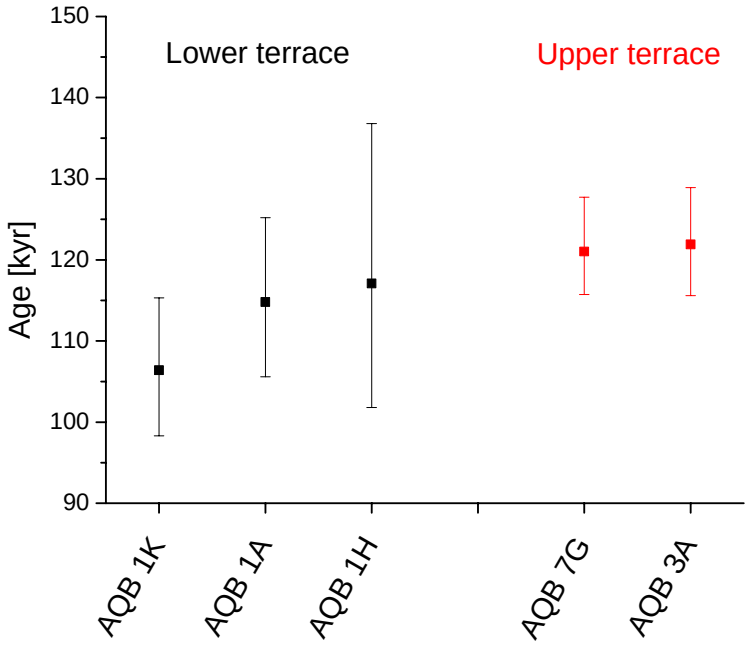

Fig. 4.18: Compilation of the calculated isochron ages according to the terraces where the corals have been collected. The red symbols indicate the corals from the upper terrace the black symbols those from the lower one. Isochron age errors are quoted at 2σ-level (95% confidence). The 2σ-uncertainties are clearly larger than those of common TIMS measured U-series ages of fossil reef corals, but it must be emphasized that this mainly results from the rather large distance of the data points from the seawater evolution curve. If the points lay closer, the resulting errors were remarkably smaller.

Isochron dating cannot be successfully applied to coral AQB 2E, because the activity ratios of this sample are not linearly correlated (Fig. 4.15 f, page 61). As this sample has a significantly lower aragonite content (85%) than the other corals, this probably results from recrystallisation from aragonite to calcite. Although such a process would result in significant loss of U (see chapter 2.2.4), this is not described by the model, because U loss is not restricted to the additional U and does not necessarily happen simultaneously. One possible explanation of the AQB 2E data would be as follows:

(i) Different sub-samples gained different amounts of a high $\delta^{234}U$ component. This is manifested in elevated initial $\delta^{234}U$ values as well as in higher total U content compared to the recent corals (Table C3, Appendix C).
(ii) Later on, recrystallisation from aragonite to calcite occurred in parts of the analysed sub-samples which resulted in loss of significant amounts of U that was initially incorporated in the coral skeleton. Consequently, U loss will not be proportional but independent from U addition. Decay produced ^{230}Th would not be transported away producing elevated ($^{230}Th/^{238}U$) activity ratios and higher U-series ages.

This will result in elevated $\delta^{234}U$ values and ($^{230}Th/^{238}U$) activity ratios, but not in a linear correlation between both of them. Possibly, coral AQB 2E was affected by a combination of the processes described by the model and aragonite recrystallisation.

It is clear from the modelling results in chapter 4.1.6 that the isochron slope contains information about the diagenetic history of the coral (i.e. the timing of U addition and loss). The isochron slopes of the Last Interglacial corals from Aqaba are given in Table 4.4, page 67. While the values for corals AQB 3A, AQB 1K, AQB 1H, and AQB 1A are rather similar, for coral AQB 7G a much higher value is calculated. In consequence, the isochron age of this coral is higher than the U-series ages of its sub-samples, while the other Last Interglacial and the Holocene coral AQB 10B yield isochron ages which are significantly lower than the U-series ages of their sub-samples (Tables C2, C3, and C4, Appendix C). The difference between coral AQB 7G and the other corals indicates that the diagenetic history of this coral must be different. This confirms the results from the estimation of the additional components (chapter 4.1.5) and from modelling (chapter 4.1.6).

It is remarkable that the activity ratios of corals AQB 1K, AQB 1A, and AQB 1H which all stem from the lower terrace together plot on an isochron (correlation coefficient R=0.947) (see Fig. 4.8, page 49). This suggests a very similar diagenetic history for those three corals, especially for the timing of U addition and loss, respectively. The calculation of one isochron age from the data of all three corals results in an age of 113 (+6.5 –5.9) kyr. This isochron age is concordant with the three single isochron ages within uncertainty. As these three corals have been collected relatively close together (<100 m distance), it can be concluded that the diagenetic processes which affected the Aqaba corals did not happen on microscopic or centimetre to metre scales, but rather were the result of specific hydrologic conditions in our

study region. However, it is evident from Fig. 4.8 that these conditions must have been significantly different for corals AQB 7G and AQB 3A.

Finally, it must be mentioned that rather constructive scenarios can be created that produce an isochron with an intersection point corresponding to a wrong age. This would be the case if U loss was not restricted to the additional U, but was proportional to the total U content of the sample. In such a scenario the intersection point would be shifted towards too old isochron ages. In the same way, if U loss was not proportional to U addition, but if all sub-samples would lose the same amount of U, the resulting data points would plot on a curve which would be very close to a straight line. In this case the whole isochron (curve) would be shifted towards ages that are too old. Although it cannot be ruled out completely that this is the case for the Aqaba corals, two facts directly argue in favour of the proposed isochron approach: (i) all well preserved corals from Aqaba show a strong linear correlation and no tendency towards a curve and even more important (ii) the concordance between the isochron age and the ^{14}C age of the Holocene coral AQB 10B.

4.1.8 The paleo sea level reconstruction at Aqaba

The ages calculated for the two corals from the upper terrace suggest that this terrace corresponds to the Last Interglacial (MIS 5e) sea level peak (see Fig. 3.4, page 39, for comparison). Because of the rather large age uncertainties, a differentiation between both terraces by their age is not possible, but in general for the lower terrace younger ages are calculated. This suggests that the lower terrace might represent a second sea level peak which was subsequent to the Last Interglacial highstand. Because of the large uncertainty of the isochron ages it could also be possible that the lower terrace corresponds to MIS 5c (timing: ~105-100 kyr, see Fig. 4.18). But as the magnitude of the MIS 5c sea level peak was about 15 to 20 m lower than the MIS 5e peak (see Fig. 3.4), this seems to be rather unlikely.

In addition to the large isochron age errors, further difficulties arise from the lack of knowledge about the vertical uplift rate at the study region. To calculate paleo sea levels with equations (3.2) or (3.3), an estimate of the vertical uplift rate is essential (see chapter 3.1.2), but there are no values available for the sampling location at Aqaba from the literature. For the southern tip of the Sinai Peninsula (lying 150-200 km southwards of Aqaba, see Fig. 4.1, page 44) values between 0.085 m/kyr (*Gvirtzman, 1994*) and tectonically stable conditions (*El-Asmar, 1997*) have been reported. If this was the case at Aqaba, the Last Interglacial sea level peak had a magnitude of +7-10 m r.p.s.l. according to the elevation of the upper terrace. As this value is higher than the values reported from other locations worldwide (+3-6 m r.p.s.l., compare Fig. 3.4 and the discussion in chapter 3.1.5), it seems unlikely that the Aqaba region is tectonically stable though it cannot be excluded from the data. If an upper limit of 0.08 m/kyr for the uplift rate is used, values about –1 m r.p.s.l. for the upper terrace and –4 to

-5 m r.p.s.l. for the lower one are calculated. This suggests that sea level was lower during the Last Interglacial than today. As it is widely accepted that sea level was a few meters higher than at present during that time, an uplift correction of 0.08 m/kyr seems to be too large. Another possibility to estimate the uplift rate is to assume that the upper terrace corresponds to the MIS 5e sea level peak and to calculate an average uplift rate from its actual height. This means that the upper terrace (+7-10 m above present sea level) would have lifted up about ~4 m since the Last Interglacial (+3-6 m r.p.s.l.). Assuming an average age of 125 kyr for MIS 5e results in an average uplift rate of 0.032 ± 0.017 m/kyr (the uncertainty has been calculated by linear error propagation). As there is only one in situ coral from the upper terrace (AQB 7G) and the associated isochron error is rather large (~5.5%), this is only a rough approximation, but based on the available data a more accurate determination is not possible. The resulting paleo sea levels are shown in Fig. 4.19.

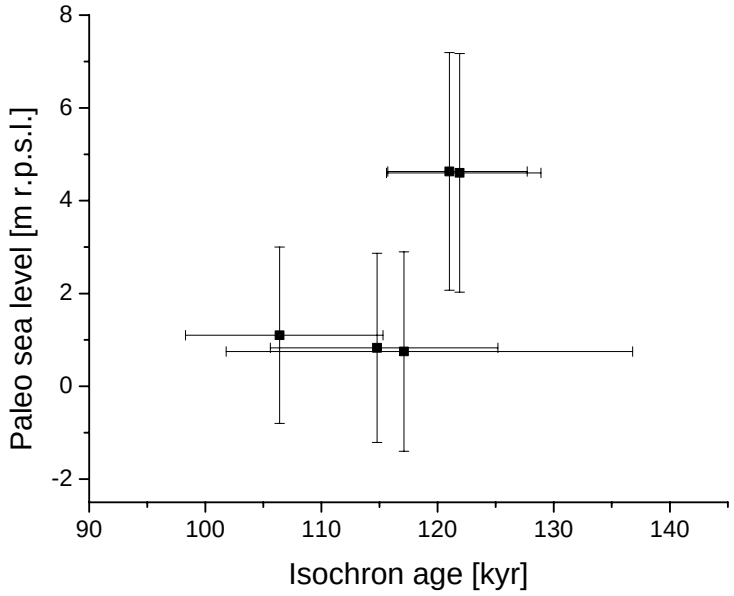

Fig. 4.19: The paleo sea levels at Aqaba based on the calculated isochron ages. Paleo sea levels have been calculated using equation (3.2) and assuming an uplift rate of 0.032 ± 0.017 m/kyr. Uncertainties have been calculated using linear error propagation.

It is evident from Fig. 4.19 that the sea level reconstruction based on the Aqaba corals is associated with large uncertainties in magnitude as well as in timing. In equation (3.3) the living depth of the corals is considered as well (see chapter 3.1.2). If this equation had been used to calculate the paleo sea levels, the resulting uncertainties would be even larger as *Porites* corals grow in water depths down to 50 m at Aqaba (*Felis et al., 2003*). However, if an uplift rate between the above mentioned values is assumed, the range of paleo sea levels calculated for both terraces is consistent with Last Interglacial sea levels reported in other studies from the Red Sea (*Gvirtzman, 1994; El-Asmar, 1997; Siddall et al., 2003*).

The likeliest interpretation of the terrace structure at Aqaba is that the lower terrace corresponds to a second sea level highstand that occurred after the MIS 5e peak and was a few meters lower. Such a sea level regression-transgression cycle during the Last Interglacial has also been detected on the Bahamas (*Wilson et al., 1998; Hearty & Neumann, 2001*). An extended discussion of the stability of the Last Interglacial climate can be found in *Holzkämper* (*2004*). Unfortunately, the sea level data from Aqaba do not allow an accurate determination of the timing as well as the magnitude of the sea level fluctuations.

4.1.9 Improving the calculation of isochron ages and errors

As described in chapter 4.1.7, the uncertainty of isochron ages can be estimated using confidence bands at a confidence level of interest (see Figs. 4.14 (page 60) and 4.15 (page 61)). While this method is adequate and yields reliable error ranges in many cases, problems may arise if correlation coefficients are low or data point distances are small. In such cases more complex methods of error calculation should be used to avoid significant over- or underestimation. In this chapter a more elaborate method is presented which is based on a Monte-Carlo-approach.

From a statistical point of view the method that has been used to calculate the isochron ages and errors has some slight weaknesses:

a) For linear fitting a conventional y-on-x least squares regression has been used. Such fitting algorithms only weight the y-errors. In the case of the isochron plots both x- (i.e. (^{230}Th/^{238}U)) and y-values (i.e. (^{234}U/^{238}U)) are afflicted with analytical errors. To minimize this problem a x-on-y least squares regression has been performed, because normally the analytical uncertainty associated with Th measurements is larger than that of U measurements.
b) The fitting algorithm does not account for possible correlations between x-and y-errors.
c) In the same way, the calculation of the confidence limits does neither consider the analytical errors nor the respective correlations that are associated with the data.
d) Even worse, the confidence limits are only valid for the data range. Therefore, strictly speaking they should not be extrapolated.
e) In addition, the initial δ^{234}U value is also associated with some uncertainty, because it is based on analytical measurements of recent corals. This uncertainty is of course propagated to the construction of the seawater evolution curve.

In the following, an approach is presented which regards all the above mentioned points.

4.1.9.1 The recalculation of the isochron ages

The application of isochrons for age determinations is common practice in geochronology and especially in U-series dating of samples with detrital contamination (see chapter 2.1.3). All these approaches have in common that the analytical data are fitted linearly and the sample age can be obtained from either the slope or the y-intercept of the isochron (*Ludwig, 2003*). Since the late 1960's several algorithms have been published that can be used to perform such linear fits. All these so-called EWLS (error-weighted-least-squares)-algorithms account for x- and y-values being associated with analytical errors, but only some of them pay attention to error correlations (*York, 1969; Titterington & Halliday, 1979; Kent et al., 1990*). Therefore, the application of an EWLS-algorithm to obtain the coral isochrons would solve problems a) and b). The results that are presented in the following have been obtained using the EWLS-algorithm provided by *Albarède* (*1995*).

In contrast to usual isochrons the coral isochron ages cannot be simply calculated from either the slope or the y-intercept. In this special case the slope as well as the intercept are needed, because the isochron age is calculated from the intersection point of the isochron with the seawater evolution curve (see Figs. 4.14 and 4.15). The isochron age can be calculated either graphically or numerically. The isochron is given as:

$$\left(\frac{^{234}U}{^{238}U}\right) = a + b\left(\frac{^{230}Th}{^{238}U}\right), \tag{4.7}$$

where a and b are the y-intercept and the slope, respectively, which are calculated by the EWLS-algorithm.

The seawater evolution curve can be described by combining the closed system equations (2.5) and (2.6) respectively and inserting the appropriate initial $\delta^{234}U$ value. The following calculations have been performed using a value of 1.1466 ± 0.0014 which has been obtained by measurements on modern corals from various regions worldwide (see *Delanghe et al.* (*2002*) and also chapters 2.2.1 and 2.2.3). By combining equation (4.7) with the seawater evolution curve the isochron age equation can be calculated:

$$(1-a) + \left(\left(\frac{^{234}U}{^{238}U}\right)_{init.} - 1\right)\cdot e^{-\lambda_{234}\,t} + b\left(e^{-\lambda_{230}\,t} - 1\right) + \tag{4.8}$$

$$+ \frac{\left(\left(\frac{^{234}U}{^{238}U}\right)_{init.} - 1\right)\cdot b\cdot e^{-\lambda_{234}\,t}\cdot\lambda_{230}\cdot\left(e^{(\lambda_{234}-\lambda_{230})\,t} - 1\right)}{\lambda_{230}-\lambda_{234}} = 0$$

The isochron age can be calculated by solving equation (4.8) numerically for t.

The recalculation of the isochron ages of the Last Interglacial corals from Aqaba results only in slight variations compared to those given in Table 4.4, page 67. The differences range from 0 to 0.5 kyr and are negligible if the isochron age uncertainties are taken into account. They arise from (i) the usage of the slightly different initial $\delta^{234}U$ value (146.6‰ instead of 150‰) and (ii) from the differences in the fitting procedure as now x- and y-errors and the respective error correlations are considered. The recalculated ages are given in Table 4.5**,** page 81.

4.1.9.2 The recalculation of the isochron age errors

All EWLS-algorithms estimate the error of the slope and y-intercept, respectively, by propagating errors and error correlations of the input data using first order expansion (*Ludwig, 2003*). Generally, the error of the isochron age could also be estimated this way using equation (4.8) and the uncertainties given for a, b, and $(^{234}U/^{238}U)_{initial}$, but in the case of asymmetric distributions or large isochron errors first order methods of error estimation are inadequate, and more accurate methods should be used (*Ludwig, 2003*). A very flexible method of error estimation regardless of the complexity of the problem is the Monte-Carlo-method (*Albarède, 1995; Fishman, 1997; Gentle, 2003*). The basic idea behind this method is to generate a large number (N) of realizations of the input data (in the case of the coral isochrons: a, b, and $(^{234}U/^{238}U)_{initial}$) according to their assigned errors, error correlations and probability distributions. Then, the parameter of interest (i.e. the isochron age) is calculated with each of these N sets of the generated input data. In this manner a probability distribution for the parameter of interest can be obtained. Confidence limits of any desired confidence level can be constructed from this distribution. Though it is inelegant and computationally expensive, the Monte-Carlo-method is one of easiest methods of error estimation to understand and implement (*Ludwig, 2003*).

It can be shown that – if the analytical errors are normally distributed – the errors of the regression slope and intercept estimated by EWLS-algorithms are also normally distributed (*Kent et al., 1990*). If it is assumed that the modern seawater value also follows a normal distribution, the estimation of the isochron age error by a Monte-Carlo-method would be rather simple: There had just N normally distributed values for a, b, and $(^{234}U/^{238}U)_{initial}$ to be generated and inserted into equation (4.8). Then N isochron ages could be calculated, and the appropriate error distribution could be obtained. An error estimation like this would solve problems c), d) and e).

Unfortunately, in most cases the situation is more complex. All EWLS-algorithms rely on two basic assumptions: (i) All of the observed scatter of the data about the regression line arises from data-point analytical error and (ii) data point errors are known to conform a

normal distribution (*Ludwig, 2003*). While the latter normally should be valid for TIMS measured U-series activity ratios, the former assumption needs to be tested for any particular dataset. Therefore, all EWLS-algorithms calculate a statistical parameter that enables to compare the observed scatter with the average amount of scatter expected from the analytical errors. This so-called MSWD (Mean Square of Weighted Deviates) parameter is given by equation (4.9) (*McIntyre et al., 1966; Kent et al., 1990; Albarède, 1995; Ludwig, 2003*):

$$MSWD = \frac{1}{n-2}\sum_{i=1}^{n}\left(\frac{resid_i}{\sigma_{y_i}}\right)^2 = \frac{1}{n-2}\,S^2, \qquad (4.9)$$

where $resid_i$ is the difference between the measured y_i and the y_i predicted from the regression slope and intercept, for each x_i. σ_y is the analytical error of the respective data point, and n the number of data points. S^2 is often also referred to as the *residual sum of squares*.

MSWD values much greater than one indicate the presence of more scatter than predicted by the analytical errors and imply that either the analytical errors were underestimated or that some non-analytical source of scatter (often also referred to as *geological scatter*) exists. In contrast, values much less than one suggest that the analytical errors were overestimated (*Ludwig, 2003*). But all for that, the MSWD is an inadequate parameter to test for the presence of geological scatter, because the highest MSWD value considered to justify the assumptions of an isochron strongly depends on the number of data points. The probability that the assigned analytical errors would produce the observed amount of scatter can be calculated from the χ^2-distribution of (n-2) × MSWD about (n-2). This is usually referred to as the *probability of fit* (*Ludwig, 2003*). By convention, probabilities exceeding 0.05 are considered to satisfy the isochron assumptions, while lower probabilities indicate the presence of geological scatter. Such isochrons are often called *excess scatter isochrons* or *errorchrons*. The MSWD values and probabilities of fit calculated for the Aqaba corals are given in Table 4.5, page 81. The probabilities of fit range from 2.54×10^{-6} (AQB 1K) to 3.94×10^{-11} (AQB 1A) indicating the presence of non-analytical scatter for all Last Interglacial corals from Aqaba. It must be emphasized that this is not uncommon for real-world systems, where it often is a matter of dealing with low probabilities of fit and high MSWD values, especially with the very small errors produced by TIMS- or ICP-MS analyses (*Kent et al., 1990; Ludwig, 2003*).

Usually, ages obtained from excess scatter isochrons are not discarded, but rather the additional uncertainty is accounted for by enlarging the isochron age errors. The most common method is to expand the slope and intercept errors by the square root of MSWD (sometimes also referred to as an *overdispersion* or *excess scatter* parameter), which is equivalent to assuming that the geological scatter in the data has a Gaussian distribution about the regression line and is proportional to the analytical errors (*Kent et al., 1990; Albarède,*

1995; Ludwig, 2001; Ludwig, 2003). As the estimation of the MSWD value is based on a finite number of data points, strictly speaking the distribution of the regression/slope errors is no longer Gaussian. The additional uncertainty arising from this fact can be included by multiplying the respective errors by a Student's t factor to construct a confidence level of interest (*Ludwig, 2003*). According to *Kent et al.* (*1990*), the distribution of the excess scatter parameter MSWD is:

$$MSWD \sim \frac{S^2}{\chi^2_{n-2}}, \tag{4.10}$$

where χ^2_{n-2} is the χ^2-distribution with n-2 degrees of freedom.

Generally, in the case of excess scatter there are two possible ways of estimating the uncertainty of the coral isochron age by a Monte Carlo simulation. One possibility is to use the results that are calculated by the EWLS-algorithm for the slope/intercept errors. Then the isochron age uncertainty can be computed as listed below (Algorithm A):

1) Set up the isochron (i.e. plot the measured data on a ($^{234}U/^{238}U$)-($^{230}Th/^{238}U$)-diagram) and perform an EWLS regression.
2) Calculate the residual sum of squares, S^2, using equation (4.9) (the S^2 values for the Aqaba corals can be calculated by multiplying the MSWD values by (n-2) in Table 4.5**,** page 81).
3) Generate a χ^2_{n-2} distributed random number (for methods of random number generation see for example *Fishman* (*1997*) or *Gentle* (*2003*)).
4) Calculate the appropriate MSWD value with equation (4.10).
5) Expand all entries of the slope/regression covariance matrix (which is provided by the EWLS-algorithm) by $\sqrt{MSWD}$.
6) Generate normally distributed values for intercept a and slope b using this expanded covariance matrix. As a and b usually are strongly anti-correlated, it is very important that the respective error correlation is taken into account.
7) Generate a normally distributed initial ($^{234}U/^{238}U$) value according to the values of *Delanghe et al.* (*2002*).
8) Calculate the corresponding coral isochron age by numerically solving equation (4.8).
9) Repeat steps 3) – 8) for an adequate number of times N.
10) Sort the isochron ages.
11) Build the plus- and minus-errors at the confidence level of interest by subtracting the isochron age from the i^{th} and j^{th} elements of the array, where $i = 0.5 \times (100\text{-}C) \times N/100$, $j = N - i + 1$, and C is the confidence level in percent (*Ludwig, 2003*).

Generally, Algorithm A solves all the above listed problems (c-e), but there may arise some problems from the results of the EWLS-algorithm. As mentioned above, the regression slope/intercept errors of EWLS-algorithms are estimated by first-order-expansion. The results from one algorithm to another may differ, but as long as the assumptions of an isochron are met and the errors of the slope/intercept are not too large these differences will be slight (*Ludwig, 2003*). Unfortunately, these requirements are not fulfilled for all of the Aqaba corals. For example, for coral AQB 7G large differences are calculated if different EWLS-algorithms are used. While the fitting routine of ISOPLOT (*Ludwig, 2001*) which uses the algorithm of *York* (*1969*) gives 95% confidence intervals of a = -2.28 ± 11 and b = 4.5 ± 15, the EWLS-algorithm by *Albarède* (*1995*) calculates values that are three times higher (a = -2.28 ± 34, b = 4.5 ± 45). These differences would be directly propagated to the isochron age error if Algorithm A was used. As a consequence, the isochron age error would strongly depend on the choice of the EWLS-algorithm. Therefore, a different method of error estimation in the case of excess scatter must be found.

The following Monte-Carlo-algorithm (Algorithm B) acts on the same two assumptions as the previous one (i.e. (i) the geological scatter is normally distributed and proportional to the analytical errors, and (ii) the MSWD value is distributed according to equation (4.10)), but avoids the use of the slope/intercept errors calculated by an EWLS-algorithm. The single steps of Algorithm B are listed below. The most important steps of the Monte-Carlo-simulation and the resulting distributions are illustrated in Figs. 4.20-4.24 considering coral AQB 3A as an example.

1) Set up the isochron and perform an EWLS regression.
2) Calculate the residual sum of squares S^2.
3) Generate a χ^2_{n-2} distributed random number.
4) Calculate the appropriate MSWD value with equation (4.10) (Fig. 4.20).
5) Expand the analytical errors of each data point spanning up the isochron by $\sqrt{MSWD}$ (i.e. multiply all entries of the covariance matrix of each data point by $\sqrt{MSWD}$).
6) Generate n “new” normally distributed data points according to the expanded analytical errors and the respective correlations (Fig. 4.21).
7) Fit the “new” set of data points linearly with an EWLS-algorithm (Fig. 4.22).
8) Generate a normally distributed initial ($^{234}U/^{238}U$) activity ratios according to the values of *Delanghe et al.* (*2002*) (Fig. 4.23).
9) Calculate the corresponding coral isochron age by numerically solving equation (4.8) (Fig. 4.24).
10) Repeat steps 3) – 9) for an adequate number of times N.
11) Sort the isochron ages.
12) Build the plus- and minus-errors at the confidence level of interest by subtracting the isochron age from the i^{th} and j^{th} elements of the array.

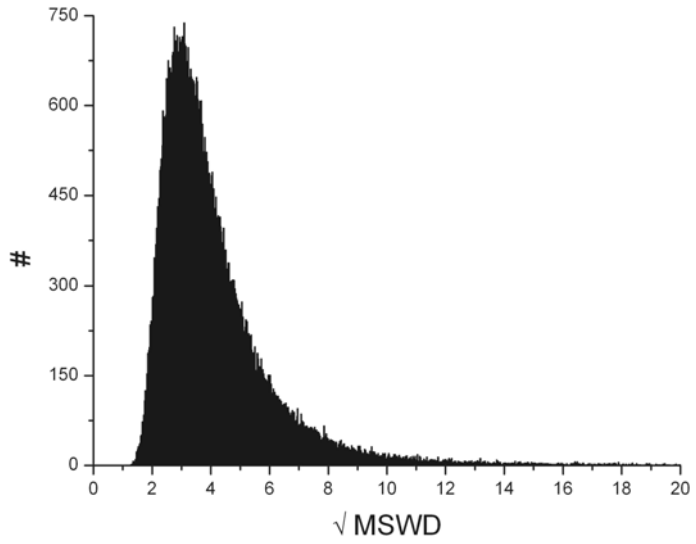

Fig. 4.20: The resulting distribution of 100,000 $\sqrt{MSWD}$ -values calculated for coral AQB 3A. $\sqrt{MSWD}$ -values have been calculated using equation (4.10). The values range from 1.28 to 67.41, with a mean of 4.11. To illustrate the shape of the distribution adequately the largest values are not shown in this plot. The higher mean value compared to that calculated from equation (4.9) ($\sqrt{MSWD}$ = 3.28) arises from the additional uncertainty because of the rather small number of data points (n = 6).

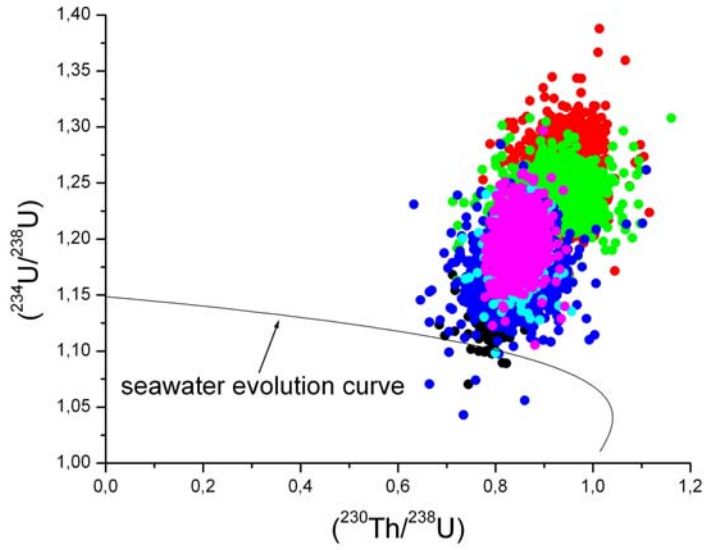

Fig. 4.21: 100,000 realizations of the six data points of coral AQB 3A (see Fig. 4.15, page 61, for the 'original' plot). The analytical errors have been expanded by the 100,000 values generated for $\sqrt{MSWD}$ (mean value: 4.11, Fig. 4.20) and are assumed to be Gaussian distributed. The shape of the scatter-plot of each data-point indicates the correlation between x- and y-errors which range from 0.065 to 0.185 for coral AQB 3A. Points that plot far from their respective scatter-plots result from very high $\sqrt{MSWD}$ values (Fig. 4.20).

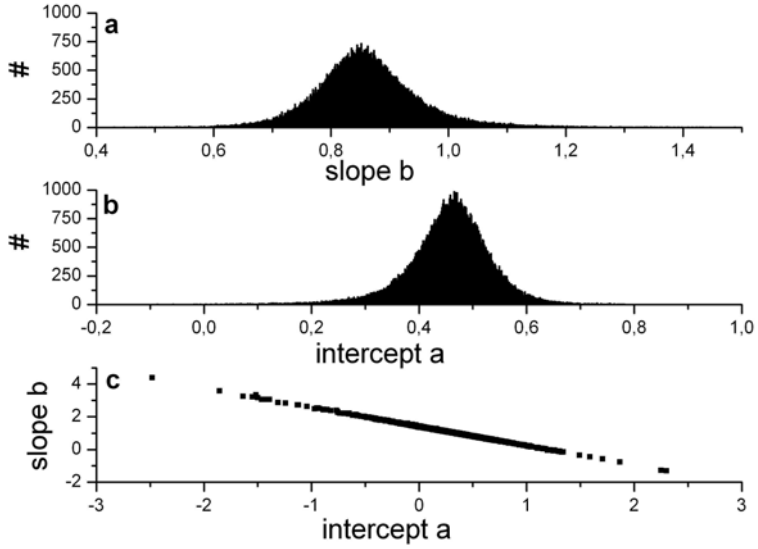

Fig. 4.22: (**a** and **b**) The resulting distributions of 100,000 EWLS-regressions through the generated data points for coral AQB 3A (Fig. 4.21). To illustrate the shape of the distributions adequately not all values are shown. The distributions of both parameters a and b are not perfectly symmetric. The distribution of the slope has a slightly larger tail towards higher values and – because of the strong anti-correlation (Fig. 4.22 c) – that of the intercept towards lower ones. For coral AQB 3A the 95% confidence intervals of both regression parameters are comparable with those calculated by usual EWLS-algorithms – except for the slight asymmetry.
(**c**) The intercept a and the slope b are strongly anti-correlated (ρ_{ab} = -0.999).

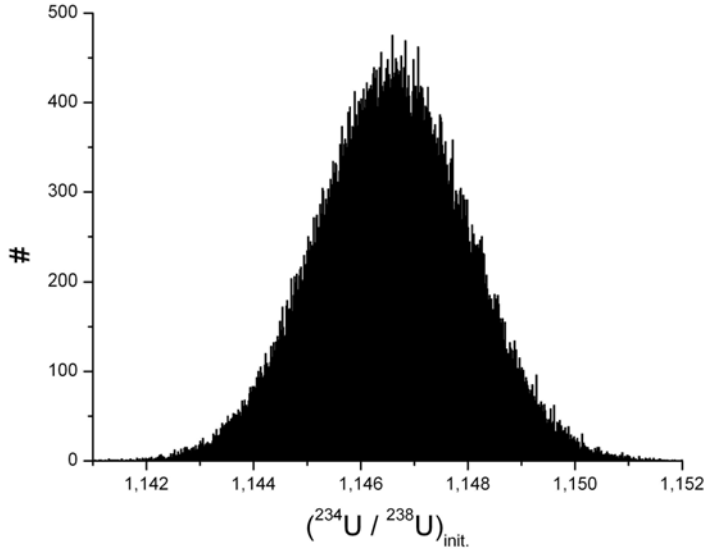

Fig. 4.23: 100,000 normally distributed values for the initial coral ($^{234}U/^{238}U$) activity ratio (modern seawater value). The values have been generated using $\mu((^{234}U/^{238}U))$ = 1.1466 and σ = 0.0014 according to the results of *Delanghe et al.* (*2002*).

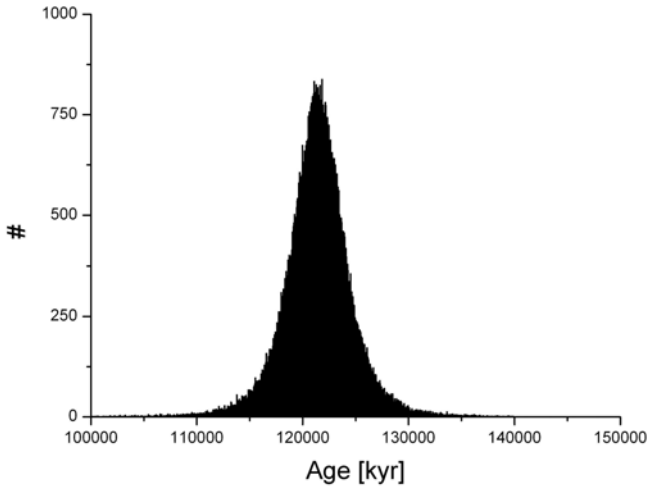

Fig. 4.24: The resulting isochron age distribution for coral AQB 3A (N = 100,000 values). The mean value agrees with the calculated isochron age of 121.4 kyr (Table 4.5, page 81). The error distribution is rather symmetric (+6.6 –6.8 kyr), showing that the slight asymmetry of the fit parameters is at least partly compensated by the isochron age calculation.

The great advantage of Algorithm B compared to the traditional methods of error estimation is that the computation is rather simple and the mathematical treatment of the complex and non-linear equations that are used by the EWLS-algorithms (*Albarède, 1995*) is avoided. Furthermore, it is not necessary to assume that a and b are normally distributed.

It must be pointed out that this approach can be also used to estimate the errors of the slope/intercept values if Algorithm B is slightly modified: Steps 8) and 9) are not necessary for such an estimation. Instead, the resulting N values for intercept a and slope b, respectively, must be sorted. The confidence levels for the fitting results can then be obtained from these arrays. In consequence, Algorithm B can also be used to calculate confidence limits for all kinds of isochrons used for age determination in geochronology.

The Visual Basic script of Algorithm B that has been used to perform the calculations presented in this work is given in Appendix B3.

4.1.9.3 Results and discussion of the recalculation of the Aqaba isochron age errors

An important aspect of error estimation by Monte-Carlo-methods is that a sufficient number of iterations, N, needs to be performed. If N is chosen too small, the involved distributions are not correctly approximated and repeated simulations will yield varying results. For the isochron ages of the Aqaba corals N = 100,000 iterations proved to yield reproducible age errors.

The results of the recalculation of the isochron ages and errors are presented in Table 4.5:

Sample	Isochron age using a x-on-y least squares regression and confidence bands [kyr]	Isochron age using an EWLS-algorithm [kyr][a]	MSWD	Probability of fit	Isochron age error using Algorithm B [kyr][d]
AQB 3A	121.9 (+7 –6.3)	121.4	10.75	1.03×10^{-8}	+6.6 –6.8
AQB 7G	121.0 (+6.7 –5.3)	121.5	10.73	4.77×10^{-7}	+out of range –51.3
AQB 1K	106.4 (+8.9 –8.1)	106.4	9.58	2.54×10^{-6}	+8.3 –9.0
AQB 1A	114.8 (+10.4 –9.2)	114.3	13.65	3.94×10^{-11}	+9.3 –9.8
AQB 1H	117.1 (+19.7 –15.3)	116.7	10.45	1.84×10^{-8}	+17.7 –35.9

Table 4.5: Comparison of the results calculated by the 'original' method (chapter 4.1.7) and the approach presented in chapters 4.1.9.1 and 4.1.9.2. The isochron ages in the second column are calculated graphically (Fig. 4.15, page 61), and those in the third column according to equation (4.8). MSWD values are calculated using equation (4.9). The calculation of the Probability of fit values is described in chapter 4.1.9.2. The Monte-Carlo-simulation based errors are calculated using Algorithm B. N = 100,000 iterations have been performed.

For corals AQB 3A, AQB 1K, and AQB 1A the recalculation results in error ranges comparable to those calculated using confidence bands. Instead, the isochron age error of coral AQB 1H is about two times larger, and that of AQB 7G is extremely enlarged.

The large differences observed for coral AQB 7G are not due to larger MSWD- or lower Probability of fit-values (Table 4.5), but rather due to the smaller distance of the data points spanning up this isochron. If the points lie very close to each other, the regression slope/intercept errors are substantially enlarged. This is also the case if conventional first-order-expansion methods are used (see page 77, chapter 4.1.9.2, where significantly different results for coral AQB 7G are obtained by ISOPLOT (*Ludwig, 2001*) and the EWLS-algorithm proposed by *Albarède* (*1995*)). With Algorithm B highly asymmetric 95% confidence intervals are calculated for the intercept (a = 2.28 +5.72 –0.05) as well as the slope (b = 4.5 +0.07 –7.51) of the isochron of coral AQB 7G. In addition, the Algorithm B intervals are only half as wide as the ISOPLOT ones. This illustrates very nicely that the assumption of normally distributed slope/intercept errors may be violated in the case of large uncertainties for the fitting parameters. Of course, asymmetric error distributions for a and b directly result in asymmetric coral isochron age distributions. It is remarkable that Algorithm B produces larger minus- than plus-errors for all Aqaba corals except for coral AQB 7G, while the estimation with confidence limits always resulted in larger plus-than minus-errors (Table 4.5).

In extreme cases (i.e. very large $\sqrt{MSWD}$ values and consequently large uncertainties in the fitting parameters) the isochron and the seawater evolution curve do not intersect. If the isochron slope is positive, the seawater evolution curve is missed to the left (suggesting an isochron age <0 kyr), if the slope is negative, it is missed to the right (suggesting an infinite isochron age). In such cases the calculation of the isochron age is not possible. In general, this

happens very seldom (e.g. in 21 out of 100,000 cases for coral AQB 3A), but for coral AQB 7G the seawater evolution curve is missed 4,988 times to the right and 192 times to the left. This arises from the very large slope/intercept uncertainties and the highly asymmetric shape of the respective distributions (see above). Even though the error range calculated by Algorithm B is about two times smaller than that calculated by ISOPLOT (*Ludwig, 2001*) and about six times smaller than that estimated by *Albarède's* (*1995*) EWLS-algorithm, the relative error ranges still exceed 100% (253% for intercept a, 168% for slope b). This is directly propagated to the isochron age uncertainty. If N = 100,000 iterations are performed, the 95% confidence intervals are constructed from the 2500^{th} and $97{,}500^{th}$ value of the sorted ranked array, respectively (see chapter 4.1.9.3). Because more than 2,500 isochrons result in uncalculable (i.e. infinite) isochron ages, it is not possible to give a plus-error for the isochron age of coral AQB 7G (Table 4.5).

4.1.9.4 Using additional information to improve the isochron age accuracy

It has been shown in chapter 4.1.8 that it is difficult to reconstruct past sea level changes from the Aqaba data because of the rather large isochron age uncertainties. This problem cannot be solved with the Monte Carlo approach presented in the previous chapter as for some corals the age uncertainties are even enlarged.

However, Monte Carlo methods can also be used to deal with more subtle questions of error estimation (*Ludwig, 2003*). For example, if there is additional knowledge about the sample age, this can be included into the Monte Carlo routine as a prior constraint (*Bernardo & Smith, 2000*). This is clearly the case for the Aqaba corals, because (i) the elevation of the fossil terraces is in the range reported for Last Interglacial reef terraces along the Red Sea coast (see chapter 4.1.1), (ii) the U-series ages of all analysed sub-samples range from 113.7 ± 1.2 to 151.6 ± 1.3 kyr (see Tables C3 and C4, Appendix C and chapter 4.1.3), and (iii) all isochron ages – especially those associated with the smallest errors – are between 106.4 +8.3 –8.1 and 121.4 +6.6 –6.8 kyr (Table 4.5). Therefore, it can be concluded that all Aqaba corals most likely grew during MIS 5. Furthermore, as discussed in chapter 4.1.8, the likeliest interpretation of the terrace structure is that there have been two sea level highstands within the Last Interglacial (MIS 5e) with the later one being a few meters lower than the first one.

If all this is taken into account, it can be assumed that all Aqaba corals grew between 150 and 100 kyr. This additional age information can be included in the Monte Carlo error estimation. With the *a priori* assumption of a coral age between 150 and 100 kyr all trials resulting in isochron ages outside of this range can be ignored, because they violate the *a priori* constraints (*Ludwig, 2003*). The confidence interval for the isochron age can then be obtained from the remaining ("successful") trials in the same way as before (see chapter

4.1.9.2). The resulting distribution of the isochron ages for coral AQB 3A is shown in Fig. 4.25:

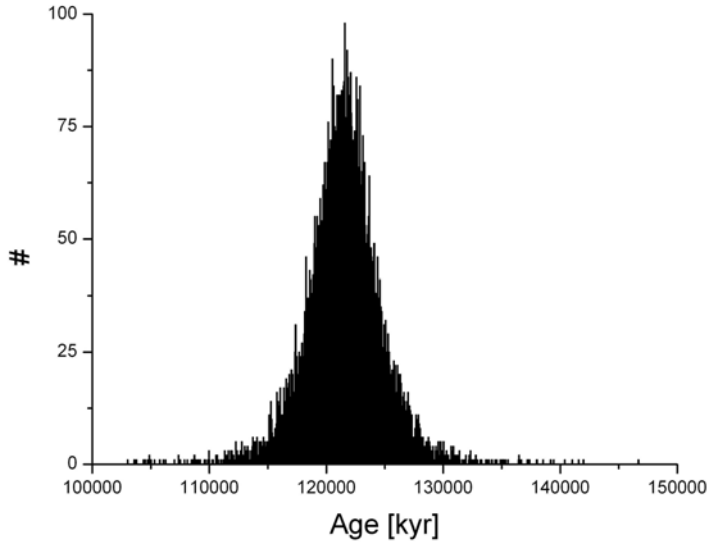

Fig. 4.25: The resulting distribution of the isochron ages using the *a priori* assumption that the true coral age is between 150 and 100 kyr. Algorithm B was iterated until 10,000 successful (i.e. yielding an isochron age within the age constraints) trials had been performed. The shape of the distribution is very similar to that of the simulation without age constraints (Fig. 4.24, page 80). This arises from the minor influence of the age constraints on the results of the Monte Carlo simulation, because 95 % of the computed ages are between 114.6 and 128 kyr. Therefore, only a few ages are ignored by the new Algorithm and the total error range remains almost the same. However, while Algorithm B yielded larger minus- than plus-errors, the simulation with *a priori* constraints results in larger plus- than minus-errors (Table 4.6). This slight modification is generated, because the isochron age lies closer to the lower (100 kyr) than to the upper bound (150 kyr).

Table 4.6 shows a comparison of the isochron age errors calculated with the three different approaches:

Sample	Isochron age using an EWLS-algorithm [kyr][a]	Age error using confidence bands [kyr]	Age error using Algorithm B [kyr]	Isochron age error using Algorithm B and a priori age constraints [kyr][d]
AQB 3A	121.4	+7.0 –6.3	+6.6 –6.8	+6.8 –6.5
AQB 7G	121.5	+6.7 –5.3	+out of range –51.3	+15.6 –18.7
AQB 1K	106.4	+8.9 – 8.1	+8.3 –9.0	+8.4 –5.3
AQB 1A	114.3	+10.4 –9.2	+9.3 –9.8	+9.4 –8.8
AQB 1H	116.7	+19.7 –15.3	+17.7 –35.9	+15.0 –12.8

Table 4.6: Comparison between the isochron age errors as they are calculated by the three different approaches (confidence bands, Monte Carlo, and Monte Carlo with *a priori* constraints).

For corals AQB 3A and AQB 1A the isochron age errors are only slightly reduced (<5%), because most of the computed ages already lay within the age constraints. For coral AQB 1K mainly the minus-error is reduced (~41%), because the isochron age (106.4 kyr) lies very close to the lower bound (100 kyr). The total reduction of the isochron age error is ~21%. The rather large error of coral AQB 1H is nearly halved by the new method. This indicates the great potential of the inclusion of additional age information into a Monte Carlo simulation. The greatest improvement is of course achieved for coral AQB 7G. While it was not possible to assign an isochron age error to this coral with Algorithm B, the new routine yields a 95% confidence interval of +15.6 –18.7 kyr that is comparable with that of coral AQB 1H.

Obviously, the resulting error ranges could be further reduced by a choice of closer age constraints such as assuming that all corals grew during MIS 5e, but it has to be emphasized that the usage of wrong age constraints could result in incorrect error ranges. For example, if they are chosen too narrow, the calculated error range will be too narrow as well. For this reason, such an approach should only be used with some caution. In this work the constraints have been chosen rather wide, because the intention rather was to indicate the potential of such an approach than to improve the age precision.

4.1.10 Conclusions I

The six Last Interglacial and the Holocene *Porites* corals from Aqaba, Jordan, show a very high degree of diagenetic alteration. This is manifested in extremely elevated initial $\delta^{234}U$ values as well as slightly higher ^{238}U and ^{232}Th content. In contrast, the analysed recent corals from the Gulf of Aqaba show no evidence of alteration.

The correlation between ^{238}U content and $\delta^{234}U$ suggests that the elevated $\delta^{234}U$ values have been produced by addition of a high $\delta^{234}U$ component after deposition, but the mechanism of addition as well as the gaining component remain unidentified. Modelling of the data has shown that the activity ratios cannot be explained by U addition alone, but by U addition followed by partly remobilisation of the added U. It has been shown that post-depositional addition of ^{230}Th as assumed by other authors can be ruled out. Furthermore, the application of the other models results in controversial coral ages.

The activity ratios of different sub-samples of the Holocene and five of the six Last Interglacial corals are strongly linearly correlated on a $\delta^{234}U$-($^{230}Th/^{238}U$)-diagram. The intersection point of the isochron with the seawater evolution curve represents a coral which has behaved as a closed system. Consequently, the corresponding activity ratios can be used to calculate the true age of the coral. This is confirmed by the concordance of the isochron age and the calibrated ^{14}C age of the Holocene coral AQB 10B.

The isochron age uncertainty can be calculated from the intersection points of confidence bands at 95% confidence level with the seawater evolution curve. In the case of larger errors for the slope/intercept values, a Monte Carlo approach should be used to calculate the isochron age uncertainty. If additional prior knowledge about the true coral age is available, this can also be included into the Monte Carlo routine.

The isochron ages of the corals from the upper terrace range from 121 (+6.7 –5.3) to 121.9 (+7 –6.3) kyr. Those from the lower terrace are between 106.4 (+8.9 – 8.1) and 117.1 (+19.7 –15.3) kyr. Because of the rather large uncertainties in the isochron ages and the vertical uplift rate at the study site, a reconstruction of past sea level fluctuations is difficult. The likeliest interpretation is that both terraces correspond to the Last Interglacial with the lower one representing a second highstand which occurred after the first one and was a few meters lower in magnitude.

The presented isochron dating method enables to assign a reliable U-series age even to corals that have been extremely diagenetically altered. Even if the resulting age uncertainties are larger than that of TIMS or ICP-MS ages, it represents an important improvement as the majority of fossil corals have been affected by diagenetic alteration and could not be dated at all with the conventional methods. Therefore, it will help to enlarge the database of reliable U-series coral ages.

4.2 The study of fossil reef corals from Barbados, West Indies

4.2.1 Description of the study region

The island of Barbados is located in the eastern Caribbean Sea, approximately 150 km east of the Lesser Antilles, between 13°02' and 13°10' N latitude and 59°25' and 59°39' W longitude (Fig. 4.26). The island extends about 32 km from north to south, 24 km from east to west , and is approximately 430 km^2 large (Fig. 4.28 A, page 89). From a geographic point of view Barbados belongs to the Lesser Antilles, but in terms of tectonics and geology it is unique in this region, as it neither belongs to the presently active volcanic island chain, nor to the older volcanic island arc (Fig 4.26).

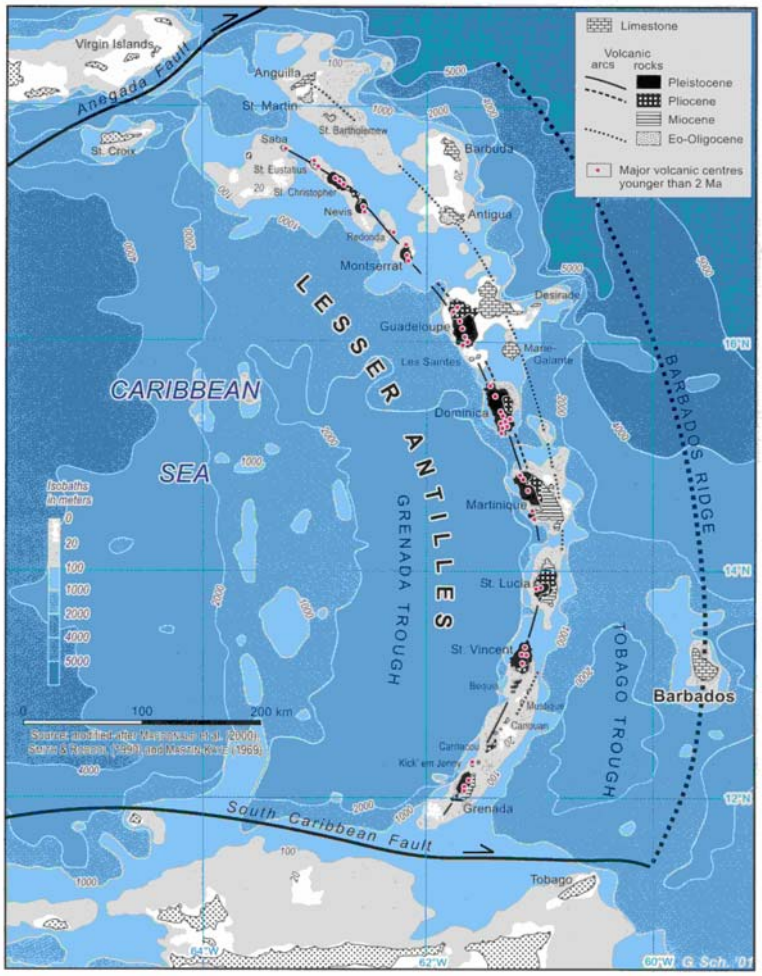

Fig. 4.26: Geographic position of Barbados, West Indies. Red circles indicate volcanically active centres. Also indicated is the Barbados Ridge. The picture has been taken from *Schellmann & Radtke* (*2004*).

Even more extraordinary is the tectonic position of the island. Barbados is located in the subduction zone of the Atlantic oceanic crust of the North American Plate which slides under the Caribbean Plate in westward direction (Fig. 4.27). This results in thick sediment layers being scraped off the ocean floor in the vicinity of Barbados since the late Eocene. These sediments are piled up and form an elongated accretionary complex, the so-called "Barbados Ridge Accretionary Prism" (Fig. 4.27). Barbados is the highest elevation of this ridge and the only part of it which is presently above sea level (*Schellmann & Radtke, 2004*). Therefore, Barbados has been the subject of tectonic uplift throughout the Pleistocene.

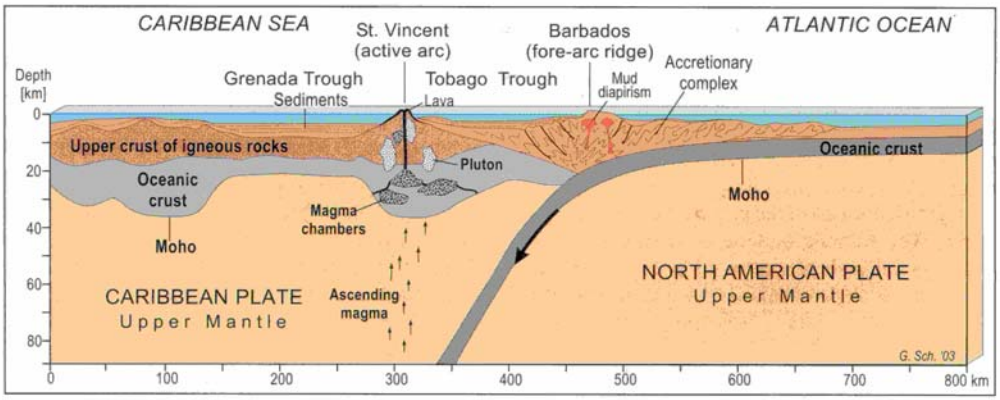

Fig. 4.27: Cross section of the subduction zone in the vicinity of Barbados. The picture has been taken from *Schellmann & Radtke* (*2004*).

Barbados consists of two principal natural regions: The northern, western, and southern parts of the island are dominated by coral reef terraces, in the eastern part lies the Scotland district which is determined by the Tertiary basement that is located beneath the Pleistocene coral cap (Fig. 4.28 A). While the Tertiary sedimentary rocks account for 15% of the surface of Barbados only, the remaining 85% are covered by coral limestone that ranges from 15 to 130 m in thickness (*Schellmann & Radtke, 2004*). During the Pleistocene emergence of Barbados, new fringing reefs were repeatedly produced under the influence of numerous sea level fluctuations and resulted in the characteristic terrace structure (see Fig. 3.3, page 35).

4.2.2 The studied coral reef terraces

Since the pioneering work of *Mesolella et al.* (*1969*), Barbados has been the "Mecca" for sea level reconstructions using fossil reef corals. Subsequently, numerous studies and publications on fossil coral dating and the sea level history of Barbados have followed. A detailed summary of the history of sea level reconstruction on Barbados and the development of the so-called "Barbados Model" is given in *Schellmann & Radtke* (*2004*). In the same publication a detailed overview of the distribution and chronostratigraphy – based on the

available U-series and Electron Spin Resonance (ESR) (see e.g. *Scholz* (*2001*) for a description of this method) data – of the several fossil coral reef terraces of Barbados can be found (*Schellmann & Radtke, 2004*).

During an excursion in November 2002 fossil reef corals from four locations have been collected. In the southern part of the island from the sites *Paragon* and *Inch Marlow Point* (Fig. 4.28, A and C), and in the south-western part from *Batts Rock Bay* and an outcrop below the *University of the West Indies* (Fig. 4.28, A and B). All these locations have already been studied to a greater or lesser extent by other workers. A detailed compilation of the existing U-series- and ESR-data from the locations *Batts Rock Bay*, *Inch Marlow Point*, and *Paragon* can be found in *Schellmann & Radtke* (*2004*) and *Potter et al.* (*2004*).

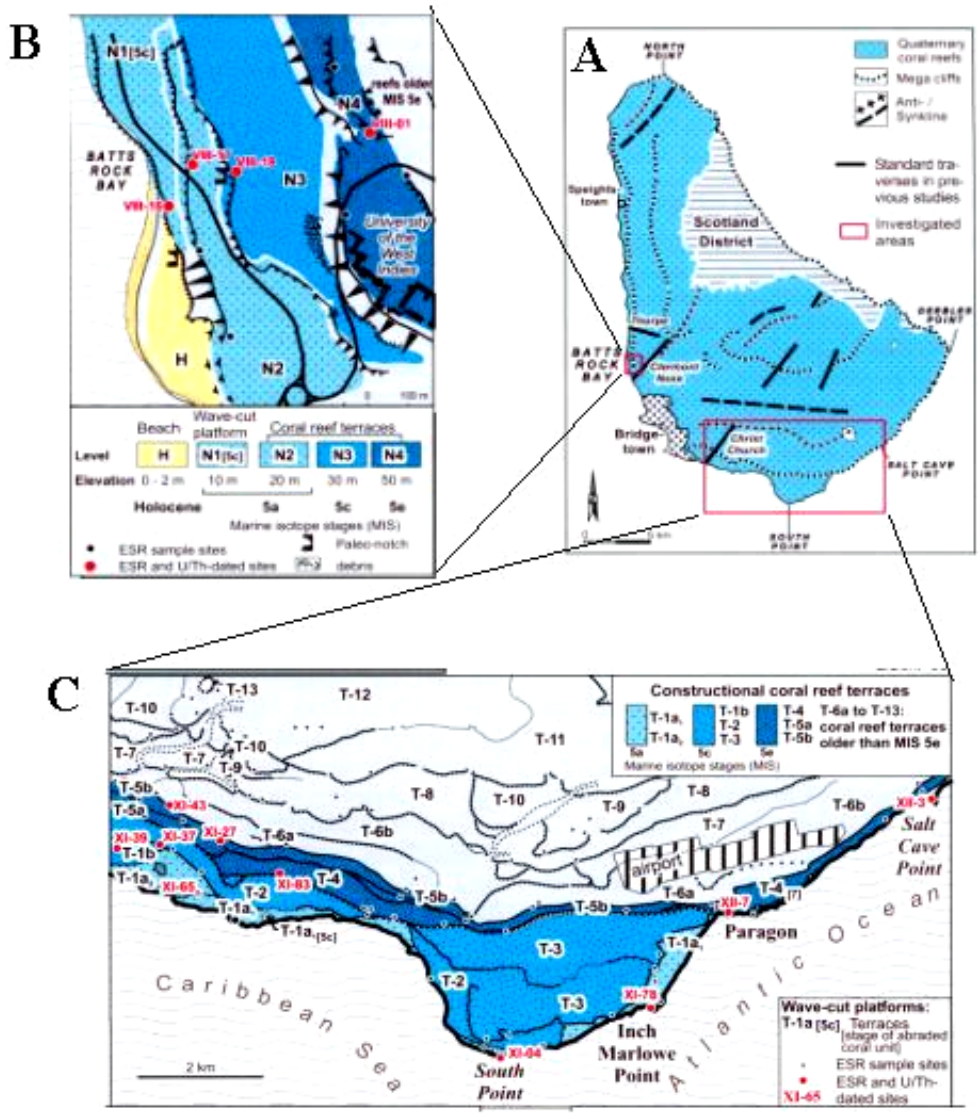

Fig. 4.28: (A) Map of Barbados. (B) and (C) Enlarged maps of the southern and south-western parts of the island, showing the locations of coral sampling. All pictures have been taken from *Schellmann & Radtke* (*2004*).

In contrast to the study of the Aqaba corals, where complete coral colonies have been sampled (see chapter 4.1.1), on Barbados drill cores have been taken, using a drilling machine equipped with a water-cooling device and hollow drills ranging from 1.5 to 5 cm in diameter (Fig. 4.29). The main advantage of this sampling method compared to the use of hammers and chisels is that the interior parts of the reef can be accessed more easily.

Fig. 4.29: Picture showing the sampling technique that has been applied on Barbados.

As the main intention of this study was to apply isochron dating (see chapter 4.1 and *Scholz et al.* (*2004*)) to the collected samples, at each location several close-by holes have been drilled. This is shown in Fig. 4.30. At some locations all holes have been drilled into one and the same coral, at others into different corals that were located closely to each other. Overall, 53 drill cores have been taken during the excursion. A detailed listing of all samples can be found in Appendix D.

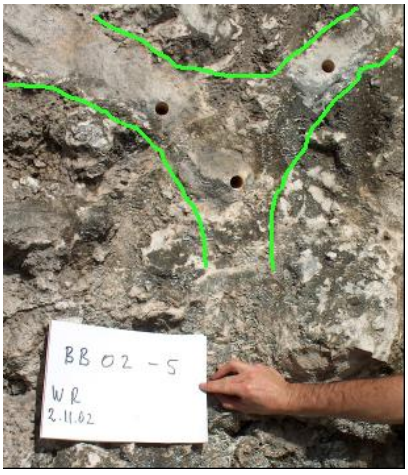

Fig. 4.30: Photography showing the applied sampling strategy exemplarily for location BB02-5. The green lines indicate the typical "elkhorn form" of the *Acropora palmata* coral (see chapter 2.2.2) showing that this sample is still in its natural growth position (*D. Meischner, pers. communication*). The locations where the drill cores have been taken are clearly visible. After the photography was taken, one more core (named BB02-5-4) has been drilled about 20 cm below the lowermost hole.

In this work, the U-series results of the samples which have been taken below the *University of the West Indies* (Fig. 4.28 B) will be presented. The outcrop is a road cut section at the University Road which is part of the classical Clermont Nose traverse (Fig. 4.28 A). It is ideally suited for sea level reconstructions using fossil reef corals, because it has the highest uplift rate on the island (0.44 m/kyr (*Taylor & Mann, 1991*)). Fossil corals from this location have already been investigated by U-series methods in another study (*Gallup et al., 2002*). Fig. 4.31 shows a cross-section of the study site which is based on the results of *Gallup et al.* (*2002*).

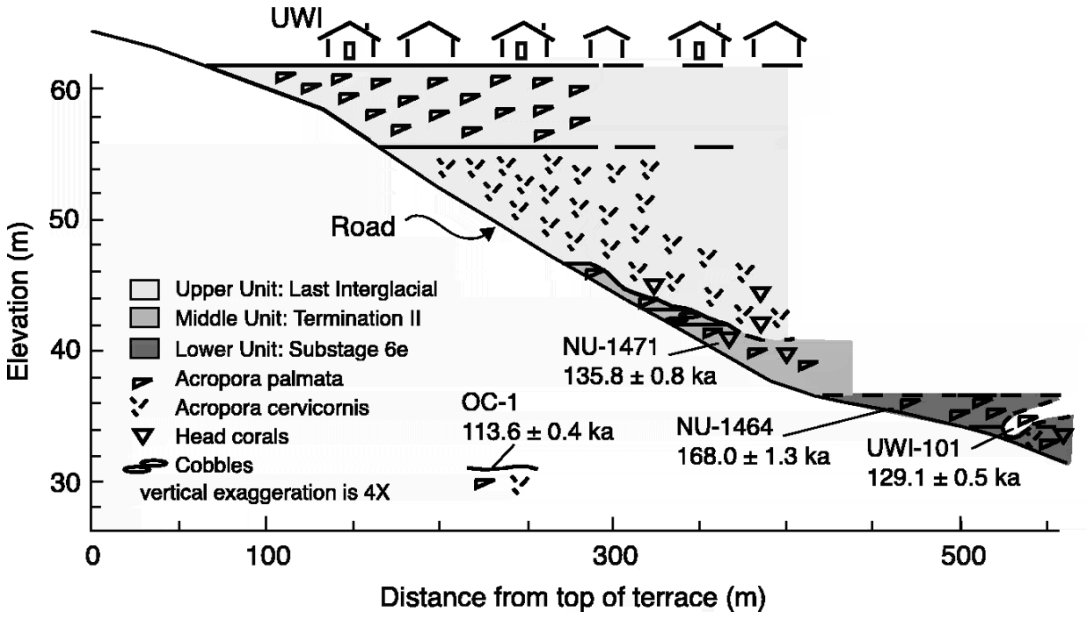

Fig. 4.31: Transect of the terrace below the University of the West Indies. The site is divided into three units: an upper one (elevation: ~45–60 m asl) which represents the Last Interglacial reef, a middle one (~35–45 m asl) which contains corals that grew during the transition from MIS 6 to MIS 5e, the so-called "Termination II", and a lower one (~30–35 m asl) which contains corals with a Last Interglacial age as well as older corals with ages around 170 kyr. Note that the vertical exaggeration is 4×. The drawing has been taken from *Gallup et al.* (*2002*).

The samples from the outcrop at the University Road stem from six different locations. Overall, at the middle unit (see Fig. 4.31 captions) four locations have been sampled. According to the results of *Gallup et al.* (*2002*) these corals should have grown during the transition from MIS 6 and the Last Interglacial (Termination II) suggesting an age of ~130 kyr (see Fig. 3.4). At this unit corals of the genus *Acropora palmata* as well as *Diploria strigosa* have been sampled.

At the lower unit samples from two locations have been taken. The results of *Gallup et al.* (*2002*) showed that the lower unit contains corals with a Last Interglacial age as well as corals which grew during MIS 6.5, a substage within the glacial period MIS 6 corresponding to the northern summer insolation peak around 175 kyr. To date, the outcrop below the University of the West Indies is the only location worldwide where MIS 6.5 corals have been found. At the lower unit only corals of the genus *Acropora palmata* have been sampled. Fig. 4.32 shows a photography of the lower unit. The locations where the samples have been taken are indicated (Fig. 4.32).

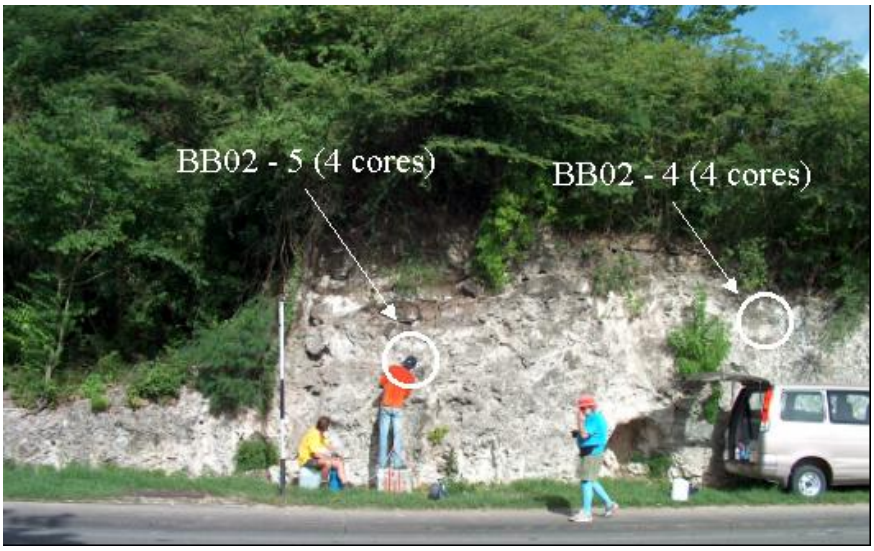

Fig. 4.32: Photography of the lower terrace which corresponds to MIS 6.5 (*Gallup et al., 2002*). The white circles indicate the locations of coral sampling (BB02-4 and BB02-5).

Table 4.7 gives a compilation of all samples which have been collected at the outcrop below the University of the West Indies.

Location	Terrace	No. of drill cores	Coral genera*
BB02-1	middle unit (Termination II)	4	Diploria strigosa (2) Acropora palmata (2)
BB02-2	middle unit (Termination II)	3	Diploria strigosa (3)
BB02-3	middle unit (Termination II)	3	Acropora palmata (3)
BB02-4	lower unit (MIS 6.5)	4	Acropora palmata (4)
BB02-5	lower unit (MIS 6.5)	4	Acropora palmata (4)
BB02-6	middle unit (Termination II)	3	Diploria strigosa (3)

Table 4.7: Compilation of the drill cores collected below the University of the West Indies.
* Numbers in brackets denote how many drill cores of the respective coral genera have been taken.

4.2.3 Coral pre-treatment and U-series measurements

In contrast to the Aqaba corals which have also been used in a high-resolution paleoclimate study (*Felis et al., 2004*), the corals from Barbados have been collected with the objective of sea level reconstruction. Therefore, they have not been investigated that detailed (i.e. using X-radiograph positive prints and thin sections) before the U-series measurements were conducted.

Each drill core has been examined under ultraviolet light to identify parts that have been mineralogically altered. Although aragonite and calcite cannot be strictly distinguished from each other by their fluorescence-colours, for example high Mn contents can be identified by their intensive red coloration (*Seilnacht, 2004*). Precise measuring of aragonite and calcite contents, respectively, is only possible by X-ray diffraction analysis (see chapter 4.1.2). Therefore, some material from each of the analysed samples has been stored for such measurements.

All U-series data have been measured by TIMS. The sample preparation and details of the measuring procedure are described in Appendix A. In contrast to the Aqaba data (chapter 4.1), the U-series data presented in this chapter have already been calculated with the recalibrated spike concentrations (see Appendix A for an extended discussion of the spike recalibration).

For the U-series measurements several sub-samples have been sawn off each drill core. This is exemplarily shown for drill core BB02-5-1 in Fig. 4.33.

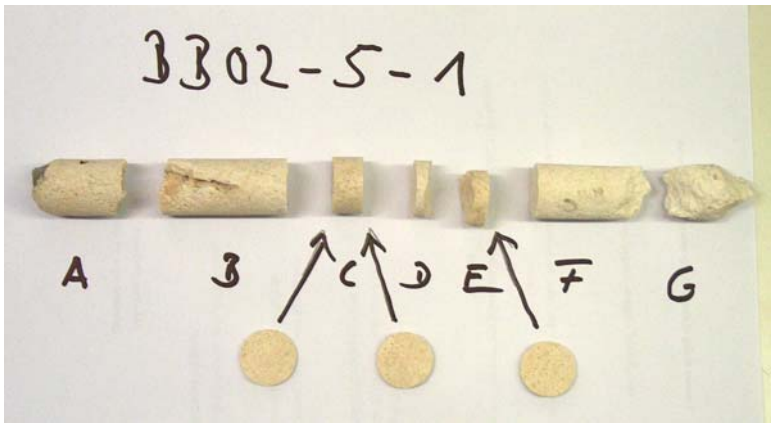

Fig. 4.33: Photography of drill core BB02-5-1 (*Acropora palmata* sample). The sub-samples have been taken from that parts of the core (indicated by the black arrows) which showed the least signs of diagenetic alteration. Each sub-sample is between 1 and 3 mm thick. Even surface areas (e.g. at the ends of pieces B and F) indicate where previous samples have been taken. Rough surface areas (e.g. at the other ends of pieces B and F) indicate natural sites of fracture or where the core broke during the drilling procedure.

4.2.4 The corals from the middle unit (Termination II)

4.2.4.1 Results and discussion of the U-series measurements

The U-series data of the analysed ten sub-samples from the middle unit are listed in Table C5 in Appendix C. From each drill core taken at locations BB02-1, -2, and –3 one sub-sample has been analysed. The drill cores from location BB02-6 are currently measured.

The U-series ages of all sub-samples range from 127.5 ± 1.7 to 133.7 ± 4.4 kyr suggesting a Last Interglacial origin. The ^{232}Th concentrations are between 0.04 and 0.59 ppb and are generally in the range measured for surface corals (see chapter 2), although the mean value of the five *Diploria strigosa* samples (0.23 ppb) is slightly higher than that of the five *Acropora palmata* samples (0.09 ppb). This indicates that non-radiogenic ^{230}Th, $^{230}Th_{nr}$ (see chapter 4.1.4), has neither been incorporated during growth nor post-depositionally added to these corals. Nevertheless, all activity ratios and ages listed in Table C5 (Appendix C) have been routinely corrected assuming a silicate source with a ^{232}Th/^{238}U weight ratio of 3.8 (*Wedepohl, 1995*) and with ^{230}Th, ^{234}U, and ^{238}U in secular equilibrium. Because of the very low ^{232}Th contents, the resulting differences between uncorrected and corrected ages are generally within the ±2σ error range of the ages.

The ^{238}U contents range from 2.61 to 2.79 ppm (mean value: 2.68 ppm) for the *Diploria strigosa* samples and from 3.14 to 3.3 ppm (mean value: 3.19 ppm) for the *Acropora palmata* samples. This indicates that the ^{238}U concentration of *Acropora palmata* corals is generally higher than that of corals of the genus *Diploria strigosa*. It is a well known fact that the ^{238}U content of fossil corals is – at least partly – species dependent (*Cross & Cross, 1983*). However, both values lie within the usual range (see chapter 2 and the references therein).

The initial δ^{234}U values vary between 148 ± 2 and 169 ± 4 ‰. If the reliability criterion of *Stirling et al.* (*1998*) is applied (i.e. initial δ^{234}U = 149 ± 3 ‰), only four of the ten sub-samples can be considered as strictly reliable (Table C5, Appendix C). This clearly shows that all other sub-samples have not behaved as closed systems.

It has been shown for the corals from Aqaba, Jordan, that the elevated δ^{234}U values have been produced by post-depositional addition of a high δ^{234}U component (see chapter 4.1.5). With the available data it cannot be evaluated if this process has produced the elevated initial δ^{234}U values of the Barbados corals. As five cores have been drilled into corals of the genus *Diploria strigosa* and the other ones into *Acropora palmata* corals, and both species originally incorporate different amounts of U, the data from these drill cores cannot be compared to each other. The remaining 5-point-datasets are too small to evaluate if a high δ^{234}U component has been added, because the initial ^{238}U concentrations in fossil reef corals depend on a variety of factors and show variations up 10% - even in different sub-samples of one and the same coral (see chapter 2.2.4).

4.2.4.2 The application of isochron dating

The drill cores from the middle unit have not been investigated very detailed as from each drill core only one sample has been analysed. As explained in the previous chapter, it is not possible to evaluate if the samples from Barbados have been affected by the same process as the corals from Aqaba. Nevertheless, a rough trend between $\delta^{234}U$ and ($^{230}Th/^{238}U$) can be observed in the data. This is shown on an isochron plot in Fig. 4.34.

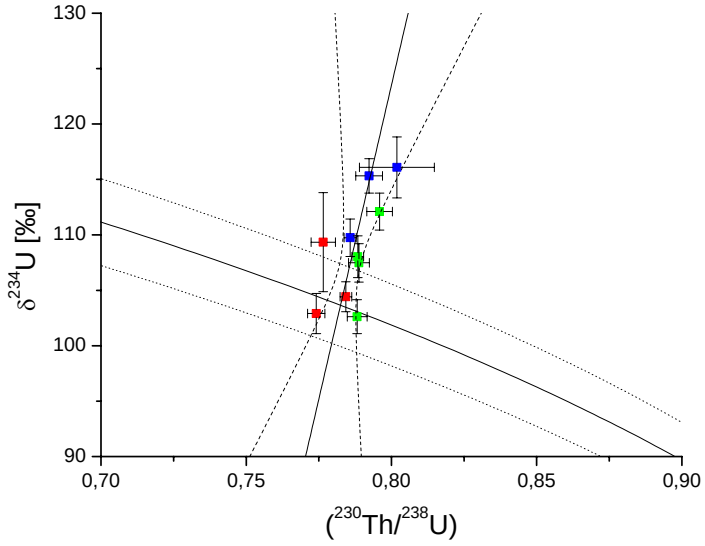

Fig. 4.34: Isochron plot for the drill cores from locations BB02-1 (shown in green), – 2 (red), and – 3 (blue). The isochron has been produced by fitting the complete dataset. Dotted lines around the linear fit are confidence bands at 2σ-level. Dashed lines around the seawater evolution curve represent the ± 5‰ range. The corresponding isochron age is 130.7 (+2 –1.4) kyr.

It is evident from Fig. 4.34 that the data of the of the single locations show very low (R= –0.01 for BB02-2, red data) to high correlations (R=0.93 for BB02-3, blue data). Because all three isochrons consist of three or four data points only, and the respective sub-samples belong to different drill cores, it cannot be decided from these data if the isochron dating method can be applied. It is interesting that the whole dataset from the middle unit shows a moderate correlation of R=0.55. This indicates that the drill cores from all three locations have been affected by similar diagenetic processes although they have been collected at a distance of ~40m. This has also been observed for the three Aqaba corals from the lower terrace (see chapter 4.1.7) and suggests again that the diagenetic processes do not happen on microscopic scales but rather are the result of the general conditions at the study region. The isochron age calculated for the middle unit is 130.7 (+2 –1.4) kyr and is in good agreement with the results of *Gallup et al.* (*2002*).

4.2.4.3 Discussion of the U-series ages

In addition to isochron dating, the usual reliability criteria have been applied to the Barbados corals. These are listed in chapter 2.2.4 (page 25). All sub-samples from the middle unit fulfil criteria two (i.e. normal ^{238}U content) and three (i.e. $^{232}Th < 1$ ppb) (see chapter 4.2.4.1 and Table C5, Appendix C). The initial $\delta^{234}U$ criterion (149 ± 3‰, (*Stirling et al., 1998*)) is fulfilled by four samples from the middle unit (Table C5, Appendix C). The U-series ages of these samples range from 127.5 ± 1.6 kyr to 132.9 ± 1.2 kyr. All ages agree within error with the isochron age (130.7 (+2 –1.4) kyr) estimated for the middle unit. Overall, all ages are in good agreement with the results of *Gallup et al.* (*2002*) who concluded that the middle unit formed during the rise to peak interglacial sea level (i.e. Termination II, compare also the sea level curve in Fig. 3.4, page 39).

4.2.5 The corals from the lower unit (MIS 6.5)

The lower unit at the outcrop below the University of the West Indies is the only location worldwide where corals from MIS 6.5 have been found (*Gallup et al., 2002*). These corals represent the only available direct measurement of sea level during this period. As MIS 6.5 is period of extraordinary climate signature (see next chapter), the sub-samples from this site have been investigated very extensively.

4.2.5.1 Climate during Marine Isotope Substage 6.5

MIS 6.5 corresponds to the northern summer insolation peak at ~175 kyr (Fig. 4.35). According to *Tzedakis et al.* (*2003*), MIS 6.5 is a period of *distinctive* climate signature which is characterised by unconventional combinations of insolation, ice sheet extent and greenhouse gas concentration. While northern summer insolation and atmospheric $\delta^{18}O$ values are at interglacial levels, there is no corresponding increase in atmospheric CO_2. In addition, the Specmap curve (*Imbrie et al., 1984*) suggests rather low sea level and accordingly rather large global ice volume. This is illustrated in Fig. 4.35.

Based on one strictly reliable coral age from *Gallup et al.* (*2002*) sea level was not as low as suggested by the Specmap curve (*Imbrie et al., 1984*), but rose to ~-40 m relative to present sea level. This implies a substantial temperature component to the benthic $\delta^{18}O$ curve due to colder temperatures in the deep sea (*Gallup et al., 2002*). The same phenomenon has also been suggested for the last glacial cycle (*Chappell et al., 1996*). A sea level reconstruction by *Lea et al.* (*2002*) has shown that there is a clear change in the planktonic $\delta^{18}O$ record during MIS 6.5 (suggesting a sea level rise), but at the same time Mg/Ca data show little or no increase in sea surface temperatures (SST).

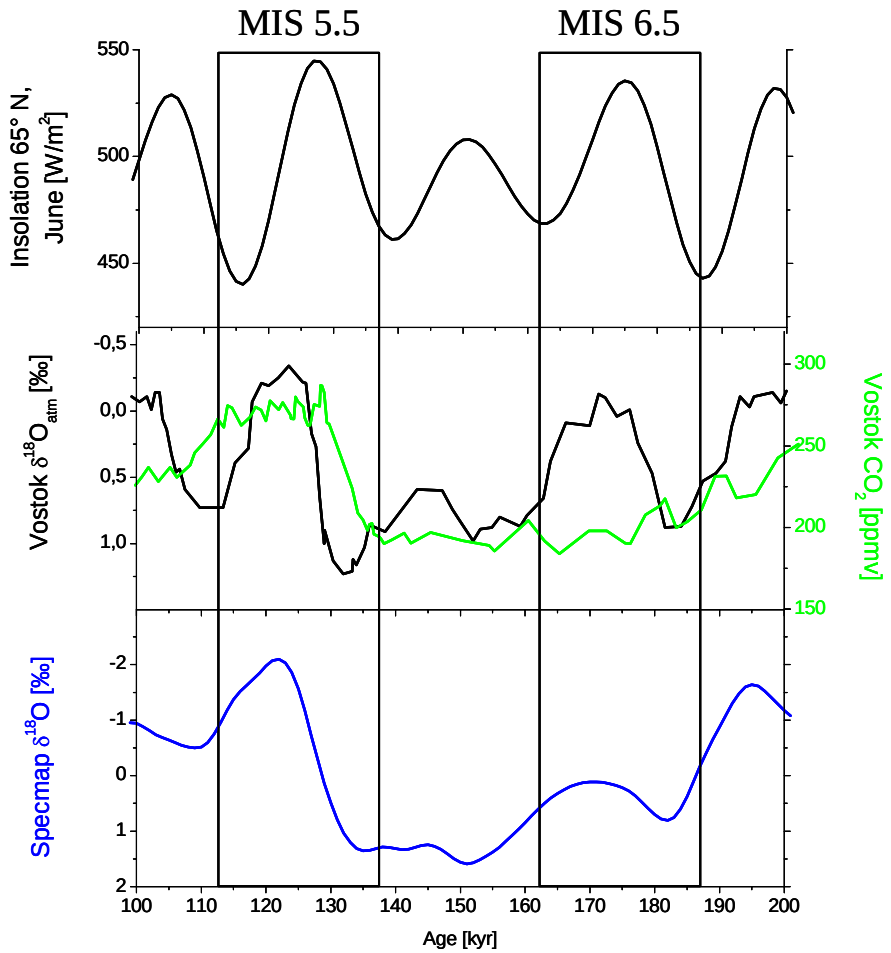

Fig. 4.35: (Upper part) 65° N summer insolation (*Berger & Loutre, 1991*), (Middle part) atmospheric $\delta^{18}O$ (black) and CO_2 content (green) from the Vostok ice core (*Petit et al., 1999*), and (Lower part) the Specmap curve (*Imbrie et al., 1984*).

In addition, several continental records indicate that MIS 6.5 was a climatically extraordinary period within the glacial period MIS 6. *Ayalon et al.* (*2002*) found a major low $\delta^{18}O$-event recorded in speleothems from the Soreq Cave, Israel, which they interpreted as a period of dramatically increased rainfall. The respective $\delta^{13}C$ values indicate the dominance of C3-type vegetation suggesting cold but humid climate (*Ayalon et al., 2002*). Interestingly, this event occurs between 180 and 178 kyr and precedes the insolation peak (i.e. 175 kyr). *Bard et al.* (*2002b*) measured a prominent negative excursion in the $\delta^{18}O$ profile of a stalagmite from Argentarola Cave, Italy, between 180 and 170 kyr which was interpreted as the result of a relatively wet period that corresponds to the deposition of the sapropel event 6 (S6). Similarly, a brief humid period between 169 and 162 kyr has been detected in a stalagmite from Clamouse Cave, in the south of France (*Plagnes et al., 2002*). In contrast to the event reported by *Ayalon et al.* (*2002*), this period slightly post-dates the insolation peak

(Fig. 4.35). The Tenaghi Philippon pollen record shows an increase in arboreal pollen, but with a minor contribution of temperate trees (*Tzedakis et al., 2003*). Overall, all these records suggest more humid and slightly warmer conditions during MIS 6.5 than during the main part of MIS 6, but much colder and less wet conditions than during an Interglacial.

Another outstanding climate feature of MIS 6.5 is an extreme minimum in the Dole effect (i.e. the natural enrichment of $\delta^{18}O$ in the atmosphere with respect to its value in the ocean, *Malaize et al., 1999*). The present day value of the Dole effect is ~23.5‰, and most of this enrichment is due to the activity of marine and terrestrial biospheres which transmit the $\delta^{18}O$ signature of oceanic and continental waters to the atmosphere via mechanisms such as respiration and photosynthesis (*Bender et al., 1994*). The past variations of the Dole effect (i.e. the difference between past and today's Dole effect, denoted as ΔDole) are calculated by subtracting the $\delta^{18}O$ measured in deep sea cores from the atmospheric $\delta^{18}O$ record measured in ice cores (*Malaize et al., 1999*). As the $\delta^{18}O$ signal in deep sea cores is also affected by deep sea temperature (see chapter 3.1.1), the calculation of the Dole effect variations is affected by this uncertainty as well. This is demonstrated by the large differences between the ΔDole reconstructions by *Shackleton* (*2000*) and *Jouzel et al.* (*2002*). While *Shackleton* (*2000*) assumed a very high MIS 6.5 sea level (see Fig. 4.53, page 117) which resulted in a ΔDole value about -0.3‰, *Jouzel et al.* (*2002*) used the sea level reconstruction by *Waelbroeck et al.* (*2002,* see Fig. 4.53) yielding a ΔDole value of approximately -0.75‰. Consequently, a coral based sea level reconstruction would allow a more accurate estimation of past Dole effect variations.

As possible explanations for the minimum of the Dole effect observed within MIS 6.5, processes induced at low latitudes have been proposed (*Mélières et al., 1997; Malaize et al., 1999*). *Malaizé et al.* (*1999*) suggested that it has been produced by an unusually strong monsoon which occurred under glacial conditions, while *Mélières et al.* (*1997*) proposed that it has been driven by low latitude insolation. However, in both cases this would represent a decoupling between high and low latitudes, the former dominated by the presence of ice (explaining the observed cold MIS 6.5 climate, see discussion above), the latter directly responding to the insolation increase (*Tzedakis et al., 2003*).

From the discussion above follows that MIS 6.5 is a period of extraordinary climatic signature within the late Quaternary. Consequently, a precise measurement of the magnitude, timing, and duration of the MIS 6.5 sea level peak would add important information which could be used to attain more precise estimates of MIS 6.5 deep sea temperatures or the Dole effect. Therefore such data would help to understand the complex climatic signature of MIS 6.5 better.

4.2.5.2 Results of the U-series measurements

The U-series data of all analysed sub-samples from the lower unit are listed in Tables C6 and C7 in Appendix C.

The ^{238}U contents of the samples collected from the two locations at the lower unit (see Fig. 4.32, page 92) show substantial differences. While the ^{238}U contents of the samples from location BB02-4 lie between 3.07 and 3.38 ppm (mean value: 3.23 ppm) and consequently within the normal range, the samples from location BB02-5 have elevated ^{238}U concentrations (3.38–4.07 ppm, mean value: 3.69 ppm). The ^{232}Th contents of all sub-samples are low (mean value: 0.33 ppb), and the U-series ages show a rather large range from 143.9 ± 1.1 to 178.9 ± 4.4 kyr.

Drill core BB02-5-4 (see Fig. 4.30, page 90) is an exception because the ^{238}U contents of its sub-samples are clearly lower than those of the other cores, ranging from 1.52 to 3.17 ppm. In the same way, the U-series ages of the respective sub-samples are substantially older than those of the other cores ranging from 168.8 ± 1.4 to 275.2 ± 4.7 kyr. The ^{232}Th contents of all sub-samples from this drill core are very low (mean value: 0.02 ppb).

The U-series results of all analysed sub-samples (excluding the BB02-5-4 samples) are shown on a $\delta^{234}U$-($^{230}Th/^{238}U$)-plot in Fig. 4.36.

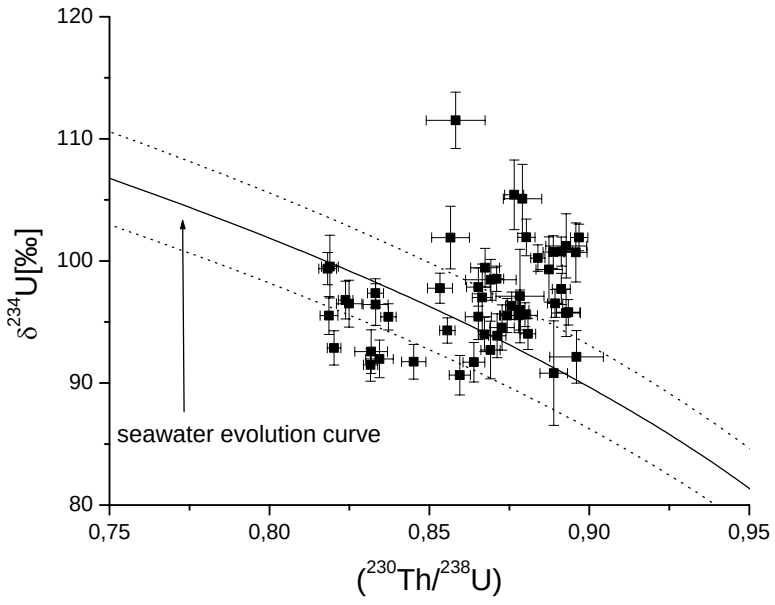

Fig. 4.36: Compilation of the U-series data measured on the drill cores from the lower unit. Sub-samples from drill core BB02-5-4 are not shown. The dashed lines represent the ± 5‰ uncertainty in the seawater evolution curve.

It is evident from Fig. 4.36 that the $\delta^{234}U$ values of these corals are generally lower than those of the Aqaba corals (compare Fig. 4.8, page 49). Nevertheless, many samples plot significantly above the seawater evolution curve indicating open system behaviour. This is also manifested in elevated initial $\delta^{234}U$ values which range from 140 ± 2 to 173 ± 4 ‰ (see Tables C6 and C7, Appendix C). Interestingly, some samples have $\delta^{234}U_{initial}$ values lower than modern seawater. This has also been reported for a few other corals from Barbados (*Potter et al., 2004*).

4.2.5.3 The application of isochron dating

The drill cores from the lower unit have been investigated very extensively. Within each drill core at least four, and in drill core BB02-5-3 even 13 sub-samples have been analysed. This should provide the optimal requirements for the application of the isochron dating method (see chapter 4.1.5). As the sub-samples of drill core BB02-5-4 have substantially less U than all other ones (see previous chapter), this drill core is an exception. Consequently, isochron dating has not been applied to this core. Fig. 4.37 shows the isochron plots for the drill cores from location BB02-4.

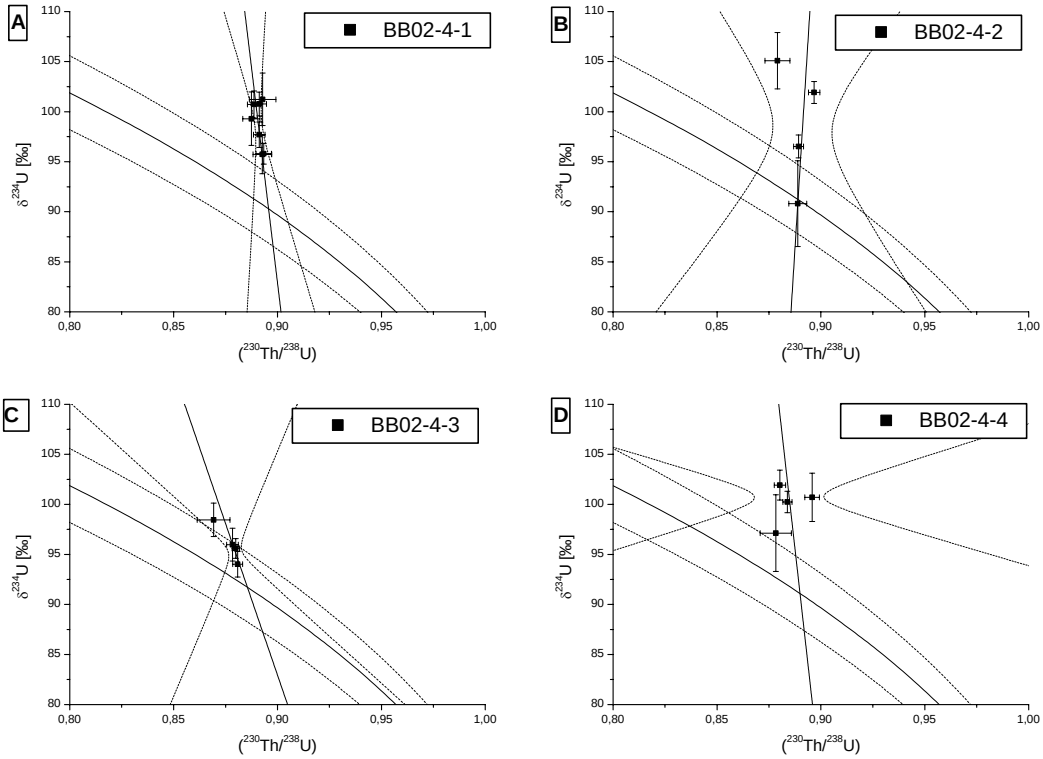

Fig. 4.37 (A-D): Isochron plots for the drill cores from location BB02-4. Dotted lines around the linear fits are confidence bands at 2σ-level. Dotted lines around the seawater evolution curve represent the ± 5‰ range.

The data from location BB02-4 show similar features as those from the middle unit (see chapter 4.2.4.2). While the data of some drill cores show medium to high correlations (BB02-4-1 (Fig. 4.37 A) and BB02-4-3 (Fig. 4.37 C)), those of the other ones result in rather low correlation coefficients (see Figs. 4.37 B and D). In the case of drill core BB02-4-4 (R= -0.1, Fig. 4.37 D) this results in extremely wide confidence bands so that no isochron age error can be calculated. Interestingly, the upper confidence band of drill core BB02-4-3 (Fig. 4.37 C) does not intersect the seawater evolution curve as well, although this drill core shows the highest correlation (R= -0.81). This shows that isochron dating cannot generally be applied to the drill cores from location BB02-4.

Fitting the data of all drill cores from location BB02-4 results in a rather low correlation (R=0.3), although the sampling distance between these drill cores is much smaller than for those of the middle unit (chapter 4.2.4.2). The corresponding isochron plot is shown in Fig. 4.38. The resulting isochron age is 172.5 (+3.6 –3) kyr. Even if the isochron dating assumptions might not be completely fulfilled for these samples, this confirms that the corals from the lower reef grew during MIS 6.5 (*Gallup et al., 2002*).

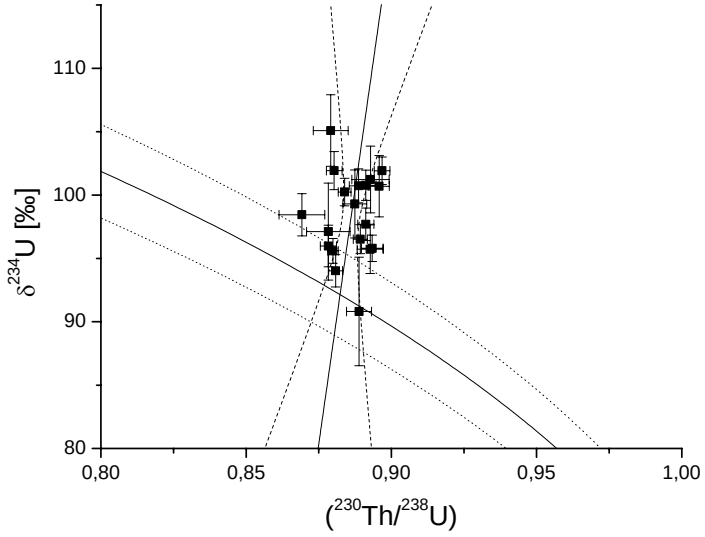

Fig. 4.38: Isochron plot for all sub-samples from location BB02-4. The corresponding isochron age for location BB02-4 is 172.5 (+3.6 –3) kyr. Dotted lines around the linear fit are confidence bands at 2σ-level. Dotted lines around the seawater evolution curve represent the ± 5‰ range.

The sub-samples of the drill cores from location BB02-5 have generally higher ^{238}U concentrations than all other samples collected on Barbados (see previous chapter). As one of most important requirements for the application of isochron dating is that all sub-samples have gained additional U, these drill cores may be better suited than the other ones. Fig. 4.39 shows the isochron plots for the drill cores from location BB02-5.

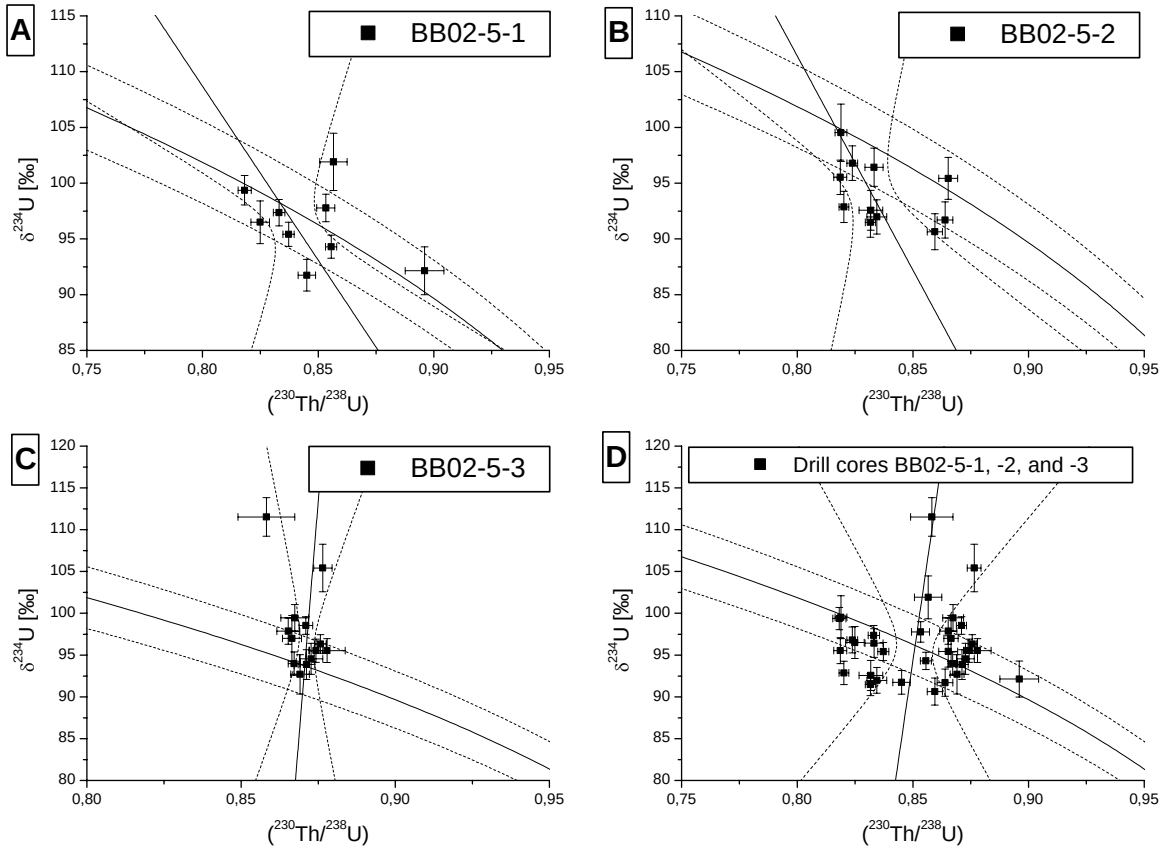

Fig. 4.39 (A-D): Isochron plots for the drill cores from location BB02-5. Dotted lines around the linear fits are confidence bands at 2σ-level. Dotted lines around the seawater evolution curve represent the ± 5‰ range.

The data of all sub-samples from location BB02-5 (Fig. 4.39 D) show substantial variations in $\delta^{234}U$ as well as in ($^{230}Th/^{238}U$), but it is obvious that they do not plot on an isochron. Instead, there is large number of samples which plot on the seawater evolution curve, but with significantly different ($^{230}Th/^{238}U$) activity ratios and in succession different U-series ages (ranging from ~140 to ~180 kyr, Tables C6 and C7 in Appendix C). As all samples stem from the same reef and should roughly have the same age, this must be a diagenetic feature.

The data of drill cores BB02-5-1 (Fig. 4.39 A) and BB02-5-2 (Fig. 4.39 B) show similar features. Even within one and the same drill core large ($^{230}Th/^{238}U$) variations are observed. As all sub-samples within one drill core must have the same age, this proves that these data have been diagenetically altered. Because the data of both drill cores do not plot on an isochron, they must have been affected by different processes than that required for isochron dating (see chapter 4.1.7).

Drill core BB02-5-3 (Fig. 4.39 C) is an exception within the samples from the BB02-5 location. The ^{238}U contents of the sub-samples from this core range from 3.38 to 3.6 ppm with an average of 3.52 ppm (Table C7, Appendix C). Although these values are higher than the usual U range of *Acropora palmata* corals, they are less elevated than those of drill cores BB02-5-1 and BB02-5-2 (compare Table C7, Appendix C). The isochron plot of drill core BB02-5-3 (Fig. 4.39 C) suggests that the method can be applied, and the calculated isochron age is 166.5 (+1.7 –1.5) kyr. In addition, the resulting age error is very small (< 1%). However, the correlation coefficient is rather small (R = 0.19) and only two out of 13 data points plot significantly above the seawater evolution curve. Therefore, it cannot be definitely decided if the isochron assumptions are fulfilled for this drill core. Furthermore, it has been shown in chapter 4.1.9 that the use of Algorithm B results in much larger isochron age errors than confidence bands if the data point distances are small.

In Table 4.8 all calculated correlation coefficients and isochron slopes are summarized.

Drill core	Number of analysed sub-samples	Correlation coefficient R	Isochron slope [‰]
BB02-4-1	7	-0.61	-1724
BB02-4-2	4	0.26	3300
BB02-4-3	4	-0.81	-588
BB02-4-4	4	-0.1	-1845
Data of all cores	**19**	**0.3**	**1608**
BB02-5-1	9	-0.51	-312
BB02-5-2	11	-0.47	-383
BB02-5-3	13	0.19	4514
Data of all cores	**33**	**0.07**	**1908**

Table 4.8: Compilation of the fitting results for all analysed drill cores. All values are based on an error-weighted x-on-y least squares regression (see chapter 4.1.9). The bold lines contain the results for fitting all data from locations BB02-4 and BB02-5, respectively. The large range in the correlation coefficients R and the isochron slopes suggests that the samples have been affected by very different diagenetic processes.

It is possible to obtain some information about the diagenetic processes from the isochron slopes. It has been shown in chapter 4.1.6 that there is a maximum range for the isochron slopes which can be produced by a U uptake scenario (see Fig. 4.16, page 62). The data of five out of six Aqaba corals which have been dated by the isochron method could not be explained by U uptake alone as they plotted to the right of the ‘early uptake’ isochron (see chapter 4.1.6). This can be evaluated on the basis of the isochron slopes for the Barbados corals as well.

An isochron is produced by addition of different amounts of a high $\delta^{234}U$ component to different sub-samples of the coral. In the case of the 'early uptake' isochron (Fig. 4.16) the addition takes place immediately after coral growth. Mathematically this means that all sub-samples start with different $\delta^{234}U$ but $(^{230}Th/U^{238}) = 0$. Consequently, the slopes of the 'early uptake' isochron and the closed-system isochron (see Fig. 2.9, page 26) of a specific age are the same. Therefore, the slope of the 'early uptake' isochron can be calculated by rearranging the closed-system age equation (2.6) and inserting the respective age. If the slope of a fitted isochron is positive but lower than this value, this shows that the data cannot have been produced by U uptake alone.

The insolation peak corresponding to MIS 6.5 is at 175 kyr. The slope of the 'early uptake' isochron of a 175 kyr old coral is 1032‰. The slopes of all isochrons from the lower unit on Barbados are higher or even negative (Table 4.8). This shows that the data of all drill cores could be described by U uptake alone. Other authors detected moderate to high correlations in Barbados corals as well (e.g. *Gallup et al., 1994; Thompson et al., 2003; Potter et al., 2004*), but the trends which have been reporteded in those studies were different.

Overall, some of the samples plot on an isochron while others do not (Figs. 4.37 A-D, 4.38, and 4.39 A-D). In addition, the data point distances are rather small which may enlarge the isochron age errors substantially (see chapter 4.1.9). Interestingly, even different sub-samples from one and the same drill core show extreme isotopic variations which cannot be explained by the isochron assumptions. Furthermore, the initial $\delta^{234}U$ values of some corals are elevated, but to a much lesser extent than at Aqaba. This makes it difficult to investigate the diagenetic processes. Therefore, the application of isochron dating to the Barbados corals is difficult. One possibility was to use the high correlation samples only, but if the isochron assumptions are not fulfilled, it is possible that wrong ages are calculated (see discussion in chapter 4.1.7).

4.2.5.4 Investigation of the diagenetic processes

Many sub-samples from the lower unit show clear evidence of diagenetic alteration. (e.g. Figs. 4.38 and 4.39 D). It has been shown in the previous chapter the processes which affected these corals must have been different than those at Aqaba. In the following these processes are investigated in more detail.

As mentioned in chapter 4.2.5.2, all samples show very low ^{232}Th contents. This indicates that non-radiogenic ^{230}Th, $^{230}Th_{nr}$ (see chapter 4.1.4), has neither been incorporated during growth nor post-depositionally added to these corals. This also follows from Fig. 4.40 as there is no correlation between ^{232}Th content and $(^{230}Th/^{238}U)$ and $\delta^{234}U$, respectively, observable.

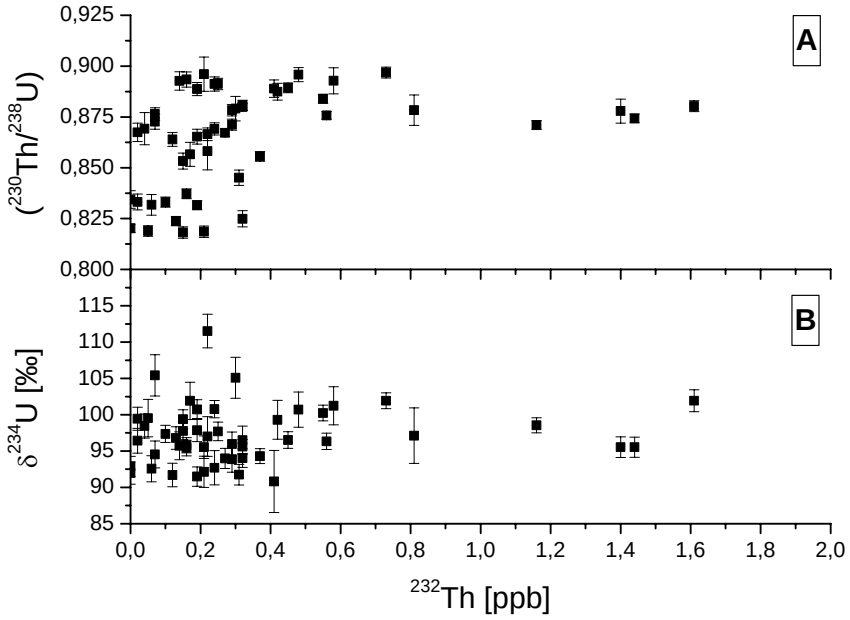

Fig. 4.40: **(A)** (^{230}Th/^{238}U)-^{232}Th- and **(B)** δ^{234}U-^{232}Th-plots for all sub-samples from the lower unit.

From this follows that all samples have not been contaminated by detrital ^{232}Th and ^{230}Th$_{nr}$. Nevertheless, all activity ratios and ages listed in Tables C6 and C7 (Appendix C) have been routinely corrected for detrital ^{232}Th assuming a silicate source with a ^{232}Th/^{238}U weight ratio of 3.8 (*Wedepohl, 1995*) and with ^{230}Th, ^{234}U, and ^{238}U in secular equilibrium. Because of the very low ^{232}Th contents, the resulting differences between uncorrected and corrected ages are generally within the $\pm 2\sigma$ error range of the ages.

The ^{238}U contents of the sub-samples from location BB02-4 are in the usual range about 3 ppm (Table C6, Appendix C). In contrast, those from location BB02-5 show substantial variations. While the sub-samples of drill cores BB02-5-1, -2, and -3 have elevated ^{238}U concentrations, those of BB02-5-4 have significantly lower ones (Table C7, Appendix C).

It has been shown for the corals from Aqaba, Jordan, that the elevated δ^{234}U values have been produced by post-depositional addition of a high δ^{234}U component (see chapter 4.1.5). Even though the δ^{234}U values of the Barbados corals are not elevated to that extent, the δ^{234}U values of at least some of them plot significantly above the seawater evolution curve (Fig. 4.36). This raises the question if the elevated δ^{234}U values of the Barbados corals have also been produced by post-depositional U uptake. Fig. 4.41 shows the data from the lower unit on a plot of δ^{234}U vs. ^{238}U content.

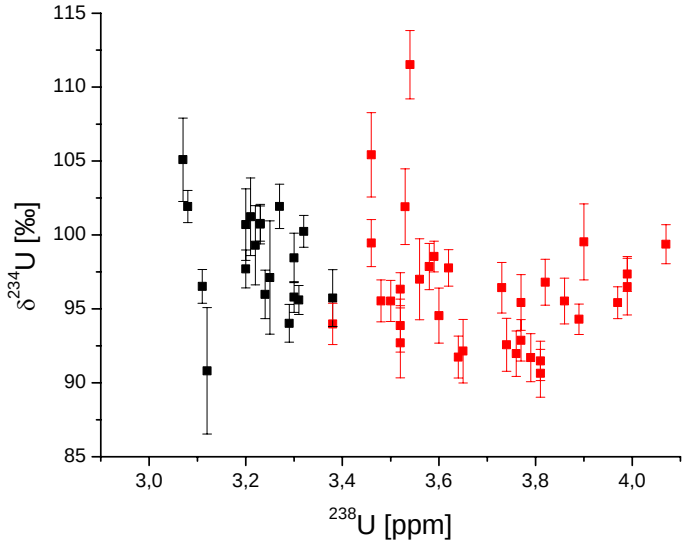

Fig. 4.41: Plot of $\delta^{234}U$ vs. ^{238}U content for the sub-samples from locations BB02-4 (shown in black) and BB02-5 (shown in red). The data of drill core BB02-5-4 are not shown as these samples have lower ^{238}U contents.

It is evident that the ^{238}U content of the BB02-4 samples (black) is generally lower than that of the BB02-5 samples (red). This suggests that all samples from location BB02-5 have gained additional U. As the normal ^{238}U content of *Acropora palmata* corals lies around 3 ppm, the data indicate that up to one ppm U has been post-depositionally added to these corals. However, there is no trend between $\delta^{234}U$ and ^{238}U content detectable suggesting that the additional U had neither a higher nor a lower $\delta^{234}U$ value than the corals.

Fig. 4.42 shows the data from the lower unit on a plot of ($^{230}Th/^{238}U$) vs. ^{238}U content.

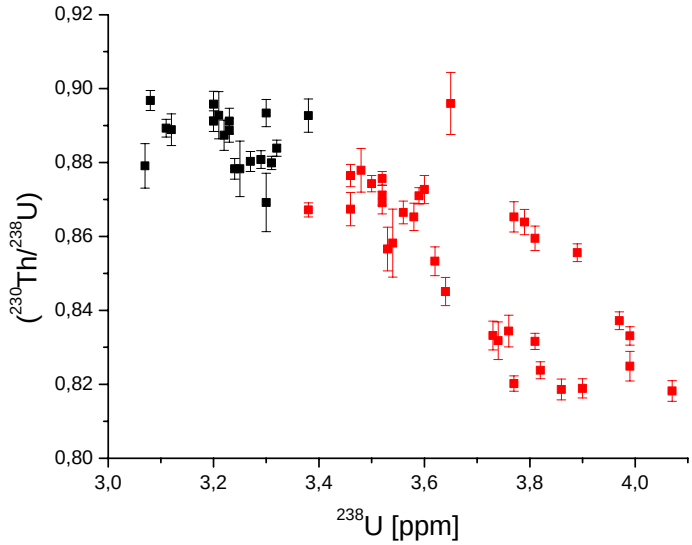

Fig. 4.42: Plot of ($^{230}Th/^{238}U$) vs. ^{238}U content for all sub-samples from locations BB02-4 (shown in black) and BB02-5 (shown in red). The data of drill core BB02-5-4 are not shown.

Fig. 4.42 confirms that the BB02-5 samples have gained additional U. While there is no trend observable in the BB02-4 data (black), the BB02-5 data (red) show a clear trend towards lower (^{230}Th/^{238}U) activity ratios with higher ^{238}U content. This indicates that the elevated ^{238}U content of the BB02-5 samples has been produced by *post-depositional* U addition, because otherwise – if higher amounts of U had been incorporated during coral growth – all sub-samples should have the same (^{230}Th/^{238}U) activity ratio. On the other hand this shows – as already has been concluded from the ^{232}Th data – that ^{230}Th has not been added to the corals along with U.

To evaluate the isotopic composition of the additional component in the drill cores from location BB02-5 in more detail, the two-component-mixing-model which has been used for the Aqaba corals (referred to as Method I in Table 4.1, page 58) has been applied. The formulas and details of this approach are explained in chapter 4.1.5. For all calculations, a true coral age of 175 kyr (corresponding to the maximum in northern summer insolation during MIS 6.5), and an initial ^{238}U content of 3.23 ppm (mean value of all analysed BB02-4 samples, Table C6, Appendix C) has been assumed. *Initial* (^{230}Th/^{238}U)$_{add}$ and (^{234}U/^{238}U)$_{add}$ activity ratios, respectively, have been calculated assuming a coral age of 175 kyr as well. Fig. 4.43 shows the calculated (^{234}U/^{238}U)$_{add}$ and initial (^{234}U/^{238}U)$_{add}$ activity ratios, respectively.

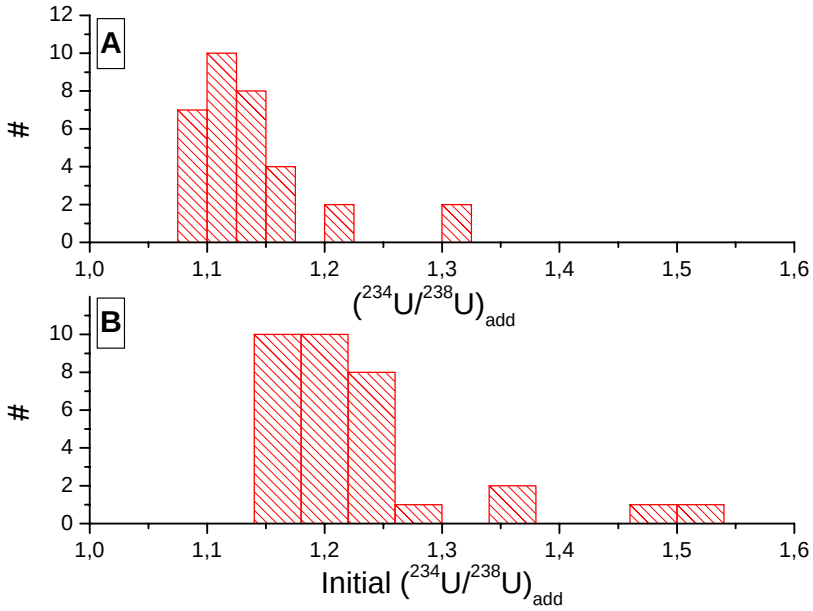

Fig. 4.43: Histograms showing the calculated (^{234}U/^{238}U)$_{add}$ (A) and initial (^{234}U/^{238}U)$_{add}$ activity ratios (B), respectively.

The $(^{234}U/^{238}U)_{add}$ values range from 1.09 to 1.32 with an average of 1.14 (Fig. 4.43 A). The initial $(^{234}U/^{238}U)_{add}$ values are between 1.14 and 1.53 with an average of 1.23 (Fig. 4.43 B). It has been explained in chapter 4.1.5 that these values – according to the timing of addition – represent maximum and minimum values, respectively, but in general, they are much lower than those calculated for the Aqaba corals (mean value: 1.65). This suggests that the additional U which has affected the Barbados corals stems from another source than at Aqaba. As the $(^{234}U/^{238}U)$ activity ratio of a 175 kyr old coral is 1.09, and if the uncertainty of the calculation method is considered (see discussion in chapter 4.1.5), it is possible that the additional U stems from surrounding corals which are coeval or slightly younger.

In Fig. 4.44 the calculated $(^{230}Th/^{238}U)_{add}$ and initial $(^{230}Th/^{238}U)_{add}$ activity ratios, respectively, are presented.

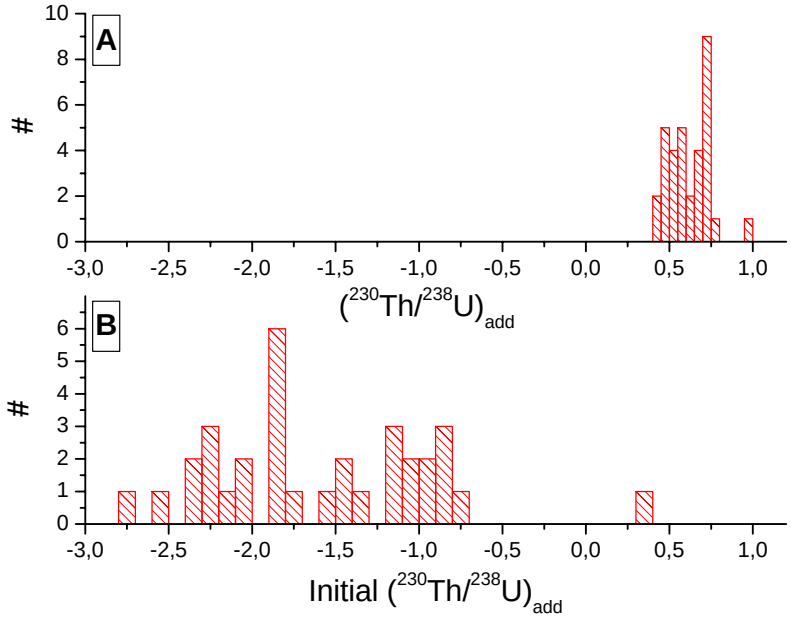

Fig. 4.44: Histograms showing the calculated $(^{230}Th/^{238}U)_{add}$ (A) and initial $(^{230}Th/^{238}U)_{add}$ activity ratios (B), respectively.

The values calculated for $(^{230}Th/^{238}U)_{add}$ range from 0.42 to 0.96 with an average of 0.62 (Fig. 4.44 A) while the initial $(^{230}Th/^{238}U)_{add}$ values are between –2.75 and 0.35 with an average of –1.58 (Fig. 4.44 B). These values represent maximum and minimum values only. The negative values result from counting back the $(^{230}Th/^{238}U)_{add}$ activity ratios using the closed system activity ratios and an age of 175 kyr. Activity ratios cannot take negative values by definition. Consequently, this shows that no ^{230}Th has been added to the corals and even more that the U has not been added 175 kyr ago, but obviously later. In the same way, the calculated $(^{230}Th/^{238}U)_{add}$ values do not necessarily indicate that ^{230}Th has been added to the corals, even if all values are greater than zero, because they result from decay of U_{add}.

The isotopic $^{230}Th/^{234}U$ ratios of the additional component range from 0.12 to 0.27 with an average of 0.17. Interestingly, these values are similar to those estimated for the Aqaba corals (additional isotopic $^{230}Th/^{234}U$ ratios between 0.17 and 0.28, see chapter 4.1.5), although the $(^{230}Th/^{238}U)_{add}$ and $(^{234}U/^{238}U)_{add}$ ratios estimated for the Barbados corals are much smaller. However, all values are much smaller than 1, which shows that the Barbados corals have not been affected by the processes proposed by other authors (*Gallup et al., 1994; Fruijtier et al., 2000; Henderson et al., 2001; Thompson et al., 2003; Villemant & Feuillet, 2003*).

To estimate the timing of U addition, two methods have been applied. First, the U-series age of the additional component has been calculated with equation (2.6) using the estimated $(^{230}Th/^{238}U)_{add}$ and $(^{234}U/^{238}U)_{add}$ activity ratios. This is equivalent to assuming that the U has been added all at once, and the system has remained closed afterwards. In the following this method is referred to as Method I. The resulting age distribution is shown in Fig. 4.45. The calculated ages are between 51.5 and 213.9 kyr with an average of 87.1 kyr.

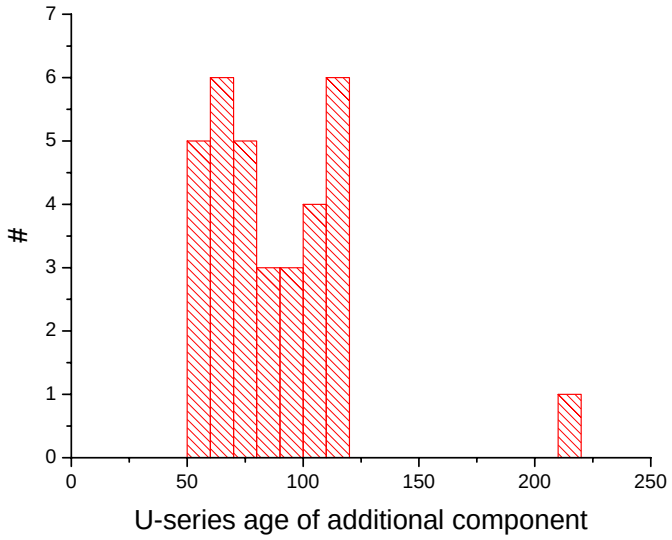

Fig. 4.45: Histogram showing the distribution of the U-series ages which have been calculated using the estimated $(^{230}Th/^{238}U)_{add}$ and $(^{234}U/^{238}U)_{add}$ activity ratios.

Another possibility to estimate the timing of U addition is to use a numerical model (Algorithm *einbau_2* in Appendix B2). The model assumes that the coral behaves as a closed system for a specific time (e.g. 25, 75, or 150 kyr). Then between 0 and 1.2 ppm of U_{add} with a $(^{234}U/^{238}U)_{add}$ activity ratio of 1.15 are added within 1,000 years. The $(^{234}U/^{238}U)_{add}$ activity ratio has been chosen such that is lies between the estimated maximum and minimum values (Fig. 4.43). Afterwards, the system remains closed again. It is assumed that the coral had an initial U concentration of 3.23 ppm and is 175 kyr old. This approach is referred to as Method II in the following. A comparison between data and the model results is shown in Fig. 4.46.

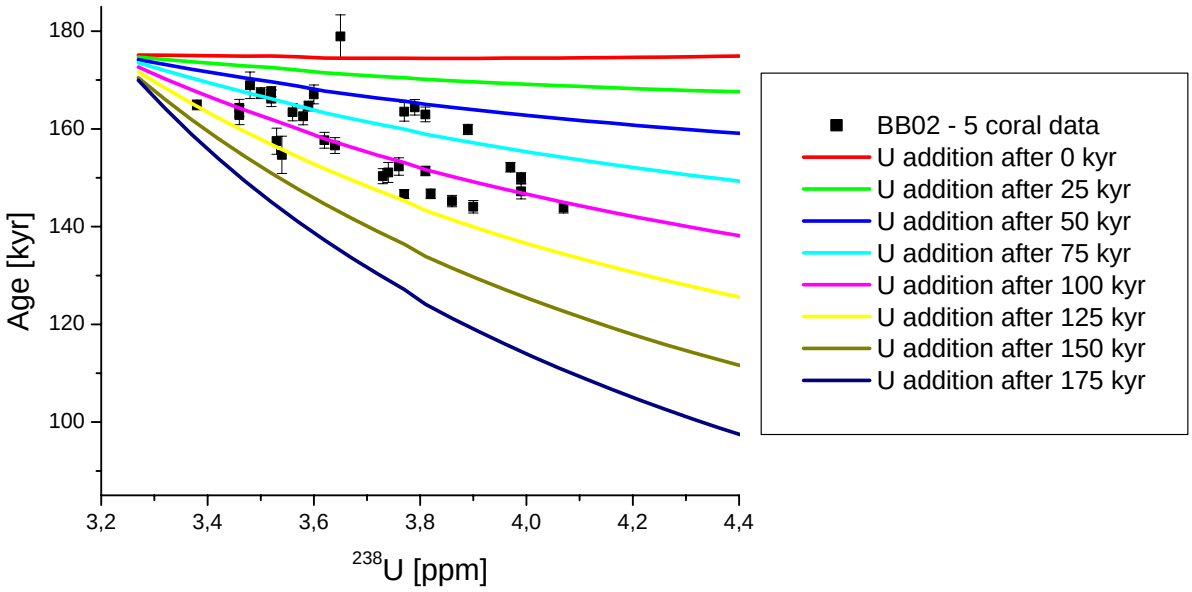

Fig. 4.46: Comparison between BB02-5 coral data and the modelling results. Each line represents U addition after a specific time (indicated by different colours, see legend).

The results show that the U_{add} has most likely been added between 50 and 125 kyr after coral growth (Fig. 4.46). If the coral is 175 kyr old, this corresponds to U addition between 50 and 125 kyr before present (BP). Overall, with both methods a similar timing of U addition is estimated. As both methods include several assumptions ('true coral' age, initial ^{238}U content, $(^{234}U/^{238}U)_{add}$ = 1.15 (Method II)) and simplifications (U is added all at once (Method I) or within 1,000 yr (Method II)), the estimated values are affected with some uncertainty. For example, if it was assumed that the U has been added continuously or batch-wise (see the modelling of the Aqaba data, chapter 4.1.6) or if a different $\delta^{234}U_{add}$ value had been used, different values for the timing would have been calculated as well.

However, both approaches show that the data can be described by U addition alone. This is a remarkable difference to the Aqaba data because those could not be modelled without assuming U loss or ^{230}Th addition (see chapter 4.1.6). The second major difference between both datasets is that the estimated $(^{234}U/^{238}U)_{add}$ activity ratios of the Barbados corals are much lower. Altogether, this suggests that the Barbados corals have possibly been affected by another process as well as another U source.

The ^{238}U contents of the sub-samples from drill core BB02-5-4 (Fig. 4.47) are lower than the usual ^{238}U contents of fossil reef corals (Table C7, Appendix C). Figs. 4.47 and 4.48 show photographs of this drill core.

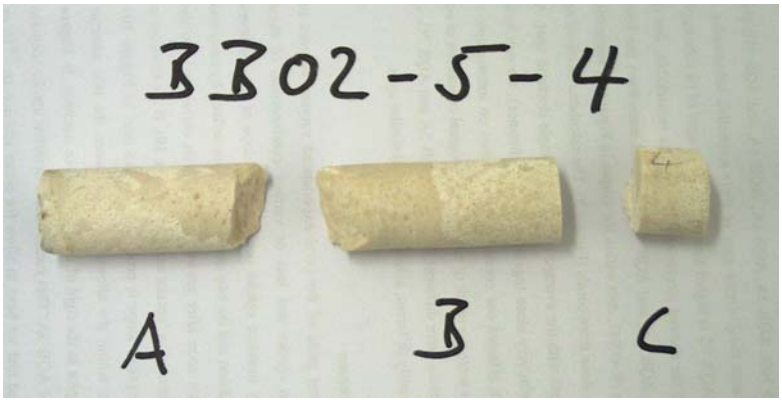

Fig. 4.47: Photography of drill core BB02-5-4. It is macroscopically visible that some parts of the core are mineralogically altered (note the difference between the left and the right part of piece B).

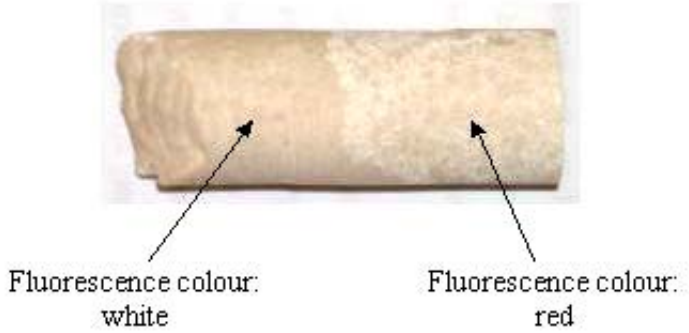

Fig. 4.48: Enlarged photography of piece B of drill core BB02-5-4 (see Fig. 4.47). While the left part looks white under ultraviolet light, the right part shows an intensive red coloration.

The sub-samples of drill core BB02-5-4 show clear differences under ultraviolet light. While the left part looks white, the right part shows an intensive red coloration (Fig. 4.48)). Overall, four sub-samples within this drill core have been analysed. One has been taken from the part showing white fluorescence colour (Fig. 4.48), another one in the red part, and two further samples which contained white as well as red parts. The variations in the ^{238}U contents of all sub-samples are substantial. While the red part shows a normal ^{238}U concentration of 3.17 ppm, the white part contains about half as much U only (^{238}U=1.52 ppm, Table C7, Appendix C). The U content of the parts showing both colours lies between these values, most likely because these samples represent a mixture of both components (Fig. 4.48). This clearly shows that the white parts have lost substantial U after deposition. Unfortunately, X–ray diffraction measurements of the respective sub-samples have not been performed yet. Therefore, it is not possible to investigate if U loss occurred due to recrystallisation from aragonite to calcite or due to another process. However, the timing of U loss can be estimated

using a numerical model (Algorithm *verlust* in Appendix B2). The model assumes that the coral behaves as a closed system for a specific time (e.g. 25, 75, or 150 kyr). Then between 0 and 80% of the initial U content (which is assumed to be 3.23 ppm) are lost within 1 year. Afterwards, the system remains closed again. It is assumed that the coral is 175 kyr old. The comparison between data and model results is presented in Fig. 4.49.

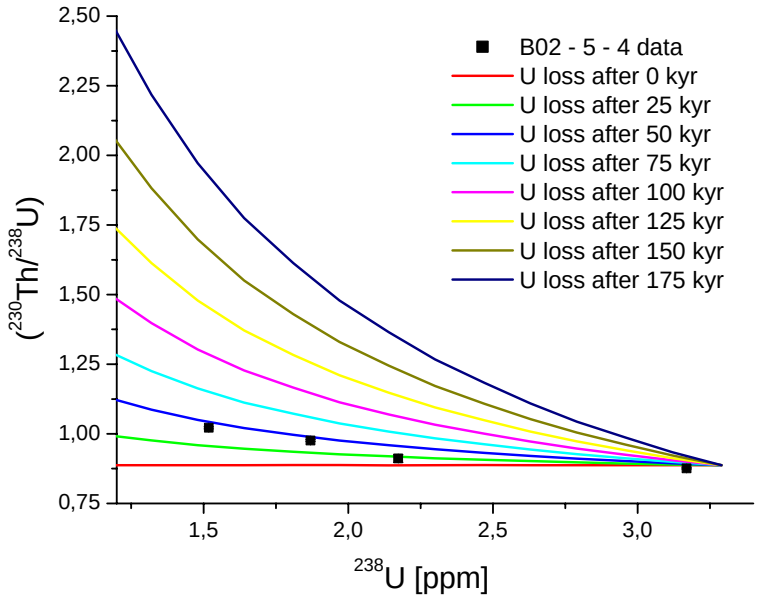

Fig. 4.49: Comparison between BB02-5-4 data and the modelling results. Each line represents U loss after a specific time (indicated by different colours, see legend).

The modelling results suggest that U was lost between 25 and 50 kyr after coral growth (i.e. between 150 and 125 kyr BP if the coral is 175 kyr old). It has to be emphasized again that this result is influenced by the modelling assumptions. However, as similar assumptions as in the U addition model have been used (i.e. addition/loss happens at once and rather fast), the results can be compared with each other. The U of the BB02-5-4 sub-samples was lost between 150 and 125 kyr BP, and the sub-samples of the other cores gained U between 125 and 50 kyr BP. Consequently, the timing of U loss and addition, respectively, allows to assume that the U which has been lost by some coral parts has been taken up by other ones. This is also confirmed by the estimated $(^{234}U/^{238}U)_{add}$ activity ratios which are in the range of the $(^{234}U/^{238}U)$ activity ratio of the corals itself suggesting that the source are surrounding corals of the same age. In the context of Fig. 2.9, page 26, this model corresponds to scenario ‘f’. This scenario provides an explanation for the U-series data of drill cores BB02-5-1 and –2 (Figs. 4.39 A and B) as well. This is explained below considering drill core BB02-5-2 as an example (Fig. 4.50).

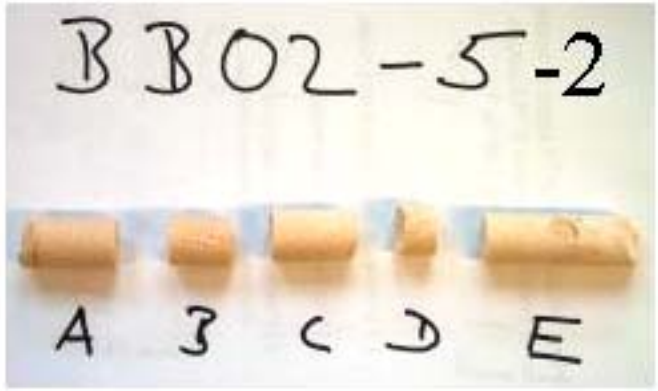

Fig. 4.50: Photography of drill core BB02-5-2. Overall, 11 sub-samples from this core have been analysed.

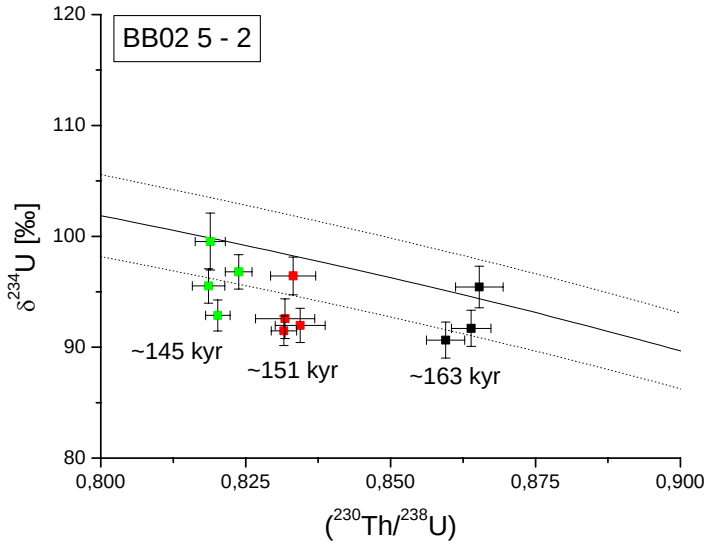

Fig. 4.51: U-series data of the sub-samples of drill core BB02-5-2. There are three clusters of ages around ~145, ~151, and ~163 kyr. As all sub-samples belong to one and the same coral, these age discrepancies clearly must have been produced by diagenesis. Nevertheless, all samples plot on or below the seawater evolution curve. This strongly supports the above proposed scenario that substantial U has been added to the cores, but with $\delta^{234}U_{add}$ in the range of the coral itself. The age differences are produced either by different amounts of additional U or by different timing of addition.

It can be concluded that the isotopic anomalies of the samples from location BB02-5 most likely result from 'U-redistribution'. If one sample within the reef looses part of its U due to dissolution or recrystallisation, the released U is taken up by surrounding corals. In this case the additional component has a similar $\delta^{234}U$ value as the gaining coral which results in lower ($^{230}Th/^{238}U$) activity ratios and U-series ages, but does not affect the measured $\delta^{234}U$.

4.2.5.5 Identification of reliable U-series ages

As it has been shown in the two previous chapters that it is not generally possible to apply isochron dating to the Barbados corals, the usual reliability criteria must be applied. These are listed in chapter 2.2.4 (page 25). Unfortunately, XRD-measurements have not been performed yet so that the aragonite content (criterion 4) of the analysed samples is not known. As the recrystallisation from aragonite to calcite results in substantial loss of U (see chapter 2.2.4), these effects can also be detected by measuring a large number of samples and comparison of their U content. In this study not only a large number of corals from the same reef, but rather many sub-samples within each drill core have been analysed. Consequently, it should be possible to detect even subtle changes in isotopic composition and coral U concentration. That the investigation of a large sample number provides an additional reliability criterion as important as the other ones, has also been suggested by other authors (*Potter et al., 2004*).

Except for four sub-samples all corals from the lower unit have ^{232}Th concentrations lower than 1 ppb. Only sub-samples BB02-4-4, BB02-5-3-A-II, BB02-5-3-C-II, and BB02–5–3-D-II have ^{232}Th contents slightly higher than 1 ppb (Tables C6 and C7, Appendix C). For the latter three this most likely results from the sample preparation, because in contrast to the other samples, they have been crushed in a mechanical crusher. However, it must be emphasized that – even if extremely high ^{230}Th/^{232}Th ratios are assumed – the resulting correction for detrital ^{230}Th was insignificant. Therefore, these three samples are not sorted out by the ^{232}Th criterion.

The ^{238}U content of the samples has been extensively discussed in the previous chapter. It has been shown that drill cores from location BB02-5 suffered substantial post-depositional U addition or loss, respectively. Consequently, the data from these drill cores cannot be considered as reliable. An exception is sub-sample BB02-5-4-B-R, because its ^{238}U content is 3.17 ppm and therefore in the normal range (Table C7, Appendix C). As this sample looked different (i.e. red) under ultraviolet light, it has most likely neither been mineralogically altered nor suffered U loss. Consequently, this sub-sample has not been sorted out by the ^{238}U content criterion. All samples from location BB02-4 have U contents within the normal range.

After application of the initial δ^{234}U criterion, six sub-samples which can be considered as strictly reliable remain. The ages of these sub-samples range from 168.9 ± 1.5 to 176.1 ± 2.8 kyr. This is shown in Table 4.9.

Drill core	^{232}Th criterion	^{238}U criterion	Initial δ^{234}U criterion	Range of reliable ages [kyr]
BB02-4-1	7/7	7/7	0/7	-
BB02-4-2	4/4	4/4	1/4	176.1 ± 2.8
BB02-4-3	4/4	4/4	3/4	168.9 ± 1.5 – 170.9 ± 1.2
BB02-4-4	3/4	3/3	1/3	168.5 ± 3.8
BB02-5-1	9/9	0/9	-	-
BB02-5-2	11/11	0/11	-	-
BB02-5-3	13/13	0/13	-	-
BB02-5-4	4/4	1/4	1/1	168.8 ± 1.4

Table 4.9: Compilation of the coral ages considered as strictly reliable. The Table must be read as follows: In each column the ratio of the number of sub-samples which fulfil the respective criterion to the total number of sub-samples is listed. Samples which do not fulfil a criterion are sorted out and consequently not listed in the next column. In the last column the ages which fulfil all criteria and therefore are considered as strictly reliable are listed.

It is interesting that most sub-samples from the drill cores from location BB02-5 fulfil the initial δ^{234}U criterion (Table C7, Appendix C). The ages of the respective sub-samples range from 143.9 ± 1.1 to 178.9 ± 4.4 kyr. As all these sub-samples have suffered significant U addition, this shows that the initial δ^{234}U criterion alone is not sufficient to identify diagenetically altered corals. If the added U has the same δ^{234}U or some U is lost, this will not affect δ^{234}U. This shows the importance of measuring a large number of sub-samples, because this enables to identify even subtle changes in ^{238}U content. Another way to identify such alterations is to apply combined Th/U- and Pa/U-dating (see chapters 2.1.2 and 2.2.5). Therefore, four sub-samples from drill core BB02-5-3 will be dated by the ^{231}Pa/U-method as well. Unfortunately, these ages which will be measured at the University of Bristol are not available yet.

The last conclusion agrees with the results of *Gallup et al.* (*2002*) who found that the initial δ^{234}U criterion is not sufficient to identify *all* samples that have experienced diagenetic alterations. Unfortunately, if the additional U has the same δ^{234}U value as the gaining coral, as well isochron dating (*Scholz et al., 2004*) as the models of other authors (*Thompson et al., 2003; Villemant & Feuillet, 2003*) cannot be used to correct the ages, because all need elevated δ^{234}U values for the correction.

4.2.5.6 Magnitude, timing and duration of the MIS 6.5 sea level peak

The lower unit below the University of the West Indies has first been extensively studied by *Gallup et al.* (*2002*). They reported U-series ages ranging from 168 ± 1.3 to 205.8 ± 2 kyr. In that study combined Th/U- and Pa/U-dating was used to identify diagenetically altered corals. *Gallup et al.* (*2002*) had only one coral sample they considered as strictly reliable. The Th/U age of this sample is 168 ± 1.3 kyr, its Pa/U age is 160.4 ± 8.5. Because of the rather large error of the Pa/U age (5.3%), it may be possible that subtle diagenetic changes have not been identified. However, the discovery of corals which grew during MIS 6.5 was the first well-documented measure of sea level from this period. Nevertheless, because only one age was considered to be strictly reliable, the timing and duration of substage MIS 6.5 could not be determined in that study.

According to *Taylor & Mann* (*1991*), the uplift rate of the study site below the University of the West Indies is 0.44 m/kyr. This value has also been used by *Gallup et al.* (*2002*). Unfortunately, *Taylor & Mann* (*1991*) do not quote errors for the uplift rate. It has been estimated from the actual height of the Last Interglacial reef terrace (60 ± 2 m r.p.s.l.), a Last Interglacial sea level of 5 ± 3 m r.p.s.l., and an age of 125 kyr for the Last Interglacial sea level peak (*Taylor & Mann, 1991; Gallup et al., 1994*). Linear error propagation of these uncertainties yields an error of 0.03 m/kyr.

The samples from location BB02-4 have been collected at an elevation of +36 ± 3 m r.p.s.l., those from location BB02-5 at an elevation of +34 ± 3 m r.p.s.l.. The corresponding paleo sea levels have been calculated by equation (3.2). The results are shown in Fig. 4.52.

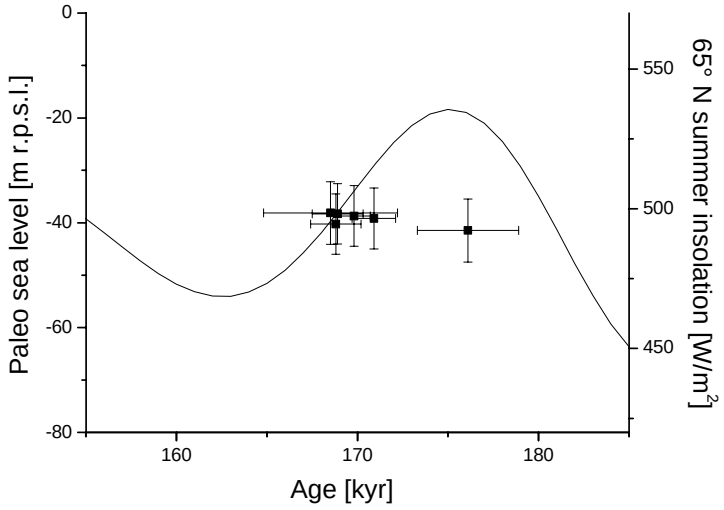

Fig. 4.52: Comparison of the calculated paleo sea level data with the 65° N summer insolation curve (*Berger & Loutre, 1991*). The black squares show the estimated paleo sea level based on the coral data which are believed to be strictly reliable. The paleo sea level errors have been calculated by linear error propagation.

Based on the strictly reliable coral data (black squares in Fig. 4.52), the estimated paleo sea levels range from –38 ± 6 to –41 ± 6 m r.p.s.l. confirming the results of *Gallup et al.* (*2002*). It is evident from Fig. 4.52 that the estimated timing and duration of the MIS 6.5 sea level highstand is in good agreement with the peak in 65° N summer insolation (*Berger & Loutre, 1991*). This suggests that insolation changes may have been the primary trigger for major ice sheet melting during that time in agreement with the Milankovitch theory (*Milankovitch, 1941*, see also chapter 3.1.1). *Gallup et al.* (*2002*) have shown by U-series dating of corals from the middle unit (see Fig. 4.31, page 91) that insolation changes have not been the trigger for global ice volume melting during Termination II. As in this study only two locations from the lower unit (i.e. MIS 6.5 reef) have been sampled, and there is only one strictly reliable coral age for the beginning of MIS 6.5 available (i.e. sample BB02-4-2-D1 with an age of 176.1 ± 2.8 kyr), it is possible that – if further sampling was applied – older corals could be found. From the existing strictly reliable coral data, there is no evidence for such a scenario.

The outcrop below the University of the West Indies is the only location worldwide where corals from MIS 6.5 have been found yet (*Gallup et al., 2002*). Therefore, the data presented in this study and *Gallup et al.* (*2002*) are the only direct measurement of sea level which is available for this period. All other MIS 6.5 sea level reconstructions are based on stable isotopes (see chapter 3.1.1) or submerged speleothems (chapter 3.1.3). Fig. 4.53 shows a comparison of the coral data with other reconstructions of MIS 6.5 sea level.

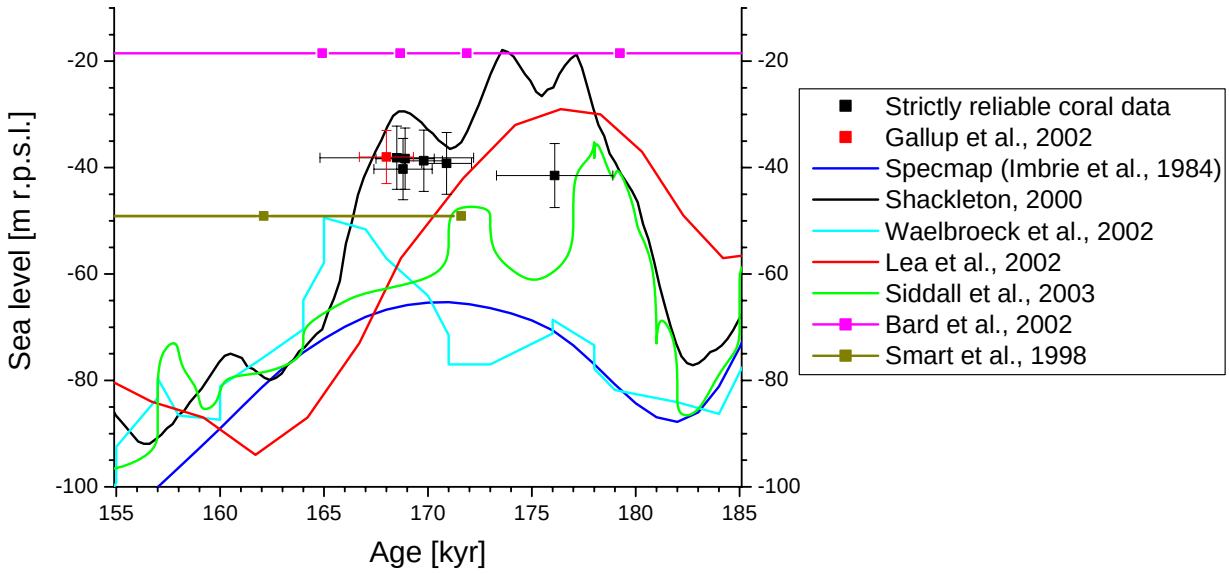

Fig. 4.53: Comparison of the coral based MIS 6.5 sea level with other reconstructions (see Figure legend for the respective references). Coral data from this study (black) and *Gallup et al.* (*2002, red*) are shown as filled squares. Straight curves represent reconstructions that are based on stable isotopes. Submerged speleothem data are shown as connected filled squares.

It is evident from Fig. 4.53 that there are large differences between the available sea level reconstructions within MIS 6.5. The strictly reliable coral data are shown as black squares, the reliable age from *Gallup et al.* (*2002*) as a red square. These data suggest that sea level was around –40 ± 6 m r.p.s.l. from 176 to 168 kyr ago.

Two reconstructions shown in Fig. 4.53 are based on submerged speleothems (plotted as connected squares). It has been explained in chapter 3.1.3 that such data only provide information such as "sea level not higher than". The first record is based on a stalagmite from Argentarola Cave, Italy, and shows continuous growth from 189.7 ± 1.5 to 145.2 ± 1.1 kyr (*Bard et al., 2002a,* shown in magenta in Fig. 4.53). As this speleothem has been sampled at a depth of –18.5 m, these data are in agreement with the coral data. Instead, some speleothem data from South Andros Island suggest that sea level was not higher than –49.1 m at 171.6 ± 4 kyr (*Smart et al., 1998,* shown in dark yellow in Fig. 4.53). Consequently, these data are in conflict with the coral based reconstruction (Fig. 4.53). However, as the morphology of the stalactitic drapery of this speleothem is complex, the earliest growth phase (i.e. the 171.6 ± 4 kyr age) cannot be readily defined (*Smart et al., 1998*).

All other curves shown in Fig. 4.53 are based on stable isotopes. In blue the Specmap curve is shown (*Imbrie et al., 1984*). As a first order approximation, it has been linearly converted to sea level using two fixed points: –120 m r.p.s.l. for the Last Glacial maximum (MIS 2) and the +6 m r.p.s.l. for the Last Interglacial (MIS 5e). The resulting reconstruction yields sea levels not higher than –65 m r.p.s.l. during MIS 6.5. If the coral based reconstruction is correct, this suggests that the $\delta^{18}O$-signal is largely affected by deep sea temperature (see chapter 3.1.1). In all other stable isotope based reconstructions shown in Fig. 4.53 additional information has been used to untangle the temperature from the ice volume component.

In the reconstruction of *Waelbroeck et al.* (*2002*, shown in cyan) relative sea level data (i.e. mostly fossil corals) have been used to derive transfer functions between sea level and benthic $\delta^{18}O$. The uncertainty of this sea level record is considered to be at least ±13 m (*Waelbroeck et al., 2002*). The resulting sea levels are not higher than –50 m r.p.s.l. for the later part of MIS 6.5 (i.e. around 165 kyr) and about –75 m r.p.s.l. around 175 kyr (Fig. 4.53). As the coral data suggest that sea level was already at –40 m r.p.s.l. at that time, this shows that the transfer functions which have been developed using data from the last climatic cycle (i.e. maximum coral age ~135 kyr) seem not to be generally applicable to the penultimate climatic cycle.

The green curve (Fig. 4.53) is the sea level record by *Siddall et al.* (*2003*). In this reconstruction a hydraulic model of the water exchange between the Red Sea and the world ocean is used to convert oxygen isotopes into global sea level. A detailed description of the method which is accurate to within ±12 m (*Siddall et al., 2003*) can be found in *Siddall et al.* (*2004*). This sea level record roughly agrees with the coral based reconstruction in the earlier part (i.e. around 175 kyr, Fig. 4.53), but suggests lower sea levels in the later part (i.e. –60 m around 170 kyr, **Fig.** 4.53).

Also included in Fig. 4.53 is a sea level reconstruction from *Lea et al.* (*2002*, shown in red). This reconstruction uses calcification temperatures from Mg/Ca to remove the temperature signal from a $\delta^{18}O$ record of planktonic foraminifera (*Lea et al., 2002*). The resulting sea levels are slightly higher (i.e. –30 m r.p.s.l.) than suggested by the coral record in the earlier MIS 6.5 period and slightly lower (i.e. –50 m r.p.s.l.) in the later part (Fig. 4.53). The uncertainty range quoted for this reconstruction is +21 -27 m. Considering these rather large error ranges the reconstruction is in good agreement with the coral data.

Finally, in black a reconstruction by *Shackleton* (*2000*) is shown (Fig. 4.53). In this paper the ice volume component of a benthic $\delta^{18}O$ signal was extracted by using the record of $\delta^{18}O$ in atmospheric oxygen trapped in the Vostok ice core (*Petit et al., 1999*). The resulting sea level curve suggests very high sea level in the earlier part (i.e. –20 m r.p.s.l. around 175 kyr, Fig. 4.53), but is in agreement with the coral data in the later part (-33 m r.p.s.l.). There is no error range given for this reconstruction. It should be mentioned that the highest MIS 6.5 sea levels resulting from this reconstruction are in contrast with the submerged speleothem data from *Bard et al.* (*2002a*) (see Fig. 4.53). This has also been discussed by other authors (*Bard et al., 2002a; Waelbroeck et al., 2002*).

It is evident from the discussion above that there are large differences between the several stable isotope based sea level reconstructions (e.g. up to 60 m between the *Shackleton* (*2000*) and the *Waelbroeck et al.* (*2002*) records around 175 kyr). This highlights the problems that are associated with such reconstruction methods. In addition, the time scales of all reconstructions have been developed by orbital tuning (see chapter 3.1.1), either by correlating with Specmap (*Lea et al., 2002; Waelbroeck et al., 2002; Siddall et al., 2003*) or by more sophisticated methods (*Shackleton, 2000*). As it has been shown for Termination II that the global sea level rise precedes the peak in northern summer insolation by several kyr (e.g.*Winograd et al., 1992; Henderson & Slowey, 2000; Gallup et al., 2002*), the timing of all reconstructions may be associated with considerable uncertainty as well. Interestingly, all records except for the *Lea et al.* (*2002*) record suggest that sea levels were higher in the early MIS 6.5 phase (~175 kyr) than in the later one (~170 kyr) (*Shackleton, 2000; Siddall et al., 2003*) or conversely (*Waelbroeck et al., 2002*). Although there is only one strictly reliable coral age for the early phase available, there is no such trend observable in the coral record.

The results of this study can also be used to verify the sea level variations proposed by conceptual models of climate change at orbital time scales. A recently published model by *Ruddiman* (*2003*) assumes that variations in global ice volume are – as proposed by *Milankovitch* (*1941*) – forced by changes in northern summer insolation, but in addition it is supposed that the insolation forcing is enhanced by responses to greenhouse gases (i.e. CO_2 and CH_4). This model proposes that sea level during MIS 6.5 was approximately as high as today (*Ruddiman, 2004*). The coral data show that this value is considerably too high. Another recent model by *Parrenin & Paillard* (*2003*) suggests that deglaciation starts when a combination of insolation *and* ice volume is large enough. Interestingly, the MIS 6.5 sea level proposed by this rather simple model (i.e. between -40 and -50 m r.p.s.l.) is in good agreement with the coral based MIS 6.5 sea level.

4.2.6 Conclusions II

Several fossil reef corals of the genus *Acropora palmata* and *Diploria strigosa* which have been collected from an outcrop below the University of the West Indies, Barbados, West Indies, have been investigated. The corals from the middle unit grew during the Last Interglacial, those from the lower unit during Marine Isotope Substage 6.5. All samples have ^{232}Th contents within the usual range. While the most samples have normal ^{238}U concentrations, the drill cores collected at one location (BB02-5) show evidence for U addition as well as loss. Many of the analysed samples show elevated initial $\delta^{234}U$ values, but to a much lesser degree than the corals from Aqaba, Jordan.

As the isotopic anomalies in the Barbados corals are less pronounced, it could not be discovered if the assumptions for isochron dating are fulfilled. While the data from some drill cores show moderate to high correlations, others show no correlation at all. Therefore, the ages which have been derived by isochron dating have not been used for sea level reconstruction. The calculated isochron slopes show that – in contrast to the Aqaba data – the Barbados data can be described by U uptake alone.

The ^{238}U content of the BB02-5 corals shows a correlation with the ($^{230}Th/^{238}U$) activity ratio, but not with $\delta^{234}U$. This suggests that these samples gained substantial U after deposition, but that the $\delta^{234}U_{add}$ value of this U was similar as in the gaining corals. This is also confirmed by the calculated activity ratios of the additional component. As some sub-samples of drill core BB02-5-4 show substantial U loss, this indicates that the U which has been lost by some corals has been gained by other ones. This is further supported by the timing estimated for U loss and uptake, respectively.

To identify unaltered corals the usual reliability criteria have been applied. The resulting ages are in good agreement with those reported by *Gallup et al.* (*2002*) for the same location. Based on the strictly reliable ages, sea level was at ~-40 m r.p.s.l. from 176 to 168 kyr BP in good agreement with the corresponding peak in northern summer insolation. Within uncertainty the coral based reconstruction is in good agreement with the reconstruction by *Lea et al.* (*2002*).

The coral data presented here and in the study of *Gallup et al.* (*2002*) are the only direct measurement of MIS 6.5 sea level worldwide. Because of its high dating precision, the presented MIS 6.5 sea level reconstruction is the most accurate in magnitude as well as in timing presently available. These results provide important information about deep sea temperatures or the Dole effect during this period of extraordinary climate signature.

5 Summary and outlook

Fossil reef corals are ideally qualified for the reconstruction of past sea level changes, because they represent a direct measurement of sea level and can be absolutely dated by U–series methods. Therefore, they provide more accurate sea level information than $\delta^{18}O$ signals from deep sea cores (which are affected by deep sea temperature as well) and submerged speleothems (which only give information such as "not higher than"). Unfortunately, many fossil reef corals show significantly elevated initial $\delta^{234}U$ values which are clear evidence for open system behaviour. Consequently, the ages of such corals are not believed to be strictly reliable.

In this study some *Porites* corals from Aqaba, Jordan, as well as corals of the genus *Acropora palmata* and *Diploria strigosa* from Barbados, West Indies, have been investigated. The corals from Aqaba show a very high degree of diagenetic alteration and could not be dated by conventional U-series methods. The activity ratios in different sub-samples of one and the same coral are strongly linearly correlated on a $\delta^{234}U$-($^{230}Th/^{238}U$)-diagram. It has been demonstrated that different sub-samples gained different amounts of a high $\delta^{234}U$ component and that this additional U component has been partly remobilised later. By modelling it has been shown that the intersection point of the isochron (i.e. the straight line fitted through the activity ratios) with the seawater evolution curve represents the true age of the coral. This is confirmed by the concordance of the isochron age and the calibrated ^{14}C age of the Holocene coral.

Two methods have been used to estimate the isochron age errors. The first approach uses confidence bands and calculates the age uncertainty from the intersection points of the confidence bands with the seawater evolution curve, the other approach is based on a Monte-Carlo-simulation. The latter method can be generally used to estimate the uncertainty of straight lines fitted to data which are associated with uncertainty in x- and y-direction. Especially, it can be applied to all kinds of so-called 'excess-scatter' isochrons or 'errorchrons'. It has been shown that – in the case of low correlation coefficients and/or small data point distances – the Monte-Carlo approach yields more realistic error ranges.

This new isochron dating approach enables to assign reliable ages to corals which could not be dated with conventional U-series methods. For example, it has been possible to calculate a reliable age of a coral which has been used in a high resolution paleoclimate study (*Felis et al., 2004*). Since the publication of the isochron dating method (*Scholz et al., 2004*) it has been successfully applied by other authors as well (*Potter et al., 2004*).

Although many of the corals from Barbados show clear evidence for diagenetic alterations, these are much less pronounced than in the Aqaba corals. It has been shown that the isochron dating method cannot be generally applied to these corals. Although some of these corals gained U as well, the $\delta^{234}U$ value of the additional U component must have been in the range of the $\delta^{234}U$ of the coral itself. As other corals from the same reef show clear evidence of U loss, it has been concluded that the Barbados corals have suffered U redistribution which means that some corals have taken up the U which has been lost by others. As a consequence of this scenario, although these corals gained substantial U which results in younger ages, the initial $\delta^{234}U$ values of the Barbados corals are not elevated. If only a small but significant amount of U has been added, the resulting alteration would not have been detected by the existing reliability criteria. Such subtle alterations can be identified by investigation of a large number of sub-samples or combined Th/U- and Pa/U-dating.

The comparison of both studies shows that the corals from the two different locations have been affected by different processes. This is for example demonstrated by the substantial differences between the isochron slopes calculated at both locations. This result disagrees with the models proposed by other authors (*Thompson et al., 2003; Villemant & Feuillet, 2003*). In addition, the results from both studies show that – in contrast to U – Th is not mobilised. This also contradicts the other models. Rather, the Aqaba as well as the Barbados corals have gained U after deposition, but while the additional U has been partly remobilised at Aqaba, this did not happen on Barbados. Furthermore, the additional U at Aqaba had a much higher $\delta^{234}U_{add}$ value. This shows that the processes which produce diagenetic alterations in fossil reef corals seem to depend strongly on the specific conditions in the study region. In addition, they seem to be influenced by the specific characteristics of the respective coral species. Consequently, one explanation for the observed differences between Aqaba and Barbados may be the substantially lower porosity of corals of the genus *Acropora palmata* than *Porites*.

It remains unidentified *which parts* of the coral gain and/or lose U and *how* this happens. Another question is if these processes are rather continuous or if they take place during specific (climatic?) periods only. On the one hand, these questions should be investigated by studying a large number of different coral species from various locations worldwide, on the other hand, important insights about the diagenetic processes may be revealed by laboratory experiments. The main problem of such experiments is that the isotopic alterations take place on very large timescales (i.e. at least several thousand years) and therefore are hard to simulate. Combined Th/U- and Pa/U-dating may also provide valuable information.

Because of the rather large uncertainties of the isochron ages and the tectonic uplift rate at Aqaba, the sea level reconstruction at this location is difficult. The likeliest interpretation of the terrace structure is that the lower one (3 to 5 m asl) represents a second highstand at the end of the Last Interglacial which was a few meters lower than the main MIS 5e sea level peak. This question cannot be finally answered with the presently available data.

The strictly reliable coral data from Barbados show that sea level was at ~-40 m r.p.s.l. between 176 and 168 kyr BP. This sea level peak corresponds to the rather small peak of MIS 6.5 in the Specmap curve. Timing and duration of the highstand are in good agreement with the Milankovitch theory. Within uncertainty, the coral based sea level record agrees best with the reconstruction by *Lea et al.* (*2002*).

The coral data presented in this work and the study of *Gallup et al.* (*2002*) are the only existing direct measurement of MIS 6.5 sea level worldwide. According to the high dating precision, this presented reconstruction is the most accurate in magnitude as well as in timing presently available. These results may provide important information for the reconstruction of deep sea temperatures or the Dole effect during this period. As the climate of MIS 6.5 seems to be unique within at least the last 250,000 years, it offers the possibility to study the complex forcing and feedback mechanisms of the climate system. Such investigations could be performed using climate models. An accurate estimate of global ice volume during this period will be very helpful for such investigations.

The available stable isotope based MIS 6.5 sea level records exhibit large differences. This highlights the problems which are associated with sea level reconstructions from stable isotope variations in deep sea cores. Therefore, future studies should try to extend the coral based sea level record to the penultimate interglacial (MIS 7). This is rather difficult, because most corals from this period show substantial diagenetic alterations. To date, only few strictly reliable ages are available for MIS 7. In this context the isochron dating method proposed in this study may help to enlarge the database of reliable corals substantially.

Appendix

A Thermal ionisation mass spectrometry (TIMS)

A1 Sample preparation

The complete sample preparation has been performed in a clean lab, and only supra-pure chemicals have been used. After coral pre-treatment and selection of the coral parts that showed the least evidence of diagenetic alteration (see chapters 4.1.2 and 4.2.3), coral pieces of 300 to 500 mg have been sawn off the colonies. The surface of these pieces has been cleaned by a brief leaching in 7N HNO_3. Then the dried samples were weighed and dissolved in 7N HNO_3. No insoluble remains were present for all samples so that no further treatment like filtration, centrifugation, or HF decomposition was necessary. Afterwards, defined amounts of U- and Th-spikes (see Appendix A4) have been added to determine the U and Th concentrations of the samples, respectively.

Thereafter, the solution was chromatographically separated using DOWEX 1□8 resin material and ion exchange columns. The single steps of the chemical separation process can be found for example in *Hoffmann* (*2002*). Finally, the resulting U- and Th-bearing HNO_3 solution has been reduced by evaporation to a droplet of ~2 µl and transferred to a rhenium filament for the mass spectrometric analysis.

A2 Thermal ionisation mass spectrometry (TIMS)

All U- and Th-measurements of this work have been performed on a solid source thermal ionisation mass spectrometer (TIMS) which enables the determination of isotope ratios with very high precision. The measurements have been conducted on a Finnigan MAT 262 RPQ (Fig. A.1) with a double filament technique. The samples are loaded on the evaporation filament from which they are thermally evaporated. A second filament, the ionisation filament, is located at a distance of about 1 mm opposite of the evaporation filament. This filament provides a high temperature (~1700° C) that enables to control the ionisation process precisely. Because of their different specific evaporation temperatures, U and Th isotopes are measured separately. First, U isotopes are measured at temperatures between 1650 and

1700° C, afterwards Th isotopes are measured at temperatures between 1730 and 1760° C. The positive ions are accelerated in a high voltage field (~10 kV) and the ion beam is focused by an electromagnetic lens system. In a strong magnetic field (~ 1 Tesla) the ion beam is separated according to the specific charge (q/m ratio) of the respective ions.

The relative abundance of the respective isotopes is then determined by Faraday cups (for ion currents higher than 1 mV) or by an Ion Counting Multiplier (ICM). A second ICM which is equipped with a Retarding Potential Quadrupol (RPQ) that effectively prohibits interferences of similar isotopes is used for Th measurements.

Fig. A.1: Photography of the Finnigan MAT 262 RPQ Thermal Ionisation Mass Spectrometer that is used at the Heidelberg Academy of Sciences.

According to the better ionisation efficiency, U and Th isotopes have been measured in their oxidized forms UO and ThO. Therefore, a correction for the relative abundances of the oxygen isotopes ^{16}O (99.756 %), ^{17}O (0.039 %), and ^{18}O (0.205 %) had to be performed. The detailed equations that have been used to perform the oxide correction can be found in *Neff* (*2001*).

An extended description of the basics of the TIMS technique, the MAT 262 RPQ, the measuring routines, and the necessary calibrations is given in *Neff* (*2001*) as well.

A3 Blanks

U as well as Th total procedural blanks (i.e. a sample which experienced exactly the same treatment (chemical separation, etc.) as the analysed samples) have been routinely measured. Because the ^{230}Th and ^{234}U concentrations of the blanks are close to the detection limit of the TIMS technique, their isotopic abundances have not been estimated from the measurements, but from the measured concentrations of ^{232}Th and ^{238}U, respectively. Such an estimation can be done similarly to the correction for detrital contamination (see chapter 2.1.3) assuming a bulk earth ^{232}Th/^{238}U ratio of 3.8 ± 1.0 (*Wedepohl, 1995*) and secular equilibrium for the U–series nuclides of the contaminants.

Fig. A.2 shows the development of the blanks during this work.

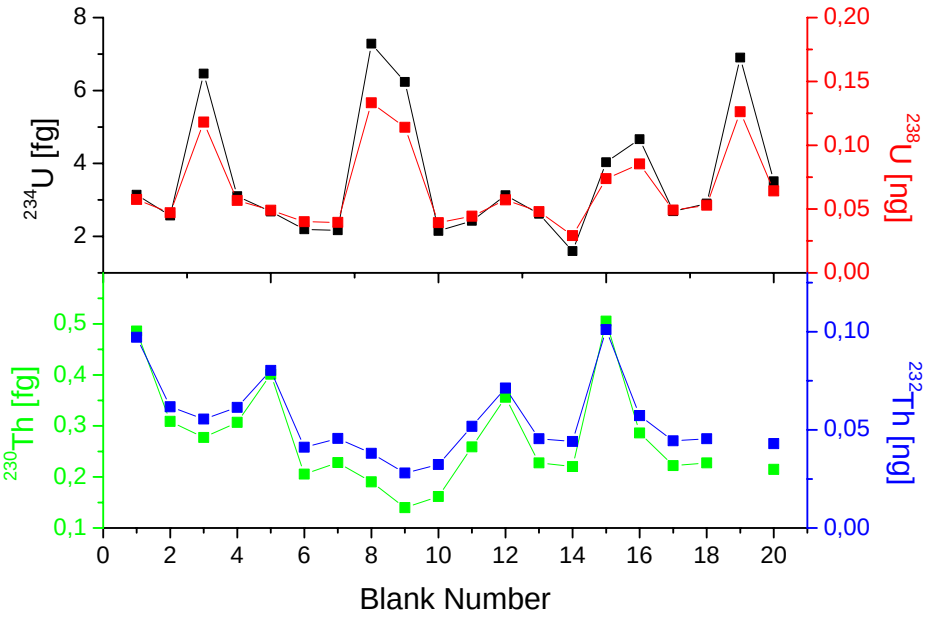

Fig. A.2: The timely development of the ^{234}U, ^{238}U, ^{230}Th, and ^{232}Th blanks, respectively.

The average blanks of the respective U-series isotopes measured in this work are:

^{234}U: 3.6 ± 1.7 fg
^{238}U: 0.07 ± 0.03 ng
^{230}Th: 0.28 ± 0.1 fg
^{232}Th: 0.06 ± 0.02 ng

Although all measured blanks are insignificant, a routinely correction for the blanks has been applied to all samples presented in this work.

A4 U and Th standards and spikes

To assign the appropriate errors to the calculated U-series ages it is required that accurate uncertainties are quoted for the measured isotope and activity ratios, respectively. For this reason, a so-called *internal* or *within run* precision is calculated by the operating software which is simply given as the 2σ-error-of-the-mean for the measured isotope ratio. However, for TIMS and ICP-MS measurements the internal precision contributes only a part of the total variance of the isotope ratio next to other (non-systematic) sources of error (see *Ludwig* (*2003*) for a listing of such potential error sources). Therefore, the true precision (or *reproducibility*) of the runs can only be reliably established by replicate analyses of natural samples or standard solutions.

At the Heidelberg Academy of Sciences the reproducibility of the TIMS measurements is estimated by regularly measuring standard solutions. The reproducibility can then be calculated by the standard deviation. For U measurements the U-standard solution 112A with a ^{238}U concentration of 4.395 ± 0.009 ppm (1σ SD, n=35) is used. Fig. A.3 shows replicate measurements of the ^{238}U concentration of standard 112A.

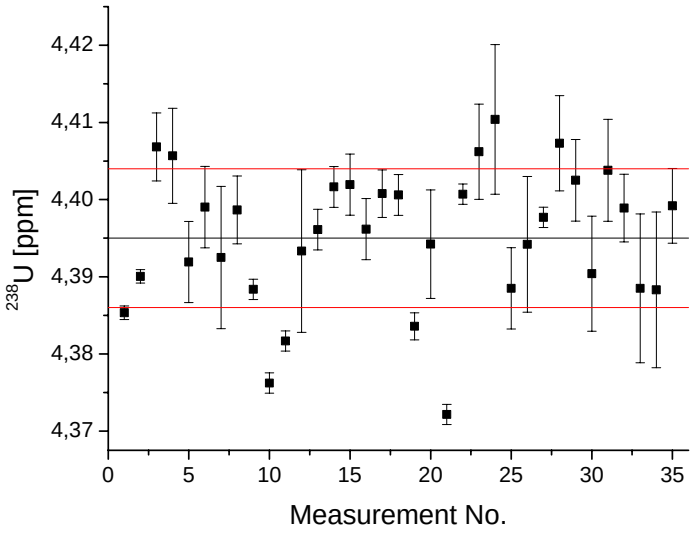

Fig. A.3: Replicate measurements of the ^{238}U concentration of U-standard solution 112A. The mean value is 4.395 ± 0.009 ppm (1σ SD, n = 35) corresponding to a reproducibility of 2‰. The black line indicates the average value, the red lines show the 1σ-error range. The error bars represent the within run precision of the single measurement. It is evident that the total precision is significantly lower than the internal precision.

The ^{234}U concentration of 112A is 0.228 ± 0.001 ppb (1σ SD, n = 35) corresponding to a reproducibility of 4.4‰.

The reproducibility of the Th analyses is checked by regular measurements of the Th standard solution HDAKT1. Fig. A.4 shows a compilation of ^{232}Th measurements between 1998 and 2004.

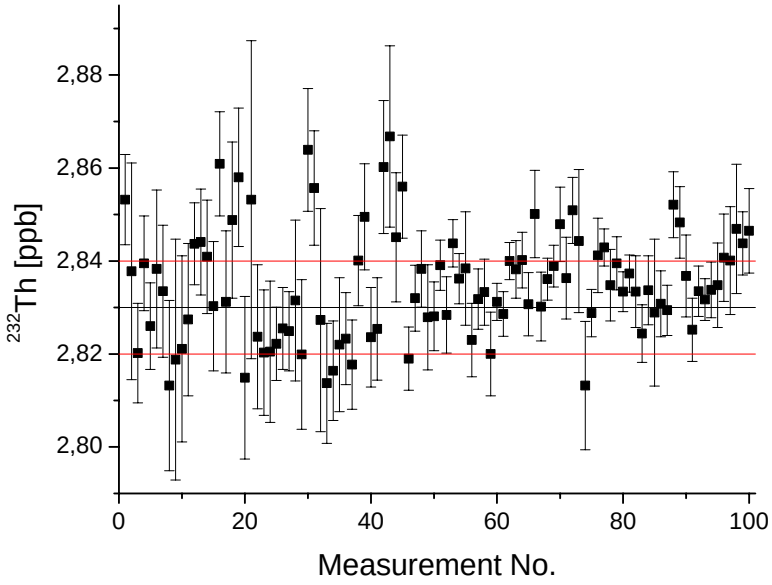

Fig. A.4: Replicate measurements of the ^{232}Th concentration of Th-standard solution HDAKT1. The mean value is 2.83 ± 0.01 ppb (1σ SD, n = 100) which corresponds to a reproducibility of 3.5‰. The black line indicates the average value, and the red lines show the 1σ-range.

The ^{230}Th concentration of HDAKT1 is 7.36 ± 0.05 ppt (1σ SD, n = 97) corresponding to a reproducibility of 6.8‰.

It must be emphasized that the values quoted for the reproducibility of the respective isotope concentration are strictly speaking only valid for the analysed standard solutions. If the U (and/or Th) contents of an analysed sample were much different, the reproducibility would be significantly different as well. For example, this is the case for a Last Interglacial coral where the ^{230}Th concentration is about one order of magnitude higher than for the HDAKT1 Th standard solution. This suggests that the reproducibility should be better than 6.8‰ as well.

The TIMS technique only allows the measurement of isotope *ratios*. Therefore, so-called U and Th *spike* solutions with accurately known concentrations of synthetic U (i.e. ^{233}U and ^{236}U) and Th (i.e. ^{229}Th) isotopes are added to the dissolved samples. Then, the U and Th isotope concentrations of the sample can be calculated from the atomic ratio of the natural to the synthetic isotope. As the spike calibration is a potential source for systematic errors affecting the accuracy of U-series dates (*Ludwig, 2003*), this must be done very carefully.

In 2004 a recalibration of the U and Th spikes used at the Heidelberg Academy of Sciences has been performed. The ^{233}U-^{236}U-double spike UDOPN99 was calibrated against two standard solutions. One was produced at the Heidelberg lab by dissolving an accurately weighed and chemically pre-treated piece of the *CRM 112-A* Uranium Metal Assay Standard which has a total U content of 99.975 ± 0.006 weight percent. A second U standard solution, the Baker Instra Analyzed Uranium ICP standard which has a total U content of 1000 µg/ml (= 994 ppm) was bought from the company J.T.Baker. The U concentration of this standard is denoted with an uncertainty of 0.2%. From each of these two primary solutions two U standard solutions have been produced by accurate dilution. The resulting solutions had a ^{238}U content between 4.4718 and 5.7809 ppm.

Similarly, a Th standard solution has been produced by accurate dilution of the Baker Instra Analyzed Thorium ICP standard solution which has a total Th concentration of 1000 µg/ml (= 987 ppm). The uncertainty of this value is quoted with 0.2% as well.

As each of the primary solutions is already affected with about 0.2% uncertainty and considering the additional uncertainty arising from the dilution process (i.e. from the weighing), the precision of the calibration of the U and Th spikes respectively cannot be better than 0.2% either. Additional uncertainty (between 0.1% and 0.2%) arises from the TIMS measurements that are used for the spike calibration. Therefore, the uncertainty in the ($^{230}Th/^{238}U$) activity ratio reclusively resulting from the spike calibration will not be less than ~4‰. As the reproducibility of the single TIMS measurements is at the same order of magnitude, it would be preferable to have a more accurate method of spike calibration.

One possibility is to use materials that are likely to have behaved as closed systems for 10^6 years or more and consequently should be in a state of secular equilibrium. A solution which has often been used as a secular equilibrium standard in alpha counting and TIMS laboratories is the Harwell uraninite (HU-1) standard solution (*Cheng et al., 2000*). Originally, this solution was prepared from pitchblende powder dissolved according to standard instructions from Harwell. For the spike calibration at Heidelberg an aliquot of a solution provided by Norbert Frank from the CNRS at Gif-sur-Yvette has been used. If this solution really is in secular equilibrium, the Th spike concentration can be adjusted such that the ($^{230}Th/^{238}U$) activity ratio measured for HU-1 is one. As the uncertainty of this activity ratio which is based on replicate measurements of the HU-1 standard solution is very small (~1‰ (2σ), n=18), the spike calibration based on this method should be more accurate than that described above. Unfortunately, a detailed investigation of several materials that were assumed to be in secular equilibrium yielded a higher ($^{230}Th/^{238}U$) activity ratio for a HU-1 solution than for all other analysed materials (*Cheng et al., 2000*). This indicates that the HU−1 solution that was analysed in that study did not behave as a closed system. Either the original powder was not in secular equilibrium, or the higher value of that solution results from the preparation or aliquoting of this particular solution. If so, it is possible that HU-1 solutions in different laboratories could have different ($^{230}Th/^{238}U$) activity ratios (*Cheng et*

al., 2000). For this reason, additional measurements will be performed on another standard solution that is likely to be in secular equilibrium provided Dirk Hoffmann (University of Bristol).

Consequently, the calibration of the U and Th spikes, respectively, has not been finally completed yet. At present, the most accurate value for the U spike concentration is based on the calibration against the mean of all measurements of the four U standard solutions. This results in the following values for the isotopic ratios and concentrations of the $^{233}U/^{236}U$ double spike UDOPN99:

$c(^{233}U)$: 0.3989 ppb
$c(^{236}U)$: 47.813 ppb
$^{233}U/^{236}U$: 0.00845

The most accurate value for the concentration of the ^{229}Th spike 01 can be obtained from the calibration against the HU-1 standard solution assuming that it is in secular equilibrium. Using the above quoted values for the U concentration this results in the following concentration:

$c(^{229}Th)$: 0.1759 ppb

The recalibration of the spike solutions results in slight but significant modifications compared to the previously used values (see e.g. *Neff, 2001; Holzkämper, 2004; Holzkämper et al., 2004; Scholz et al., 2004*). It does not only affect the calculated U and Th isotope concentrations (and consequently activities), but also the ($^{230}Th/^{238}U$) activity ratios. This in turn directly affects the calculated U-series ages.

If the old spike values are used, the average ($^{230}Th/^{238}U$) activity ratio measured on HU-1 is 0.9886 ± 0.0014 being 1.14% too low if the HU-1 solution is in secular equilibrium. As the new spike calibration has been adjusted such that the HU-1 ($^{230}Th/^{238}U$) activity ratio is one, the old values can be corrected by multiplying the measured ($^{230}Th/^{238}U$) activity ratios by a factor of 1.0115.

The entire U-series data presented in this work have been measured before the recalibration of the U and Th spikes, respectively. Of course, if the new values were used, the U and Th concentrations of the samples as well as the quoted U-series ages would be significantly different (i.e. lower values for U and Th concentrations, but higher (i.e. older) U-series ages). Due to lack of time, the U-series data measured on the corals from Aqaba, Jordan (chapter 4.1), have not been recalculated. It must be emphasized here that these changes do not affect the general conclusions which have been drawn from the Aqaba data including the correlation between $\delta^{234}U$ and ($^{230}Th/^{238}U$), the isochron dating method, and the modelling of

the diagenetic processes. As the recalculated isochron ages would be slightly older (~3 kyr), the interpretation of the terrace structure as two highstands within the Last Interglacial is even confirmed. The coral data from Barbados, West Indies (chapter 4.2), have already been recalculated with the recalibrated spike concentrations.

B Visual Basic Scripts

In the context of this work several Algorithms have been used. All Algorithms have been written in Visual Basic and can be integrated into Microsoft Excel. In this chapter the corresponding Visual Basic Scripts can be found.

B1 Calculation of U-series ages, initial δ234U and the corresponding errors

The following Algorithm (*ThU_Alter_Kombi*) has been used to calculate the U-series ages. The input variables are the measured ($^{230}Th/^{238}U$) and ($^{234}U/^{238}U$) activity ratios of the sample, respectively. *ThU_Alter_Kombi* numerically solves the Th/U-age equation (equation 2.6) using a combination of the *Bisection* and the *Newton-Raphson*-method. The Algorithm has been adopted from *Press et al.* (*1988*).

```
Function ThU_Alter_Kombi(ByVal AV!, ByVal AU!) As Variant

  Dim lan234!, lan230!, t#, WERT#, ABL#, i&, swap#, x1#, x2#, xacc#, dx#, fh#, fl#, xh#, xl#, dxold#, temp#

  AV = AV
  AU = AU
  lan234 = 0.0000028263
  lan230 = 0.0000091577

  xacc = 0.0001
  x1 = 0
  x2 = 1000000
  i = 0

  fl = ((1 - Exp(-lan230 * x1)) + (AU - 1) * (lan230 / (lan230 - lan234)) * (1 - Exp(-(lan230 - lan234) * x1))) - AV
  fh = ((1 - Exp(-lan230 * x2)) + (AU - 1) * (lan230 / (lan230 - lan234)) * (1 - Exp(-(lan230 - lan234) * x2))) - AV

  If fl * fh >= 0 Then

    ThU_Alter_Kombi = "Out of range"

  Else

    If fl < 0 Then
      xl = x1
      xh = x2

    Else
      xh = x1
      xl = x2
      swap = fl
      fl = fh
      fh = swap

    End If
```

```
    t = 0.5 * (x1 + x2)
    dxold = Abs(x2 - x1)
    dx = dxold

    WERT = ((1 - Exp(-lan230 * t)) + (AU - 1) * (lan230 / (lan230 - lan234)) * (1 - Exp(-(lan230 - lan234) * t))) - AV
    ABL = lan230 * Exp(-lan230 * t) - (AU - 1) * (lan230 / (lan230 - lan234)) * (-lan230 + lan234) * Exp((-lan230 + lan234) * t)

    For i = 1 To 100 Step 1

      If ((t - xh) * ABL - WERT) * ((t - xl) * ABL - WERT) >= 0 Then

        dxold = dx
        dx = 0.5 * (xh - xl)
        t = xl + dx

        If Abs(dx) < xacc Then

          ThU_Alter_Kombi = Application.Round(t / 1000, 4)
          Exit For

        End If

      ElseIf Abs(2 * WERT) > Abs(dxold * ABL) Then

        dxold = dx
        dx = 0.5 * (xh - xl)
        t = xl + dx

        If Abs(dx) < xacc Then

          ThU_Alter_Kombi = Application.Round(t / 1000, 4)
          Exit For

        End If

      Else

        dxold = dx
        dx = WERT / ABL
        temp = t
        t = t - dx

        If temp = t Then ThU_Alter_Kombi = Application.Round(t / 1000, 4)

      End If

      If Abs(dx) < xacc Then

        ThU_Alter_Kombi = Application.Round(t / 1000, 4)
        Exit For

      End If

      WERT = ((1 - Exp(-lan230 * t)) + (AU - 1) * (lan230 / (lan230 - lan234)) * (1 - Exp(-(lan230 - lan234) * t))) - AV
      ABL = lan230 * Exp(-lan230 * t) - (AU - 1) * (lan230 / (lan230 - lan234)) * (-lan230 + lan234) * Exp((-lan230 + lan234) * t)

      If WERT < 0 Then

        xl = t
        fl = WERT

      Else

        xh = t
        fh = WERT

      End If

    Next i

  End If

End Function
```

The uncertainties of the U-series ages presented in this work have been calculated by the Algorithm *Montealter* which is based on a Monte-Carlo-simulation (see chapter 4.1.9). The calculated errors are given at 2σ-level. The input variables are the measured ($^{230}Th/^{238}U$) and ($^{234}U/^{238}U$) activity ratios and the corresponding (2σ-) errors.

```
Function Montealter(AV, dAV, AU, dAU) As String

Dim iter%, felda!(), feldb!()
Dim res() As Variant, ausgabe(3) As String
Dim i&, j&

AV = AV
dAV = dAV
AU = AU
dAU = dAU
iter = 5000

ReDim felda!(iter), feldb!(iter)
ReDim res(iter) As Variant

   If ThU_Alter_Kombi(AV, AU) = "Out of range" Then

      Montealter = "-----"
      Exit Function

   End If

   Randomize

   For i = 1 To iter

      felda(i) = Gauss * (dAV / 2) + AV
      feldb(i) = Gauss * (dAU / 2) + AU
      res(i) = ThU_Alter_Kombi(felda(i), feldb(i))

      If res(i) = "Out of range" Then i = i - 1

   Next i

   Heapsort iter, res()

   i = (100 - 95.4) * iter * 0.5 \ 100
   j = iter - i + 1

   ausgabe(0) = "+"
   ausgabe(1) = Application.Round(res(j) - ThU_Alter_Kombi(AV, AU), 4)
   ausgabe(2) = "  -"
   ausgabe(3) = Application.Round(ThU_Alter_Kombi(AV, AU) - res(i), 4)

Montealter = Join(ausgabe)

End Function
```

The Algorithm *Gauss* which has been adopted from *Press et al.* (*1988*) generates normally distributed random numbers with a mean value of $\mu = 0$ and a standard deviation of $\sigma = 1$.

```
Function Gauss() As Double

Dim c!, r!, v1!, v2!
Static iset%, var1!


   If iset = 0 Then

      Do

         v1 = (2 * Rnd) - 1
         v2 = (2 * Rnd) - 1
         r = (v1 * v1 + v2 * v2)

      Loop While r >= 1

      c = Sqr(-2 * Log(r) / r)
      var1 = v1 * c

      iset = 1

      Gauss = v2 * c

   Else
      iset = 0
      Gauss = var1

   End If

End Function
```

Heapsort is a sorting algorithm which is used to numerically sort the calculated U-series ages into a ranked array. It has been adopted from *Press et al.* (*1988*) as well.

```
Sub Heapsort(ByVal iter&, res() As Variant)

Dim j&, k&, q&, m&
Dim t#, v#

   m = iter

   For q = iter \ 2 To 1 Step -1
      k = q
      t = res(k)
      Do While k <= iter \ 2
         j = k + k
         If j < iter Then
            If res(j) < res(j + 1) Then j = j + 1
         End If
         If t >= res(j) Then Exit Do
         res(k) = res(j)
         k = j
      Loop
      res(k) = t
   Next q
   Do
      v = res(1)
      res(1) = res(m)
```

```
      res(m) = v
      m = m - 1
      k = 1
      t = res(k)
      Do While k <= m \ 2
         j = k + k
         If j < m Then
            If res(j) < res(j + 1) Then j = j + 1
         End If
         If t >= res(j) Then Exit Do
         res(k) = res(j)
         k = j
      Loop
      res(k) = t
   Loop Until m <= 1

End Sub
```

Algorithm *Initial* calculates the initial $\delta^{234}U$ value and the corresponding 2σ-error on the basis of the measured ($^{230}Th/^{238}U$) and ($^{234}U/^{238}U$) activity ratios and the respective (2σ)–errors. The calculation of the error is based on a Monte-Carlo-simulation and uses the algorithms *Gauss* and *Heapsort* as well.

```
Function Initial(AV, dAV, AU, dAU) As String

Dim iter%, felda!(), feldb!()
Dim res() As Variant, init() As Variant, ausgabe(3) As String
Dim i&, j&, Initialcalc!

AV = AV
dAV = dAV
AU = AU
dAU = dAU
iter = 5000

ReDim felda!(iter), feldb!(iter), init(iter) As Variant
ReDim res(iter) As Variant

   If ThU_Alter_Kombi(AV, AU) = "Out of range" Then

      Initial = "-----"
      Exit Function

   End If

   Initialcalc = (AU - 1) * 1000 * Exp(0.0028263 * ThU_Alter_Kombi(AV, AU))

   Randomize

   For i = 1 To iter

      felda(i) = Gauss * (dAV / 2) + AV
      feldb(i) = Gauss * (dAU / 2) + AU
      res(i) = ThU_Alter_Kombi(felda(i), feldb(i))

      If res(i) <> "Out of range" Then

         init(i) = (feldb(i) - 1) * 1000 * Exp(0.0028263 * res(i))

      Else

         i = i - 1

      End If
```

```
    Next i

    Heapsort iter, init()

    i = (100 - 95.4) * iter * 0.5 \ 100
    j = iter - i + 1

    Debug.Print Initialcalc; init(i); init(j)

    ausgabe(0) = "+"
    ausgabe(1) = Application.Round(init(j) - Initialcalc, 4)
    ausgabe(2) = "  -"
    ausgabe(3) = Application.Round(Initialcalc - init(i), 4)

Initial = Join(ausgabe)

End Function
```

B2 U uptake/loss models

The Algorithm *einbau* has been used to model the isochrons of the Aqaba corals (see chapter 4.1.6). The corresponding Visual Basic script can be found below. The Algorithm must be integrated into Microsoft Excel and can be started from the Visual Basic Editor (Alt+F11) by pressing F5. The model parameters (such as number and duration of the events, $(^{234}U/^{238}U)_{add}$, and the U loss coefficient *c*) must be modified directly in the model code, where *h* = $(^{234}U/^{238}U)_{add}$, *c* = U loss coefficient, *anzahl* = number of events, *dauer* = duration of events, and *alter* = true coral age. The initial ^{238}U concentration of the coral must be given as atoms (*N238coral*). The values exemplarily inserted in the code below have been used for the modelling of coral AQB 3A (compare Table 4.3, page 65, and *Scholz et al.* (*2004*)).

```
Sub einbau()

Dim lan230!, lan234!, lan238!
Dim N230coral!, N234coral!, N238coral!, AVcoral!, AUcoral!, deltaUcoral!, Agecoral!, Ucoral!
Dim h!, Uin!, c!
Dim t&, alter&, i!, dauer&, anzahl&
Dim N230in!, N234in!, N238in!, AVin!, AUin!, deltaUin!, Uinresult!
Dim AVtotal!, dAVtotal!, deltaUtotal!, ddeltaUtotal!, AUtotal!, Agetotal!, Utotal!

lan230 = 0.0000091577
lan234 = 0.0000028263
lan238 = 0.000000000155125

h = 2
c = 0.00025
anzahl = 5
dauer = 10000
alter = 121900

N230coral = 0
N238coral = 8.86E+15
N234coral = (1.15 * N238coral * lan238) / lan234

Range("A18").Activate
ActiveCell = "Urankonz. Koralle"
ActiveCell.Offset(0, 1).Activate
ActiveCell = (N238coral * 238 * 1000000#) / 6.022E+23
ActiveCell.Offset(1, -1).Activate
ActiveCell = "dU in"
```

```
ActiveCell.Offset(0, 1).Activate
ActiveCell = (h - 1) * 1000
ActiveCell.Offset(1, -1).Activate
ActiveCell = "Koeffizient Verlust"
ActiveCell.Offset(0, 1).Activate
ActiveCell = c
ActiveCell.Offset(1, -1).Activate
ActiveCell = "Anzahl Störungen"
ActiveCell.Offset(0, 1).Activate
ActiveCell = anzahl
ActiveCell.Offset(1, -1).Activate
ActiveCell = "Dauer einer Störung"
ActiveCell.Offset(0, 1).Activate
ActiveCell = dauer
ActiveCell.Offset(1, -1).Activate

Range("A25").Activate

ActiveCell = "U in"
ActiveCell.Offset(0, 1).Activate
ActiveCell = "AV Koralle"
ActiveCell.Offset(0, 1).Activate
ActiveCell = "dU Koralle"
ActiveCell.Offset(0, 1).Activate
ActiveCell = "Alter Koralle"
ActiveCell.Offset(0, 1).Activate
ActiveCell = "Uran Koralle"
ActiveCell.Offset(0, 1).Activate
ActiveCell = "AV in"
ActiveCell.Offset(0, 1).Activate
ActiveCell = "dU in"
ActiveCell.Offset(0, 1).Activate
ActiveCell = "U in total"
ActiveCell.Offset(0, 1).Activate
ActiveCell = "AV total"
ActiveCell.Offset(0, 1).Activate
ActiveCell = "dU total"
ActiveCell.Offset(0, 1).Activate
ActiveCell = "Alter total"
ActiveCell.Offset(0, 1).Activate
ActiveCell = "U total"
ActiveCell.Offset(1, -11).Activate

Range("A27").Activate

For t = 1 To alter

   N238coral = N238coral - N238coral * lan238
   N234coral = N234coral + N238coral * lan238 - N234coral * lan234
   N230coral = N230coral - lan230 * N230coral + N234coral * lan234

Next t

For Uin = 0.05 To 2.01 Step 0.05

   Debug.Print Uin

   N238in = 0
   N234in = 0
   N230in = 0

   For i = 0 To alter

      If i Mod (alter / anzahl) = 0 And i < alter Then

      Debug.Print i

         For t = i To i + (dauer / 2)

            N238in = N238in - N238in * lan238 + (Uin * 0.000001 * 6E+23) / ((dauer / 2) * 238)
            N234in = N234in - N234in * lan234 + N238in * lan238 + (Uin * 0.000001 * 6E+23 * h * lan238) / ((dauer / 2) * 238 *
lan234)
            N230in = N230in - N230in * lan230 + N234in * lan234
```

```
        Next t

        For t = i + (dauer / 2) + 1 To i + dauer

            N238in = N238in - N238in * lan238 - c * N238in
            N234in = N234in + N238in * lan238 - N234in * lan234 - c * N234in
            N230in = N230in - lan230 * N230in + N234in * lan234

        Next t

        i = t - 1

      Else

      N238in = N238in - N238in * lan238
      N234in = N234in + N238in * lan238 - N234in * lan234
      N230in = N230in - lan230 * N230in + N234in * lan234

      End If

   Next i

   Debug.Print i

   AVcoral = (N230coral * lan230) / (N238coral * lan238)
   AUcoral = (N234coral * lan234) / (N238coral * lan238)
   deltaUcoral = (((N234coral * lan234) / (N238coral * lan238)) - 1) * 1000
   Agecoral = ThU_Alter(AVcoral, AUcoral)
   Ucoral = (N238coral * 238 * 1000000#) / 6.022E+23

   AVin = (N230in * lan230) / (N238in * lan238)
   AUin = (N234in * lan234) / (N238in * lan238)
   deltaUin = (AUin - 1) * 1000
   Uinresult = (N238in * 238 * 1000000#) / 6.022E+23

   AVtotal = ((N230coral + N230in) * lan230) / ((N238coral + N238in) * lan238)
   dAVtotal = 0.003 * AVtotal
   AUtotal = ((N234coral + N234in) * lan234) / ((N238coral + N238in) * lan238)
   deltaUtotal = (AUtotal - 1) * 1000
   ddeltaUtotal = 0.0015 * deltaUtotal
   Agetotal = ThU_Alter(AVtotal, AUtotal)
   Utotal = ((N238in + N238coral) * 238 * 1000000#) / 6.022E+23

   ActiveCell = Application.Round(Uin, 2)
   ActiveCell.Offset(0, 1).Activate
   ActiveCell = Application.Round(AVcoral, 4)
   ActiveCell.Offset(0, 1).Activate
   ActiveCell = Application.Round(deltaUcoral, 2)
   ActiveCell.Offset(0, 1).Activate
   ActiveCell = Application.Round(Agecoral, 2)
   ActiveCell.Offset(0, 1).Activate
   ActiveCell = Application.Round(Ucoral, 2)
   ActiveCell.Offset(0, 1).Activate
   ActiveCell = Application.Round(AVin, 4)
   ActiveCell.Offset(0, 1).Activate
   ActiveCell = Application.Round(deltaUin, 2)
   ActiveCell.Offset(0, 1).Activate
   ActiveCell = Application.Round(Uinresult, 2)
   ActiveCell.Offset(0, 1).Activate
   ActiveCell = Application.Round(AVtotal, 4)
   ActiveCell.Offset(0, 1).Activate
   ActiveCell = Application.Round(deltaUtotal, 2)
   ActiveCell.Offset(0, 1).Activate
   ActiveCell = Application.Round(Agetotal, 2)
   ActiveCell.Offset(0, 1).Activate
   ActiveCell = Application.Round(Utotal, 2)
   ActiveCell.Offset(1, -11).Activate

Next Uin

End Sub
```

The Algorithms that have been used to estimate the timing of U addition (*einbau_2*) and U loss (*verlust*) for the corals from Barbados, West Indies (chapter 4.2.5.4), are given below as well.

```
Sub einbau_2()

Dim lan230!, lan234!, lan238!, N230!, N234!, N238!, h!, m!, t&, tstör&, dauer&, alter&, AV!, AU!, age!, U!, dAU!, dAV!

lan230 = 0.0000091577
lan234 = 0.0000028263
lan238 = 0.000000000155125

Range("A1").Activate

For tstör = 0 To 175000 Step 25000

   ActiveCell = "Zeitpunkt Störung"
   ActiveCell.Offset(0, 1).Activate
   ActiveCell = tstör
   ActiveCell.Offset(2, -1).Activate

   ActiveCell = "Uran Add"
   ActiveCell.Offset(0, 1).Activate
   ActiveCell = "AV"
   ActiveCell.Offset(0, 1).Activate
   ActiveCell = "AU"
   ActiveCell.Offset(0, 1).Activate
   ActiveCell = "Alter"
   ActiveCell.Offset(0, 1).Activate
   ActiveCell = "U total"
   ActiveCell.Offset(2, -4).Activate

   For m = 0.05 To 1.21 Step 0.05

      h = 1.15
      dauer = 1000
      alter = 175000

      N230 = 0
      N238 = 8.14E+15
      N234 = (1.15 * N238 * lan238) / lan234

      For t = 0 To tstör

         N238 = N238 - N238 * lan238
         N234 = N234 + N238 * lan238 - N234 * lan234
         N230 = N230 - lan230 * N230 + N234 * lan234

      Next t

      For t = tstör + 1 To tstör + dauer

         h = (N234 * lan234) / (N238 * lan238)
         N238 = N238 - N238 * lan238 + (m * 0.000001 * 6E+23) / (dauer * 238)
         N234 = N234 - N234 * lan234 + N238 * lan238 + (m * 0.000001 * 6E+23 * h * lan238) / (dauer * 238 * lan234)
         N230 = N230 - lan230 * N230 + lan234 * N234

      Next t

      For t = tstör + dauer + 1 To alter

         N238 = N238 - N238 * lan238
         N234 = N234 + N238 * lan238 - N234 * lan234
         N230 = N230 - lan230 * N230 + N234 * lan234

      Next t

      AV = (N230 * lan230) / (N238 * lan238)
      dAV = 0.003 * AV
```

```
      AU = (N234 * lan234) / (N238 * lan238)
      dAU = 0.002 * AU
      age = ThU_Alter(AV, AU)
      U = N238 * 238 * 1000000 / 6.022E+23

      ActiveCell = m
      ActiveCell.Offset(0, 1).Activate
      ActiveCell = Application.Round(AV, 4)
      ActiveCell.Offset(0, 1).Activate
      ActiveCell = Application.Round(AU, 4)
      ActiveCell.Offset(0, 1).Activate
      ActiveCell = Application.Round(age, 2)
      ActiveCell.Offset(0, 1).Activate
      ActiveCell = Application.Round(U, 2)
      ActiveCell.Offset(1, -4).Activate
      Debug.Print m; tstör; h; AV; AU; age

   Next m

ActiveCell.Offset(-28, 6).Activate

Next tstör

End Sub



Sub verlust()

Dim lan230!, lan234!, lan238!, N230!, N234!, N238!, c#, t&, tstör&, dauer&, alter&, AV!, AU!, age!, U!, dAU!, dAV!

lan230 = 0.0000091577
lan234 = 0.0000028263
lan238 = 0.000000000155125

Range("A1").Activate

dauer = 1
alter = 175000

For tstör = 0 To alter Step 25000

   ActiveCell.Offset(2, 0).Activate
   ActiveCell = "Zeitpunkt der Störung [kyr]"
   ActiveCell.Offset(0, 1).Activate
   ActiveCell = tstör
   ActiveCell.Offset(2, -1).Activate

   ActiveCell = "Uranverlust [%]"
   ActiveCell.Offset(0, 1).Activate
   ActiveCell = "(230Th/238U)"
   ActiveCell.Offset(0, 1).Activate
   ActiveCell = "234U/238U)"
   ActiveCell.Offset(0, 1).Activate
   ActiveCell = "Alter"
   ActiveCell.Offset(0, 1).Activate
   ActiveCell = "Urangehalt"
   ActiveCell.Offset(2, -4).Activate

   For c = 0 To 0.81 Step 0.05

      N230 = 0
      N238 = 8.32E+15
      N234 = (1.15 * N238 * lan238) / lan234

      For t = 1 To tstör

         N238 = N238 - N238 * lan238
         N234 = N234 + N238 * lan238 - N234 * lan234
         N230 = N230 - lan230 * N230 + N234 * lan234

      Next t
```

```
    For t = tstör + 1 To tstör + dauer

       N238 = N238 - N238 * lan238 - c * N238
       N234 = N234 - N234 * lan234 - N234 * c + N238 * lan238
       N230 = N230 - lan230 * N230 + lan234 * N234

    Next t

    For t = tstör + dauer + 1 To alter

       N238 = N238 - N238 * lan238
       N234 = N234 + N238 * lan238 - N234 * lan234
       N230 = N230 - lan230 * N230 + N234 * lan234

    Next t

    AV = (N230 * lan230) / (N238 * lan238)
    'dAV = 0.003 * AV'
    AU = (N234 * lan234) / (N238 * lan238)
    'dAU = 0.002 * AU'
    age = 0
    U = N238 * 238 * 1000000 / 6.022E+23

    ActiveCell = Application.Round(c * 100, 0)
    ActiveCell.Offset(0, 1).Activate
    ActiveCell = Application.Round(AV, 4)
    ActiveCell.Offset(0, 1).Activate
    ActiveCell = Application.Round(AU, 4)
    ActiveCell.Offset(0, 1).Activate
    ActiveCell = Application.Round(age, 2)
    ActiveCell.Offset(0, 1).Activate
    ActiveCell = Application.Round(U, 2)
    ActiveCell.Offset(1, -4).Activate
    Debug.Print tstör; c; AV; AU; age

  Next c

Next tstör

End Sub
```

B3 Calculation of coral isochron age errors

In the following the Visual Basic script of Algorithm B (see chapter 4.1.9.2) can be found. This Algorithm can be used to estimate the 2σ-uncertainty of coral isochron ages. It is based on a Monte-Carlo simulation. A detailed explanation of Algorithm B is given in chapter 4.1.9.2.

Confidence is the main program of Algorithm B. The input variables are the measured ^{230}Th, ^{234}U, and ^{238}U activities of the sub-samples and the corresponding 2σ-errors. All sub-programs used by *Confidence* are listed below. In addition, functions *Gauss* and *Heapsort* are used. These algorithms can be found in Appendix B1.

```
Function Confidence(Th230 As Range, dTh230 As Range, U234 As Range, dU234 As Range, U238 As Range, dU238 As
Range) As String

Dim x!(49), y!(49), dx!(49), dy!(49), cov!(49)
Dim xneu!(49), yneu!(49), dxneu!(49), dyneu!(49), covneu!(49)
Dim i&, data&, j&, iter&
Dim a!, da!, b!, db!, Cqu!
Dim rest() As Variant
Dim y0!
Dim t#, age!, up#, low#
Dim konf!
```

```
Dim ex#, Cqu_fix#
Dim k$
Dim ausgabe(4)

   iter = 4999
   konf = 95

ReDim rest(iter)

   y0 = 1.1466

   a = 0: da = 0: b = 0: db = 0

   k = "Konvergenz"

   For i = 0 To Th230.Count - 1

      x(i) = Th230.Cells(i + 1) / U238.Cells(i + 1)
      dx(i) = Sqr((dTh230.Cells(i + 1) / (2 * U238.Cells(i + 1))) ^ 2 + (Th230.Cells(i + 1) * dU238.Cells(i + 1) / (2 * U238.Cells(i +
1) ^ 2)) ^ 2)
      y(i) = U234.Cells(i + 1) / U238.Cells(i + 1)
      dy(i) = Sqr((dU234.Cells(i + 1) / (2 * U238.Cells(i + 1))) ^ 2 + (U234.Cells(i + 1) * dU238.Cells(i + 1) / (2 * U238.Cells(i + 1)
^ 2)) ^ 2)
      cov(i) = (dU238.Cells(i + 1) / (2 * U238.Cells(i + 1))) ^ 2 * x(i) * y(i)

      'Debug.Print x(i), dx(i), y(i), dy(i); cov(i); cov(i) / (dx(i) * dy(i))

   Next i

   data = Th230.Count

   Linear_Fit data, x(), dx(), y(), dy(), a, da, b, db
   'a = 15: b = 0.1
   Debug.Print a; da; b; db

   Final_Fit data, x(), dx(), y(), dy(), cov(), a, da, b, db, Cqu, k

   Debug.Print data; a; da; b; db; k

   Debug.Print Cqu; Cqu / (data - 2)

   Isochronenalter y0, t, a, b

   age = t

   Debug.Print t; a; da; b; db; covba

   Open "N:\user\Denis\Konfidenz Programm\Final Version\AQB 1H\Messpunkte.txt" For Output As #1
   Close #1
   Open "N:\user\Denis\Konfidenz Programm\Final Version\AQB 1H\Fit.txt" For Output As #2
   Close #2
   Open "N:\user\Denis\Konfidenz Programm\Final Version\AQB 1H\Initials.txt" For Output As #3
   Close #3
   Open "N:\user\Denis\Konfidenz Programm\Final Version\AQB 1H\Alter.txt" For Output As #4
   Close #4
   Open "N:\user\Denis\Konfidenz Programm\Final Version\AQB 1H\chi-test.txt" For Output As #5
   Close #5

   Open "N:\user\Denis\Konfidenz Programm\Final Version\AQB 1H\Messpunkte.txt" For Append As #1
   Open "N:\user\Denis\Konfidenz Programm\Final Version\AQB 1H\Fit.txt" For Append As #2
   Open "N:\user\Denis\Konfidenz Programm\Final Version\AQB 1H\Initials.txt" For Append As #3
   Open "N:\user\Denis\Konfidenz Programm\Final Version\AQB 1H\Alter.txt" For Append As #4
   Open "N:\user\Denis\Konfidenz Programm\Final Version\AQB 1H\chi-test.txt" For Append As #5

   Cqu_fix = Cqu

   Randomize

   Debug.Print iset

   For j = 0 To iter
      k = "Konvergenz"
```

```
        ex = Cqu_fix / chi_squ(data - 2)

        Print #5, j; ";"; (Cqu_fix / ex); ";"; ex; ";"; Sqr(ex); ";"

        Print #1, j; ";";

        For i = 0 To data - 1

            dxneu(i) = Sqr(ex) * dx(i)
            dyneu(i) = Sqr(ex) * dy(i)
            covneu(i) = ex * cov(i)

            Bivariat x(i), y(i), dxneu(i), dyneu(i), covneu(i), xneu(i), yneu(i)

            Print #1, xneu(i); ";"; yneu(i); ";";

        Next i

        Print #1, Tab

        Linear_Fit data, xneu(), dxneu(), yneu(), dyneu(), a, da, b, db
        'Debug.Print a; da; b; db

        Final_Fit data, xneu(), dxneu(), yneu(), dyneu(), covneu(), a, da, b, db, Cqu, k
        'Debug.Print a; da; b; db; k

        If k = "keine Konvergenz" Then

            Linear_Fit data, xneu(), dxneu(), yneu(), dyneu(), a, da, b, db

        End If

        Print #2, j; ";"; a; ";"; b; ";"; k; ";"

        y0 = Gauss() * 0.0014 + 1.1466

        'Debug.Print y0

        Print #3, j; ";"; y0

        Isochronenalter y0, t, a, b

        rest(j) = t

        Print #4, j; ";"; t

    Next j

    Close #1
    Close #2
    Close #3
    Close #4
    Close #5

    Heapsort iter, rest()

    i = 0.5 * ((100 - konf) / 100) * (iter + 1)
    j = (iter + 1) - i - 1

    Debug.Print age; rest(i); rest(j)

    up = (rest(j) - age)
    low = (age - rest(i))

    ausgabe(0) = Application.Round(age / 1000, 2)
    ausgabe(1) = " +"
    ausgabe(2) = Application.Round(up / 1000, 2)
    ausgabe(3) = " -"
    ausgabe(4) = Application.Round(low / 1000, 2)

    Confidence = Join(ausgabe)

End Function
```

Linear_Fit performs a conventional error weighted y-on-x-least-squares-regression. The resulting values for intercept a and slope b are then used as starting values for the EWLS-algorithm. The Algorithm has been adopted from *Press et al.* (*1988*).

```
Sub Linear_Fit(ByVal data%, x!(), dx!(), y!(), dy!(), a!, da!, b!, db!)

Dim i%
Dim Wt!, t!, sxoss!, Sx!, Sy!, st2!, ss!

   b = 0
   ss = 0: Sx = 0: Sy = 0: st2 = 0

   For i = 0 To data - 1

      Wt = 1 / (dy(i) * dy(i))
      ss = ss + Wt
      Sx = Sx + (x(i) * Wt)
      Sy = Sy + (y(i) * Wt)

   Next i

   sxoss = Sx / ss

   For i = 0 To data - 1

      t = (x(i) - sxoss) / dy(i)
      st2 = st2 + t * t
      b = b + t * y(i) / dy(i)

   Next i

   b = b / st2
   a = (Sy - Sx * b) / ss
   da = Sqr((1 + ((Sx * Sx) / (ss * st2))) / ss)
   db = Sqr(1 / st2)

End Sub
```

Final_Fit performs an error-weighted-least-squares-regression which takes x- as well as –y-errors into account. The algorithm has been modified from *Albarède* (*1995*).

```
Sub Final_Fit(ByVal data%, x!(), dx!(), y!(), dy!(), cov!(), a!, da!, b!, db!, Cqu!, k$)

Dim i%, j%
Dim xacc!
Dim e!(49), w!(49), d!(49), c!(49)
Dim g1!, g2!
Dim Hxx!, Hxy!, Hyy!, Hxxinv!, Hxyinv!, Hyyinv!
Dim Sb!, Sa!, Sba!
Dim covba!, korr!

   j = 0

   xacc = 0.0001

   db = 0: da = 0: covba = 0

   Do

      For i = 0 To data - 1

         e(i) = b * dx(i) ^ 2 - cov(i)
         w(i) = (b * dx(i)) ^ 2 - 2 * b * cov(i) + dy(i) ^ 2
```

```
        d(i) = b * x(i) + a - y(i)

        'Debug.Print e(i); w(i); d(i)

    Next i

    Cqu = 0: g1 = 0: g2 = 0: Hxx = 0: Hxy = 0: Hyy = 0

    For i = 0 To data - 1

        c(i) = d(i) ^ 2 / w(i)
        Cqu = Cqu + c(i)
        g1 = g1 + (x(i) * d(i) / w(i)) - (d(i) ^ 2 * e(i) / w(i) ^ 2)
        g2 = g2 + d(i) / w(i)
        Hxx = Hxx + (x(i) ^ 2 / w(i)) + (4 * d(i) ^ 2 * e(i) ^ 2 / w(i) ^ 3 - 4 * d(i) * x(i) * e(i) / w(i) ^ 2 - d(i) ^ 2 * dx(i) ^ 2 / w(i) ^ 2)
        Hxy = Hxy + x(i) / w(i) - 2 * e(i) * d(i) / w(i) ^ 2
        Hyy = Hyy + 1 / w(i)

    Next i

    'Debug.Print Cqu; g1; g2; Hxx; Hxy; Hyy

    Hxxinv = (Hxx * Hyy - Hxy ^ 2) ^ -1 * Hyy
    Hxyinv = (Hxx * Hyy - Hxy ^ 2) ^ -1 * (-Hxy)
    Hyyinv = (Hxx * Hyy - Hxy ^ 2) ^ -1 * Hxx

    'Debug.Print Hxxinv; Hxyinv; Hyyinv

    b = b - (Hxxinv * g1 + Hxyinv * g2)
    a = a - (Hxyinv * g1 + Hyyinv * g2)

    'Debug.Print Abs(Hxxinv * g1 + Hxyinv * g2); Abs(Hxyinv * g1 + Hyyinv * g2); j
    'Debug.Print a; b

    j = j + 1

    If j > 15 Then

        k = "keine Konvergenz"
        Exit Sub

    End If

Loop Until Abs(Hxxinv * g1 + Hxyinv * g2) < xacc And Abs(Hxyinv * g1 + Hyyinv * g2) < xacc

'Debug.Print Abs(Hxxinv * g1 + Hxyinv * g2); Abs(Hxyinv * g1 + Hyyinv * g2); j
'Debug.Print a; b

Sb = 0: Sa = 0: Sba = 0

For i = 0 To data - 1

    Sb = Sb + (x(i) ^ 2 / w(i)) + (2 * x(i) * e(i) / w(i)) + (d(i) ^ 2 * dx(i) ^ 2 / w(i) ^ 2)
    Sa = Sa + (1 / w(i))
    Sba = Sba + (x(i) / w(i)) + (e(i) / w(i))

Next i

'Debug.Print Sb; Sa; Sba

db = Hxxinv ^ 2 * Sb + 2 * Hxyinv * Hxxinv * Sba + Hxyinv ^ 2 * Sa
da = Hxyinv ^ 2 * Sb + 2 * Hxyinv * Hyyinv * Sba + Hyyinv ^ 2 * Sa
covba = Hxyinv * Hxxinv * Sb + Hxxinv * Hyyinv * Sba + Hxyinv ^ 2 * Sba + Hxyinv * Hyyinv * Sa
korr = covba / (Sqr(db) * Sqr(da))

'Debug.Print a; Sqr(da); b; Sqr(db); covba; korr; Cqu; ex
'Debug.Print a; Sqr(ex * da); b; Sqr(ex * db); ex * covba; korr
'Debug.Print a; 2.78 * Sqr(ex * da); b; 2.78 * Sqr(ex * db); ex * covba; korr

End Sub
```

Isochronenalter is used to calculate the isochron age on the basis of the fitting results.

```
Sub Isochronenalter(ByVal y0!, t#, a!, b!)

Dim lan234!, lan230!
Dim xacc#
Dim yhilf#, stand#, fit#, diff#

   lan234 = 0.0000028263
   lan230 = 0.0000091577

   xacc = 0.0001

   t = 0
   yhilf = 1 + Exp(-lan234 * t) * (y0 - 1)
   stand = (1 - Exp(-lan230 * t) + (((1 - Exp(t * (lan234 - lan230))) * (yhilf - 1) * lan230) / (lan230 - lan234)))
   fit = (yhilf - a) / b

   'Debug.Print t; xhilf; stand; fit'

   Do Until fit < stand

      If t >= 500000 Then Exit Sub

      t = t + 1000
      yhilf = 1 + Exp(-lan234 * t) * (y0 - 1)
      stand = (1 - Exp(-lan230 * t) + (((1 - Exp(t * (lan234 - lan230))) * (yhilf - 1) * lan230) / (lan230 - lan234)))
      fit = (yhilf - a) / b

      'Debug.Print t; xhilf; stand; fit'

   Loop

   diff = Abs(stand - fit)

   Do Until diff < xacc

      If t <= 0 Then Exit Sub

      t = t - 1
      yhilf = 1 + Exp(-lan234 * t) * (y0 - 1)
      stand = (1 - Exp(-lan230 * t) + (((1 - Exp(t * (lan234 - lan230))) * (yhilf - 1) * lan230) / (lan230 - lan234)))
      fit = (yhilf - a) / b
      diff = Abs(stand - fit)

      'Debug.Print t; xhilf; stand; fit'

   Loop

End Sub
```

The Function *chi_squ* generates a χ_n^2-distributed random number. This algorithm has been adopted from *Fishman* (*1997*).

```
Function chi_squ(ByVal n%) As Double

Dim alpha#
Dim achi#, bchi#, mchi#, dchi#, fchi#
Dim Xchi#, Ychi#, Vchi#, Wchi#

   alpha = n / 2

   achi = alpha - 1: bchi = (alpha - 1 / (6 * alpha)) / achi: mchi = 2 / achi: dchi = mchi + 2: fchi = Sqr(alpha)

   Do

      Do

         Xchi = Rnd
         Ychi = Rnd
         Wchi = Ychi + (1 - 1.857764 * Xchi) / fchi

      Loop Until Wchi > 0 And Wchi < 1

      Vchi = bchi * Ychi / Wchi

      If mchi * Wchi - dchi + Vchi + 1 / Vchi <= 0 Then Exit Do

      If mchi * Log(Wchi) - Log(Vchi) + Vchi - 1 <= 0 Then Exit Do

   Loop

   chi_squ = 2 * achi * Vchi

End Function
```

Bivariat generates correlated normally distributed random numbers. The algorithm has been adopted from *Fishman* (*1997*).

```
Sub Bivariat(x!, y!, dx!, dy!, cov!, xneu!, yneu!)

Dim c11#, c21#, c22#
Dim X1!, X2!

   xneu = 0: yneu = 0

   c11 = dx
   c21 = cov / dx
   c22 = Sqr(dy ^ 2 - (cov / dx) ^ 2)

   X1 = Gauss()
   X2 = Gauss()
   xneu = x + c11 * X1
   yneu = y + c21 * X1 + c22 * X2

   'Debug.Print X1; X2; xneu; yneu

End Sub
```

C TIMS data

All data from Aqaba, Jordan, and Eilat, Israel, have been calculated using the old spike concentrations (see Appendix A4). As the spike recalibration yielded significantly different values for the Th- as well as U-concentrations all ages are slightly too young. To convert the listed values into the recalibrated ones the measured ($^{230}Th/^{238}U$) activity ratios must be multiplied by a factor of 1.0115 (see Appendix A4). The corresponding U-series ages and errors as well as the initial $\delta^{234}U$ values and errors can then be recalculated using these ($^{230}Th/^{238}U$) activity ratios.

Table C.1: Recent corals from Eilat, Israel

Sample	^{232}Th [ppb]	^{238}U [ppm]	$\delta^{234}U$ [‰]	initial $\delta^{234}U$ [‰]	($^{230}Th/^{238}U$)*	U-series age [yrs]
EDC 2	0.58	3.34	148 ± 4	-	-[b]	-[c]
Eilat 1a	3.85	2.88	144 ± 4	-	-[b]	-[c]
Eilat 1b	1.6	2.95	145 ± 2	-	-[b]	-[c]
Eilat 15 a	0.07	2.65	147 ± 3	-	-[b]	-[c]

* Due to low counting rates the precision of the ^{230}Th measurements was significantly affected by the background current. For this reason ($^{230}Th/^{238}U$) activity ratios and U-series ages have not been calculated.

Table C.2: Holocene corals from Aqaba, Jordan

Sample	^{232}Th [ppb]	^{238}U [ppm]	$\delta^{234}U$ [‰]	initial $\delta^{234}U$ [‰]	($^{230}Th/^{238}U$)†	U-series age [yrs]
AQB 10 B	0.7	3.31	179 ± 2	180 ± 2	0.0338 ± 0.0003	3,171 ± 27
AQB 10 B–2	0.1	3.05	178 ± 2	180 ± 2	0.0335 ± 0.0003	3,143 ± 31
AQB 10 B–3	0.43	2.99	156 ± 2	157 ± 2	0.0329 ± 0.0003	3,150 ± 25
AQB 10 B–4	0.52	3.08	156 ± 2	157 ± 2	0.0321 ± 0.0005	3,070 ± 49

† The quoted ($^{230}Th/^{238}U$) activity ratios are based on the old spike calibration. They can be converted using a factor of 1.0015 (Appendix A4).

Table C.3: Last Interglacial corals from the upper terrace at Aqaba, Jordan

Sample	^{232}Th [ppb]	^{238}U [ppm]	δ^{234}U [‰]	initial δ^{234}U [‰]	(^{230}Th/^{238}U)†	U-series age [kyrs]
AQB 3A	31.70	3.89	151 ± 2	215 ± 3	0.806 ± 0.003	126.4 ± 1
AQB 3A 2	17.40	4.30	261 ± 3	385 ± 4	0.934 ± 0.005	137.1 ± 1.6
AQB 3A 3	2.95	4.13	237 ± 2	349 ± 3	0.915 ± 0.007	137.3 ± 2
AQB 3A 4	9.05	3.73	170 ± 3	248 ± 4	0.843 ± 0.006	132.7 ± 2
AQB 3A 5	21.84	4.04	187 ± 2	271 ± 3	0.851 ± 0.003	130.9 ± 0.9
AQB 3A 6	19.40	4.00	196 ± 2	282 ± 3	0.850 ± 0.003	128.7 ± 1.1
AQB 7G	4.05	3.11	122 ± 2	171 ± 2	0.755 ± 0.002	118.3 ± 0.7
AQB 7G 2	4.2	3.24	151 ± 3	208 ± 3	0.759 ± 0.005	113.7 ± 1.2
AQB 7G 3	3.24	2.89	132 ± 2	184 ± 2	0.763 ± 0.002	118.7 ± 0.7
AQB 7G 4	1.44	3.07	128 ± 2	178 ± 2	0.753 ± 0.003	116.7 ± 0.9
AQB 7G 5	9.75	2.87	147 ± 3	203 ± 3	0.760 ± 0.005	114.6 ± 1.4
AQB 2E	1.82	3.71	152 ± 2	218 ± 2	0.810 ± 0.002	127.2 ± 0.8
AQB 2E 2	16.88	3.66	140 ± 2	215 ± 3	0.876 ± 0.003	151.6 ± 1.3
AQB 2E 3	14.02	3.21	147 ± 2	226 ± 6	0.882 ± 0.019	151.5 ± 6.9
AQB 2E 4	6.46	3.43	153 ± 4	228 ± 5	0.855 ± 0.007	140.8 ± 2.5

† The quoted (^{230}Th/^{238}U) activity ratios are based on the old spike calibration. They can be converted using a factor of 1.0015 (Appendix A4).

Table C.4: Last Interglacial corals from the lower terrace at Aqaba, Jordan

Sample	^{232}Th [ppb]	^{238}U [ppm]	δ^{234}U [‰]	initial δ^{234}U [‰]	(^{230}Th/^{238}U)†	U-series age [kyrs]
AQB 1K	1.18	4.26	278 ± 2	396 ± 3	0.904 ± 0.004	125.7 ± 1
AQB 1K 2	3.57	3.99	271 ± 3	390 ± 4	0.913 ± 0.005	129.2 ± 1.3
AQB 1K 3	35.00	3.48	213 ± 2	299 ± 3	0.831 ± 0.003	120.2 ± 0.9
AQB 1K 4	9.88	3.77	206 ± 2	288 ± 3	0.820 ± 0.002	118.6 ± 0.6
AQB 1K 5	18.03	3.98	230 ± 3	324 ± 4	0.848 ± 0.004	121.1 ± 1
AQB 1A	4.92	4.42	265 ± 2	371 ± 2	0.870 ± 0.003	119.8 ± 0.7
AQB 1A 2	1.88	3.94	270 ± 3	381 ± 4	0.881 ± 0.005	121.6 ± 1.2
AQB 1A 3	1.26	4.02	251 ± 3	351 ± 4	0.857 ± 0.006	119.3 ± 1.5
AQB 1A 4	0.92	3.98	192 ± 2	268 ± 3	0.810 ± 0.006	119 ± 1.5
AQB 1A 3 – 2	1.54	3.89	221 ± 3	308 ± 3	0.826 ± 0.002	117.2 ± 0.7
AQB 1A 4 – 2	3.58	3.75	201 ± 3	282 ± 4	0.822 ± 0.003	120 ± 1
AQB 1H 2	0.69	3.91	252 ± 4	357 ± 5	0.873 ± 0.007	122.9 ± 1.9
AQB 1H 3	0.89	3.27	219 ± 2	309 ± 3	0.845 ± 0.004	122.6 ± 1.1
AQB 1H 2 – 2	11.84	4.05	238 ± 2	332 ± 3	0.844 ± 0.005	118.5 ± 1.4
AQB 1H 3 – 2	6.28	3.5	202 ± 2	283 ± 2	0.821 ± 0.002	119.8 ±0.6
AQB 1H 4 – 2	1.36	3.31	224 ± 2	315 ± 3	0.841 ± 0.002	120.5 ± 0.6

† The quoted (^{230}Th/^{238}U) activity ratios are based on the old spike calibration. They can be converted using a factor of 1.0015 (Appendix A4).

Table C.5: Corals from the middle unit on Barbados, West Indies

Sample	^{232}Th [ppb]	^{238}U [ppm]	δ^{234}U [‰]	initial δ^{234}U [‰]	(^{230}Th/^{238}U)†	U-series age [kyrs]
BB02-1-1	0.13	2.79	107 ± 2	156 ± 2	0.789 ± 0.004	131.8 ± 1.3
BB02-1-2	0.59	2.7	103 ± 2	149 ± 2	0.788 ± 0.003	132.9 ± 1.2
BB02-1-3	0.16	3.3	108 ± 2	157 ± 3	0.788 ± 0.002	131.5 ± 0.8
BB02-1-4	0.07	3.14	112 ± 2	163 ± 2	0.796 ± 0.004	132.8 ± 1.5
BB02-2-1	0.23	2.61	109 ± 4	157 ± 6	0.777 ± 0.004	127.5 ± 1.7
BB02-2-2	0.04	2.7	103 ± 2	148 ± 2	0.774 ± 0.003	128.4 ± 1.1
BB02-2-3	0.15	2.61	104 ± 1	151 ± 2	0.784 ± 0.002	131.2 ± 0.8
BB02-3-1-1	0.08	3.22	110 ± 2	159 ± 2	0.786 ± 0.002	130.3 ± 0.8
BB02-3-1-2	0.05	3.16	116 ± 3	169 ± 4	0.802 ± 0.013	133.7 ± 4.4
BB02-3-2	0.1	3.14	115 ± 2	167 ± 2	0.792 ± 0.005	130.9 ± 1.5

† The quoted (^{230}Th/^{238}U) activity ratios are based on the new spike calibration (Appendix A4).

Table C.6: Corals from location BB02-4 on Barbados, West Indies

Sample	^{232}Th [ppb]	^{238}U [ppm]	δ^{234}U [‰]	initial δ^{234}U [‰]	(^{230}Th/^{238}U)†	U-series age [kyrs]
BB02-4-1	0.19	3.23	101 ± 1	164 ± 2	0.889 ± 0.003	171.6 ± 1.6
BB02-4-1-B	0.58	3.21	101 ± 3	165 ± 4	0.893 ± 0.006	173.2 ± 3.2
BB02-4-1-C	0.14	3.38	96 ± 2	157 ± 3	0.893 ± 0.005	175.6 ± 2.4
BB02-4-1-D	0.42	3.22	99 ± 3	161 ± 4	0.887 ± 0.004	171.6 ± 2.3
BB02-4-1-B-li	0.25	3.2	98 ± 1	160 ± 2	0.891 ± 0.003	174 ± 1.4
BB02-4-1-C-li	0.16	3.3	96 ± 1	158 ± 2	0.893 ± 0.004	175.9 ± 1.8
BB02-4-1-C-re	0.24	3.23	101 ± 1	164 ± 2	0.891 ± 0.004	172.7 ± 1.7
BB02-4-2	0.3	3.07	105 ± 3	168 ± 4	0.879 ± 0.006	165.6 ± 2.9
BB02-4-2-B1	0.73	3.08	102 ± 1	167 ± 2	0.897 ± 0.003	174.7 ± 1.4
BB02-4-2-C1	0.45	3.11	97 ± 1	158 ± 2	0.889 ± 0.002	173.7 ± 1.2
BB02-4-2-D1	0.41	3.12	91 ± 4	149 ± 7	0.889 ± 0.004	176.1 ± 2.8
BB02-4-3	0.29	3.24	96 ± 2	155 ± 2	0.878 ± 0.003	168.9 ± 1.5
BB02-4-3-A1	0.04	3.3	98 ± 2	156 ± 3	0.869 ± 0.008	164 ± 3.4
BB02-4-3-A2	0.32	3.31	96 ± 1	154 ± 1	0.88 ± 0.002	169.8 ± 0.9
BB02-4-3-A3	0.32	3.29	94 ± 1	152 ± 2	0.881 ± 0.002	170.9 ± 1.2
BB02-4-4	1.61	3.27	102 ± 2	164 ± 2	0.88 ± 0.003	167.3 ± 1.4
BB02-4-4-A	0.48	3.2	101 ± 2	165 ± 4	0.896 ± 0.004	174.8 ± 2
BB02-4-4-C1	0.55	3.32	100 ± 1	162 ± 2	0.884 ± 0.002	169.6 ± 1.1
BB02-4-4-C2	0.81	3.25	97 ± 4	156 ± 6	0.878 ± 0.008	168.5 ± 3.8

† The quoted (^{230}Th/^{238}U) activity ratios are based on the new spike calibration (Appendix A4).

Table C.7: Corals from location BB02-5 on Barbados, West Indies

Sample	^{232}Th [ppb]	^{238}U [ppm]	δ^{234}U [‰]	initial δ^{234}U [‰]	(^{230}Th/^{238}U)†	U-series age [kyrs]
BB02-5-1	0.15	4.07	99 ± 1	149 ± 2	0.818 ± 0.003	143.9 ± 1.1
BB02-5-1-D	0.32	3.99	97 ± 2	146 ± 3	0.825 ± 0.004	147.2 ± 1.6
BB02-5-1-C-re	0.1	3.99	97 ± 1	149 ± 2	0.833 ± 0.003	150 ± 1.1
BB02-5-1-E	0.16	3.97	95 ± 1	147 ± 2	0.837 ± 0.002	152.2 ± 1
BB02-5-1-2	0.17	3.53	102 ± 3	159 ± 4	0.857 ± 0.006	157.5 ± 2.7
BB02-5-1-B	0.31	3.64	92 ± 1	143 ± 2	0.845 ± 0.004	156.6 ± 1.6
BB02-5-1-F	0.37	3.89	94 ± 1	148 ± 2	0.856 ± 0.002	159.9 ± 1.1
BB02-5-1-C-li	0.15	3.62	98 ± 1	153 ± 2	0.853 ± 0.004	157.7 ± 1.6
BB02-5-1-3	0.21	3.65	92 ± 2	153 ± 4	0.896 ± 0.008	178.9 ± 4.4
BB02-5-2	-*	3.77	93 ± 1	141 ± 2	0.82 ± 0.002	146.7 ± 0.9
BB02-5-2-3	0.05	3.9	100 ± 3	150 ± 4	0.819 ± 0.003	144.1 ± 1.3
BB02-5-2-E1	0.13	3.82	97 ± 2	147 ± 2	0.824 ± 0.002	146.7 ± 1
BB02-5-2-E2	0.21	3.86	96 ± 2	144 ± 2	0.819 ± 0.003	145.2 ± 1.2
BB02-5-2-2	0.19	3.81	91 ± 1	140 ± 2	0.832 ± 0.002	151.4 ± 1
BB02-5-2-C1	-*	3.76	92 ± 2	141 ± 2	0.834 ± 0.004	152.3 ± 1.8
BB02-5-2-C2	0.06	3.74	93 ± 2	142 ± 3	0.832 ± 0.005	151.1 ± 2.1
BB02-5-2-C3	0.02	3.73	96 ± 2	147 ± 2	0.833 ± 0.004	150.3 ± 1.6
BB02-5-2-A1	-*	3.77	95 ± 2	152 ± 3	0.865 ± 0.004	163.5 ± 1.9
BB02-5-2-A2	-*	3.81	91 ± 2	144 ± 2	0.86 ± 0.003	163 ± 1.5
BB02-5-2-A3	0.12	3.79	92 ± 2	146 ± 2	0.864 ± 0.003	164.4 ± 1.6

* ^{232}Th content was below detection limit.

† The quoted (^{230}Th/^{238}U) activity ratios are based on the new spike calibration (Appendix A4).

Table C.7 (continued): Corals from location BB02-5 on Barbados, West Indies

Sample	^{232}Th [ppb]	^{238}U [ppm]	δ^{234}U [‰]	initial δ^{234}U [‰]	(^{230}Th/^{238}U)†	U-series age [kyrs]
BB02-5-3	0.19	3.58	98 ± 2	155 ± 2	0.865 ± 0.004	162.6 ± 1.7
BB02-5-3-2	0.02	3.46	99 ± 2	158 ± 2	0.867 ± 0.005	162.8 ± 2
BB02-5-3-3	0.07	3.6	95 ± 2	152 ± 3	0.873 ± 0.004	167.1 ± 1.9
BB02-5-3-A	0.24	3.52	93 ± 2	148 ± 4	0.869 ± 0.003	166.2 ± 1.7
BB02-5-3-B	0.29	3.52	94 ± 2	150 ± 3	0.871 ± 0.003	166.7 ± 1.4
BB02-5-3-C	0.27	3.38	94 ± 1	150 ± 2	0.867 ± 0.002	164.9 ± 1
BB02-5-3-D	0.22	3.56	97 ± 3	154 ± 4	0.867 ± 0.003	163.4 ± 1.8
BB02-5-3-E	0.07	3.46	105 ± 3	168 ± 4	0.877 ± 0.003	164.3 ± 1.7
BB02-5-3-F	0.22	3.54	112 ± 2	173 ± 4	0.858 ± 0.009	154.7 ± 3.8
BB02-5-3-A-II	1.4	3.48	96 ± 1	154 ± 2	0.878 ± 0.006	168.9 ± 2.7
BB02-5-3-C-II	1.44	3.5	96 ± 1	153 ± 2	0.874 ± 0.002	167.3 ± 1.1
BB02-5-3-D-II	1.16	3.59	99 ± 1	157 ± 2	0.871 ± 0.002	164.7 ± 1
BB02-5-3-E-II	0.56	3.52	96 ± 1	155 ± 2	0.876 ± 0.002	167.6 ± 1
BB02-5-4	0.01	1.87	86 ± 2	165 ± 3	0.976 ± 0.003	231.9 ± 3
BB02-5-4-B-W	0.01	1.52	86 ± 2	186 ± 3	1.022 ± 0.004	275.2 ± 4.7
BB02-5-4-B-R	0.03	3.17	94 ± 2	151 ± 3	0.876 ± 0.002	168.8 ± 1.4
BB02-5-4-B-M	0.02	2.17	95 ± 3	160 ± 6	0.911 ± 0.013	185.2 ± 7.4

† The quoted (^{230}Th/^{238}U) activity ratios are based on the new spike calibration (Appendix A4).

D List of samples collected during the Barbados excursion

Sample	Date of sampling	Location	Collected coral species	Number of samples
BB02 – 1	2.11.02	15 m von Gallup-Stelle nach unten	Head-Coral + Palmata	4
BB02 – 2	2.11.02	Siehe Meischner	Head Coral	3
BB02 – 3	2.11.02	Zwischen BB02-1 und BB02-2	Palmata	3
BB02 – 4	2.11.02	Vom Autodach gegenüber Fence	Palmata	4
BB02 – 5	2.11.02	Palmata Riff in Lebendstellung	Palmata	4
BB02 – 6	2.11.02	War mit „13“ bezeichnet	Head Coral + Palmata	4
BB02 – 7	3.11.02	Rendezvous Hill	Head Coral + Palmata	8
BB02 – 8	3.11.02	Strand	Palmata	4
BB02 – 9	3.11.02	„nicht 5c“, weil zu hoch	Head Coral + Palmata	3
BB02 – 10	3.11.02	5c – Notch von Exkursion	Palmata	2
BB02 – 11	4.11.02	Sea Dragon Cave	Stalagmit aus Tropfwasser + Palmata	7
BB02 – 12	4.11.02	Um die Kurve	Palmata	3
BB02 – 13	5.11.02	Cave am Strand	Palmata	2
BB02 – 14	5.11.02	5a - Bushaltestelle	Palmata	2

References

Albarède, F. (1995): Introduction to Geochemical Modeling, Cambridge University Press. Cambridge

Al-Rifaiy, I. A. and Cherif, O. H. (1988): The fossil coral reefs of Al-Aqaba, Jordan. - *Facies 18*: 219-230.

Amiel, A. J., Friedman, G. M. and Miller, D. S. (1973a): Distribution and nature of incorporation of trace elements in modern aragonitic corals. - *Sedimentology 20*: 47-64.

Amiel, A. J., Miller, D. S. and Friedman, G. M. (1973b): Incorporation of uranium in modern corals. - *Sedimentology 20*: 523-528.

Ayalon, A., Bar-Matthews, M. and Kaufman, A. (2002): Climatic conditions during marine oxygen isotope stage 6 in the eastern Mediterranean region from the isotopic composition of speleothems of Soreq Cave, Israel. - *Geology 30*: 303-306.

Bak, R. P. M. (1977): Coral reefs and their zonation in the Netherland Antilles. - *Studies in Geology 4*: 3-16.

Bard, E., Antonioli, F. and Silenzi, S. (2002a): Sea-level during the penultimate interglacial period based on a submerged stalagmite from Argentarola Cave (Italy). - *Earth and Planetary Science Letters 196*: 135-146.

Bard, E., Delaygue, G., Rostek, F., Antonioli, F., Silenzi, S. and Schrag, D. P. (2002b): Hydrological conditions over the western Mediterranean basin during the deposition of the cold Sapropel 6 (ca. 175 kyr BP). - *Earth and Planetary Science Letters 202*: 481-494.

Bard, E., Fairbanks, R. G. and Hamelin, B. (1992): How accurate are the U-Th ages obtained by mass spectrometry on coral terraces, in: Kukla, G. and Went, E. (Eds.), Start of a Glacial, Springer-Verlag, Berlin

Bard, E., Fairbanks, R. G., Hamelin, B., Zindler, A. and Hoang, C. T. (1991): Uranium-234 anomalies in corals older than 150,000 years. - *Geochimica et Cosmochimica Acta 55*: 2385-2390.

Bard, E., Hamelin, B., Arnold, M., Montaggioni, L., Cabioch, G., Faure, G. and Rougerie, F. (1996): Deglacial sea-level record from Tahiti corals and the timing of global meltwater discharge. - *Nature 382*: 241-244.

Bard, E., Hamelin, B. and Fairbanks, R. G. (1990a): U-Th ages obtained by mass spectrometry in corals from Barbados: sea level during the past 130,000 years. - *Nature 346*: 456-458.

Bard, E., Hamelin, B., Fairbanks, R. G. and Zindler, A. (1990b): Calibration of the ^{14}C timescale over the past 30,000 years using mass spectrometric U-Th ages from Barbados corals. - *Nature 345*: 405-410.

Bar-Matthews, M., Wasserburg, G. J. and Chen, J. H. (1993): Diagenesis of fossil coral skeletons: Correlation between trace elements, textures, and $^{234}U/^{238}U$. - *Geochimica et Cosmochimica Acta 57*: 257-276.

Barnes, J. W., Lang, E. J. and Potratz, H. A. (1956): The ratio of ionium to uranium in coral limestone. - *Science 124*: 175-176.

Barnes, R. S. K. and Hughes, R. N. (1988): An introduction to marine ecology, Blackwell Scientific Publications. Oxford

Bender, M. L., Fairbanks, R. G., Taylor, F. W., Matthews, R. K., Goddard, J. G. and Broecker, W. S. (1979): Uranium-series dating of the Pleistocene reef tracts of Barbados, West Indies. - *GSA Bulletin 90*: 577-594.

Bender, M. L., Sowers, T. and Labeyrie, L. (1994): The Dole effect and its variations during the last 130,000 years as measured in the Vostok ice core. - *Global Biogeochemical Cycles 8*: 363-376.

Berger, A. and Loutre, M.-F. (1991): Insolation values for the climate of the last 10 million years. - *Quarternary Science Reviews 10*: 297-317.

Bernardo, J. M. and Smith, A. F. M. (2000): Bayesian Theory, John Wiley & Sons. New York

Bischoff, J. L. and Fitzpatrick, J. A. (1991): U-series dating of impure carbonates: An isochron technique using total-sample dissolution. - *Geochimica et Cosmochimica Acta 55*: 543-554.

Blanchon, P. and Eisenhauer, A. (2001): Multi-stage reef development on Barbados during the Last Interglaciation. - *Quarternary Science Rewiews 20*: 1093-1112.

Bourdon, B., Turner, S. P., Henderson, G. M. and Lundstrom, C. C. (2003): Introduction to U-series geochemistry, in: Bourdon, B., Henderson, G. M., Lundstrom, C. C. and Turner, S. P. (Eds.), Uranium-series Geochemistry, Mineralogical Society of America, Washington, DC

Broecker, W. S. (1963): A preliminary evaluation of uranium series inequilibrium as a tool for absolute age measurement on marine carbonates. - *Journal of Geophysical Research 68*: 2817-2834.

Broecker, W. S. (1995): The Glacial World according to Wally, Lamont-Doherty Observatory, Columbia University. Palisades, NY

Broecker, W. S., Thurber, D. L., Goddard, J. G., Ku, T.-L., Matthews, R. K. and Mesolella, K. J. (1968): Milankovich hypothesis supported by precise dating of coral reefs and deep sea sediments. - *Science 159*:

Cabioch, G. and Ayliffe, L. K. (2001): Raised coral terraces at Malakula, Vanatu, Southwest Pacific, indicate high sea level during Marine Isotope Stage 3. - *Quaternary Research 56*: 357-365.

Chabaux, F., Riotte, J. and Dequincey, O. (2003): U-Th-Ra Fractionation during weathering and river transport, in: Bourdon, B., Henderson, G. M., Lundstrom, C. C. and Turner, S. P. (Eds.), Uranium-series Geochemistry, Mineralogical Society of America, Washington, DC

Chappell, J. (2002): Sea level changes forced ice breakouts in the Last Glacial cycle: new results from coral terraces. - *Quaternary Science Reviews 21*: 1229-1240.

Chappell, J., Omura, A., Esat, T. M., McCulloch, M. T., Pandolfi, J., Ota, Y. and Pillans, B. (1996): Reconciliation of late Quaternary sea levels derived from coral terraces at Huon Peninsula with deep sea oxygen isotope records. - *Earth and Planetary Science Letters 141*: 227-236.

Chappell, J. and Polach, H. (1991): Post-glacial sea-level rise from a coral record at Huon Peninsula, Papua New Guinea. - *Nature 349*:

Chen, J. H., Curran, H. A., White, B. and Wasserburg, G. J. (1991): Precise chronology of the last interglacial period: ^{234}U-^{230}Th data from fossil coral reefs in the Bahamas. - *GSA Bulletin 103*: 82-97.

Chen, J. H., Edwards, R. L. and Wasserburg, G. J. (1986): ^{238}U-^{234}U-^{232}Th in seawater. - *Earth and Planetary Science Letters 80*:

Cheng, H., Edwards, R. L., Hoff, J., Gallup, C. D., Richards, D. A. and Asmerom, Y. (2000): The half-lives of uranium-234 and thorium-230. - *Chemical Geology 169*: 17-33.

Cheng, H., Edwards, R. L., Murrell, M. T. and Benjamin, T. M. (1998): Uranium-thorium-protactinium dating systematics. - *Geochimica et Cosmochimica Acta 62*: 3437-3452.

Cobb, K. M., Charles, C. D., Cheng, H., Kastner, M. and Edwards, R. L. (2003): U/Th-dating living and young fossil corals from the central tropical Pacific. - *Earth and Planetary Science Letters 210*: 91-103.

Cross, T. S. and Cross, B. W. (1983): U, Sr and Mg in Holocene and Pleistocene corals *A. palmata* and *M. annularis*. - *Journal of Sedimentary Petrology 53*: 587-594.

Cutler, K. B., Edwards, R. L., Taylor, F. W., Cheng, H., Adkins, J., Gallup, C. D., Cutler, P. M., Burr, G. S. and Bloom, A. L. (2003): Rapid sea-level fall and deep-ocean temperature change since the last interglacial period. - *Earth and Planetary Science Letters 206*: 253-271.

Delanghe, D., Bard, E. and Hamelin, B. (2002): New TIMS constraints on the uranium-238 and uranium-234 in seawaters from the main ocean basins and the Mediterranean Sea. - *Marine Chemistry 80*: 79-93.

Dunk, R. M., Jenkins, W. J. and Mills, R. A. (2002): A re-evaluation of the oceanic uranium budget. - *Chemical Geology 190*: 45-67.

Edwards, R. L. (1988): High precision Th-230 ages of corals and the timing of sea level fluctuations in the late Quaternary - PhD Dissertation; California Institute of Technology, Pasadena, California

Edwards, R. L., Beck, J. W., Burr, G. S., Donahue, D. J., Druffel, E. R. M. and Taylor, F. W. (1993): A large drop in atmospheric $^{14}C/^{12}C$ and reduced melting during the Younger Dryas, documented with ^{230}Th ages of corals. - *Science 260*: 962-968.

Edwards, R. L., Chen, J. H., Ku, T.-L. and Wasserburg, G. J. (1987): Precise Timing of the Last Interglacial Period from Mass Spectrometric Determination of Thorium-230 in Corals. - *Science 236*: 1547-1553.

Edwards, R. L., Chen, J. H. and Wasserburg, G. J. (1986): ^{238}U-^{234}U-^{230}Th-^{232}Th systematics and the precise measurement of time over the past 500,000 years. - *Earth and Planetary Science Letters 81*: 175-192.

Edwards, R. L., Cheng, H., Murrell, M. T. and Goldstein, S. J. (1997): Protactinium-231 dating of carbonates by Thermal Ionization Mass Spectrometry: Implications for Quaternary climate change. - *Science 276*: 782-786.

Edwards, R. L., Gallup, C. D. and Cheng, H. (2003): Uranium-series dating of marine and lacustrine carbonates, in: Bourdon, B., Henderson, G. M., Lundstrom, C. C. and Turner, S. P. (Eds.), Uranium-series Geochemistry, Mineralogical Society of America, Washington, DC

El-Asmar, H. M. (1997): Quaternary isotope stratigraphy and paleoclimate of coral reef terraces, Gulf of Aqaba, South Sinai, Egypt. - *Quaternary Science Reviews 16*: 911-924.

Esat, T. M., McCulloch, M. T., Chappell, J., Pillans, B. and Omura, A. (1999): Rapid fluctuations in sea level recorded at Huon Peninsula during the penultimate deglaciation. - *Science 283*: 197-201.

Fairbanks, R. G. (1989): A 17,000-year glacio-eustatic sea level record: influence of glacial melting rates on the Younger Dryas event and deep-ocean circulation. - *Nature 342*: 637-642.

Felis, T., Lohmann, G., Kuhnert, H., Lorenz, S. J., Scholz, D., Pätzold, J., Al-Rousan, S. A. and Al-Moghrabi, S. M. (2004): Increased seasonality in Middle East temperatures during the last interglacial period. - *Nature 429*: 164-168.

Felis, T. and Pätzold, J. (2003): Climate records from corals, in: Wefer, G., Lamy, F. and Mantoura, F. (Eds.), Marine Science Frontiers for Europe, Springer-Verlag, Berlin

Felis, T., Pätzold, J. and Loya, Y. (2003): Mean oxygen-isotope signatures in *Porites spp.* corals: inter-colony variability and correction for extension-rate effects. - *Coral Reefs 22*: 328-336.

Felis, T., Pätzold, J., Loya, Y. and Wefer, G. (1998): Vertical water mass mixing and plankton blooms recorded in skeletal stable carbon isotopes of a Red Sea coral. - *Journal of Geophysical Research 103*: 30731-30739.

Fishman, G. S. (1997): Monte Carlo: Concepts, Algorithms, and Applications, Springer-Verlag. New York

Friedman, G. M. (1968): Geology and geochemistry of reefs, carbonate sediments, and waters, Gulf of Aqaba (Elat), Red Sea. - *Journal of Sedimentary Petrology 38*: 895-919.

Fruijtier, C., Elliott, T. and Schlager, W. (2000): Mass-spectrometric ^{234}U-^{230}Th ages from the Key Largo Formation, Florida Keys, United States: Constraints on diagenetic age disturbance. - *GSA Bulletin 112 (2)*: 267-277.

Gallup, C. D., Cheng, H., Taylor, F. W. and Edwards, R. L. (2002): Direct Determination of the Timing of Sea Level Change During Termination II. - *Science 295*: 310-313.

Gallup, C. D., Edwards, R. L. and Johnson, R. G. (1994): The timing of High Sea Levels over the past 200,000 years. - *Science 263*: 796-800.

Geiselhart, S. (1998): Late Quaternary paleoceanographic and paleoclimatologic history of the Red Sea during the last 380,000 years: Evidence from stable isotopes and faunal assemblages. - *Tübinger Mikropaläontologische Mitteilungen 17*: 87.

Gentle, J. E. (2003): Random number generation and Monte Carlo methods, Springer. New York

Geyh, M. A. and Schleicher, H. (1990): Absolute age determination. Physical and chemical dating methods and their application, Springer-Verlag. Berlin

Gvirtzman, G. (1994): Fluctuations of sea level during the past 400 000 years: the record of Sinai, Egypt (northern Red Sea). - *Coral Reefs 13*: 203-214.

Gvirtzman, G., Friedman, G. M. and Miller, D. S. (1973): Control and distribution of uranium in coral reefs during diagenesis. - *Journal of Sedimentary Petrology 43*: 985-997.

Gvirtzman, G., Kronfeld, J. and Buchbinder, B. (1992): Dated coral reefs of southern Sinai (Red Sea) and their implication to late Quaternary sea levels. - *Marine Geology 108*: 29-37.

Hamelin, B., Bard, E., Zindler, A. and Fairbanks, R. G. (1991): $^{234}U/^{238}U$ mass spectrometry of corals: How accurate is the U-Th age of the last interglacial period? - *Earth and Planetary Science Letters 106*: 169-180.

Hearty, P. J. and Neumann, A. C. (2001): Rapid sea level and climate change at the close of the Last Interglaciation (MIS 5e): evidence from the Bahama Islands. - *Quarternary Science Reviews 20*: 1881-1895.

Henderson, G. M. (2002): Seawater ($^{234}U/^{238}U$) during the last 800 thousand years. - *Earth and Planetary Science Letters 199*: 97-110.

Henderson, G. M. and Anderson, R. F. (2003): The U-series toolbox for paleoceanography, in: Bourdon, B., Henderson, G. M., Lundstrom, C. C. and Turner, S. P. (Eds.), Uranium-series Geochemistry, Mineralogical Society of America, Washington, DC

Henderson, G. M., Cohen, A. S. and O'Nions, R. K. (1993): $^{234}U/^{238}U$ ratios and ^{230}Th ages for Hateruma Atoll corals: implications for coral diagenesis and seawater $^{234}U/^{238}U$ ratios. - *Earth and Planetary Science Letters 115*: 65-73.

Henderson, G. M. and Slowey, N. C. (2000): Evidence from U-Th dating against Northern Hemisphere forcing of the penultimate deglaciation. - *Nature 404*: 61-65.

Henderson, G. M., Slowey, N. C. and Fleisher, M. Q. (2001): U-Th dating of carbonate platform and slope sediments. - *Geochimica et Cosmochimica Acta 65*: 2757-2770.

Hoffmann, D. (2002): Kombinierte Elektronen-Spin-Resonanz- und Uranreihen-Datierung von Zahnschmelz - PhD Thesis; Heidelberg Academy of Sciences, Heideleberg

Hoffmann, D. and Mangini, A. (2003): A method for coupled ESR/U-series dating of teeth showing post-depositional U-loss. - *Quaternary Science Reviews 22*: 1367-1372.

Holzkämper, S. (2004): Dating and interpretation of secondary carbonate deposits from the Last Interglacial - PhD Thesis; Heidelberg Academy of Sciences, Heidelberg

Holzkämper, S., Mangini, A., Spötl, C. and Mudelsee, M. (2004): Timing and progression of the Last Interglacial derived from a high alpine stalagmite. - *Geophysical Research Letters 31*: L07201.

Hughen, K. A., Schrag, D. P., Jacobsen, S. B. and Hantoro, W. (1999): El Nino during the last interglacial period recorded by a fossil coral from Indonesia. - *Geophysical Research Letters 26*: 3129-3132.

Imbrie, J., Hays, J. D., McIntyre, A., Mix, A. C., Morley, J. J., Pisias, N. G., Prell, W. L. and Shackleton, N. J. (1984): The orbital theory of Pleistocene climate: Support from a revised chronology of the marine $\delta^{18}O$ record., in: Berger, A., Imbrie, J., Hays, J., Kukla, G. J. and Saltzman, E. (Eds.), Milankovitch and Climate, D. Reidel, Boston

Ivanovich, M. and Harmon, R. S. (1992): Uranium-series Disequilibrium: Applications to Earth, Marine, and Environmental Sciences, Oxford University Press. Oxford

Jouzel, J., Hoffmann, G., Parrenin, F. and Waelbroeck, C. (2002): Atmospheric oxygen 18 and sea-level changes. - *Quaternary Science Reviews 21*: 307-314.

Kaufman, A. (1993): An evaluation of several methods for determining ^{230}Th/U ages in impure carbonates. - *Geochimica et Cosmochimica Acta 57*: 2303-2317.

Kent, J. T., Watson, G. S. and Onstott, T. C. (1990): Fitting straight lines and planes with an application to radiometric dating. - *Earth and Planetary Science Letters 97*: 1-17.

Ku, T.-L., Ivanovich, M. and Luo, S. (1990): U-Series dating of Last Interglacial high sea stands: Barbados revisited. - *Quaternary Research 33*: 129-147.

Ku, T.-L., Knauss, K. G. and Mathieu, G. G. (1977): Uranium in open ocean: concentration and isotopic composition. - *Deep-Sea Research 24*: 1005-1017.

Lazar, B., Stein, M., Enmar, R., Bar-Matthews, M. and Halicz, L. (2002). The effect of diagenesis on the U system in live and Holocene corals from the Red Sea. Goldschmidt Conference, Davos, Switzerland.

Lea, D. W., Martin, P. A., Pak, D. K. and Spero, H. J. (2002): Reconstructing a 350 ky history of sea level using planctonic Mg/Ca and oxygen isotope records from a Cocos Ridge core. - *Quaternary Science Reviews 21*: 283-293.

Levinton, J. S. (2001): Marine Biology: Function, Biodiversity, Ecology, Oxford University Press, Inc. New York

Linsley, B. K., Dunbar, R. B., Wellington, G. M. and Mucciarone, D. A. (1994): A coral-based reconstruction of Intertropical Convergence Zone variability over central America since 1707. - *Journal of Geophysical Research 99*: 9977-9994.

Ludwig, K. R. (2001): Isoplot/Ex rev. 2.49: A geochronological toolkit for Microsoft Excel. - *Berkley Geochronolgy Center Special Publication No. 1a*:

Ludwig, K. R. (2003): Mathematical-statistical treatment of data and errors for ^{230}Th/U geochronology, in: Bourdon, B., Henderson, G. M., Lundstrom, C. C. and Turner, S. P. (Eds.), Uranium-series Geochemistry, Mineralogical Society of America, Washington, DC

Ludwig, K. R., Muhs, D. R., Simmons, K. R., Halley, R. B. and Shinn, E. A. (1996): Sea-level records at ~80 ka from tectonically stable platforms: Florida and Bermuda. - *Geology 24*: 211-214.

Ludwig, K. R. and Titterington, D. M. (1994): Calculation of ^{230}Th/U isochrons, ages, and errors. - *Geochimica et Cosmochimica Acta 58*: 5031-5042.

Luo, S. and Ku, T.-L. (1991): U-series isochron dating: A generalized method employing total-sample dissolution. - *Geochimica et Cosmochimica Acta 55*: 555-564.

Malaize, B., Paillard, D., Jouzel, J. and Raynaud, D. (1999): The Dole effect over the last two glacial-interglacial cycles. - *Journal of Geophysical Research 104*: 14,199-14,208.

Matthews, R. K. (1968): Carbonate diagenesis: Equilibration of sedimentary mineralogy to the subaerial environment; coral cap of Barbados, West Indies. - *Journal of Sedimentary Petrology 38*: 1110-1119.

McCulloch, M. T. and Esat, T. (2000): The coral record of last interglacial sea levels and sea surface temperatures. - *Chemical Geology 169*: 107-129.

McIntyre, G. A., Brooks, C., Compston, W. and Turek, A. (1966): The statistical assessment of Rb-Sr isochrons. - *Journal of Geophysical Research 71*: 5459-5468.

Mélières, M.-A., Rossignol-Strick, M. and Malaizé, B. (1997): Relation between low latitude insolation and $\delta^{18}O$ change of atmospheric oxygen for the last 200 kyrs, as revealed by Mediterranean sapropels. - *Geophysical Research Letters 24*: 1235-1238.

Mesolella, K. J., Matthews, R. K., Broecker, W. S. and Thurber, D. L. (1969): The astronomical theory of climatic change: Barbados Data. - *Journal of Geology 77*: 250-274.

Milankovitch, M. M. (1941): Canon of Insolation and the Ice Age Problem (English Translations, Washington, D.C.). - *Königlich Serbische Akademie, Beograd*

Min, G. R., Edwards, R. L., Taylor, F. W., Recy, J., Gallup, C. D. and Beck, J. W. (1995): Annual cycles of U/Ca in coral skeletons and U/Ca thermometry. - *Geochimica et Cosmochimica Acta 59*: 2025-2042.

Moore, W. S. (1981): The thorium isotope content of ocean water. - *Earth and Planetary Science Letters 53*: 419-426.

Muhs, D. R., Simmons, K. R. and Steinke, B. (2002): Timing and warmth of the Last Interglacial period: new U-series evidence from Hawaii and Bermuda and a new fossil compilation for North America. - *Quaternary Science Reviews 21*: 1355-1383.

Neff, U. (2001): Massenspektrometrische Th/U-Datierung von Höhlensintern aus dem Oman: Klimaarchive des asiatischen Monsuns - PhD Thesis; Heidelberg Academy of Sciences, Heidelberg

Nozaki, Y. and Nakanishi, T. (1985): ^{231}Pa and ^{230}Th profiles in the open ocean water column. - *Deep-Sea Research 32*: 1209-1220.

Parrenin, F. and Paillard, D. (2003): Amplitude and phase of glacial cycles from a conceptual model. - *Earth and Planetary Science Letters 214*: 243-250.

Petit, J. R., Jouzel, J., Raynaud, D., Barkov, N. I., Barnola, J.-M., Basile, I., Bender, M. L., Chappellaz, J., Davis, M., Delaygue, G., Delmotte, M., Kotlyakov, V. M., Legrand, M., Lipenkov, V. Y., Lorius, C., Pepin, L., Ritz, C., Saltzman, E. and Stievenard, M. (1999): Climate and atmospheric history of the past 420,000 years from the Vostok ice core, Antarctica. - *Nature 399*: 429-436.

Plagnes, V., Causse, C., Genty, D., Paterne, M. and Blamart, D. (2002): A discontinous climatic record from 187 to 74 ka from a speleothem of the Clamouse Cave (south of France). - *Earth and Planetary Science Letters 201*: 87-103.

Porcelli, D. and Swarzenski, P. W. (2003): The behaviour of U- and Th-nuclides in groundwater, in: Bourdon, B., Henderson, G. M., Lundstrom, C. C. and Turner, S. P. (Eds.), Uranium-series Geochemistry, Mineralogical Society of America, Washington, DC

Potter, E.-K., Esat, T. M., Schellmann, G., Radtke, U., Lambeck, K. and McCulloch, M. T. (2004): Suborbital-period sea-level oscillations during marine isotope substages 5a and 5c. - *Earth and Planetary Science Letters 225*: 191-204.

Potter, E.-K. and Lambeck, K. (2003): Reconciliation of sea-level observations in the Western North Atlantic during the last glacial cycle. - *Earth and Planetary Science Letters 217*: 171-181.

Press, W. H., Flannery, B. P., Teukolsky, S. A. and Vetterling, W. T. (1988): Numerical recipes in C. The art of scientific computing, Cambridge University Press. Cambridge

Quinn, T. M., Crowley, T. J., Taylor, F. W., Henin, C., Joannot, P. and Join, Y. (1998): A multicentury stable isotope record from a New Caledonia coral: Interannual and decadal sea surface temperature variability in the southwest Pacific since 1657 A.D. - *Paleoceanography 13*: 412-426.

Reeder, R. J., Nugent, M., Lamble, G. M., Tait, C. D. and Morris, D. E. (2000): Uranyl incorporation into calcite and aragonite: XAFS and luminescence studies. - *Environmental Science & Technology 34*: 638-644.

Reiss, Z. and Hottinger, L. (1984): The Gulf of Aqaba: Ecological Micropaleontology, Springer-Verlag. Berlin

Richards, D. A. and Dorale, J. A. (2003): Uranium-series chronology and environmental applications of speleothems, in: Bourdon, B., Henderson, G. M., Lundstrom, C. C. and Turner, S. P. (Eds.), Uranium-series Geochemistry, Mineralogical Society of America, Washington, DC

Richards, D. A., Smart, P. L. and Edwards, R. L. (1994): Maximum sea levels for the last glacial period from U-series ages of submerged speleothems. - *Nature 367*: 357-360.

Richter, F. M. and Turekian, K. K. (1993): Simple models for the geochemical response of the ocean to climatic and tectonic forcing. - *Earth and Planetary Science Letters 119*: 121-131.

Ruddiman, W. F. (2003): Orbital insolation, ice volume, and greenhouse gases. - *Quaternary Science Reviews 22*: 1597-1629.

Ruddiman, W. F. (2004): The role of Greenhouse Gases in orbital-scale climatic changes. - *Eos 85*: 1, 6-7.

Ruppert, E. E. and Barnes, R. D. (1994): Invertebrate Zoology, Saunders College Publishing. Fort Worth

Schellmann, G. and Radtke, U. (2004): The Marine Quaternary of Barbados, Selbstverlag: Geographisches Institut der Universität zu Köln - Kölner Geographische Arbeiten -. Köln

Scholz, D. (2001): ESR-Datierung von Foraminiferen - Staatsexamensarbeit; Heidelberg Academy of Sciences, Heidelberg

Scholz, D., Mangini, A. and Felis, T. (2004): U-series dating of diagenetically altered fossil reef corals. - *Earth and Planetary Science Letters 218*: 163-178.

Schuhmacher, H. (1988): Korallenriffe, BLV Verlagsgesellschaft mbH. München

Seilnacht, T. (2004): Vergleich Calcit - Aragonit, http://www.seilnacht.com/Minerale/ calcarag. htm

Shackleton, N. J. (2000): The 100,000-year ice-age cycle identified and found to lag temperature, carbon dioxide, and orbital eccentricity. - *Science 289*: 1897-1902.

Shackleton, N. J., Chapman, M., Sanchez-Goni, M. F., Pailler, D. and Lancelot, Y. (2002): The classic marine isotope substage 5e. - *Quaternary Research 58*:

Shemesh, A., Luz, B. and Erez, J. (1994): Carbon isotopes, dissolved oxygen, and the carbonate system in the northern Gulf of Aqaba (Elat). - *Israel Journal of Earth Sciences 43*: 145-155.

Shen, G. T. and Dunbar, R. B. (1995): Environmental controls on uranium in reef corals. - *Geochimica et Cosmochimica Acta 59*: 2009-2024.

Siddall, M., Rohling, E. J., Almogi-Labin, A., Hemleben, C., Meischner, D., Schmelzer, I. and Smeed, D. A. (2003): Sea-level fluctuations during the last glacial cycle. - *Nature 423*: 853-858.

Siddall, M., Smeed, D. A., Hemleben, C., Rohling, E. J., Schmelzer, I. and Peltier, W. R. (2004): Understanding the Red Sea response to sea level. - *Earth and Planetary Science Letters 225*: 421-434.

Smart, P. L., Richards, D. A. and Edwards, R. L. (1998): Uranium-series ages of speleothems from South Andros, Bahamas: Implications for Quaternary sea-level history and palaeoclimate. - *Cave and Karst Science 25*: 67-74.

Stein, M., Wasserburg, G. J., Aharon, P., Chen, J. H., Zhu, Z. R., Bloom, A. and Chappell, J. (1993): TIMS U-series dating and stable isotopes of the last interglacial event in Papua New Guinea. - *Geochimica et Cosmochimica Acta 57*: 2541-2554.

Stirling, C. H., Esat, T. M., Lambeck, K. and McCulloch, M. T. (1998): Timing and duration of the Last Interglacial: evidence for a restricted interval of widespread coral reef growth. - *Earth and Planetary Science Letters 160*: 745-762.

Stirling, C. H., Esat, T. M., Lambeck, K., McCulloch, M. T., Blake, S. G., Lee, D.-C. and Halliday, A. N. (2001): Orbital forcing of the Marine Isotope Stage 9 Interglacial. - *Science 291*: 290-293.

Stirling, C. H., Esat, T. M., McCulloch, M. T. and Lambeck, K. (1995): High-precision U-series dating of corals from Western Australia and implications for the timing and duration of the Last Interglacial. - *Earth and Planetary Science Letters 135*: 115-130.

Strasser, A., Strohmenger, C., Davaud, E. and Bach, A. (1992): Sequential evolution and diagenesis of Pleistocene coral reefs (South Sinai, Egypt). - *Sedimentary Geology 78*: 59-79.

Swart, P. K. and Hubbard, J. A. E. B. (1982): Uranium in scleractinian coral skeletons. - *Coral Reefs 1*: 13-19.

Szabo, B. J., Ludwig, K. R., Muhs, D. R. and Simmons, K. R. (1994): Thorium-230 ages fo corals and duration of the Last Interglacial Sea-level High-stand on Oahu, Hawaii. - *Science 266*: 93-93.

Taviani, M. (1998): Post-Miocene reef faunas of the Red Sea:glacio-eustatic controls, in: Purser, B. H. and Boscene, J. (Eds.), Sedimentation and tectonics of rift basins: Red Sea-Gulf of Aden, Chapman & Hall, London

Taylor, F. W. and Mann, P. (1991): Late Quaternary folding of coral reef terraces. - *Geology 19*: 103-106.

Thompson, W. G., Spiegelmann, M. W., Goldstein, S. L. and Speed, R. C. (2003): An open-system model for U-series age determinations of fossil corals. - *Earth and Planetary Science Letters 210*: 365-381.

Titterington, D. M. and Halliday, A. N. (1979): On the fitting of parallel isochrons and the method of maximum likelihood. - *Chemical Geology 26*: 183-195.

Toscano, M. A. and Lundberg, J. (1999): Submerged Late Pleistocene reefs on the tectonically-stable S.E. Florida margin: high-precision geochronology, stratigraphy, resolution of Substage 5a sea-level elevation, and orbital forcing. - *Quaternary Science Reviews 18*: 753-767.

Tudhope, A. W., Chilcott, C. P., McCulloch, M. T., Cook, E. R., Chappell, J., Ellam, R. M., Lea, D. W., Lough, J. M. and Shimmield, G. B. (2001): Variability in the El Nino-southern oscillation through a glacial-interglacial cycle. - *Science 291*: 1511-1517.

Tzedakis, C., McManus, J. F., Hooghiemstra, H., Oppo, D. W. and Wijmstra, T. A. (2003): Comparison of changes in vegetation in northeast Greece with records of climate variability on orbital and suborbital frequencies over the last 450000 years. - *Earth and Planetary Science Letters 212*: 197-212.

Villemant, B. and Feuillet, N. (2003): Dating open systems by the ^{238}U-^{234}U-^{230}Th method: application to Quaternary reef terraces. - *Earth and Planetary Science Letters 210*: 105-118.

Waelbroeck, C., Labeyrie, L., Michel, E., Duplessy, J. C., McManus, J. F., Lambeck, K., Balbon, E. and Labracherie, M. (2002): Sea-level and deep water temperature changes derived from benthic foraminifera isotopic records. - *Quaternary Science Reviews 21*: 295-305.

Walter, R. C., Buffler, R. T., Bruggemann, J. H., Guillaume, M. M. M., Berhe, S. M., Negassi, B., Libsekal, Y., Cheng, H., Edwards, R. L., von Cosel, R., Neraudeau, D. and Gagnon, M. (2000): Early human occupation of the Red Sea coast of Eritrea during the last interglacial. - *Nature 405*: 65-69.

Wedepohl, H. K. (1995): The composition of the continental crust. - *Geochimica et Cosmochimica Acta 59*: 1217-1232.

Wilson, M. A., Curran, H. A. and White, B. (1998): Paleontological evidence of a brief global sea-level event during the last interglacial. - *Lethaia 31*: 241-250.

Winograd, I. J., Coplen, T. B., Landwehr, J. M., Riggs, A. C., Ludwig, K. R., Szabo, B. J., Kolesar, P. T. and Revesz, K. M. (1992): Continuous 500,000-year climate record from vein calcite in Devils Hole, Nevada. - *Science 258*: 255-259.

York, D. (1969): Least squares fitting of a straight line with correlated errors. - *Earth and Planetary Science Letters 5*: 320-324.

Zhu, Z. R., Wyrwoll, K.-H., Collins, L. B., Chen, J. H., Wasserburg, G. J. and Eisenhauer, A. (1993): High-precision U-series dating of Last Interglacial events by mass spectrometry: Houtman Abrolhos Islands, Western Australia. - *Earth and Planetary Science Letters 118*: 281-293.

Danksagung

Mein ganz besonderer Dank gilt meinem Doktorvater Prof. Dr. Augusto Mangini, der stets großes Interesse an meiner Arbeit zeigte. Er hatte immer ein offenes Ohr für Fragen, und seine zahlreichen, guten Ideen haben maßgeblich zum Gelingen der Arbeit beigetragen. Zudem ließ er mir immer viel Raum für eigene Ansätze. Dennoch haben sich seine Ratschläge nicht nur auf wissenschaftliche Themen beschränkt: „Ich überlege die ganze Zeit, ob ihr nicht andere Musik machen solltet ...“

Prof. Dr. Kurt Roth danke ich dafür, dass er spontan bereit war als Gutachter dieser Arbeit zu fungieren.

Dr. Thomas Felis von der Universität Bremen hat die „außergewöhnlichen“ Korallen aus Aqaba zur Verfügung gestellt und sämtliche Voruntersuchungen durchgeführt. Hieraus hat sich in den letzten drei Jahren eine äußerst produktive Zusammenarbeit ergeben, die hoffentlich noch lange andauert.

Prof. Dr. Dieter Meischner war eine große Hilfe bei der Probennahme auf Barbados. Ohne seine Unterstützung hätten wir das MIS 6.5 Riff wahrscheinlich nicht gefunden.

Außerdem möchte ich mich bei allen Mitgliedern meiner Arbeitsgruppe bedanken. Die kollegiale, freundliche Atmosphäre am Institut erleichtert das neuerdings sehr frühe Aufstehen ungemein.

Insbesondere danke ich meinem Zimmerkollegen René Eichstädter, der mich das TIMS-Messen gelehrt hat und sich auf Barbados immer „ganz selbstlos“ (und mit letzten Kräften) um übriggebliebene Cocktails „gekümmert“ hat.

Marcus danke ich dafür, dass er trotz ernormem Stress meine Arbeit korrekturgelesen hat. Außerdem war er immer die erste Anlaufstelle bei Computer-Problemen.

Auch bei Andrea möchte ich mich für das sorgfältige (und zügige!!!) Korrekturlesen bedanken.

Auch einige „Ehemalige“ dürfen nicht unerwähnt bleiben:

Mit meinem (Ex)-DEKLIM-Kollegen und Namensvetter Steffen „Scholzkämper“ habe ich einige Tagungen und Exkursionen besucht und so manchen feuchtfröhlichen Abend (auch am Institut) erlebt.

Meinem Vorgänger am Institut und jetzigen Bandkollegen Uli möchte ich dafür danken, dass ich mich (wie er es sagen würde) „ins gemachte Nest setzen durfte“.

Clemens war mir eine große Hilfe bei Diskussionen zum Thema Fehlerrechnung.

Steffi möchte ich für ihr Verständnis in Stressphasen während des Zusammenschreibens und überhaupt für alles danken.

Allerherzlichsten Dank auch an meine Eltern, die mir mein Studium und damit diese Arbeit erst ermöglicht haben, und an die übrigen Familienmitglieder.